Alkali Effect on the Iron Making Processes

Thesis Submitted by

Maharshi Ghosh Dastidar

DOCTOR OF PHILOSOPHY (ENGINEERING)

Department of Metallurgical & Material Engineering
Faculty Council of Engineering and Technology
Jadavpur University

Kolkata-700032

India

2021

JADAVPUR UNIVERSITY

KOLKATA-700032, INDIA

INDEX NO. 205/16/E

1. TITLE OF THE THESIS:

Alkali Effect on the Iron Making Processes

2. NAME, DESIGNATION & INSTITUTION OF SUPERVISORS:

Prof. Rajib Dey

Professor

Department of Metallurgical & Material Engineering

Jadavpur University

Kolkata-700032

Prof. Manoj Kumar Mitra

Former-Professor

Department of Metallurgical & Material Engineering

Jadavpur University

Kolkata-700032

3. LIST OF PUBLICATIONS

THESIS RELATED PAPERS IN JOURNAL:

- **Alkali Effect on the Iron Making Processes**, **Maharshi Ghosh Dastidar**, Bitan Kumar Sarkar, Rajib Dey, Manoj Kumar Mitra, *Material Sci. & Eng. 2018;2(6):304–313.*
- **The effect of alkali on the reaction kinetics and strength of blast furnace coke, Maharshi Ghosh Dastidar,** Anrin Bhattacharyya, Bitan Kumar Sarkar, Rajib Dey, Manoj Kumar Mitra, Johannes Schenk; *Fuel 268 1-10 (2020); 117388.*

OTHER PAPERS IN JOURNAL:

- **Optimization of Reduction Parameters of Quenched Titaniferous Magnetite Ore by Boiler Grade Coal Using Box–Behnken Design**; Bitan Kumar Sarkar, **Maharshi Ghosh Dastidar**, Rajib Dey, Gopes Das, Souryadipta Chowdhury & Dhiman Mahata; *Journal of the Institution of Engineers (India)* (2019). 10.1007/s40033-019-00184-3.
- **A study on isothermal reduction kinetics of titaniferous magnetite ore using coke dust, an industrial waste;** Bitan Kumar Sarkar, **Maharshi Ghosh Dastidar**, Rajib Dey, Gopes Das, *Canadian Metallurgical Quarterly* (2018). 58. 1-9. 10.1080/00084433.2018.1553750.
- **Study on reduction kinetics of iron ore sinter using coke dust;** Arghya Majumder, Bitan Kumar Sarkar, **Maharshi Ghosh Dastidar**, Gopes Chandra Das & Rajib Dey; *International Journal of Metallurgical & Materials Science and Engineering (IJMMSE)*, (2018), 8. 19-26.
- **Utilisation of low grade chromite ore for the production of carbon free ferrochrome;** Rajib Dey, Siddhartha Mukherjee, **Maharshi Ghosh Dastidar**, Amit Kumar Bhandary, Mahua Ghosh Chaudhuri; MGMI Transactions, 114 (2017-18), 13-23.

4. LIST OF PATENTS: NIL

5. LIST OF PRESENTATIONS (NATIONAL/INTERNATIONAL):

1. **Recovery of Metal Values from a Blast Furnace Waste; Maharshi Ghosh Dastidar**, Ishita Sarkar, Bitan Kumar Sarkar, Riddhi Sarkar, Arghya Majumder, Rajib Dey; Waste Management in Metallurgical Industries: Effective Industry Practices & Research Initiatives,2018; CGCRI, Kolkata.

2. **Utilization of Iron Making Plant Waste for Production of Iron using Briquetting Process; Maharshi Ghosh Dastidar**, Ishita Sarkar, Bitan Kumar Sarkar, Rajib Dey, Arghya Majumder; Prospects and Challenges in Metallurgical & Allied Industries with Special Emphasis on Quality, Safety and Environment: IIM- Kolkata Chapter 2018, Floatel, Kolkata.

3. **Effect of Alkali present in Iron Ore on Direct Reduction using Box Behnken Design Modelling; Maharshi Ghosh Dastidar**, Bitan Kumar Sarkar, Anrin Bhattacharyya, Riddhi Sarkar, Rajib Dey, Manoj Kumar Mitra; NMD-ATM 2018, J.W. Marriott Hotel, Kolkata.

STATEMENT OF ORIGINALITY

I Maharshi Ghosh Dastidar registered on 02/02/2016 do hereby declare that this thesis entitled "Alkali Effect on the Iron Making Processes" contains literature survey and original research work done by the undersigned candidate as part of Doctoral studies.

All information in this thesis have been obtained and presented in accordance with existing academic rules and ethical conduct. I declare that as required by these rules and conduct, I have fully cited and referred all materials and results that are not original to this work.

I also declare that I have checked this thesis as per the "Policy on Anti-Plagiarism, Jadavpur University, 2019", and the level of similarity as checked by iThenticate software is 8 %.

Signature of Candidate:

Date:

Certified by Supervisor(s):

(Signature with date and seal)

1.

2.

CERTIFICATE FROM THE SUPERVISORS

This is to certify that the thesis entitled "**Alkali Effect on Iron Making Processes**" submitted by **Shri. Maharshi Ghosh Dastidar**, who got his name registered on **2nd February, 2016** for the award of **Ph.D. (Engg.)** degree of Jadavpur University is absolutely based on his own work under the supervision of **Prof. Rajib Dey and Prof. Manoj Kumar Mitra** and that neither his thesis nor any part of the thesis has been submitted for any degree/diploma or any other academic award anywhere before.

Prof. Rajib Dey
Professor
Dept. of Metallurgical & Material Engineering
Jadavpur University
Kolkata- 700032
India

Prof. Manoj Kumar Mitra
Former-Professor
Dept. of Metallurgical & Material Engineering
Jadavpur University
Kolkata- 700032
India

Dedicated to my

Family

Acknowledgement

Pursuing this PhD has been an immense experience. This journey has been a memorable one because of all the people that I have worked with over the years; who have helped me, guided me and motivated me during this time. I would like to take this opportunity to express my gratitude towards them.

Foremost, I would like to express my sincere gratitude to my advisors Prof. Rajib Dey and Prof. Manoj Kumar Mitra for their continuous support during my tenure as a research scholar, for their patience, motivation and immense knowledge. Their guidance helped me during the time of my research and writing of this thesis. They have always provided me with valuable advice, inputs and shown me the direction whenever I was in a befuddled state during my thesis work.

I also revere Prof. Gopes Chandra Das, Prof. Saradindukumar Ray, Prof. Siddhartha Mukherjee, Prof. Prasanta Kumar Dutta, Prof. Subir Paul, Prof. Pravash Chandra Chakraborti and Prof. Akshay Kumar Pramanick for their valuable suggestions and guidance. I also acknowledge the help rendered by Mr. Sudhir Ghosh, Mr. Subhasis Das, Mr. Bigneshwar Behra, Mr Jayanta Bhattacharya and Mr. Amitava Das during my execution of work. My special thanks to Dr. Chanchal Biswas, Dr. Bitan Kumar Sarkar, Amit Kumar Bhandary, Arnab Swarnakar, Sourav Adhikary and Pritha Pal for helping me throughout my project work, without them this thesis would not have been possible. I also deeply acknowledge the advice & support of Dr. Arghya Majumder, Director, School of Mining and Metallurgy, Kavi Nazrul University, Asansol.

I would also like to thank Dr. Anrin Bhattacharyya and Prof Johannes Schenk of Montanuniversität, Leoben, Austria for providing me the opportunity to work with them and pick their brain on occasions. I also thank all my friends and research scholars of Metallurgical & Material Engineering Department, Jadavpur University for providing me aspirations during my

work. I would like to take this opportunity to thank all my friends whose cooperative attitude helped me very much. I also like to acknowledge the cooperation of all the other faculty and staff members of the department during my project work.

I would also like to thank Mr Anirban Sur for providing me with the WDXRF results of the raw materials used for this thesis work. I would also like to thank Dr. Piyal Mondal, from IIT Guwahati my batch mate and friend from my undergraduate days of National Institute of Technology, Durgapur who helped me with XRD analysis for my thesis during the COVID-19 restrictions. I would also like to thank Mr. V.V.N. Harishchandra Prasad, Manager (QATD), Vizag Steel plant for helping me with the ICP-OES analysis for my thesis.

I would like to extend special thanks to Dr. Anrin Bhattacharyya and Dr. Bitan Kumar Sarkar. Other than my two supervisors these two seniors have helped me all along my PhD tenure giving me valuable suggestions and inputs any time I needed them. It has been a great experience and pleasure working with them.

Most importantly I would like to pay my indebted acknowledgement to my parents for providing me endless support and confidence during my thesis work. My father, mother and elder brother have always believed and supported my every decision. Their indefatigable faith in me has helped me throughout my life.

Finally, I gratefully acknowledge the funding sources i.e. West Bengal State Fellowship (2015-2019) and COE Project TEQIP-Phase III (2019-2020) that made my PhD work possible in India. I would also like to thank OeAD-GmbH for funding and facilitating my research work in Montanuniversität Leoben, during my brief stays in Leoben, Austria during 2017 and 2019.

Maharshi Ghosh Dastidar

List of Contents

List of Figures

List of Tables

Abstract

The impurities in raw materials pose many problems to the smooth operation of the iron making processes and have adverse effects on the final product. One amongst such impurities are the alkali elements (Na/K). Alkali elements enter the iron making processes mainly from the charge materials (Iron ore and Coke). The type of iron ore charge materials (lumps/ sinter/ pellets/ briquettes) also influences the alkali intake. The effects of alkali elements, present in iron ore charge and coke are different and have to be tackled accordingly. The adverse impacts of alkali content are decrement in mechanical strength of the charge materials, formation of low melting phase, alkali recirculation, process irregularities and refractory damage. The influence of alkali present in different charge materials has to be studied methodically to understand the adverse effects of alkali elements on the iron making processes. In this thesis, an attempt has been made to study the impact of alkali present in different forms of iron ore charge materials i.e. lump ore, sinters, pellets and briquettes, have on the reducibility of the ore under various alkali concentrations with varying time and temperature. Different iron ore charge materials have been tested under both direct reduction conditions as well as conditions replicating a blast furnace. Optimal alkali load that can be allowed to enter the furnace without causing too much of irregularities, has been found out with the help of statistical modelling via Box Behnken Design Modelling. The effect on the strength of the charge (where possible) has also been investigated to understand the contribution of alkali elements towards generation of fines. Similar type of experiments, have also been carried out for coke to understand the effect of alkali on coke along its catalytic effect on Boudouard reaction. Kinetic study of the reduction of different iron ore charge material under varied alkali loading and reduction conditions has also been done followed by characterization of the reduced samples. The kinetic study of bouduard reaction of coke under different alkali loading has also been carried out. The alkali effect on the activation energy of bouduard reaction has also been carried out. At last, an attempt has been made to find out some remedies to control the irregularities caused by the alkali intake; through alkali removal via smelting.

Chapter-1

Introduction

1.1 Background

The iron and steel sector is an important indicator of the socio-economic development of any country. Iron and steel provide the raw materials required for a wide range of different industries. Many different developed countries have declared the steel industry as sun down industry, whereas the developing countries rely a lot on iron and steel for development in different sectors. Iron and Steel gain importance as any country witnesses a shift to urbanisation and modernisation. There is a push in the construction sector, automobile sector, all of which require different grades of steel. In the recent years many countries have been concentrating on the growth of their own steel industry. The growth in steel production in different countries around the world over the last 50 years has been shown in Fig. 1.1. India also seen increase of steel production over the last few years. Steel produced in the world by different countries and India in the recent times have been shown in Fig. 1.2 and Fig. 1.3, respectively.

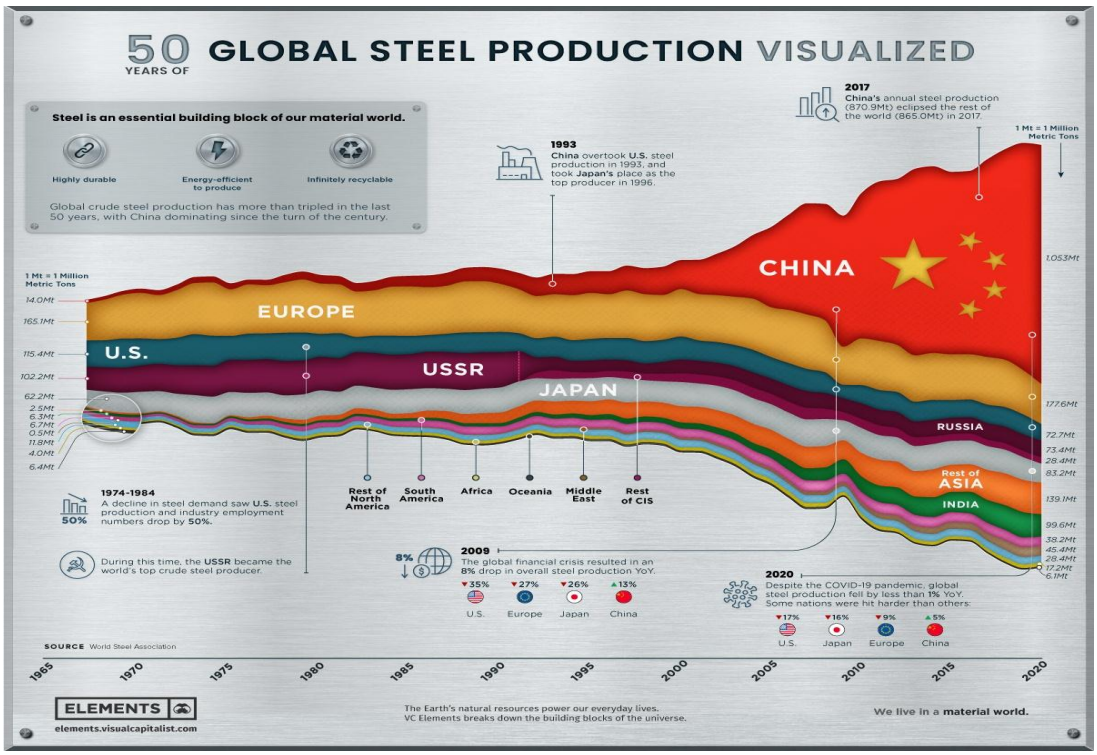

Fig. 1.1: Annual growth in steel production globally [1]

Top 10 steel-producing countries				
Rank	Country	2020 (Mt)	2019 (Mt)	%2020/2019
1	China	1053.0	1001.3	5.2
2	India	99.6	111.4	-10.6
3	Japan	83.2	99.3	-16.2
4	Russia (e)	73.4	71.6	2.6
5	United States	72.7	87.8	-17.2
6	South Korea	67.1	71.4	-6.0
7	Turkey	35.8	33.7	6.0
8	Germany	35.7	39.6	-10.0
9	Brazil	31.0	32.6	-4.9
10	Iran (e)	29.0	25.6	13.4

Fig. 1.2: Top ten steel producing countries in the world (million tonnes) [2]

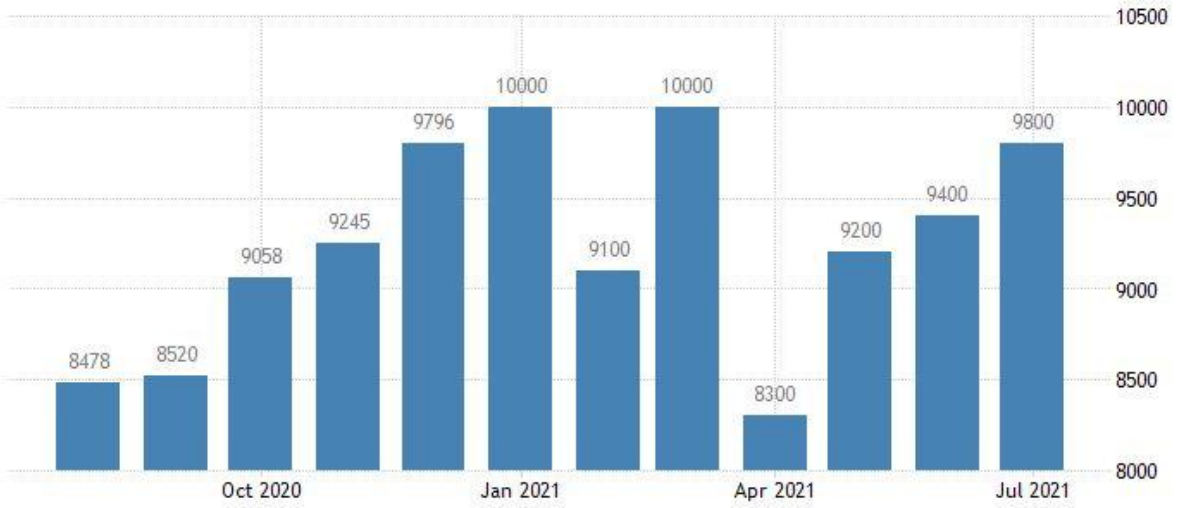

Fig. 1.3: Steel production in India (thousand tonnes) [3]

India itself overtook Japan as the second largest producer of steel in the world in the year 2018. The main problem with iron and steel industry is that the raw material reserves are limited. The demand for steel is increasing which is putting a pressure on the conservation of these resources. The most important thing for steelmaking are the raw materials: iron ore and

coke/coal (reductant). The first thing after gathering the raw materials is to produce iron from the iron ore i.e. Iron making process. There are two types of iron making processes: direct reduction and smelting (reduction followed by melting) process. In direct reduction the iron ore gets reduced in the solid state with the help of a reductant (solid or gas). In smelting processes, the iron ore is reduced followed by melting. All these processes are very much dependent on the composition of the raw materials. It is very important to carefully choose the raw materials for each process so as to produce iron of the required quality in an efficient way. After iron making the next step is to move onto the steel making processes. There are two types of commonly used steel making processes: pneumatic steel making - basic oxygen furnace (LD Converter) and slag transfer steel making- the electric arc furnace. Similar to iron making processes steel making process depends a lot on the quality of hot metal, DRI, scrap along with other raw materials and the process parameters. The quality of iron produced during iron making processes has a very big impact on the process parameters and efficiency of the following steel making process. So, it means that a better grade of iron ore gives a higher productivity for the entire plant as a whole. The quality of iron produced during iron making again depends on the iron ore charge materials (lumps, pellets, sinters and briquettes) quality. The unwanted materials present in the iron ore charge materials are known as gangue. The process parameters need to be set depending on the gangue materials. The gangue needs to be removed from the charge material during the iron making processes. The main gangue materials which need to be removed are sulphur, silica and phosphorous. The other gangue materials like alumina have different effects on the iron making processes. Alumina for example increases the viscosity of slag which is bad for the process. Apart from these there are some gangue materials which even present in lower quantities have a very adverse impact on the entire process. Alkali materials are one such gangue material which even in low percentages have very bad impact on the process as well as the furnace [4]. Alkali materials like sodium and potassium have the following effects on the iron making

processes: decrease in strength of raw materials, form cracks in the refractory, causing irregularities such as hanging and scaffoldings [5][6][7][8]. The main problem with alkali in raw materials is that it is very difficult to get rid of them since they recirculate in the blast furnace which is the most commonly used iron making route [8][9][10].

1.2 Steel Making: It can be carried out in two ways: Integrated steel Plant and Mini Steel plant. In an integrated steel plant, the raw materials are converted to iron which is then converted to steel using basic oxygen furnace or an electric arc furnace. The output of one shop is the input for the next shop. It consists of agglomeration units, iron making units, steel making units as well as the caster. In an integrated steel plant, we get the finished steel form the initial iron ore. In a mini steel plant steel is made from pig iron, DRI and scrap. They mainly consist of EAF or an Induction furnace for steel making.

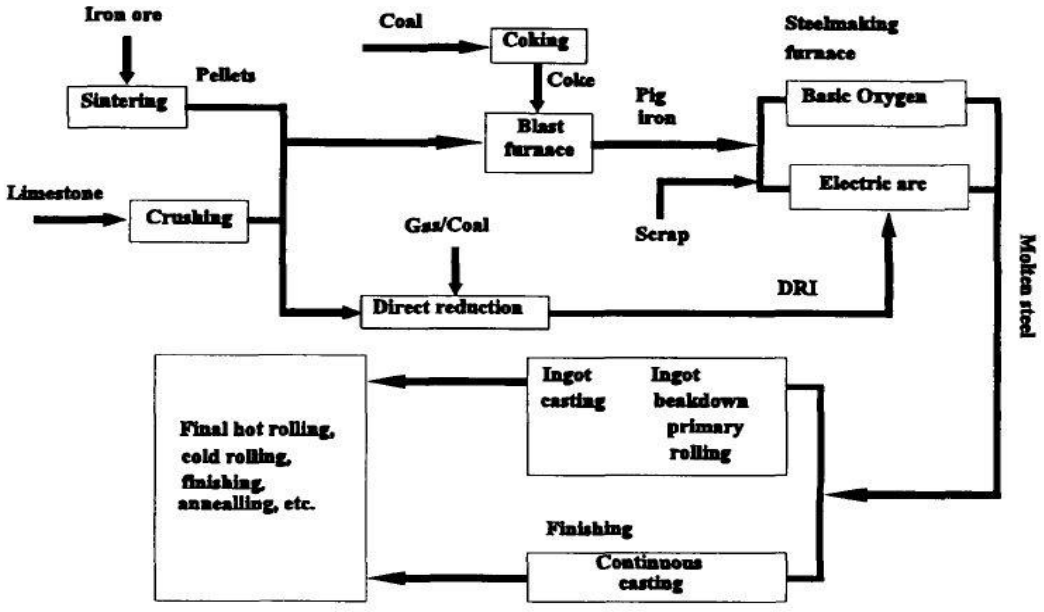

Fig. 1.4: Flow sheet of an integrated steel plant [11]

1.3 Iron Making: Iron making is the process of getting iron from its ore maintaining a specific composition. The iron making processes are classified in two types: smelting and direct reduction. The different iron making processes have been shown in Fig.1.5.

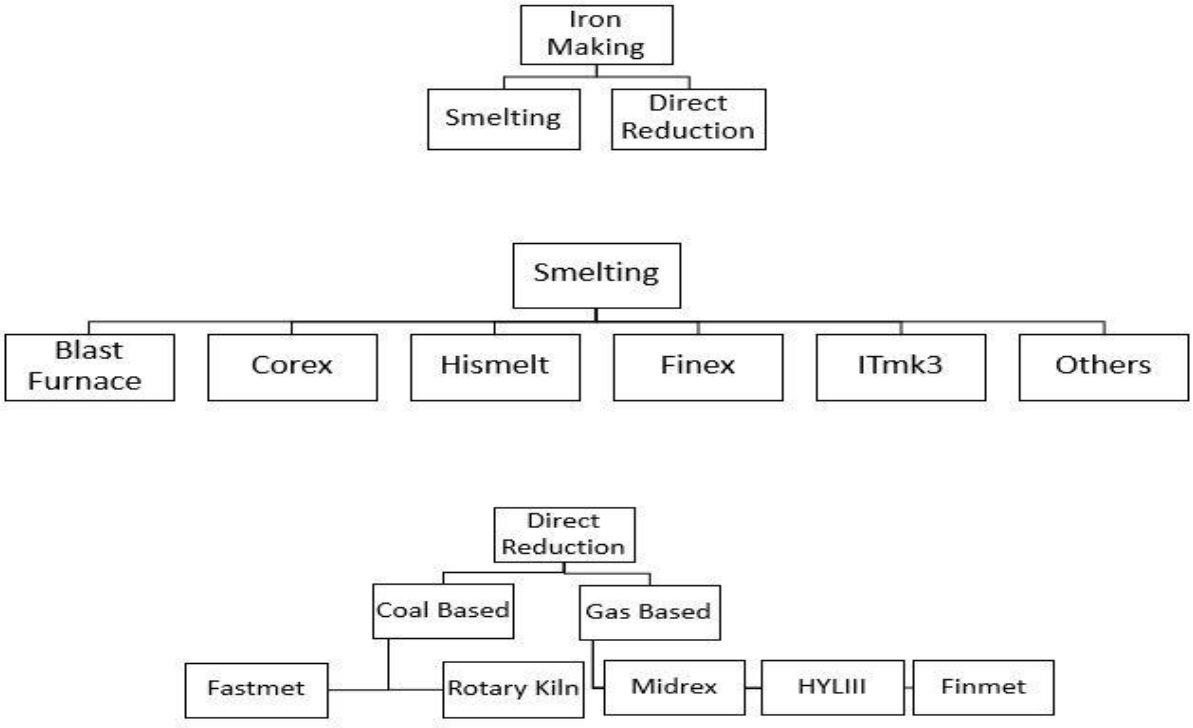

Fig. 1.5: The different iron making processes

1.3.1 Smelting

In smelting processes iron is made from iron ore using a reductant where reduction is followed by melting where the gangue phases are separated from the metal phase. Among all the smelting process for iron making the most widely used process is Blast Furnace. Other smelting processes include: Finex, Corex, Romelt, Hismelt, FASTMET, FASTMELT and Itmk3.

1.3.1.1 Overview of Blast Furnace

The blast furnace is the most popular of all iron making processes. The BF is a counter-current heat exchanger where hot gas ascends in the furnace giving heat to the descending raw materials while reducing iron oxides. The gas exits the furnace from the top where it has a temperature between 373K and 423K. The hot metal and slag are separated during tapping in the bottom of the furnace in a tapping channel which has a skimmer. The skimmer has a small opening underneath it where iron flows since it is denser than slag. Iron is tapped into torpedo cars and slag into ladles.

1.3.1.2 Temperature Profile in the Blast Furnace

The BF is divided mainly into three distinct temperature zones depending on the temperature and the physical state of the material. The temperature profile of the BF along with important reactions is shown in Fig. 1.6.

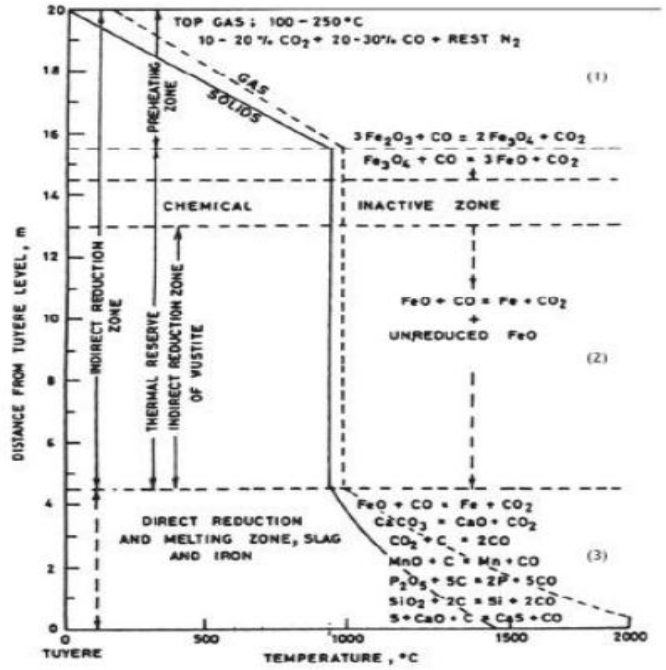

Fig. 1.6: Temperature profile of the blast furnace [8]

The other smelting and direct reduction processes are called the alternative iron making processes. Alternative iron making processes are not dependent on coke as the main source of reductant.

1.3.2 Direct Reduction

Iron produced from iron ore in solid form with the help of reductant (solid or gas) is known as direct reduced iron. In this process non coking coal is used as reductant for example in case of rotary kiln. Other direct reduced iron making processes break down natural gas into reformer gas and water vapour which help in the direct reduction process. The coal based iron making processes are SL/RN (rotary kiln) and FASTMET (rotary hearth furnace). The gas based iron making processes are: MIDREX, Finmet and HYL-III. The most commonly used coal based direct iron making process is the rotary kiln iron making processes whereas for gas based the MIDREX is the most widely used route. The main problem with direct reduced iron is that since there is no melting the gangue phase remains in the final product depending on their initial composition. The iron ore loses its oxygen in solid state giving it a sponge like appearance which is why it is often referred to as sponge iron. There are many problems with the transportation of sponge iron. Sponge iron is pyrophoric and coupled with its high surface area sponge iron cargo have been known to catch fire during shipping. It is therefore, formed into briquettes (hot briquetted iron) via hot briquetting to increase the bulk density and prevent any disaster during transportation.

1.4 Raw Materials for Iron Making Processes

The most important part to consider for any iron making process are the raw materials. The iron ore, the reductant and the flux are the main raw materials. The gangue present in the iron ore plays a very vital role in an iron making process.

1.4.1 Iron Ore: Iron ore that is charged into a furnace for iron making can be in many different forms. Different iron ores are hematite, magnetite, limonite, siderite, goethite, etc. Hematite is the most important iron ore followed by magnetite. Most commonly and oldest form of iron ore charge is the iron ore in the lump form.

The total reserves of haematite in India (2015) is estimated at 22,487 million tonnes of which 5,422 million tonnes (24%) are under 'Reserves' category and the balance 17,065 million tonnes (76%) are under 'Remaining Resources' category. By grades, Lumps constitute about 56% followed by Lumps with Fines (17%), Fines (16%), and the remaining 11% are black Iron ore, lump low & medium grade, beneficiable grade, Others, Unclassified, Not-known and Lump & fines & blue dust unclassified grade [12]. The total reserves/resources of magnetite in India (2015) are estimated at 10,789 million tonnes of which 'Reserves' constitute a mere 53 million tonnes and 10,736 million tonnes are placed under 'Remaining Resources'. The iron ore production of past 10 years is shown below. India produced 201426 and 206446 thousand tonnes of iron ore in 2017-18 and 2018-19, respectively.

The mining and crushing of iron ores generate a lot of fines which in earlier days have been wasted, but with time as the reserves of good quality iron ore started to decrease the focus shifted on the utilisation of the fines generated during mining and crushing of iron ores. The iron ore fines cannot be used in most of the iron making processes except for a few like Finex. The processes to use iron fines is known as agglomeration. The different agglomeration processes used for iron making processes are as follows:

Sintering: Sintering is an agglomeration technique where iron ore, iron ore return fines along with other plant wastes and coke have been agglomerated together into a size suitable for charging in a blast furnace. There are different heating zones for the dehydration of hydroxides and getting rid of the moisture. Air is introduced into the mix where the coke reacts with air generating the heat required for the fusion of the mix. The flame front

gradually moves down agglomerating the entire raw materials. The best sinter quality based upon the quality indices, amount of porosity along with amount of primary hematite along with amount of ferrites is reached during sintering at 1225–1275^{o}C [13].

Pelletizing: Pelletization is the agglomeration technique where iron ore fines below 150 micrometers are mixed with water and suitable binder and agglomerated into a ball. The mix put into a drum or disc pelletizer where it obtains its shape. The pellets lack the strength in this condition which is why the pellets are fired at around 1200-1400^{o}C. The fired pellets have the required mechanical strength to be fed into the blast furnace.

Briquetting: One of the easiest ways of agglomeration. A mixture of iron ore fines, water and a binder (molasses, bentonite, starch or tar pitch) is pressed into a compact with the help of a pressure using a die or vacuum stiff extrusion process.

Nodulizing: This is very similar to sintering no separate binder is required. The iron ore concentrate along with carbon is fed into a rotary kiln. Nodules are formed in the kiln due to rotating under high temperature. The mixture softens due to high temperature but not fuse it. The nodules have very high density lacking the porosity required for the iron making processes. This process is also very similar to briquetting, since iron ore wastes in steel plants can be used for nodulization [13].

1.4.2 Coal: Iron making processes require a fuel to act as a reductant. The blast furnace uses coke made from coking coal in a coke oven as a reductant whereas in direct reduction and other smelting reduction processes non coking coal is used as a reductant. There are various varieties of coal. Depending upon their composition and calorific values they are used in different sectors.

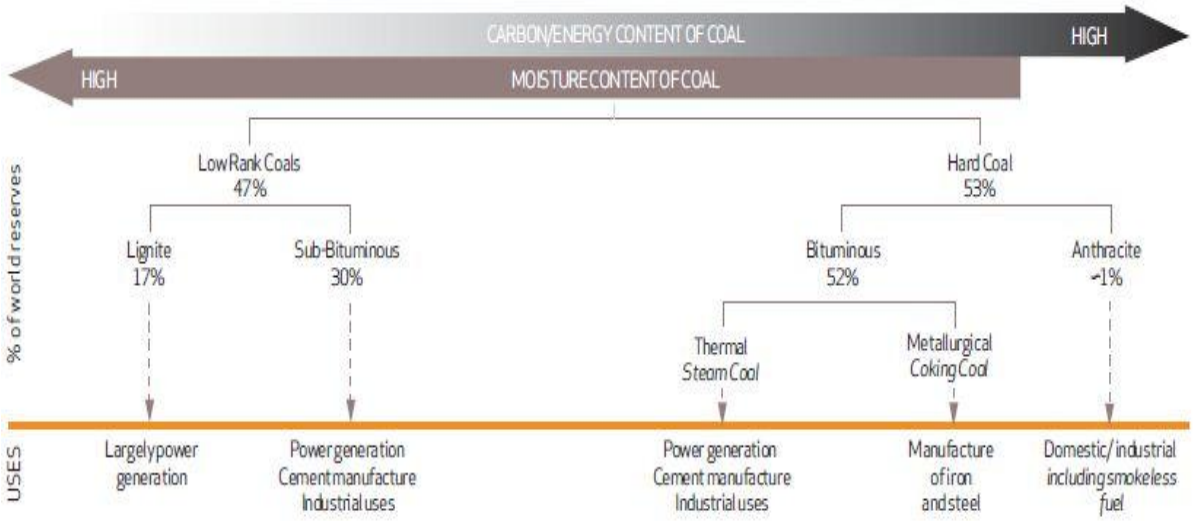

Fig.1.7: Different kinds of coal and their uses [14]

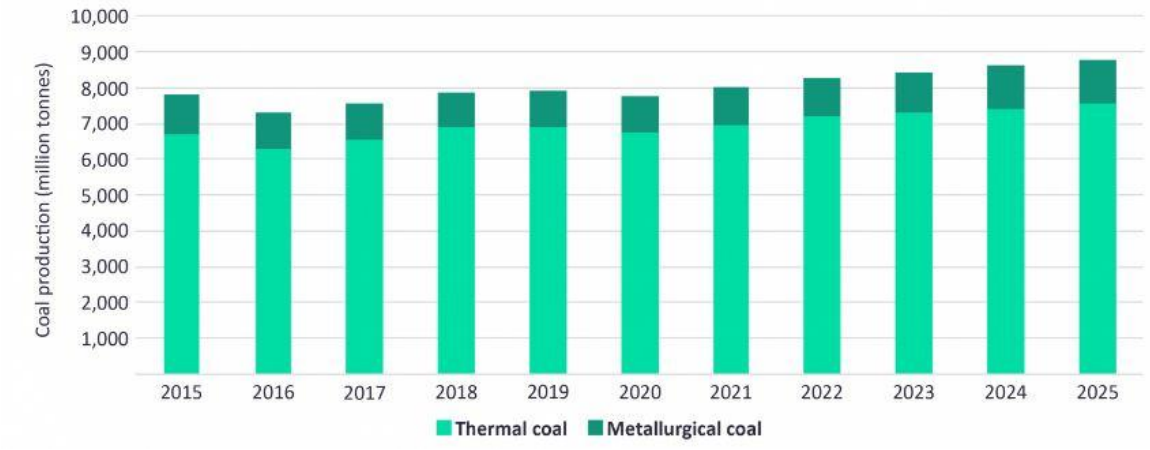

Fig. 1.8: Global coking coal production [15]

India has about 319.02 Billion tonnes of Geological Resources of Coal as estimated in the country as of 2018 [16]. The Type and Category-wise Coal resources of India as on 2018 are given in Table 1.1.

Type of Coal	Proved/Measured	Indicated	Inferred	Total
Grand Total	**148787**	**139164**	**31069**	**319020**
(A) Coking :-				
-Prime Coking	4649	664	0	5313
-Medium Coking	13914	11709	1879	27502
-Semi-Coking	519	995	193	1708
Sub-Total Coking	19082	13368	2073	34522
(B) Non-Coking :-	129112	125697	28102	282910
(C) Tertiary Coal :-	594	99	895	1588

Table 1.1: The coal reserves in India (million tonnes) [17].

It can be seen that the reserves of coking coal are very low compared to that of non-coking coal in India. The ash quantity of coal makes it very difficult to use these coals for making good quality coke. The high ash percentage in coke caused problems in removal of sulphur and silicon from hot metal in blast furnace. India is known to import a lot of coking coal from Australia to meet its demand in iron and steel sector. It is important to prioritise the use of iron making processes using non coking coal as the main source of fuel instead of coking coal.

1.5 Alkali Effect on the Iron Making Processes:

Among the gangue materials found in iron ore charge material one of the most detrimental are the alkaline elements. The alkaline elements mainly enter the iron making processes through the raw materials i.e. iron ore lumps, sinters, pellets and coke. The alkaline elements increase the reducibility of the iron ore charge materials but they also reduce the strength of the raw materials [18, 19]. Alkali cause swelling in iron ore charge materials and coke [20, 21]. Generation of fines takes place which in turn leads to decrease in permeability, leading to many irregularities like hanging, flooding and scaffolding inside the furnace [22]. These irregularities result in the inefficient performance of the furnace. Alkaline elements are also known to catalyse the bouduard reaction in the blast furnace [23, 24]. This leads to an increased coke rate and a decrease in productivity. The alkali elements also cause cracking of the refractory. They enter the refractory through the pores and form silicates which expand causing cracks [25]. In case of carbide bricks the alkali form alkali carbides leading to deterioration of the refractory. Inside the blast furnace the alkaline elements become vapours at higher temperatures and rise up and when they are in lower temperature regions they condense on the surface of the raw materials and come down with them to the lower parts of the furnace. They keep on re-circulating inside the furnace leading to an alkali build up inside the furnace. The removal of alkaline elements is difficult because of the recirculation [26]. Some of the sodium exits the furnace along with the slag whereas potassium being volatile exits along with the off gas. The other problem with the removal of alkaline elements from the blast furnace is that the conditions required for their removal contradicts that's for sulphur removal [27]. The main problem regarding alkali is that the alkali intake cannot be stopped completely. It becomes imperative to keep a check on the input and output of alkali of the reactor as the circulation & buildup of alkali adversely affect the iron production. In case the raw materials have high alkali content, the operator should adapt working on acidic slag for

some period of time to remove the alkali already in circulation in the furnace. There has been some work to understand the effect alkali elements have on the blast furnace process but not much work has been done to understand their effect on the direct reduction processes.

1.6 Scope of Research

Most of the work has been done on effect of alkali metals on blast furnace operations rather than the other iron making processes. It is very important to understand the effect alkali have, on the reduction properties of other iron making processes like direct reduction of iron. Since, in recent years the increase in price of scrap has led to DRI being used as replacement, this makes it imperative to study and understand the effect of alkali on the direct reduction processes of iron. Alkali effect on the reaction kinetics of iron ore reduction under different conditions and Bouduard reaction needs to be studied. Alkali effect on briquette reduction has not yet been studied as such. Alkali effect on the reduction kinetics and reaction mechanism of lumps and agglomerates like briquettes, pellets and sinters needs to be carried out under relevant conditions. Alkali effect on sinters with magnetite as the major phase is still a grey area. The removal of alkali from metal via slag transfer without hampering the final composition of hot metal also needs to be studied.

Most of the work done till now is all qualitative work. In this thesis quantitative analysis of the content of alkali and its effect on various processes and their raw materials has been studied. The effect of alkali on the direct reduction of iron and as well as in blast furnace conditions has been carried out. The effect of alkali on the reduction kinetics and reaction mechanisms of different iron ore charge materials in different iron making conditions has been studied. Statistical modelling has also been used to optimise the alkali intake for direct reduction processes depending on the response i.e. extent of reduction. The effect of alkali on the strength and reactivity of coke along with its effect on the activation energy of Bouduard

reaction has been evaluated. An attempt has been made to remove alkali from metal via slag through smelting.

1.7 Delimitation of Research:

The alkali effect on the modern iron making processes (eg. Finex, Corex, iTMK3 etc.) have not been carried out. Magnetite lumps and pellets have not been considered for this work. Alkali effect on refractory has not been studied. Alkali effect on strength of raw materials has been evaluated only for the cases where it is possible. A lot of work has been done previously on the morphological and structural changes brought about by alkali in the raw materials. We have mainly concentrated on making a quantitative analysis of alkali content and its effect on kinetics of different reactions taking place during iron making processes.

1.8 Reference:

1. https://elements.visualcapitalist.com/50-years-of-global-steel-production.
2. https://www.worldsteel.org/media-centre/press-releases/2021/Global-crude-steel-output-decreases-by-0.9--in-2020.html.
3. https://tradingeconomics.com/india/steel-production
4. Kurunov IF, Titov VN, Emel'yanov VL. et al. Analysis of the behavior of alkalis in a blast furnace. Metallurgist. (2009);53(9):533–542.
5. Gridasov VP, Logachev, GN, Pishnograev SN, et al. Behavior of Alkalis in Blast Furnaces. Metallurgist. 2016; 59(9):761–765.
6. Davies J, Moon JJ, Raice FB. Alkalis in Blast Furnace Iron making and steel making. 1978:151–161.
7. Rankin WJ, SEE JB. The alkali problem in blast furnace Mineral Science Engineering. 1977; 9(2):68–82
8. A. K. Biswas, Principles of Blast Furnace Ironmaking, SBA Publications, Calcutta, 1984, pp. 8.
9. Yusfin YS, Chernousov PI, Garten V. et al. The role of alkalis and conserving resources in blast-furnace smelting. Metallurgist. 1999; 43(2):54–58.
10. Kejiang Li, Rita Khanna, Jianliang Zhang, et al. 'The evolution of structural order, microstructure and mineral matter of metallurgical coke in a blast furnace: A review'. Fuel. 2014; 133:194–215.
11. Zervas, T., McMullan, J.T. and Williams, B.C. (1996), Direct smelting and alternative processes for the production of iron and steel. Int. J. Energy Res., 20: 1103-1128.
12. Indian Mineral Year Book 2017 (Part III- Minerals Review), 56th Edition Iron Ore, Indian Bureau of Mines 28-2 – 28-3.

13. Iron Ore Agglomeration Technologies, Daniel Fernández-González, Juan Piñuela-Noval and Luis Felipe Verdeja, Intech Open, 2018, 62-66.
14. Coal & Steel Report, World Coal Institute, 2007, pp 7.
15. https://www.globaldata.com/global-coal-production-expected-rise-3-5-2021-says-globaldata.
16. Indian Mineral Year Book 2018 (Part III- Minerals Review), 57th Edition Coal and Lignite, 28-2 – 28-3.
17. https://www.coal.nic.in/content/coal-reserves.
18. Iljana, Mikko & Mattila, Olli & Alatarvas, Tuomas & Kurikkala, Jari & Paananen, Timo & Fabritius, Timo. (2013). Effect of Circulating Elements on the Dynamic Reduction Swelling Behaviour of Olivine and Acid Iron Ore Pellets under Simulated Blast Furnace Shaft Conditions. ISIJ International. 53. 419-426.
19. Pichler, A., Schenk, J., Hanel, M., Mali, H., Thaler, C., Hauzenberger, F., & Stocker, H. (2014). Influence of alkalis on mechanical properties of lumpy iron carriers during reduction. In Conference Proceedings to the 23rd International Conference on Metallurgy and Materials (pp. 40-40).
20. Song, Wei, Luo, Guo-Ping, Sun, Chen-Chen, Zhang, Jing and Zhu, Jian-Guo. "Effect of K and Na on reduction swelling performance of oxidized roasted briquettes" High Temperature Materials and Processes, vol. 40, no. 1, 2021, pp. 241-252.
21. Hiroshi Haraguchi, Tetsu Nishi, Yoshiaki Miura, Miyoshi Ushikubo, Tamio Noda, Some Aspects of Deterioration of Coke in Blast Furnace, Transactions of the Iron and Steel Institute of Japan, 1985, Volume 25, Issue 3, Pages 190-197.
22. Narita K. Effects of alkalis and Zinc on the wear of blast furnace refractories and tuyere displacement. Transactions ISIJ. 1981;21(12):839–845.

23. Zeng ZH, Zou C, She Y, Yang J, Ma C, He JY. Effects of alkali metal enrichment on structure and gasification reactivity of blast furnace tuyere coke. Journal of Iron and Steel Research. 2020; 32(6):452–461.
24. Lv QQ, Tian YS, Du P, Zhou JL, Wang GH. A study on the characteristics of coke in the hearth of a super large blast furnace. PLoS One. 2021; 16(3):e0247051.
25. Silva NS. Wear mechanism for blast furnace hearth refractory lining. Iron making and Steel making. 2005; 32:459–467.
26. Evgueni Jak, Peter Hayes; The Use of Thermodynamic Modelling to Examine Alkali Recirculation in the Iron Blast Furnace; High Temp. Mater. Proc. 2012; 31(4-5):657–665.
27. Kurunov FI. Analysis of the behavior of alkalis in the blast furnace. Metallurgist. 2009; 53:9–10.

Chapter-2

Literature Review

2.1 Introduction

The blast-furnace operator's main objective is, maximum production of pig iron of the required chemical composition at lowest cost. This can be achieved on the basis of quality of raw materials and by ensuring trouble free operation of blast-furnace. Both parameters are influenced by the presence of undesirable elements. The unwanted elements of the blast-furnace raw materials cause many technical problems in the sintering process as well as in the blast-furnace iron making [1]. It is widely known that alkali metals like potassium and sodium cause operational problems in the iron blast furnace [2, 3]. Alkalis get introduced in the furnace mainly via the raw materials, in different forms such as silicates, oxides, carbonates or halides as a part of the gangue in the iron ore charge and coke [4]. These alkali elements entering the furnace leave the blast furnace by mixing with slag and with the suspended fines in the top gas, except those absorbed by the refractories. Alkalis are known to cycle and accumulate in the blast furnace. The impact of alkalis on blast furnace operation has been a major concern to the iron making industry. Under certain conditions, the alkali materials, even in relatively low concentration in the burden, can rapidly accumulate in the furnace.

There are many ways in which alkalis affect the furnace production some of them are given below which have been discussed in detail in the later segment of this chapter [5].

I. Alkali present in the iron ore charge material diminishes their resistance to degradation, cause swelling and loss in strength of iron ore lumps, as well as pellets and sinters.

II. Alkali are responsible for scaffold formation in the furnace. The presence of which reduces its working volume and thus increasing the gas velocity and in turn the tendency to fluidization and channeling. Now some times scaffolds break away from the furnace walls, leading to chilled hearth. The wind rate reduces and hence the productivity of the furnace decreases.

III. The presence of alkalis even increases the coke consumption which increases the coke rate leading to decrease in the productivity of the furnace and also decreases the coke strength [6], which is crucial for gas permeability [7].

IV. The physical and chemical properties of slag are adversely influenced which gives rise to an earlier onset of hanging.

V. Alkalis attack the refractory lining in the furnace this necessitates more frequent relining during which the production is stopped [8].

The input of alkali should be monitored properly as the best way to avoid alkali circulation. In cases where the ore has higher alkali content many different methods can be employed to remove alkali. Most of the alkali is removed through slag and the rest fly off with the off gasses while the remaining alkali circulate in the furnace [9]. The conditions that facilitate alkali removal through slag cause other serious problems like the composition of the hot metal its sulphur, silicon and manganese content are altered [7, 10]. Many works have been done for the removal of alkali keeping the hot metals final composition intact like for example addition of quartzite, olivine, dunite and calcium chloride [4, 11, 12]. These facilitate the transfer of alkali to slag keeping the basicity in check. The alkali intake of a furnace should thus be kept in check in order to avoid the various problems of alkali circulation.

Alkali metals have different effects on some other iron making processes and other parts of an Integrated steel plant. Stjernberg and Ion C. have reported that alkali metals have deteriorating effect on the refractory of the rotary kiln for iron ore pellet production [13]. It has been proposed that potassium vapors penetrate the refractory bricks through voids and brick joints and get entrapped. This potassium reacts with entrapped liquids and condenses for diffusion through the bulk. On reacting with the refractory material secondary mullites form around the primary mullite, this mechanism has been considered responsible for the degradation of the refractory lining. Das et. al. have reported that the flue dust from sinter

plants have many value added products but there use is a problem because of presence of alkali [14]. The alkali have been removed with help of scrubbing and washing still alkali remain present.

2.2 Alkali Effect on Blast Furnace

Among all the iron making processes the blast furnace is the dominant process all over the world. The study of effect of alkali has been mainly studied in blast furnace conditions. It is reported that alkali enter blast furnace mainly through the raw materials. The problem mainly occurs because of their circulation of alkali in the blast furnace which leads to their accumulation in the blast furnace. The alkali have effect on the iron ore charge as well as the coke which in turn effects the entire operation and its efficiency.

2.3 Alkali Circulation in the Blast Furnace

The important facts about alkali circulation in the blast furnace:

A. The alkali movement in the blast furnace can be represented with the help of two loops: first as vapors/ cyanides/ carbonates or fine droplets with the ascending gases; second is their downward movement as condensed phases on charge materials [4].
B. In the lower parts of the furnace although the blast is free from alkali, the high temperature and reducing power of the gases turn the condensed phases of alkali into vapors.
C. Many alkali compounds are formed as the alkalis travel through the blast furnace.
D. The charge materials have higher oxygen potential than in the bulk gas stream. At the iron oxide and gas interface the wustite would oxidize the various alkali compounds to form oxides. Due to interaction of alkalis, iron oxide, the reducing gases and silica in the gangue complex alkali silicates are formed. Under the blast furnace condition alkali silicates have high stability [15]. These alkali silicates need to be transported to lower regions with higher temperature and reducing power for their reduction.
E. The phase diagrams of silica ferrous oxide along with alkali oxides indicate that the melting point of iron silicate gangue and viscosity of slags is reduced drastically because of the

presence of alkalis [16, 17].

It can be concluded that alkali content in the raw material is not an accurate measure of alkali content in the furnace as the alkali accumulate in the furnace, iron oxides and gangue phases containing silica form low melting phases with alkali. Fig. 2.1 illustrates the circulation of potassium in the blast furnace. The favorable conditions for the reduction of alkali oxides, halides or silicates to metallic state can be found in the bosh and hearth zones. In the high temperature zone alkali silicates can be reduced by carbon, as in Ellingham diagram. The alkali silicates are reduced by carbon to alkali vapors. Alkali silicates can also be reduced by freshly reduced iron into alkali vapor in high temperature zones. The extents to which these reactions occur are dependent upon the partial pressure of carbon monoxide and temperature [18]. Alkali vapors being produced by the reactions mentioned below, are carried upwards along the rapidly moving gas stream [19]. Alkali oxides can be reduced either by solid carbon or gaseous carbon monoxide whereas alkali carbonates cannot be reduced by carbon in the blast furnace at lower temperatures. But at lower temperatures the alkali oxides are reduced by carbon monoxide.

At some point the temperature in the furnace becomes so high, that the alkali oxide is displaced by lime from the complex silicates along which it enters the furnace. Alkali cyanides are formed as this alkali oxide reacts with carbon and nitrogen, which, at the temperatures involved, must be entirely in the vapor phase. Cyanides are then converted either to silicates or carbonates after reacting with carbon monoxide and carbon dioxide, which then get deposited on the charge material coming down to the region where the cyanides form. Alkali silicates are the most stable alkali compounds under the blast furnace conditions. Alkali carbonates are stable till 1400°C then liquid cyanide becomes more stable than liquid carbonates.

All the reactions mentioned above are given here (A stands for Potassium, K or Sodium, Na):

$$2A_2SiO_3 + 2C = 2A(g) + 2SiO_2 + 2CO \text{ (1823K for Na and 1923 K for K)}$$

$$2A_2SiO_3 + 6C = 4A(g) + 2Si + 6CO \text{ (1823K for Na and 1923 K for K)}$$

$$A_2CO_3 + CO = 2A + 2CO_2 \text{ (Above 1473K)}$$

$$2ACN + 4CO = A_2CO_3 + 5CO + N_2 \text{ (At 1373K)}$$

A certain portion of alkali goes through into the slag and another portion escapes with the top gases. Some of the alkali enters the refractory whereas some of the alkali which have not been removed with the slag accumulate in the above fashion in the furnace.

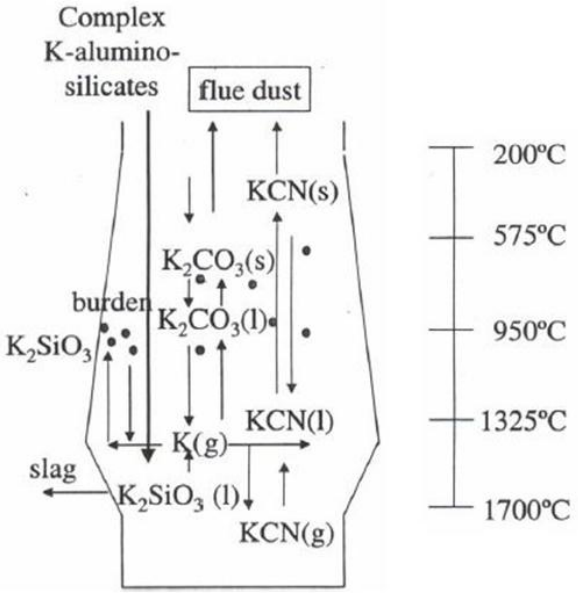

Fig. 2.1: Potassium circulations in the blast furnace [18]

2.4 Alkali Effect on Iron Ore Charge Materials in Blast Furnace

Alkali metals entering the blast furnace along with the raw materials pose many problems to their mechanical strength. The alkalis keep on circulating in the furnace. The alkali vapors rising from below condense on the surface of lump, sinter and pellets leading to a decrease in mechanical strength leading to their fracture hence, deterioration in the gas permeability of the stock [20, 21]. Pellet disintegration occurs particularly rapidly under the influence of alkalis. Anton has reported in his work the effect alkali have on degradation of charge and

generation of fines which has been determined by reduction and mechanical tests [22]. They found coarser metallic iron nuclei under the microscope, which have been observed in soaked materials as opposed to in untreated ones. In work done earlier it has been seen that alkali chlorides have a catalytic effect on the reduction of hematite to iron all the stages [23]. It has been seen that although the reduction of hematite to magnetite is accelerated but in case of magnetite to wustite the rate of reduction is lower than in case of hematite. It has been stated that due to reduction from hematite to magnetite that magnetite structure would have more pores compared to magnetite in first stage of reduction. The pore morphology did not change although the volume increase gave rise to greater surface area for contact with the reducing gases. In one of the works it has been seen that doping with potassium affected only the surface of the charge materials it has been seen that potassium increased the reduction rate of wustite [24]. It has also been found to be responsible for the growth and nucleation of iron. When potassium has been added to partly reduced wustite it increases the transfer of reactants by making it much more permeable to gases. In another work it has been found that the addition of alkali oxide has a significant effect on the reduction of wustite [25]. The reduction rate decreased with increasing the alkali percent. The oxygen removal from doped wustite samples has been higher than pure wustite due to faster whisker formation, this leads to the formation of a porous structure which in turn facilitates the access of the reducing gas. It has been observed that swelling and compact disintegration took place clearly by decreasing the alkali content to give the maximum value with pure and less doped sample, this is attributed to the active whisker formation at higher reduction temperatures in pure wustite samples compared to doped samples.

2.4.1 Alkali Effect on Pellets

Alkali metals enter the blast furnace along with the raw materials and circulate in the furnace. In the lower portions of the furnace the alkali vapors come up with the ascending gases and in the lower temperature zones they condense on the pellets surface and move down along with them. Alkali metals have been reported to have bad effect on the reduction rate of pellets [22]. It has been seen that the rate of reduction increases with alkali which can be due to the loss in strength of the pellets leading to cracking which enhances the mass transfer of reducing gases between the iron oxide grains. Many mechanisms have been proposed for the decrease in strength of the pellets due to alkali. Both acid as well as olivine pellets have been tested to study the effect of alkali on the pellets. The alkali present on the charge reacts to form alkali iron silicates which have very low liquidus temperature [26]. The alkali silicates for the case of acid pellets form bridges between the iron oxide grains which help to release stress during transformation thus giving a better protection from degradation and swelling than basic pellets [27]. In one of the earlier studies the alkali oxides effect on the reduction swelling behavior of hematite has been investigated. Abnormal swelling has been reported when synthetic Fe_2O_3 crystals reacted with alkali oxides. According to the study, the addition of alkali has the following effects on the swelling behavior of Fe_2O_3 crystals. In the initial stages, stress induced by the migration of Na_2O and K_2O inwards the crystal lead to fine cracks in the crystal due to formation of the alkali metal carbonates during the reduction. Then, a remarkable growth of the fibrous iron occurs inside the crack. The growth is enhanced due to the lattice defects which are introduced by the presence of alkali metal ions in hematite crystals. Fig. 2.2 illustrates the average reduction swelling indices of pellet sample as a function of the average degree of reduction under certain reducing conditions. The figure indicates that sulphur in reducing atmosphere leads to pellet volume decrease, but in case of large amounts of potassium the volume increase is found to be 10.5% at the most [27].

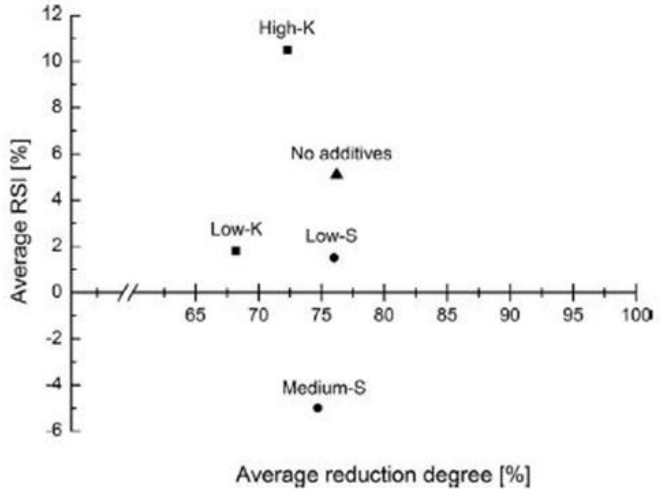

Fig. 2.2: Average reduction swelling indices as a function of the average degree of reduction under certain reducing conditions [27]

2.4.2 Alkali Effect on Sinter

Alkali metals reduce the resistance to cracking of sinters. In a chloride environment, the deposition of chlorides on the sinter surface reduces the surface area in contact with the reducing gases leading to decrease in reduction. Pure alkali atmosphere facilitates the reduction of hematite to magnetite at much lower temperatures leading to development of stresses in the sinter structure finally leading to cracking responsible for disintegration [28]. In case of pure Cl atmosphere, due to the inhibiting nature the degradation is avoided in the earlier stages of reduction. Alkali atmosphere increases the reduction kinetics at lower temperatures. The effect of alkali on the strength and reduction of sinters is shown in figures below. P Besta et al. found that most of the alkali carbonates enter the furnace through the sinter mixture and coke. He even reported that the alkali removal depended a lot on the basicicty, FeS, and chlorides present. Increase in basicity of the sinter leads to decrease in the alkali content of sinter whereas sulphides inhibit the alkali transfer into the gas phase. The presence of chlorides supports the removal of alkali from the furnace [29]. Fig. 2.3 & Fig. 2.4 represent the alkali effect on the abrasion of sinter and on the reduction of sinters respectively.

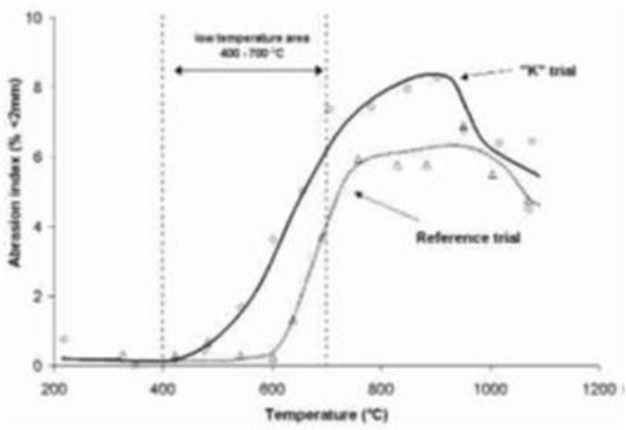

Fig. 2.3: Abrasion curve of sinter in alkali atmosphere [28].

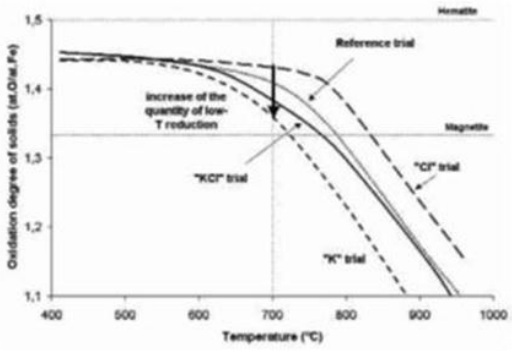

Fig. 2.4: Reduction curves of sinter for the 4 types of trials [28].

2.4.3 Alkali effect on Metallurgical Coke

Coke is used as reductant in the blast furnace process. Coke being the fuel determines the productivity of the furnace. The coke strength, the mineral matter, reactions during its descent, determine how well the process commences. Alkali metals have been known to have a detrimental effect of the blast furnace cokes strength, which generates fines leading to a lower permeability in the coke bed decreasing the productivity. Alkali are also known for their catalytic action on the gasification reaction along with their tendency to form intercalation compounds [19]. This leads to both chemical and mechanical weakening of the

coke structure. The penetration into the coke results in differential volume expansion of the lattice. Crack formation takes place in the structure to relieve the stresses leading to higher contact area for high temperature reactions. The different effects due to alkali presence in coke are: intercalation with coke, swelling and buildup of stresses leading to degradation. The effect of alkali on coke strength is uncertain as certain reports suggest the lead to abrasion of the alkali rich layer of coke whereas on the other hand another report suggests that alkali up to 5% does not have any adverse effect on the coke strength [30, 31]. High ash content of coke leads to higher alkali input leading to liquid phase formation and volume expansion causing cracks. But it has also been reported that the alkali effect as catalyst on Boudouard reaction has been the main factor in the process of coke degradation [32]. The loss of strength of coke is high if the alkali is present at high temperatures even in the absence of carbon monoxide gas. In one of the works it has been shown that both sodium and potassium have a huge effect on the CSR and CRI of the coke. The coke consumption increases due to the high alkali rate leading to irregularities and instability. The ionic radius of alkali is higher than carbon, this causes pronounced lattice disturbance at high temperature due to diffusion of alkali into the graphite crystal system [33]. In cokes with lower CRI the catalytic effect of alkali is higher when compared to cokes with higher CRI. The gasification of coke is accelerated with addition of alkali, the activation energy also gets reduced but the effect is not seen at higher temperatures [34, 35]. The alkali concentration has been observed to increase as the coke descended through the furnace [36].

The reactivity of coke with oxidizing gases depends on the structure of the coke material and hence in turn influences the coke behavior in the blast furnace. Various components of optical texture of coke affect its performance. S. Gupta has reported that the reactive maceral derived components have been less reactive than the inert maceral derived components at high temperatures [37]. Metallurgical coke has a microstructure which is composed of anisotropic carbon in the form of mosaics together with flow-type anisotropy as well as isotropic carbon.

The fluidity of the carbonization system which determines the size and shape of the resultant anisotropy primarily depend on the physical and chemical properties of the coal. The interlocked and randomly orientated units of the mosaics sow higher resistance to crack propagation and fracture than the isotropic carbon or the flow-type anisotropic carbon. Anisotropic carbon is more resistant to gasification than isotropic carbon and this factor is important for the discussion of Boudouard reaction in the blast furnace. On gasification the mosaic units of anisotropic carbon, do not develop the fissures which occur in the flow-type anisotropy, resulting in better strength. The mosaics, a major part of the optical texture of metallurgical cokes, are more resistant to alkali attack than the flow-type anisotropy. The isotropic carbon is probably much more resistant [38]. Co-carbonization has been used to produce cokes with suitable optical textures. The isotropic carbon has higher reactivity with CO2 which can be explained with the help of surface area and intrinsic reactivity. Isotropic carbon has been reported to have a higher chemical reactivity, [39] and surface area for unit weight compared to anisotropic carbon [40]. The isotropic carbon has lower bulk density compared to anisotropic carbon [40]. Metallurgical cokes microstructure contains many disordered carbon units along with complex mixture of alumino-silicates. During the descent of the coke morphological changes take place by formation of ordered carbon layer planes and intercalated species. It has been reported that the circulation of alkali in the furnace are responsible for the morphological changes in the structure of coke mentioned above [41].

The alkali content of coke shows a similar trend in the different locations of the furnace although their concentration and distribution fluctuated in the radial direction. It has been reported that the alkali concentration increases in the coke as it descended through the blast furnace, and are evenly distributed throughout the coke matrix [42]. In the upper zone of the furnace the reactivity of CO_2 with coke is much less compared to the lower zone coke owing to the increased alkali concentration. Due to the adsorption of the circulating alkali in the furnace the alkali level in the tuyere zone is quite high. The coke in the dead man zone has

been found to have the largest interlayer spacing and small crystallite dimensions. Alkali have not been observed in raceway cokes whereas highest alkali concentration has been observed in the deadman coke. The average number of lattice layers is quite large for deadman coke leading to interaction with alkali through diffusion or adsorption rather than intercalation [43]. The potassium content of deadman cokes has been more than fifteen times of that present in the feed coke. The coke in the tuyere level contains graphite crystals. The formation of graphite crystals on the coke surface decreases the reactivity in turn allowing the coke pieces to slide over each other affecting the mechanical stability of coke [44]. Deformation of graphite crystals can be attributed to the vaporization of intercalate present in graphite. This causes dismembering of the crystals into sheets. This leads to generation of fines contributing to higher blast furnace dust. The amount of potassium intake by cokes at the tuyere level is also found to be inversely proportional to the temperature of the tuyere zone as well as to the degree of coke graphitization. The principal forms in which potassium exists have been identified as potassium enriched silicates, aluminosilicates, bonded to carbon and distributed throughout the carbonized minerals. Silicates and aluminosilicates act as alkali receptors yet half of the potassium has been reported to be bonded to the carbonized minerals [45]. It has been seen that the alkali increased as the coke descended the furnace but the potassium content on the surface and core have not been different indicating full penetration of potassium into the coke, results have indicated intergranular diffusion of potassium through the coke matrix [46]. Coke with higher alkali content is carburized slower. Additional alkali load from injection of waste and recycling materials in the blast furnace is not all bad from the viewpoint of coke consumption. Coke preferentially reacts at its surface. The ash from injected materials forms many small globules on the coke surface, protecting the coke from degradation [47]. The catalytic effect of formed iron coke can be used to bring down the thermal reserve zone where the reactivity of coke is enhanced by the presence of condensed alkali vapors [48].

2.4.3.1 Catalytic Influence of Alkali on Coke Reactivity

Many research works have been done over the years proposing different mechanisms of catalysis of the gasification reaction. Work has been done not only on coke but also on char [49]. In test of coke doped with alkali, the catalytic effect of different alkali has been found to be in the order of: Li<Na<K [50]. Alkali metals reduce the activation energy of the gasification reaction; with the addition of alkali the catalyst sites are increased. Alkali carbonates have been tested to find out the catalytic effect on coke. Effect of sodium and potassium carbonates has been studied separately. It has been seen that potassium carbonate has higher catalytic effect than sodium carbonate. The vapour cycle mechanism is the reason for the catalytic effect. The reduced carbonates again get converted back to carbonates as soon as they come in contact with CO [51].

It has been reported that for the gasification reactions to take place it is necessary that the alkali carbonates be reduced as to provide the area for the reaction to take place [52]. It has been seen that during high alkali loading the alkali would act as the extra reactant on the other hand the carbon acts the limiting surface area, a carbon monoxide concentration profile with time has been observed. It has been also reported that the interior of coke structure has lower content of alkali and carbon dioxide due to which the reactions have not been so severe in the center although the alkali reaches the interior of coke structure [53]. It has been reported that potassium is the main variable in determining the rate of reaction of gasification reaction in ferromanganese production [54]. The different mechanisms of catalysis of gasification of carbon have been reviewed by Mackee [55]. It has been reported that the catalytic effect on gasification of carbon could be best understood by sequence of cyclic redox process. In this mechanism the alkali salts react with carbon substrate and are again reoxidised in oxidizing atmosphere. It has been also reported that alkali intermediates might react with the substrate to form intercalation compounds. In one of the experiments it has been found that K_2CO_3 has the most pronounced effect on the coke oxidation and it has also been seen that it catalyzed

specifically the less ordered crystal structure [56].

2.5 Alkali Effect on Refractory Lining of Blast Furnace

The refractory lining in the blast furnace, from the shaft to the hearth is affected by alkali metals. The different zones of the furnace have different refractory bricks and the alkali attack is also different owing to the different temperature in the different zones. It has been observed that in the region between shaft and bosh, and the hearth region the wear resistance of the lining is poor. The life of the refractory lining is affected primarily by thermal shock. Unwanted materials like alkali and zinc coming down the furnace along with the charge material have deteriorating effect on the lining life. The deteriorating effect of alkalis on the wear resistance properties of the refractory lining changes with the composition and type. In this portion the deteriorating effect of alkali on different refractory bricks used in the blast furnace has been discussed. Among the alkali circulating inside the furnace, potassium mainly affects the refractories since sodium gets removed along with slag. $A120_3$-$Si0_2$ bricks are commonly used in the blast furnace; alkali oxides react with these at temperatures above 700^{o}C. The product of alkali oxides with alumina silicates depends a lot on the temperature and the alumina composition of the bricks. The reaction products lead to expansion in volume and hence formation of cracks [57].

Primarily carbon based and silicon carbide bricks are used in the lower part of the shaft and the bosh region. These bricks do not show any significant increase in volume upon interaction with alkalis. This can be credited to the amorphous structure of carbon which is resistant to the formation of intercalation compounds. On the other hand, refractory in the lower parts of the furnace are highly affected by alkali attack. In between the lower part of the stack to the bosh the refractories have been observed to completely wear off, whereas for bosh to the tuyere zone the effect on the refractory linings are almost similar. The refractory in the vicinity of shaft to tuyere where penetrated by foreign elements. It has been observed that potassium is present in these refractory in the form of kalsilite. The wear of fireclay bricks is

mainly due to kalisilite and its corresponding volume expansion [58]. It has also been reported that alkali upon reaction with glass even form liquid phase other than alumino silicates which might lead to wear of the refractory [59].

Study has also been carried out to understand the effect of alkali on carbon refractories. To prolong the life of blast furnace carbon refractories in the high temperature zones it is necessary to know the effect of alkalis on their wear resistance properties. The alkali penetrates the carbon bricks through pores and cracks and takes part in reactions that accompany cracking and swelling of the refractory. Refractories with higher number of pores and cracks are less resistant to alkali attack. Inside the refractory $KAlSiO_4$ is the main phase. The formation of $KAlSiO_4$ is accompanied with volume expansion. Most of the carbon refractories of blast furnace in china are made of calcined anthracite as the main constituent. The effect depends a lot on the micro porous structure of the calcined anthracites [60]. In case of refractories with calcined anthracite as main constituent the micro porous structure is hampered leading to higher alkali attack. The presence of β-SiC helps in determining the micro porous structure of the refractory, and is much more resistant to alkali attack as compared to SiO_2.

The amount of alkali oxides affecting the refractory is different in different regions of the furnace i.e. in the upper stack only 5-10% K_2O whereas at higher temperature 20-30% of K_2O [61]. Alkali peeling of fire-clay brick below the tuyere zone is related to K_2O attacking the bonding constituents along the formation of high specific volume minerals like leucite and kaliophilite. Alkali attack above the tuyere can be prevented by enough liquid formation to prevent damage. A high silica refractory reacts with alkali oxides at lower temperatures to prevent the subsurface from alkali attack, this happens since silica is attacked first by alkali.

High alumina bricks there are a rapid formation of kaliophilite, which suggests that the use of high alumina under alkali attack deteriorates the lining. It has been reported that silicon nitride has higher resistance to alkali attack at higher temperatures and can be used to protect

silicon carbide refractories used in the blast furnace [62]. Blast-furnace slag at high temperatures reacts with silicon nitride to yield complex silicides of transition metals and nitrides of these metals. In case of alumina carbide refractories, the pore structure is controlled by silicon addition of pore structure, permeability, microstructures, and alkali resistance of Al_2O_3-C refractories. Addition of silica helps in controlling the pore structure of alumina carbide refractories by promoting insitu formation of mullite and SiC whiskers. It has been reported that the refractories with higher silicon carbide whiskers have a denser structure with less pores. The smaller pore size of the refractories means higher the alkali resistance of the alumina carbide bricks [63]. In case of higher alkali percentage cracks appear in the refractory lining of the blast furnace stove [64]. T. Cheng has previously reported that along with the refractory temperatures even the iron flow in the hearth region plays an important role on the alkali attack on the refractory [65].

2.6 Alkali Effect on Other Parts of Blast Furnace

2.6.1 Tuyere Displacement

Fireclay bricks show remarkable swelling behavior due to the formation of alkali aluminosilicates. The furnace lining above the tuyere, particularly the bosh lining, disappears, that makes the tuyere brick less sustained. It has been suggested that such a displacement of the tuyere brick leads to the movement of the tip of the tuyere in the same direction [58]. It becomes imperative to use bricks with lower porosity and higher resistance to alkali attack, in order to avoid tuyere displacement which might eventually lead to tuyere burnout. This technique provides effective cooling of the tuyere zone helping to delay the alkali reaction. The main cause for the wear of refractories of the furnace walls is from alkali attack due to penetration of alkali vapor. Formation and the growth of alkali aluminosilicate such as kalsilite in fireclay brick lead to cracking and remarkable swelling.

2.6.2 Scaffold Formation

The high alkali content of the raw materials – iron ore, limestone, coke in the form of halides, silicates and the erratic working of the blast furnace leads to the formation of scaffolds inside the furnace. A scaffold forms in the low temperature region of the blast furnace i.e. mid and upper stack. The scaffolds in the furnace lead to the reduction in the working volume of the furnace, impeding the smooth downward movement of the burden materials and the ascending gases which reducing the contact time of gas and charge which in turn reduces the process efficiency. In one of the works while the inner layer contained high carbon with low alkali content, the intermediate layer contained about 10% alkali with low carbon content and the outer layer contains relatively lower alkali (4.43%) and carbon contents comparable to those in the intermediate layer [58]. Figure 2.5 shows influence of alkali on scaffold formation.

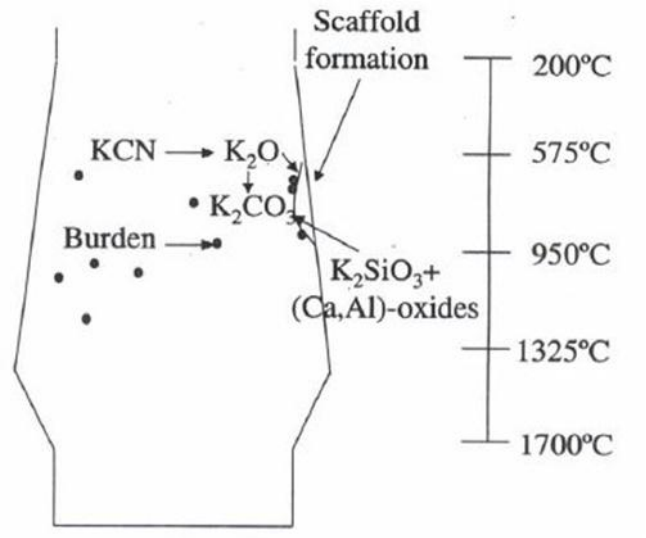

Fig. 2.5: Suggested influence of potassium on the formation of scaffolds in blast furnace [18]

2.7 Removal of Alkali from Blast Furnace

The rate at which the alkali accumulate in the blast furnace depends primarily on their input and output rates. The tolerable level or the maximum amount of accumulation depends on the quality of the raw materials being used, composition of hot metal, and mode of operation. Alkali metals exit the blast furnace either along with the top gas or with the slag. Potassium is the alkali which predominantly exits with the top gas sodium is mainly removed with the slag.

The retention of alkalis in the slag results from slow reaction rate rather than due to the thermodynamics. Alkali reacts with silica to form alkali silicates which are removed from the furnace along with slag. The use of limestone is a common practice in blast furnace. In excess it reacts with silica to form calcium silicates which does not allow the formation of alkali silicates. This makes it very important to keep the basicity in check which is given by $(CaO+MgO)/(Si0_2+Al_2O_3)$ [66]. Here, as we can see CaO percentage is proportional to the basicity. It is therefore necessary to maintain a slag regime with low basicity i.e. lower CaO content to avoid the accumulation of alkali in the furnace the conditions required for the removal of alkali from the furnace via slag have detrimental effect on the blast furnace operation and the final hot composition [67].

Some of the main problems been faced are the pickup of silicon from slag on to metal, sulphur in metal and manganese partition. The manganese oxides are much more stable than alkali oxides so any presence of alkali oxides in the slag reduces the manganese in the metal. The condition for sulphur removal contradicts those of alkali removal. The conditions need to be balanced so as to get the required composition of hot metal without much of alkali accumulation. Addition of quartzite, which provides silica for the formation of silicates is one of the many remedies used for the removal of alkali from the furnace through slag. It is important to keep the basicity of slag in check so that the sulphur content in the hot metal can be controlled but the addition of silica reduces the basicity leading to higher sulphur values in

the hot metal. Among other remedies the addition of olivine has been quite useful since it provides useful oxides required to remove the alkali as well as maintain the sulphur content of the hot metal. Another such method is the use of dunite which contains high percentage of silicate hydroxides which are ideal for alkali removal [68]. Another work done states addition of mixture of dunite and high MgO bearing materials, this helps get rid of alkalis well as helps maintain proper basicity for low Sulphur content [69].

Many works have proved before that the addition of Calcium chloride helps in the removal of alkali and scaffolds in the blast furnace [12]. $CaCl_2$ weakens the structure of alkalis present. It has been seen that the addition of $CaCl_2$ increases the alkali uptake by slag [70]. Even the removal of alkali from the raw materials has been suggested by chloride volatilization. The addition of $CaCl_2$ during the agglomeration processes for pellets and sinters helps to bring down the alkali percentage in the final product. This way the entry of alkali into the blast furnace can be controlled.

2.8 Alkali Effect on Alternative Iron Making Processes

The alkali effect on the other iron making processes is different for the other iron making processes. Corex has this advantage over the blast furnace that they are insensitive to the alkali attack. In Corex since pure oxygen is used there is no cyanide formation in the tuyere level rather vapors of alkali carbonates are formed from the silicate reduction which depends on the CO2 content of the raw gas [71]. The alkali output remains the same as input. In many of the direct reduction as well as smelting processes coal is used, which makes it important to understand the effect of alkali on the coal gasification reaction. The effect of alkali on the gasification of char has also been studied in which they reported that the alkali salts reacted with the char substrate to crate sites on the surface where gasification could take place [72]. Study of steam gasification of coal revealed that the alkali carbon complex determined the reaction rate. It has been seen that the activation energy is lower for K doped samples compared to original coal [73]. One work on the nature of the catalytic site revealed that

potassium carbonate has been dispersed all over the substrate, reacted with carbonaceous material at the edges of carbon micro layers to form groups. These sites have been reported to be the dominant sites of gasification [75]. It has also been reported in some works that the alkali showed the strongest influence on the reaction rate of the bouduard reaction which leads to higher coke consumption and electric power consumption in ferromanganese production [75, 77, 78].

2.9 References

1. Gridasov VP, Logachev, GN, Pishnograev SN, et al. Behavior of Alkalis in Blast Furnaces. Metallurgist. 2016; 59(9):761–765.

2. Davies J, Moon JJ, Raice FB. Alkalis in Blast Furnace Ironmaking and steel making. 1978:151–161.

3. Rankin WJ, SEE JB. The alkali problem in blast furnace Mineral Science Engineeing. 1977; 9(2):68–82.

4. Kurunov IF, Titov VN, Emel'yanov VL. et al. Analysis of the behavior of alkalis in a blast furnace. Metallurgist. (2009); 53(9):533–542.

5. A. K. Biswas, Principles of Blast Furnace Ironmaking, SBA Publications, Calcutta, 1984, pp. 110-115.

6. Raipala K. Deadman and hearth phenomena in the blast furnace.Scandinavian Journal of Metallurgy. 2000; 29(1):39–46.

7. Gladkov NA, Nikolaev SA, Budnik LG. Effect of alkalis on blast-furnace smelting. Metallurgist. 1986; 30(2):44–46.

8. Ghosh A, Chatterjee A, Iron Making and Steel Making: Theory and Practice book, PHI Learning Pvt. Ltd, 2008.

9. Yusfin YS, Chernousov PI, Garten V. et al. The role of alkalis and conserving resources in blast-furnace smelting. Metallurgist. 1999; 43(2):54–58.

10. Kundu AL, Prasad SC, Prakash HS et al. 'Strategies for the production of low silicon and low sulpher hot metal at Rourkela steel plant'. Transactions of the Indian Institute of Metals. 2004; 57(2):109–121.

11. Ellenbaum. United States Patent; 1976:29.

12. Ashton JD, Gladysz CV, Holditch JER, et al. Alkali control at Dofasco. JOM. 1974;26(40):47–54.

13. Stjernberg J, Antti M-L, Nordin L-O, et al. Degradation of Refractory Bricks Used as

Thermal Insulation in Rotary Kilns for Iron Ore Pellet Production. International Journal of Applied Ceramic Technology. 2009; 6(6):717–726.

14. Das B, Prakash S. Effective utilization of blast furnace flue dust of integrated steel plants. European Journal of Mineral Processing and Environmental protection. 2002; 2(2):61–68.

15. Evgueni Jak. Peter Hayes High Temp. Mater Proc. 2012;31(4):657–665.

16. H Kim, W Kim, J Park, et al. A Study on the Effect of Na_2O on the Viscosity for Ironmaking Slags. Steel Res Int. 2010; 81(1);17–24.

17. Besta P, Samolejova A, Janovska K, et al. The effect of harmeful elements in production of iron in relation to input and output material balance. Metabk. 2012; 51(3):325–328.

18. Sammuelsson C. Impurity flow due to waste recycling. MiMeR Report nb. 2000;3(4):4.

19. Kejiang Li , Rita Khanna , Jianliang Zhang , et al. 'The evolution of structural order, microstructure and mineral matter of metallurgical coke in a blast furnace: A review'. Fuel. 2014; 133:194–215.

20. Gladkov NA, Nikolaev SA, Budnik LG. 'Effect of alkalis on blast-furnace smelting'. institute of Ferrous Metallurgy. 1986; 30(2)12–14.

21. Al-ajeel Wahab A, Sahar AN. Effect of Some alkali additives on the reducibility of Al-Hussainiyat Iron ore From Iraqi western Desert. Iron Bulletin of Geology and Mining. 2009;5(1):119–131.

22. Pichler, A., Schenk, J., Hanel, M., Mali, H., Thaler, C., Hauzenberger, F., & Stocker, H. (2014). Influence of alkalis on mechanical properties of lumpy iron carriers during reduction. In Conference Proceedings to the 23rd International Conference on Metallurgy and Materials (pp. 40-40).

23. Nakagawa H, OnoY. Effects of potassium chloride on the reduction of iron oxides, Transactions ISIJ. 1985:25.

24. Gougeon M, Dupre B, Gleitzer C. An investigation of the critical influence of potassium on reduction of Wustite. Metallurgical Transaction B. 1986; 17(4):657–663.

25. Bhagat M, Halim Abdel SK, El-Kelesh AH, et al. Metallic iron whisker formation and growth during iron oxide reduction: K_2O Effect. Iron and Steel Making. 2009; 36(5):379–387.

26. Elkasabgy T. Effect of Alkalis on Reduction Behavior of Acid Iron Ore Pellets. Transactions ISIJ. 1984; 24.

27. Iljana M, Mattila O. Effect of circulating elements on the dynamic Reduction Swelling Behaviour of Olivine and Acid Iron Ore Pellets under simulated blast furnace Shaft conditions. ISIJ International. 2013; 53(3):419–426.

28. Lectard E, Hess E, Lin R. Behaviour of chlorine and alkalis in the blast furnace and effect on the sinter properties during reduction. La Revue de Metallurgie. 2004;101(1):31–38.

29. Besta P, Samolejova A. Alkaline carbonates in blast furnace process. Metalurgija. 2014; 53(4):549–552

30. Gupta S. Minerals and iron making reactions in blast furnace. Progress in Energy and Combustion Science. 2008. 34 p.

31. Haraguchi H, Nishi T. Some aspects of deterioration of coke in blast furnace. Transactions ISIJ. 1985; 25(3):190–197.

32. Van Niekerk HW. The influence of potassium on the reactivity and strength of coke, with special reference to coke ash, J.S. Afr. Inst. Min. Metall. 1986; 86(1):25–29.

33. Bhattacharya A, Schenk J. Effect of Alkaline elements on the reactivity, strength and structural properties of blast furnace coke, Metallurgia. 2014; 54(3) 503–506.

34. Babich A, Senk D. Coke quality for a modern blast furnace. RWTH Aachen University.

35. Babich A, Sen. D. Guden. Effect of coke reactivity and nut coke on blast furnace operations, Iron Making and Steel making, 2009; 36(3):222–229.

36. Hilding T, Gupta S, Sahajwalla V, et al. Structural and alkali content of coke in an experimental blast furnace and their gasification reaction. AISTech. 2004:1.

37. Gupta S, Kazuberns K. Coke Mineral Transformation in the Experimental Blast Furnace. Energy and Fuels. 2008; 22(5):3407–3419.

38. Marsh H. Metallurgical coke: formation, structure and properties. In: Proceedings of ironmaking conference, University of Newcastle upon Tyne, England; 1982:2p.

39. Marsh H, Asao O, Qian Z. A structural study of cokes using optical microscopy and X-ray diffraction. Fuel. 1983; 2:9–17.

40. Crawford D, Marsh H. High resolution electron microscopy of carbon structure. J Microsc. 1977; 109(1):145–52.

41. Shevlin FJM, Fryer RJ. Microstructural Analysis of metallurgical cokes and intercalated species. Carbon. 1986; 24:527–534.

42. Hilding T, Gupta S, Sahajwalla V., et al. Degradation behaviour of a high CSR coke in an experimental blast furnace: effect of carbon structure and alkali reactions. ISIJ Int. 2005; 45(7):1041–1050.

43. Dong S, Paterson N. Characterization of Tuyere level core drill coke samples from blast furnace operation, Energy & Fuel, 2007:21:3446–3454.

44. Gornostayev S. Graphite crystals in blast furnace coke. Carbon. 2007; 45(6):1145–1151.

45. Huffman PG, Huggins EF. Investigation of the structural forms of potassium in coke by electron microscopy and X-ray absorption spectroscopy. Fuel. 1986; 65(5):621–632.

46. Morland A. The structure and strength of metallurgical coke, thesis. Loughborough University; 1990.

47. H. W. Gudenau, D. Senk, K. Fukada, A. Babich and C. Fröhling: Proc. Int. Blast Furnace Lower Zone Symposium, Wollongong, Australia, November 2002, 11·1.

48. Nomura S, Higuchi K. Reaction behavior of formed iron coke and its effect on decreasing thermal reserve zone temperature in blast furnace. ISIJ International. 2010; 50(10)1388–1395.

49. Duman G, Yanik J. The effect of char properties on gasification reactivity, Fuel

processing technology. 2014; 118:75–81.

50. Huhn F, Klein J. Investigations on the alkali-catalysed steam gasification of coal: kinetics and interactions of alkali catalyst with carbon. Fuel. 1983; 62(2):196–199.

51. Adjorlolo AA, Rao KY. Effect of potassium and sodium carbonate catalysts on the rate of gasification of metallurgical coke. Carbon. 1984; 22(2):173–176.

52. Shadman F, Punjak AW. Catalyst transformation during alkali catalyzed carbon gasification. University of Arizona. 1986; 31(7):143–149.

53. Pang, Qing Hai, Zhang. et al. K2CO3 catalysis on the reactivity of top charged coke and stamp charged coke. IJMMM. 2013; 1:17.

54. Lindstad T, The influence of Alkalis on the bouduard reaction. Tenth International Ferroalloys Congress. 2004:1–4.

55. Mckee WM. Mechanisms of the alkali metal catalyzed gasification of carbon. Fuel. 1983:62(2):170–175.

56. Vallova S, Slovak V, The influence of selected oxides and carbonates on thermal oxidation of coke. Journal of Thermal analysis and calorimetry. 2003; 71(3):875–881.

57. Fredman PT. Accretions in the blast furnace stack- background factors. Canadian Metallurgical Quarterly, 2002; 41(4):475–486.

58. Narita K. Effects of alkalis and Zinc on the wear of blast furnace refractories and tuyere displacement. Transactions ISIJ. 1981; 21(12):839–845.

59. Silva NS. Wear mechanism for blast furnace hearth refractory lining. Iron making and Steel making. 2005; 32:459–467.

60. Chen Xilai. Effect of carbon aggregates on the properties of carbon refractories for blast furnace. Metallurgical and Materials Transactions A. 2010:42.

61. McCune ES. Reaction between K_2O-Al_2O_3-SiO_2 refractories as related to blast furnace linings. Journal of American Ceramic Society. 1985; 40:6.

62. Pitak VN., The effect of reducing and oxidizing gases and molten slag and alkalis on the properties and resistance of Nitride based refractory materials. Refractories and Industrial ceramics, 2002;43(1):32–35.

63. Yibia Xu, Pore structure, permeability, and alkali attack resistance of Al_2O_3-C refractories. Metallurgical and Materials Transactions A. 2014;45(6):2885–2893.

64. Ghosh NB, Rao B. Alkali attack on blast furnace stove refractories. Transactions of the indian ceramic society.1970; 29:1–7.

65. Cheng TW, Huang NC. Simulation of iron flow and heat transfer in the hearth of the blast furnace, Department of Chemical Engineering, National Chung Hsing University. 2004;15: 55–59.

66. Shaopeng Chen, Wei Wang, Runsheng Xu, Shuliang Deng & Heng Zheng (2020) Influence of multiple factors on the alkali metal enrichment in blast furnaces by a thermodynamic model, Ironmaking & Steelmaking, 47:3, 219-227.

67.Kurunov FI. Analysis of the behavior of alkalis in the blast furnace. Metallurgist. 2009; 53:9–10.

68. Lopez AF. Caloremetric and fourier transform infrared spectrophotometric studies of potassium elimination by dunite. Metallurgical and Materials Transactions B, 1995; 26(1):51–58.

69. Somolinos E. Increasing the value in use of magnesium silicate fluxes: tailor made (MgO)/SiO2 ratio for each application, Metech, 2nd ed. 2015.

70. Aydin S, Dikec F. The removal of alkalis from iron ores by chloride volatilization. Canadian Metallurgical quarterly. 1990; 29(3):213–216.

71. Amit Chatterjee. Hot metal production by smelting reduction of iron oxide. PHI Learning Pvt. Ltd, Second Edition 2014, 97-98.

72. McKee, D. W., Spiro, C. L., Kosky, P. G., & Lamby, E. J. (1982, January). Catalytic effects of alkali metal salts in the gasification of coal char. In Symposium on coal gasification (pp. 74-86).

73. Huhn F. Investigations on the alkali catalyzed steam gasification of coal: Kinetics and interactions of alkali catalyst with carbon. Fuel. 1983; 62(2):196–199.

74. Mims, C. A., & Pabst, J. K. (1980). Alkali-catalyzed carbon gasification. I. Nature of the catalytic sites. Am. Chem. Soc., Div. Fuel Chem., Prepr.; (United States), 25 (CONF-800814-P2).

75. Kaczorowski J, Lindstad T. The effect of potassium impregnation on the boudouard reactivity of selected single source and commercial cokes. INFACON XI. 2007:583–593.

76. Lindstad T, Syverstsen M. The influence of alkalis on the Bouduard reaction. INFACON X. 2004:261–271.

77. Kaczorowski J, Lindstad T. The Influence of Potassium on the Boudouard Reaction in Manganese Production. ISIJ International. 2007; 47(11):1599– 1604.

Chapter-3

Methodology

3.1 Background

This chapter summarizes the methodology adopted in this thesis to study and understand the effect of alkali elements on the iron making processes. In this chapter the steps adapted to understand the effect alkali elements have on the raw materials i.e. different iron ore charge material and carbon bearing reductant (strength, reactivity and their reaction mechanism), under different iron making conditions have been highlighted. Iron ore lumps have been collected from different sources (Steel Plants). Iron ore briquettes have been made using the iron ore fines. Pellets and sinters have also been collected from different sources i.e. Tasmania, Australia and Donawitz, Austria, respectively. In case of reductant, boiler grade coal has been used for direct reduction processes. Coke samples have been collected from different sources i.e. from India, Austira and Germany. Coke is used to understand the effect alkali have on the reductant strength and reactivity under blast furnace conditions. Alkali has been added to different raw materials depending on their composition. Different fluxes have been collected to make an attempt for the removal of alkali through slag via smelting. The steps taken have been noted down systematically in this chapter.

3.2 Characterisation of the Raw Materials

The iron ore charge materials i.e. lumps, pellets and sinters along with the reductants i.e. coal and coke have been crushed into fines for general characterisation of raw materials. The raw materials have been broken down using a hammer followed by the primary crusher i.e. jaw crusher followed by secondary crusher i.e. roll mill and at last the disc pulveriser to collect fines. The iron ore fines below 75µm have been used for WDXRF and XRD analysis. The raw materials of different size range have been collected using a sieve shaker.

The composition of different iron ore charge materials has been studied using WDXRF. The MagiX 2424 model of PAN analytical has been used, which is a sequential wavelength dispersive x-ray fluorescence spectrometer. The WDXRF has been performed by Mr. Anirban Sur at GSI, Kolkata. The analysis of the different phases present has been done with the help of XRD analysis. The phase analysis is performed using X-ray diffraction spectrometer via Bragg-Barentano geometry (Rigaku Ultima III, Japan) of raw ore and several treated products (reduced). Data is collected from the positions and intensities of peaks compared with those of the standards given in PDF database (PCPDF-WIN software, JCPDS-International Centre for Diffraction Data). The XRD has been performed partly at Jadavpur University and rest has been done in IIT Guwahati.

Boiler grade coal fines have been used as reductant under the direct reduction conditions. The TG/DTA and proximate analysis of the boiler grade coal has been carried out. Coke has been used to study the effect under the blast furnace conditions. The TG/DTA and proximate analysis of the coke samples used has also been carried out. The TG/DTA analysis has been investigated using a Pyris Diamond Thermo gravimetric /Differential Thermal Analysis (Perkinelmer, Singapore). The α-alumina fine powder is taken as a reference. The ground specimen and a reference material have been measured accurately and then placed inside their respective cells.

The iron ore lumps have been crushed using primary crusher i.e. Jaw Crusher to select samples for the tests of reduction of iron ore lumps under direct reduction conditions. Samples in the size range of -18.75 to +12.5 have been selected. The lumps of the particular size have been separated using standard BSS sieves, for this purpose the sieves of size ¾ and ½ inch have been used. The iron ore has further been crushed using secondary crushers i.e. roll crusher followed by pulveriser. The sieve of 200 mesh size (75μm) has been selected. The particles below the 200 mesh size have been selected for making briquettes which have

been tested under the direct reduction conditions. Briquettes have been made using iron ore fines, bentonite, water and alkali solution (where required). All these components are mixed together and put in a die which is then placed under an automatic hydraulic press. The force to be applied is set on the press and force is applied, and after some time the die is taken out. The briquettes are then taken out from the die and heated to get rid of the excess moisture.

The Sinters have also been broken down using hammer, sieved and collected in the size range of -12.5 - +10mm. The collected pellets have also been sieved and pellets in the size range of -12.5 - +10 mm have been selected. The sinters and pellets of the selected size range have been used to study the alkali effect on their reduction, strength and reaction mechanism under blast furnace conditions. Coke samples collected have been broken down using a hammer and sieved. Cokes in the size range of -22.4 - +19mm have been selected for the tests on coke under the blast furnace conditions to study the alkali effect on the reactivity, strength and reaction mechanism of Bouduard reaction.

3.3 Impregnation of Raw Materials with alkali elements:

Most of the iron ore charge materials and coke used for the tests have very low alkali content (0.02-0.06%). In our study the alkali has been introduced into the different raw materials (where required) so as to help make a quantitative assessment of the alkali effect on their reactivity strength and reaction mechanisms. The different solutions of Sodium hydroxide and potassium hydroxide have been made having different strengths i.e. 1M, 2M, 3M, 4M and 5M. The iron ore charge materials and coke samples have then been put in the beaker with the alkali solution. The beaker with the solution containing the samples has then been transferred into a desiccator connected to a vacuum pump. The suction is started as the pump gets switched on, the container is then left inside the desiccator until the bubbling ends. Due to the vacuum the air leaves the pores of the raw materials and the alkali then settles into the

pores. This process continues till air has been removed from all the pores at which point the bubbling stops. The samples have then been taken out and they have been heated at 120^{o} C to get rid of the moisture for about 2 hours. The samples weight has been recorded before and after impregnation. The difference between the weight of the samples before and after impregnation has been calculated to find out the alkali gain by the iron ore charge materials. The alkali solution which gives acceptable alkali gain has been selected for alkali impregnation of all the raw materials i.e. iron ore lumps, briquettes, pellets, sinters and coke samples separately.

3.4 Response Surface Methodology

Nowadays statistical analysis using design of experiments has gained a lot of interest in the field of research [1, 2, 3, 4]. To perform the carbothermal reduction experiments on the impregnated hematite samples, a statistical approach has been made using response surface methodology to optimize the effect of variable parameters on reduction.

- It is a set of statistical and mathematical methods that can be utilised for modelling and analysing different problems.
- It also quantifies the link amongst the controllable input parameters and the obtained response surfaces.
- It is an economical method of obtaining the optimum amount of data in a short period of time and with lesser number of tests.
- Box- Behnken design is one of the experimental design models which has been chosen to establish the link between the response function and the variables [5, 6, 7].

3.4.1 Box-Behnken Design

Multivariate techniques have gained popularity for the optimization of analytical methods [8, 9, 10]. They can be used for preliminary examination of experimental variables in analytical processes and/or for the determination of concerned conditions (maximum or minimum) of the concerned variables [11]. Factors with more than three levels are used, and they help form quadratic models. Box– Behnken, Central composite, and Doehlert designs are the most popular amongst the response surface methodologies.

Box–Behnken design uses an experiment number depending on $N = k^2 + k + c_p$, where (k) is the variable number and (c_p) is the replicate number of the central point. The central composite design generally has a greater number of trials, which can be calculated according to $N = k^k + 2k + c_p$, where (k) is the variable number and (c_p) is the number of central points [12]. Box–Behnken is also considered as a spherical, revolving design. It can also be viewed as a cube (Fig. 3.1a), it consists of a central point and the middle points of the edges. However, it can also be considered as comprising of three interlocking 22 factorial designs and a central point (Fig. 3.1b) [13]. It has been applied for optimization of several chemical and physical processes [14].

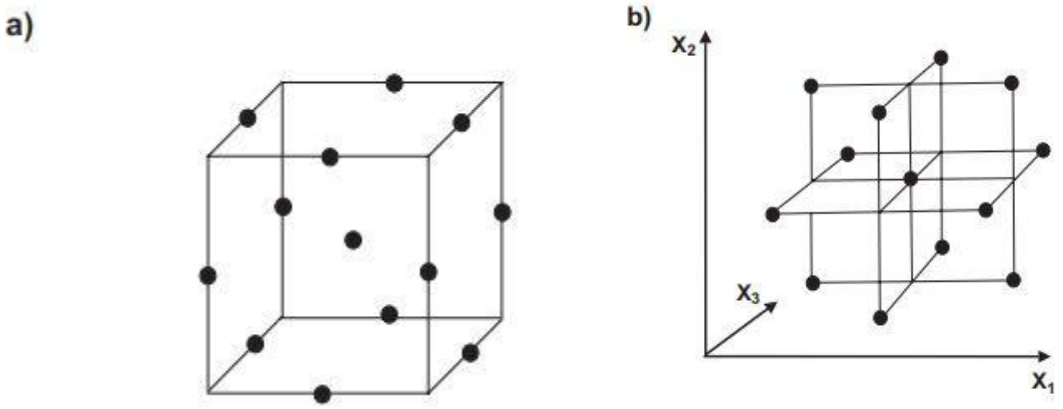

Fig. 3.1: Box–Behnken design. a.) The design, as derived from a cube; b.) Representation as interlocking 22 factorial experiments [15]

Box–Behnken design (BBD) is very handy as it can provide a second-order polynomial model as a function of the independent process parameters with the lowest possible experimental runs. The experimental design has 17 trials and the dependent response is provided as the mean of three duplicates. The BBD is performed with three chosen, independent variables at three levels coded as −1 (low), 0 (central point), and 1 (high) as shown in Table 3.1. The relationship between the response and the independent variables can be fitted by a second-order quadratic polynomial equation:

$$Y\ (\text{response}) = X + a_1A + a_2B + a_3C + a_4AB + a_5BC + a_6AC + a_7A^2 + a_8B^2 + a_9C^2$$

Where Y represents the response (% extent of reduction), X is a constant, a_i (i=1 to 9) are the coefficients for linear and quadratic interaction effects, respectively, and A, B and C are the chosen independent variables. According to statistical theory, the three-factor (*k*=3) three-level, and five central points (C0 =5) BBD needs 17 sets of experiments (N=17). Table 3.2 shows all the 17 set of reactions. The software Design-Expert (version 7.0.0) is applied to design and analyse the experiments. The analysis of variance (ANOVA) has been employed to determine the statistical significance and competency of the model. Using Design-Expert 7.0.0 the relationship between the responses and the levels of each variable could be allegorized actively by expressing the fitted polynomial equation in the form of a three-dimensional (3D) surface plot.

Serial	Parameters	Lower	Middle	Higher
1	A	-1	0	+1
2	B	-1	0	+1
3	C	-1	0	+1

Table 3.1: Coded parameter levels of experimental variables used for Box–Behnken design

Sl. No.	A	B	C
1	-1	-1	0
2	-1	0	-1
3	-1	0	+1
4	-1	+1	0
5	0	-1	-1
6	0	-1	+1
7	0	0	0
8	0	0	0
9	0	0	0
10	0	0	0
11	0	0	0
12	0	+1	-1
13	0	+1	+1
14	+1	-1	0
15	+1	0	-1
16	+1	0	+1
17	+1	+1	0

Table 3.2: Box Behnken Design for 3 factors

These 17 set of experiments are carried out. The response is evaluated experimentally and the data is put in the software Design Expert 7.0.0. The software then analyses the data and gives the optimised conditions and the second-order polynomial quadratic equation. The statistical data i.e. Annova provides various information which help to determine whether the model is significant or not. The software provides different graphs like normal plot of residuals, predicted vs. actual which also help in determining if the model is significant. At last the contour and 3-D surface plots are generated to understand the effect of different factors on the response.

3.5 Isothermal Reduction Kinetic Study:

The reaction of dried iron ore charge materials with coal and coke will be carried out isothermally in their respective reaction vessels. The conventional gas-solid reaction mechanisms for isothermal kinetic study are mentioned hereunder [16][17].

$\alpha^2 = kt$	Parabolic (D_1)	1
$[\alpha + (1-\alpha)\ln(1-\alpha)] = kt$	ValensiBarrer(D_2)	2
$[1-2/3\ \alpha - (1-\alpha)^{2/3}] = kt$	GinstlingBrounsthein(D_3)	3
$[1-(1-\alpha)^{1/3}]^2 = kt$	Jander(D_4)	4
$[(1+\alpha)^{1/3}-1]^2 = kt$	Anti Jander(D_5)	5
$[(1-\alpha)^{-1/3}-1]^2 = kt$	Zhuralevet al. (D_6)	6
$\alpha = kt$	Linear Growth (CG_1)	7
$[1-(1-\alpha)^{1/2}] = kt$	Cylindrical (CG_2)	8
$[1-(1-\alpha)^{1/3}] = kt$	Spherical (CG_3)	9
$[-\ln(1-\alpha)] = kt$	First- order Chemical Reaction (R_1)	10
$[(1-\alpha)^{-1/2}-1] = kt$	One&Half - order Chemical Reaction (R_2)	11
$[(1-\alpha)^{-1}-1] = kt$	Second -order Chemical Reaction (R_3)	12

In the above kinetic equations, the abbreviations like D, CG and R correspond to diffusion, contracting geometry and chemical reaction controlled mechanism, respectively. The equations represent the different mechanisms involved in the kinetics of reaction in the solid-solid and solid-gas interface.

In order to identify the mechanism(s) of reduction, reduced time analysis is carried out. For a particular mechanism,

$$g(\alpha) = kt \qquad 13$$

α is the fractional conversion ranging from 0 to 1, where g(α) is the functional form representing a reaction mechanism, t is the time and k is the rate constant.

Assuming, α =0.5,

$$g(\alpha_{0.5}) = kt_{0.5} \qquad 14$$

$t_{0.5}$ is the time required for fraction of conversion of 0.5. Dividing equation 3 by equation 4, we get

$$g(\alpha) / g(\alpha_{0.5}) = t/t_{0.5} = \theta \qquad 15$$

Where, θ, a dimensionless quantity, is known as reduced time. Reaction rate constant k is a function of mechanism and temperature. The kinetic study has been carried out to determine how the reaction mechanism changes for different alkali percentages.

3.6 Effect of Alkali on Iron Ore Charge Material under Direct Reduction Conditions

The iron ore lumps (before alkali impregnation) in the size range of -18.75 - +12.5 have been selected. They have been reduced using boiler grade coal fines using an inconel tube inside a tube furnace. Reduction experiments are carried out in a conventional resistance furnace (up to 1623 K) containing silicon carbide as heating element with PID controller. The lumps and briquettes have been reduced at 1000^{o}C, 1050^{o}C and 1100^{o}C for 5, 10, 15, 30, 45 and 60 minutes. Iron ore has been collected from three different sources i.e. Tata Steel, JSW and Vizag Steel Plant. All the ores have very low alkali percentage. In order to select a specific ore for this test, all lumps of all three ores have been reduced in a tube furnace at the lowest temperature i.e. 1000^{o}C for 60 minutes. The iron ore lump with maximum extent of reduction has been selected for further testing. The isothermal kinetic study has been carried out. The same has been done for both the alkali impregnated iron ore lumps and briquettes. The molar concentration of sodium hydroxide and potassium hydroxide selected is 2M and 4M. The kinetic study has been carried out for the iron ore lumps and pellets with and without alkali, to understand the alkali effect on the reaction mechanism of the iron ore charge material. Surface Response Methodology via Box Behnken statistical design model using Design Expert 7.0 software, has been used with the response as extent of reduction (EOR) to understand the effect the alkali elements have on the reducibility of iron ore charge material under direct reduction conditions. The reduced samples of iron ore lumps and briquettes have been analysed using XRD analysis to find out the main phases present.

3.7 Effect of Alkali on Iron Ore Charge Material under Blast Furnace Conditions:

The selected pellets and sinters without and with alkali content have been subjected to reducibility test according to the standard ISO-4695. In ISO 4695 test the iron ore charge material is reduced using CO gas at 950^{o}C. The effect of alkali on the strength of the sinters

has been studied according to the standard ISO-4696-1. In IS0 4696-1 test the low temperature reduction degradation (LTD) indices have been calculated for the selected sinters i.e. they are reduced in conditions similar to upper stack zone of blast furnace. The sinter with the best LTD test results has been used for further testing. ISO-4695 and ISO-4696-1 (where applicable) tests have been carried out for both sinters and pellets to understand the effect alkali have on their reduction and strength, respectively under the blast furnace conditions. This test has been carried out in the vertical retort furnace present in Montanuniversität, Leoben, Austria in the year 2019. The isothermal kinetic study has been carried out to understand the effect alkali have on the reaction mechanism for the reduction of sinters and pellets. The XRD analysis of the reduced samples has been carried out to study the main phases present.

3.8 Effect of Alkali on Coke under Blast Furnace Conditions:

Coke samples have been collected from two different sources. The BET analysis of both the coke samples has been carried out using a Micro Meritics Tristar 3020 model to find out the available surface area. The coke reactivity index and coke strength after reduction of the coke sample with and without alkali has been calculated according to the standard ISO 18894 (here the tests have been performed on two different coke samples but with only one range of alkali percentage). The alkali effect on the reactivity and strength of the coke samples has been studied. The abrasion values have also been evaluated. The kinetics of the Bouduard reaction has been carried out to have a better understanding of the effect alkali elements have on the Bouduard reaction. To have a better understanding an analytical study of effect of different percentages of different alkali on the Bouduard reaction has also been carried out. The ISO 18894 test has been carried out in the vertical retort furnace present in Montanuniversität, Leoben, Austria during 2017. The reacted coke samples have been analysed using XRD analysis to find out the main phases present.

3.9 Alkali Removal from the Blast Furnace

The reduced iron ore charge materials with the highest alkali content have been smelted with added flux. Other than lime; dunite, magnesium hydroxide as a source of MgO and magnesium silicate has been used stoichiometrically with the reduced samples and smelted in a graphite crucible using a raising hearth furnace. The composition of the metal has been analysed by induced coupled plasma-optical emission spectroscopy (ICP-OES) to study the removal of alkali through slag.

3.10 Reference

1. S. Biswas, S. Chakraborty, M. G. Chaudhuri, P. C. Banerjee, S. Mukherjee, R. Dey, Optimization of process parameters and dissolution kinetics of nickel and cobalt from lateritic chromite overburden using organic acids, J Chem Technol Biotechnol, 89 (2014), 1491-1500.
2. S. Biswas, K. Bhattacharjee, Fungal assisted bioleaching process optimization and kinetics: Scenario for Ni and Co recovery from a lateritic chromite overburden, Separation and Purification Technology, 135 (2014), 100-109.
3. N. Aslan, Y. Cebeci; Application of Box–Behnken design and response surface methodology for modeling of some Turkish coals; Science Direct Fuel 86 (2007) 90–97.
4. Sébastien Lefèvrea, Jean-Henry Ferrassea, Olivier Boutina, Michelle Sergentc, Rémy Faucherandb, Alain Viandb; Process optimisation using the combination of simulation and experimental design approach: Application to wet air oxidation; chemical engineering research and design 8 9 (2011) 1045–1055.
5. Application of Response Surface Methodology and Box–Behnken Design for the Optimization of the Stability of Fibrous Dispersion Used in Drilling and Completion Operations; Mohammed Alhajabdalla, Husameldin Mahmoud, Mustafa S. Nasser, Ibnelwaleed A. Hussein, Ramadan Ahmed, and Hamidreza Karami ACS Omega 2021 *6* (4), 2513-2525.
6. Box-Behnken Design Optimization of Sand Casting Process Parameters; Blessing Ngozi Goodluck Aliemeke and M. H. Oladeinde, INTERNATIONAL JOURNAL of ENGINEERING TECHNOLOGIES, 2020, Vol.6, No.2, 25-36.

7. Peng, X., Yang, G., Shi, Y. *et al.* Box–Behnken design based statistical modeling for the extraction and physicochemical properties of pectin from sunflower heads and the comparison with commercial low-methoxyl pectin. *Sci Rep* **10,** 3595 (2020).
8. M.S. Dopico Garcia, J.M. Lo´pez, V.R. Bouza, M.J. Abad, E. Gonza´lez Soto, M.V. Gonza´lez Rodrı´guez, Extraction and quantification of antioxidants from low-density polyethylene by microwave energy and liquid chromatography, Anal. Chim. Acta 521 (2004), 179–188.
9. M.C.B. Quaresma, R.J. Cassella, M.F.B. Carvalho, R.E. Santelli, Focussed microwave-assisted sample preparation: total phenol determination in petroleum refinery effluents by flow injection spectrophotometry, Microchem. J. 78 (2004) 35–40.
10. A.C. Ferreira, A.C.S. Costa, M.G.A. Korn, Preliminary evaluation of the cadmium concentration in seawater of the Salvador City, Brazil, Microchem. J. 78 (2004) 77–83.
11. B.B. Neto, I.S. Scarminio, R.E. Bruns, Como fazer Experimentos: Pesquisa e Desenvolvimento na Cieˆncia e na Industria, Editora da UNICAMP, Sa˜o Paulo, 2001.
12. S.L.C. Ferreira, W.N.L. dos Santos, C.M. Quintella, B.B. Neto, J.M. Boque-Sendra, Doehlert Matrix: a chemometric toll for analytical chemistry—review, Talanta 63 (2004) 1061– 1067.
13. D.L. Massart, B.G.M. Vandeginste, L.M.C. Buydens, S. de Jong, P.J. Lewi, J. Smeyers-Verbeke, Handbook of Chemometrics and Qualimetrics Part A, Elsevier, Amsterdam, 2003.

14. Statistical optimization parameter for lean grade self-reducing nuggets by surface response modelling to produce pig iron Chanchal Biswas, Saikat Samanta, Anrin Bhattacharyya, Mahua Ghosh Chaudhuri, Rajib Dey, International journal of Mineral Processing and Extractive Metallurgy (Trans. Inst. Min. Metall. C), pp. 1-10
15. Souza, A. S., dos Santos, W. N., & Ferreira, S. L. (2005). Application of Box–Behnken design in the optimisation of an on-line pre-concentration system using knotted reactor for cadmium determination by flame atomic absorption spectrometry. Spectrochimica acta part B: atomic spectroscopy, 60(5), 737-742.
16. Wang H, Chu M, Guo B, Bao J, Zhao W, Liu Z, et al. Investigation on Gasification Reaction Behavior and Kinetic Analysis of Iron Coke Hot Briquette under Isothermal Conditions. Steel Res Int 2019;90:1–10. doi:10.1002/srin.201800354.
17. Sarkar BK, Samanta S, Dey R, Das GC. A study on reduction kinetics of titaniferous magnetite ore using lean grade coal. Int J Miner Process 2016;152:36–45. doi:10.1016/j.minpro.2016.05.011.

Chapter-4

Special Equipments and Test Facilities

4.1 Tube Furnace Direct Reduction Conditions

Reduction experiments are carried out in a conventional resistance furnace containing silicon carbide as heating element with PID controller. Size of alumina tube is 50 mm outer diameter (O.D) and 40 mm inner diameter (I.D) with length (L) 700mm. Heating zone in the furnace is about 10 cm from the furnace inlets (from either side) as shown in the schematic diagram below. The temperature is calibrated and standardized by using a Pt/Rh thermocouple. After the experiment the sample is cooled in the furnace to room temperature. A picture of the instrument is shown in Fig. 4.1.

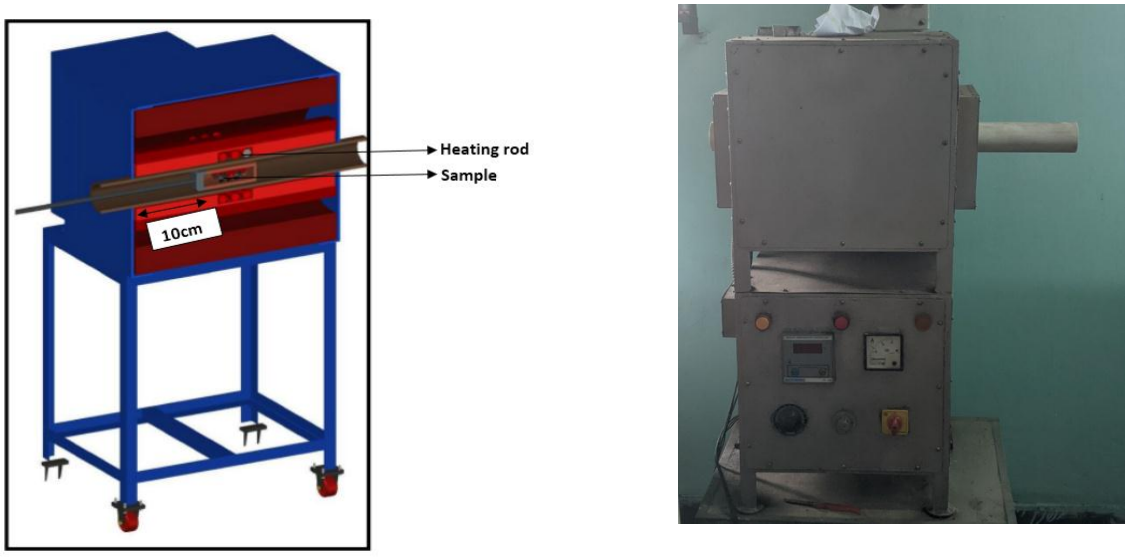

Fig. 4.1: Tube furnace schematic and the furnace used for this research work, respectively.

4.2 Vertical Retort Furnace used for Tests under Blast Furnace Conditions

A vertical retort furnace has been used for experiments of iron ore charge materials and coke. The entire system is digitalized and has different gas systems attached to the furnace. In this furnace the different environments depicting various iron making processes can be replicated according to the saved standards in the system. The furnace can be opened and the retort containing the samples is put inside the furnace and closed. A standard is selected according to the experiment that needs to be performed. The retorts dimensions are different for tests

with iron ore charge materials and coke. A perforated plate is used inserted in the retort. Two layers of porcelain balls are inserted in between the perforated plates and the test samples to maintain a uniform gas flow. The retort is then inserted in the furnace centrally hanging by the weighing device, making sure that the retort does not touch the furnace walls. The standard is selected in the test is started. Different standards used are ISO-4695, ISO-4696-1 and ISO 18894 for iron ore reduction, strength of sinters and coke reactivity, respectively. The image, layout and design of the retort furnace are shown in Fig. 4.2, Fig. 4.3 and Fig. 4.4, respectively.

Fig. 4.2: Vertical retort furnace used for tests under blast furnace conditions

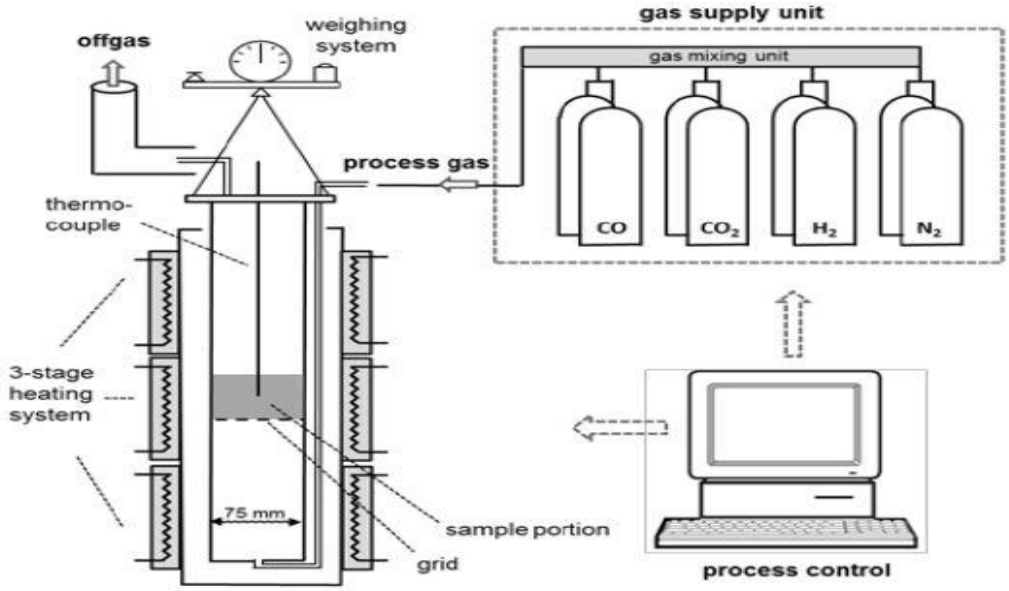

Fig. 4.3: Layout of the vertical retort furnace including the gas system [1]

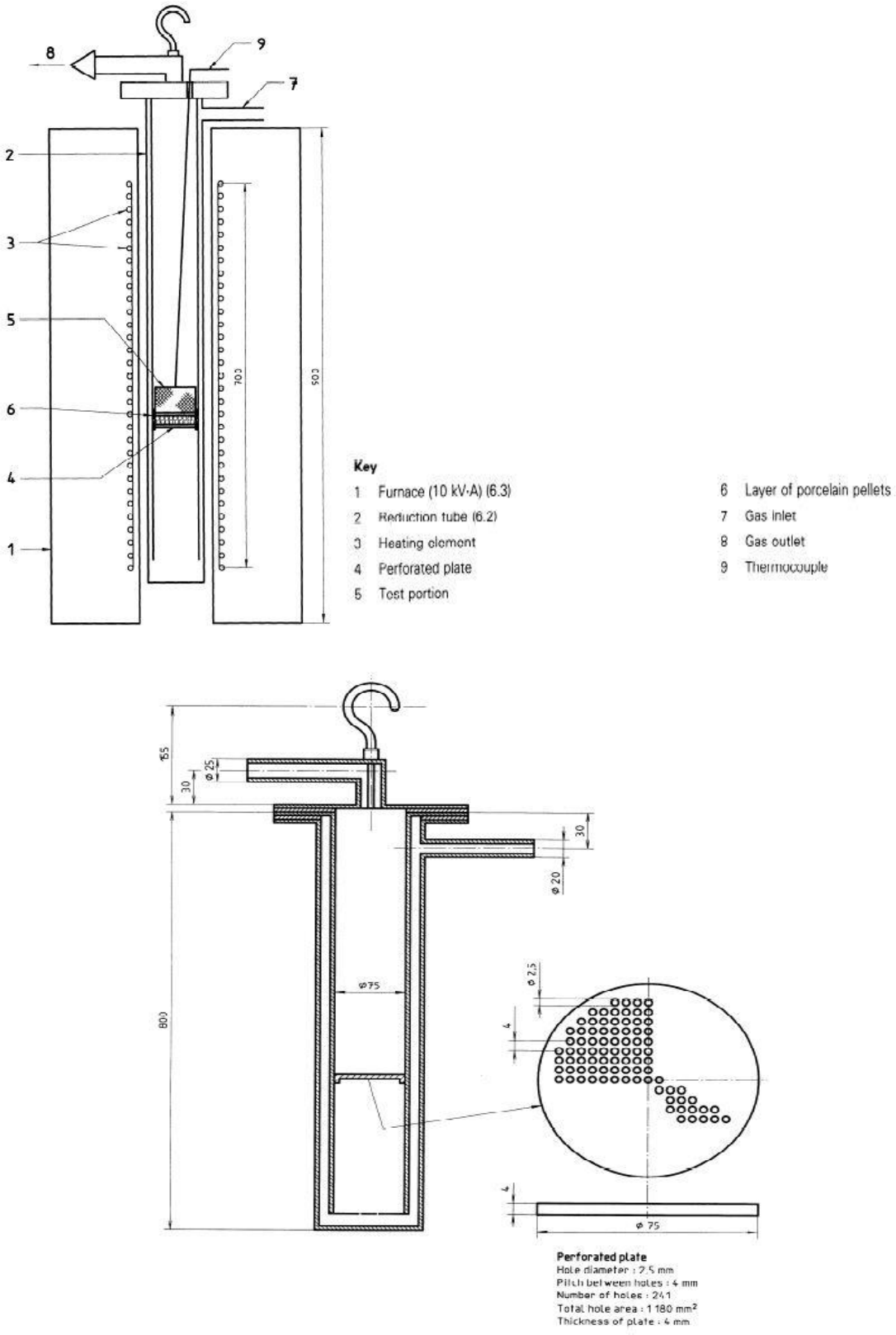

Fig. 4.4: Reduction tube design (the diameter of the tube and perforated plate differ for iron ore and coke tests rest is the same) [2]

4.3 Tumbler:

4.3.1 For Iron Ore Charge Materials:

The reduced iron ore charge materials are inserted into a tumble drum after weighing. The mouth of the drum is closed shut and the drum is rotated for 300 revolutions at rate of 30revs/min. The sample is then collected and weighed followed by manual sieving using 6.3mm, 3.15mm and 500µm. The weights of samples retained on these sieves are recorded. The material lost due to dust has to be considered a part of -500 µm. Then the reduction degradation index is calculated using the following formulas:

$$RDI\text{-}1_{6.3} : (m_1/m_0)*100$$

$$RDI\text{-}1_{3.15}: \{[m_0-(m_1+m_2)]/m_0\}*100$$

$$RDI\text{-}1_{0.5}: \{[m_0-(m_1+m_2+m_3)]/m_0\}*100$$

where;

m_0 is the mass of sample after reduction and before tumbling.

m_1 is the mass of sample retained on the 6.3mm sieve

m_2 is the mass of sample retained on the 3.15mm sieve

m_3 is the mass of sample retained on the 500µm sieve

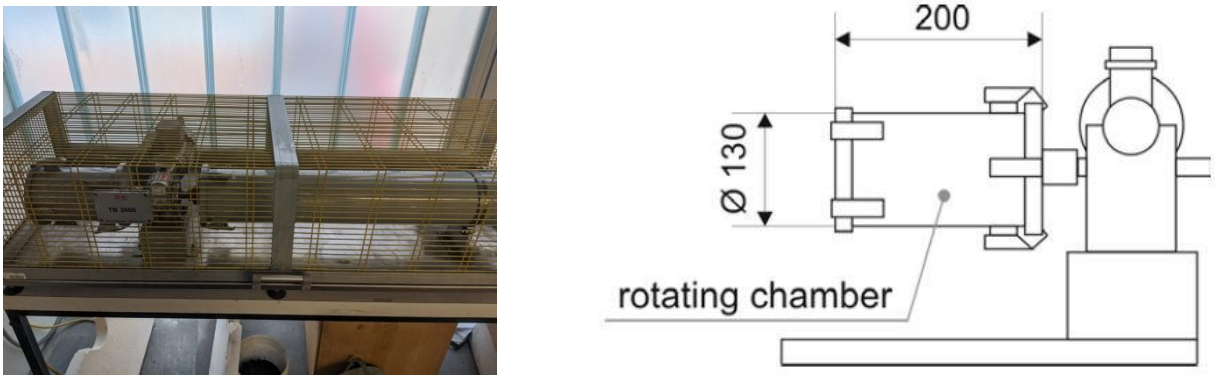

Fig 4.5: Iron charge material tumbler picture and schematic diagram [1]

4.3.2 For Coke:

The coke samples after reaction in the vertical retort furnace are taken out and weighed. These samples are then inserted into a tumbler for coke samples. Tumbler has a revolving drive, controlled by revolution counter and time relay. The sample is put inside the drum and the drum lid is closed. The tumbler is designed to stop after 600 revolutions at the rate of 20revs/min. The Coke strength after reduction (CSR) and abrasion value is calculated as follows:

CSR: $(m_2/m_1)*100$

AV: $(m_3/m_1)*100$

Where;

m_2 is the weight of coke samples larger than 10mm in size after tumbling.

m_1 is the weight of coke samples in gram after reaction.

m_3 is the weight of coke samples less than 500 μm in size after tumbling.

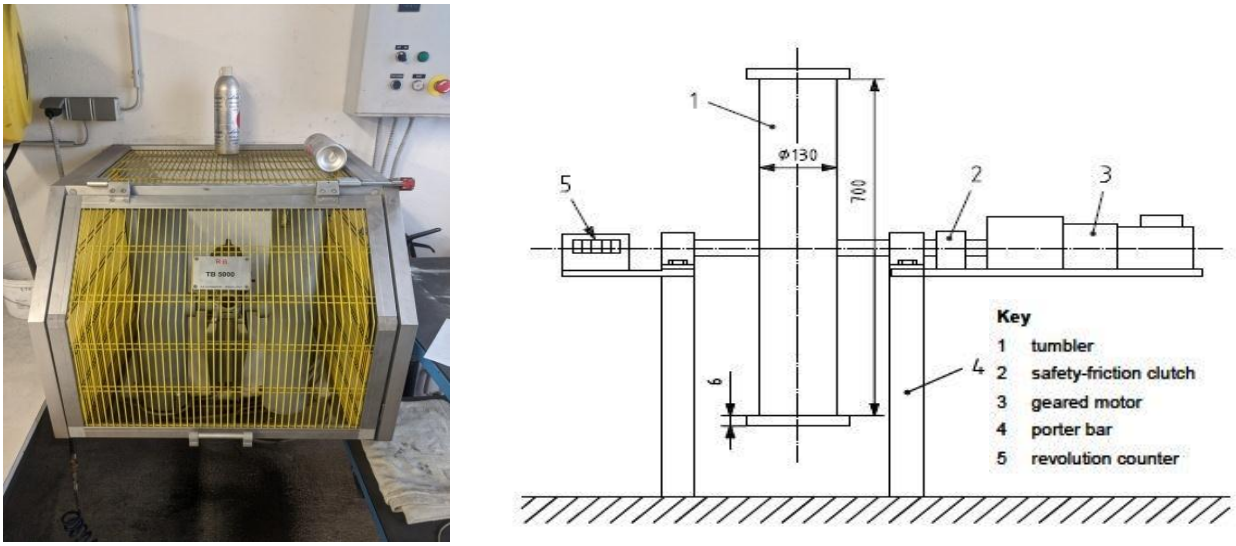

Fig 4.6: Coke tumbler picture and schematic diagram [3]

4.4 Raising Hearth Furnace:

Raising hearth furnace is used for experiments which require higher operating temperatures (1550^{o}C) as compared to tube furnace mainly for melting of reduced samples and slag metal separation experiments. It consists of platform section which can be brought down to charge the samples after which it is raised into the furnace. The samples are charged in the furnace using a graphite crucible after the intended temperature is reached. The platform with the crucible is then raised into the heating zone. There is an exhaust fan to take out the hot air and for cooling purposes. Proximate analysis of boiler grade coal and LOI calculation of iron ore charge materials is carried out in this furnace. The image of the raising hearth furnace has been shown in Fig. 4.7.

Fig. 4.7: Raising hearth furnace

4.5 Reference

1. Hanel, M. B., Mali, H., Schenk, J.L., Skorianz, M., Hauzenberger, F., Thaler, C.; Stocker, H., Characterization of Different Lump Ore Brands According to Industrial Scale Process Conditions by Means of Reducibility Testing and Morphological Investigation, Proceedings of AISTech2013- Pittsburgh, USA, 2013, 447-456.
2. International Organization for Standardization: ISO 4695 Iron ores - Determination of reducibility (1995)
3. International Organization for Standardization: ISO 18894, 2006. Coke – Determination of Coke Reactivity Index (CRI) and Coke Strength after Reaction (CSR).

Chapter-5

Raw Material Characterisation, Selection and Preparation

5.1 Characterisation of Raw Materials

The samples have been characterized by X-ray diffraction (XRD) for phase analysis and wave length X-ray florescence (WDXRF) for composition analysis.

5.1.1 Iron Ore Charge Material

5.1.1.1 Iron Ore Lump

Iron ore samples have been collected from 3 different sources. The samples have been characterised using WDXRF and XRD analysis. {All the three samples will be subjected to reduction under the same conditions and the ore with the best extent of reduction will be considered for the research work}

5.1.1.1.1 WDXRF: The sized ore have been subjected to wave length dispersive x-ray florescence, the result is given in Table 5.1.

	Total Fe	SiO_2	Al_2O_3	MnO	MgO	CaO	TiO_2	Na_2O	K_2O	S, P_2O_5
Vizag	67.17	1.3	1.5	0.03	0.04	0.16	0.08	0.02	0.02	neg.
JSW	64.4	3.84	2.15	0.053	0.011	0.056	0.112	0.016	0.019	neg.
TATA Steel	64.4	3.3	2.05	0.019	0.001	0.05	0.31	0.032	0.047	neg.

Table 5.1: WDXRF result of the iron ore samples

It can be seen from the WDXRF data that the iron ore lumps have very less alkali content. The alkali (Na, K) have been introduced into the lumps artificially for this work.

5.1.1.1.2 X-Ray Diffractometer Analysis*:* Phase analysis of the iron ore samples has been carried out using X-ray diffraction spectrometer, the results are shown in Fig. 5.1 to 5.3 below. The d-values of high intensity peaks have been matched with the corresponding standards from PDF database.

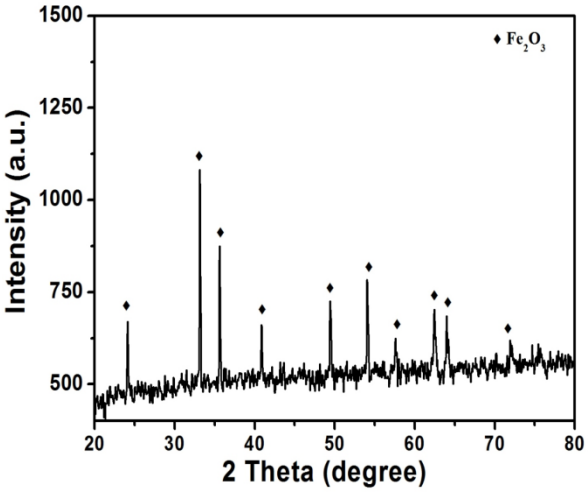

Fig. 5.1: XRD result of the iron ore from Vizag Steel plant

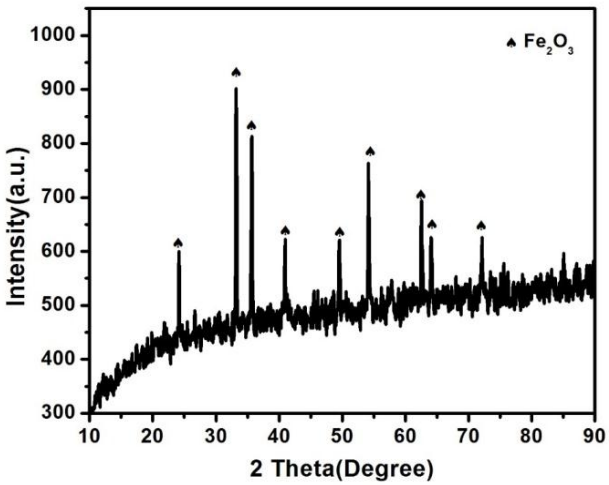

Fig. 5.2: XRD result of the iron ore from JSW

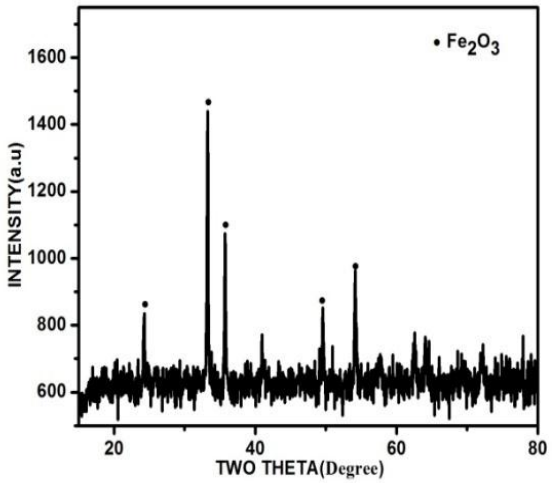

Fig.5. 3: XRD result of the iron ore from Tata Steel

From the diffractogram, hematite (Fe_2O_3) phase is present predominantly as the main phase in all the three iron ore lumps.

5.1.1.2 Pellets: Iron ore pellets have been collected from Tasmania, Australia and subjected to wave length dispersive x-ray florescence, the result is given in Table 5.2.

T Fe	FeO	Fe_2O_3	CaO	MgO	SiO_2	Al_2O_3	Mn	TiO_2	P	K_2O	Na_2O	S
65.47	0.8	92.47	0.19	1.86	2.56	0.54	0.07	0.79	0.012	0.03	0.03	Neg.

Table 5.2: WDXRF result of the iron ore pellet

It can be seen from the WDXRF data that the iron ore pellet has very less alkali content. The alkali (Na, K) have been introduced into the pellets artificially for this work.

5.1.1.2.1 XRD analysis of Pellet

Phase analysis of the iron ore pellets has been carried out by X-ray diffraction spectrometer, the result is shown in Fig. 5.4 below.

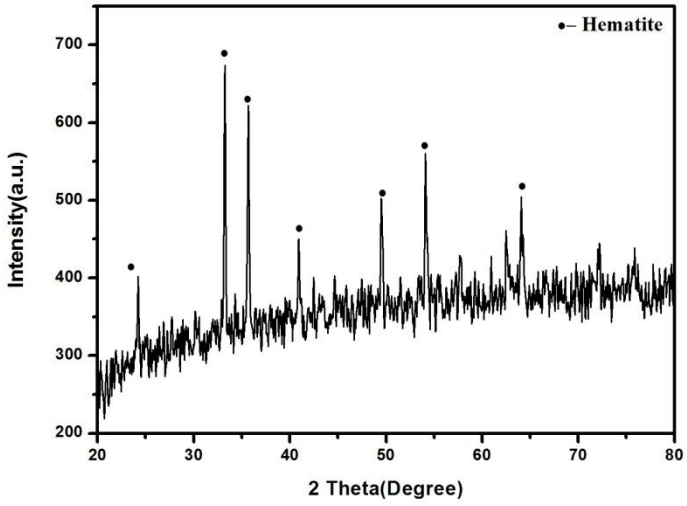

Fig.5.4: XRD result of the iron ore pellets

From the diffractogram, it can be seen that hematite (Fe_2O_3) phase is present predominantly as the main phase.

5.1.1.3 Sinter: Iron ore sinter has been collected from Vost Alpine Donawitz Steel plant, the sinter has been subjected to wave length dispersive x-ray florescence, the result is given in Table 5.3.

T Fe	FeO	Fe_3O_4	CaO	MgO	SiO_2	Al_2O_3	Mn	TiO_2	P	K_2O	Na_2O	S,P
54.805	8.255	66.81	8.805	2.64	6.88	1.875	1.58	0.12	0.05	0.48	0.06	Neg.

Table 5.3: WDXRF result of the iron ore sinter

It can be seen from the WDXRF data that the iron ore sinter has high potassium content. Sodium has been introduced into the sinters artificially for this work.

5.1.1.3.1 XRD Analysis of Sinter

Phase analysis of the iron ore sinters has been carried out by X-ray diffraction spectrometer, the result is shown in Fig. 5.5 below.

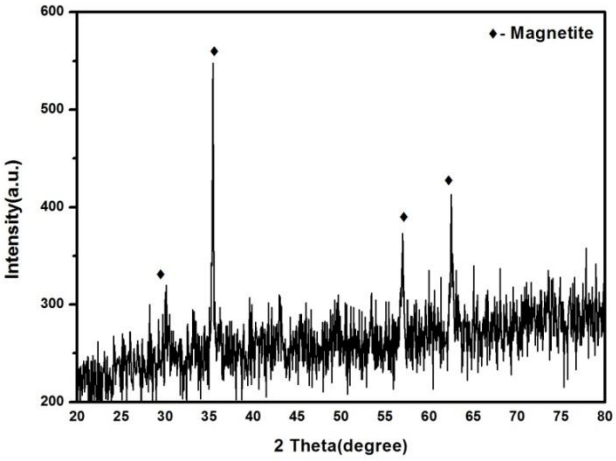

Fig.5.5: XRD result of the sinter

From the diffractogram, magnetite (Fe_3O_4) phase is present predominantly as the main phase.

5.1.2 Reductant

5.1.2.1 Boiler Grade Coal

Boiler grade coal has been used in these experiments. This coal is supplied by Vizag steel plant, along with the proximate analysis and the TG/DTA of the coal has been performed for its characterization.

5.1.2.1.1 Proximate Analysis: The results of the proximate analysis of the coal have been given in Table 5.4.

Percentage (%)	Boiler Grade Coal
Fixed Carbon	28.08
V.M	28.31
Moisture	7.40
Ash	36.21

Table 5.4: Proximate analysis of boiler grade coal

5.1.2.1.2 TG/DTA Analysis for Boiler Coal

The TG/DTA study of boiler grade coal is essential for the design of the direct reduction part of this work using coal as a reductant. The green line is the TG curve and the red line is the DSC curve. The nature of the weight loss agrees with the data from the proximate analysis of the boiler coal. The graph shows a weight loss up to 383K, which is due to the loss of moisture (7-8 %) from the coal. The major weight loss from 673-823K is because to the expulsion of the volatile matter (25-30 %). This is the single most important step during the gasification. The following weight loss which takes place at a very slow rate occurs due to mild oxidation or soot formation by the trace amount of oxygen present in nitrogen which is used as a shielding gas in the experiment

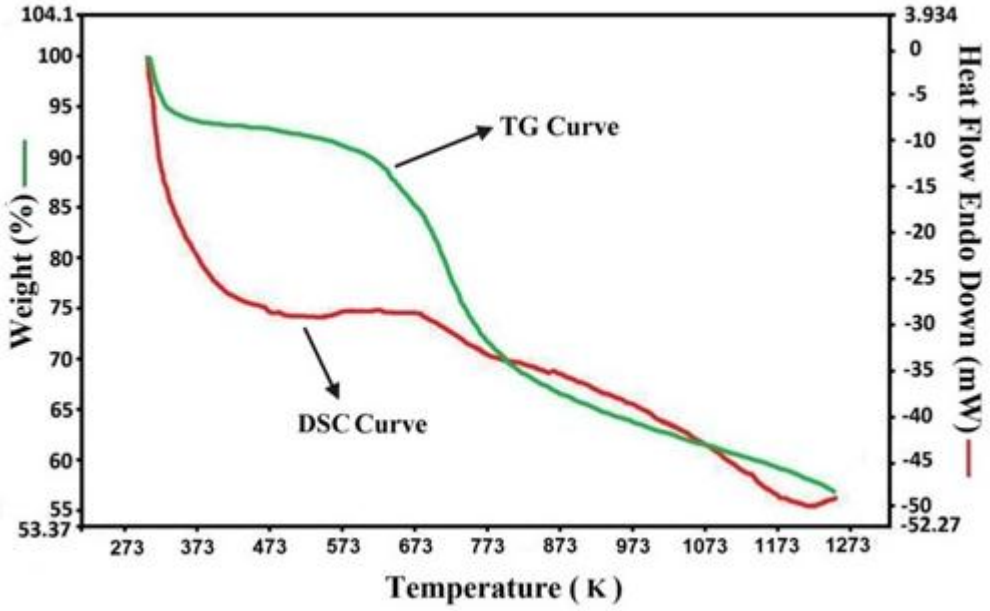

Fig.5.6: TG/DTA analysis for boiler coal

5.1.2.2 Coke

Two different industrial coke samples collected from Tata Steel and Vizag Steel plant have been used for the purpose of experiments.

5.1.2.2.1 Proximate Analysis

The results from proximate analysis of the coke samples are shown in Table 5.5.

Percentage (%)	Tata Steel	Vizag Steel Plant
Fixed Carbon	76.83	72.28
V.M	7.56	8.54
Moisture	0.65	0.84
Ash	14.96	18.43

Table 5.5: Proximate analysis of different coke samples

5.1.2.2.2 TG/DTA Analysis for Coke

Thermo gravimetric-differential thermal analysis of coke samples has also been performed in nitrogen atmosphere starting from room temperature to about 1000°C (1273 K) and is shown in Fig. 5C.1. From TG curve, initial weight loss has been observed at around 100°C (373 K)–200°C (473 K) because of the removal of moisture content from coke. Over the next temperature range of 400°C (673 K) to 600°C (873 K), weight loss takes place due to release of volatile matter of coke. The gradual weight loss up to 1000 °C (1273 K) has taken place due to the removal of residual volatile matter in coke.

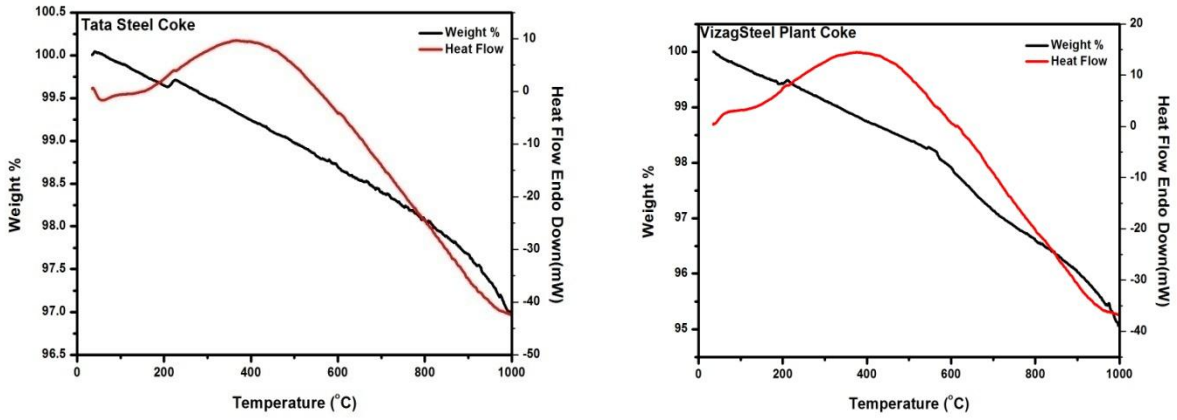

Fig. 5.7: The TG/DTA analysis of Tata steel coke and Vizag steel plant coke, respectively

5.1.3 Bentonite

Bentonite is generally used as the binding agent in pellet and briquette making in an iron and steel plant. Bentonite has swelling properties. The absorption of water leads to the swelling of bentonite which leads to restructuring of the atoms giving a higher bonding capacity to bentonite. Bentonite has been collected from Tata Steel Jamshedpur, Jharkhand, India. The composition of the bentonite used in this research work has been given in Table 5.6.

Typical constituents	Contents
SiO_2	59.10%
Al_2O_3	18.60%
Fe_2O_3	4.40%
CaO	1.90%
MgO	4.00%
K_2O	0.30%
Na_2O	2.50%
Moisture	6-12%
Loss on Ignition	8.90%

Table 5.6: Chemical composition of bentonite

5.1.4 Lime

Lime is used as flux in iron and steel making industry. Lime as well as dolomite is used to get rid of the gangue material present in the charge materials through slag metal separation to get a product of desired compositions. The addition of lime is very important since it is an indicator of the slag basicity due to presence of CaO. The composition of lime used in this research work has been collected from Tata Steel Plant, Jharkhand, India. The composition of lime used has been given in Table 5.7.

Typical constituents	Contents
Acid Insoluble Matter	2.00%
SiO_2	1.00%
Alumina	0.10%
Fe	0.25%
CaO	74.00% (Available lime as Calcium Oxide – 70%
MgO	0.60%
Carbon Dioxide	0.80%
Mn	0.01%
Moisture	0.30%
Calcium Carbonate ($CaCO_3$)	1.8%
Calcium Hydroxide [$Ca(OH)_2$]	95.00%

Table 5.7: Composition of lime

5.1.5 Dunite

Dunite is an ultrabasic igneous rock mainly consisting of olivine. Dunite is also used a flux in iron and steel making plant. Dunite has been used to attempt the removal of alkali from blast furnace conditions through slag metal separation. Dunite has been procured from Industrial Minerals and Refractories, Salem, Tamil Nadu, India. The composition of Dunite is given in Table 5.8.

Constituents	Content(%)
MgO	44.55
SiO2	39.6
Fe2O3	9.12
Al2O3	1.64
CaO	1.68
LOI	2.05

Table 5.8: Composition of dunite

5.1.6 Other Chemical Compounds

Alkali compound have been used to artificially increase the alkali content of the iron ore charge materials and coke samples. Sodium hydroxide and potassium hydroxide pellets have been used to make alkali solutions of different concentration depending on the amount of alkali we want to introduce in the raw materials. These alkali pellets have been acquired from Merk Life Science Private ltd.. The composition of the alkali hydroxide pellets used has been given below.

Assay (Na, KOH)>= 97%

Carbonate (Na, K_2CO_3)=<2%

Other chemicals like magnesium hydroxide and magnesium silicate have also been acquired. These chemicals have been used as flux during smelting for removal of alkali through slag.

5.2 Iron Ore Selection

5.2.1 Reduction of Iron Ore Samples under Similar Direct Reduction Conditions

The collected iron ore samples have been reduced under the same conditions i.e. 1000^{o}C, time 60 minutes. The samples have been reduced in a tube furnace. The iron ore samples of specific size range (-18.75mm - +12.5mm) have been selected. The iron ore lump along with stoichiometric amount of reductant, in this case boiler grade coal; have been put inside an inconel tube. When the furnace has reached the desired temperature the inconel tube is placed inside the tube in such a way that the sample is located in the main heating zone of the tube furnace. After 60 minutes of reduction the mouth of the inconel tube is closed so that no re-oxidation can take place as the inconel tube cools. When the inconel tube cools down the sample is taken out and separated from the burnt coal and weighed. The final weight of the sample is used to calculate the extent of reduction (EOR). Calculation of EOR has been shown in Appendix-I. The results of the reduction for iron ores from different sources is given in the Table 5.9 below:

Iron Ore Source	Extent of Reduction (EOR in %)
TATA STEEL	64.63
VIZAG STEEL PLANT	60.52
JSW	58.76

Table 5.9: EOR of different iron ore lumps

The iron ore collected from Tata Steel, Jamshedpur has the highest extent of reduction under the same direct reduction conditions among the other sources. For the purpose of our work in this thesis we have chosen the iron ore sample with the highest degree of reduction.

5.2.2 Impregnation of Iron Ore Charge Material with Alkali

Only in the case of sinters, we have chosen a sample which innately possess high percentage of alkali; in this case potassium. There is no need to dope the sinter samples with potassium (only sodium) since it contains high potassium load. The iron ore lumps, briquettes and pellets have been impregnated with alkali using different methods depending on the iron ore charge material, which have been discussed in the next part.

5.2.2.1 Impregnation of Iron Ore Lumps, Pellets and Sinters with Sodium and Potassium

The iron ore lumps collected from Tata Steel have been crushed using a hammer. The collected iron ore lump pieces have been separated according to size. In our experiments we have chosen lumps in the size range of (-18.75mm - +12.5mm), previously tested samples showed if more pieces of samples have been added to the inconel tube during reduction they reduced differently. This happened due to the limited main heating zone in the tube furnace. These iron ore lumps have been taken and put in different alkali solutions. Solutions of sodium hydroxide and potassium hydroxide have been made at five different concentrations (1M, 2M, 3M, 4M and 5M).

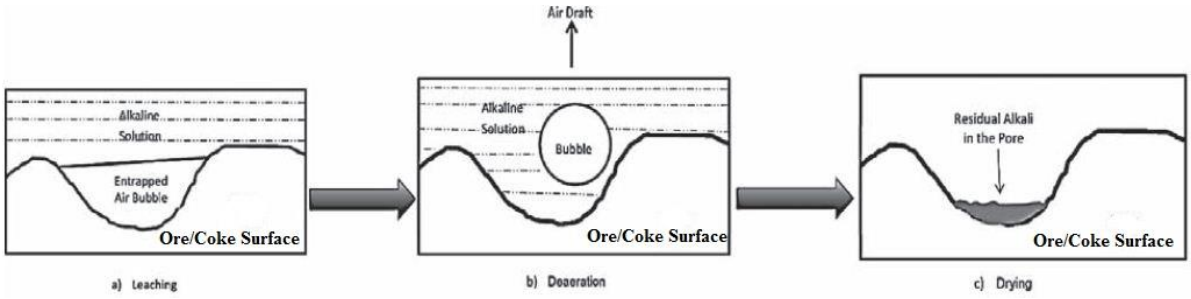

Fig. 5.8: Schematic of alkali impregnation process

The solution along with the iron ore lumps have been kept in a desiccator; which has vacuum pump attached to it. After the pump is switched on there is bubbling due to the solution entering the pores of the iron ore lumps. The pump is switched off after the bubbling stops. The samples are taken out and heated at 100^{o}C for 2 hrs to remove the excess moisture. After the samples have completely dried we measure the final weight and find out the amount of alkali gained. Analysing the final alkali gain percentage and along with the literature two different concentration of alkali solutions have been selected (too high alkali gain percentage will lead to decrease in reduction and strength of the iron ore lumps). In case of iron ore lumps 2M and 4M concentrations have been selected. The average alkali gain is given below:

Alkali Solution Concentration	Alkali Gain (%)
2M NaOH	0-0.10
4M NaOH	0.20-0.35
2M KOH	0-0.15
4M KOH	0.20-0.40

Table 5.10: Alkali gain in iron ore lumps

Similarly, in case of iron ore pellets the pellets have been doped with alkali using 2M and 4M sodium hydroxide and potassium hydroxide solutions. The collected sinters innately have high percentage of potassium so; sinters have been doped only with 2M and 4M sodium hydroxide solutions.

5.2.2.2 Iron ore Briquetting and Addition of Sodium and Potassium

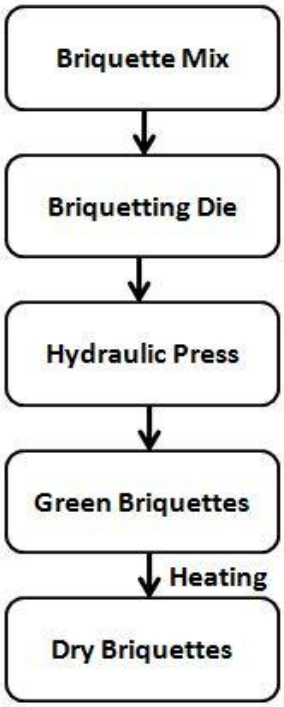

The iron ore fines, bentonite and alkali solution have been mixed together and then put in the die. The die has been put in an automatic hydraulic press which puts load on the die. After this, 200kg load is applied on to the die; we wait for few minutes and take the die out. The briquettes have been taken out and heated to get rid of the excess moisture. Iron ore briquettes could not be impregnated in the same way as the other iron ore charge materials. The briquettes break as soon as they are put in the alkali solution. The alkali has been added with the help of micropipette along with the other briquetting materials while making the briquette mix (calculation shown in Appendix-II).

Fig. 5.9: Flow diagram of briquetting

Alkali Solution Concentration	Alkali Gain (%)
2M NaOH	0.20
4M NaOH	0.40
2M KOH	0.225
4M KOH	0.45

Table 5.11: Alkali gain in iron ore briquettes

Chapter-6

Optimization of the Alkali Content in Iron Ore Lumps by the Use of Statistical Modelling via Box Behnken Design and Its Effect on Reducibility and Kinetics under Direct Reduction Conditions

6 Design of Experiment

Reduction of iron ore lumps with and without added alkali by boiler grade coal has been performed at varying time, temperature and concentration of alkali content. Response surface methodology i.e. Box Behnken design in this case has been adopted to find the optimum process parameters.

6.1 Box Behneken Design

The Box Behnken Design modelling has been used as discussed in chapter 3, section 3.4.1. The different parameters and their range have been given in Table 6.1. The model uses these parameters and their range to provide us with 17 set of tests under different conditions. The 17 set of test conditions have been given in a tabulated form in Table 6.2.

Serial	Parameters	Unit		Lower	Higher	-1	0	1
1	Temperature	Deg C	C	1000	1100	1000	1050	1100
2	Time	Minutes	B	30	60	30	45	60
3	Alkali(KOH/NaOH)	M	A	0	4	0	2	4

Table 6.1: Range and coded parameter levels of experimental variables used to reduce iron ore lumps for Box–Behnken design

Sl.No.	Temperature (Degree C)	Time (Minutes)	Concentration (M)
1	1000	30	2
2	1000	45	0
3	1000	45	4
4	1000	60	2
5	1050	30	0
6	1050	30	4
7	1050	45	2
8	1050	45	2
9	1050	45	2
10	1050	45	2
11	1050	45	2
12	1050	60	0
13	1050	60	4
14	1100	30	2
15	1100	45	0
16	1100	45	4
17	1100	60	2

Table 6.2: Details of all 17 sets of reactions as provided by BBD

6.2 Reduction of Iron ore lumps under Direct Reduction Conditions

A tube furnace has been used for the reduction of alkali impregnated iron ore lumps according to set of reactions given by box behnken design. An inconel tube is used to provide a closed environment for reduction of lumps. The lumps are placed in an inconel tube along with stoichiometric amount of coal required for reduction. During reduction the gases come out of the outlet tube. When the furnace is switched off the outlet is closed so that air does not enter leading to re-oxidation. After the inconel tube has cooled down the sample is taken out and the extent of reduction (EOR) is calculated.

6.3 Box Behnken Design Model for Iron Ore Lumps

The results of the 17 set of reductions of iron ore lumps under direct reduction conditions according to the Box Behnken design have been given in the Table 6.3. (Calculation of extent of reduction is shown in Appendix-I).

Sl.No.	Temperature (Degree C)	Time (Minutes)	Concentration (M)	Extent of Reduction of Lump with KOH (%)	Extent of Reduction of Lump with NaOH (%)
1	1000	30	2	41.22	40.55
2	1000	45	0	42.03	42.03
3	1000	45	4	57.32	66.35
4	1000	60	2	65.98	75.82
5	1050	30	0	40.41	40.41
6	1050	30	4	65.22	60.40
7	1050	45	2	64.91	68.67

8	1050	45	2	63.45	67.42
9	1050	45	2	66.23	66.89
10	1050	45	2	65.78	69.34
11	1050	45	2	64.50	68.10
12	1050	60	0	67.60	67.60
13	1050	60	4	85.76	78.10
14	1100	30	2	57.27	61.92
15	1100	45	0	66.31	66.31
16	1100	45	4	59.75	91.60
17	1100	60	2	88.33	80.39

Table 6.3: Extent of reduction of iron ore lump samples with added potassium and sodium for the 17 set of reactions (Box Behnken Design)

6.3.1 Statistical Analysis of the Reduction of Alkali Added Iron Ore Lumps

Optimization of the process variables (alkali concentration, time and temperature) has been carried out in order to maximize the extent of reduction (%) of the iron ore lumps with added potassium and sodium within the framework of BBD (Table 6.3). This design predicted the optimum combination of potassium hydroxide concentration of 1.82M, time of 60 min and temperature of $1100^{O}C$ for an optimized EOR of 85.89%. This design predicted the optimum combination of sodium hydroxide concentration of 4M, time 57.34 min at a temperature of $1100^{O}C$ for an optimized EOR of 84.5%. Fig. 6.1 shows the Normal probability plot of the studentized residuals which confirms the normality of residuals. Fig. 6.2 shows the plot of predicted versus actual extent of reduction of iron ore lumps impregnated with potassium and

sodium, respectively. From this figure, it can be seen that the points are lying close to the straight line and this thus indicates that the experimental yield is fairly close to the yield predicted by the BBD.

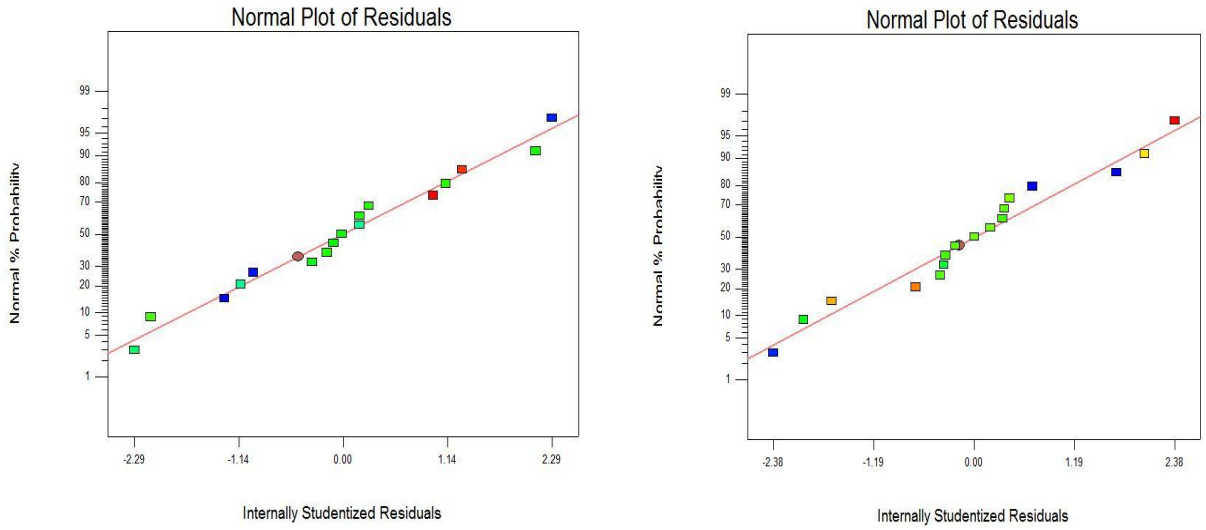

Fig. 6.1: The normal plot of residuals for iron ore lumps with added a) Potassium and b) Sodium

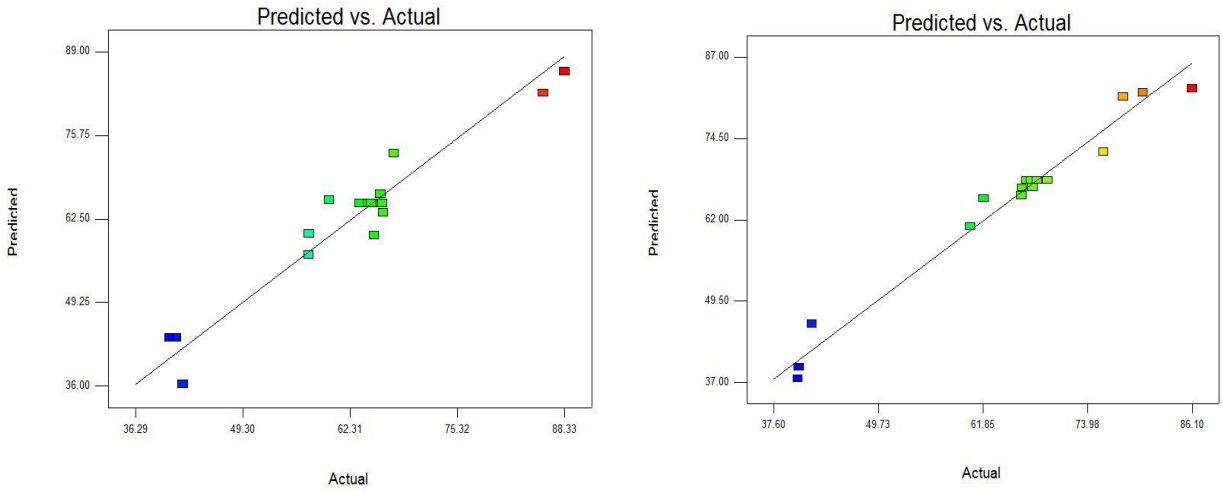

Fig. 6.2: The predicted vs. actual plots of iron ore lumps with added a) Potassium and b) Sodium

6.3.2 Analysis of Variance (ANOVA)

The ANOVA of the quadratic model for the optimization of reduction of lumps of iron ore with boiler grade coal with added alkali i.e. potassium hydroxide and sodium hydroxide have been listed in the Table 6.4 below.

Model for added Potassium:

The Model F-value of 27.19 implies that the model is significant. There is only a 0.01% chance that a "Model F-Value" this large could occur due to noise. Values of "Prob > F" less than 0.0500 indicate model terms are significant. In this case A, B, C and AB are significant model terms. Values greater than 0.1000 indicate the model terms are not significant. "Adeq Precision" measures the signal to noise ratio. A ratio greater than 4 is desirable. Here, the ratio of 17.432 indicates an adequate signal. This model can be used to navigate the design space. The R-srquared value of 0.9722 is also very good.

Model For added Sodium:

The Model F-value of 11.23 implies that the model is significant. There is only a 0.22% chance that a "Model F-Value" this large could occur due to noise. Values of "Prob > F" less than 0.0500 indicate model terms are significant. In this case A, B, C are significant model terms. Values greater than 0.1000 indicate the model terms are not significant. "Adeq Precision" measures the signal to noise ratio. A ratio greater than 4 is desirable. Here, the ratio of 12.868 indicates an adequate signal. This model can be used to navigate the design space. The R-srquared value of 0.9352 is also very good.

Statistical Results	KOH Model	NaOH Model
Model *F*-value	11.23	27.19
Model prob.> F	<.05	<.05
R-Squared	0.9352	0.9722
CV%	8.04	6.77
Adjusted R- squared	0.8519	0.9364
Adequate precision	12.868	17.432

Table 6.4: Statistical results of ANOVA for iron ore with lumps added potassium and sodium

6.3.3 Extent of Reduction of Iron Ore Lumps with Added Potassium and Sodium

Data obtained from the 17 batch runs have been analyzed using the Design Expert 7.0.0 software and the following second-order polynomial equations for extent of reduction (%) of iron ore lumps with added potassium and sodium have been generated:

$$EOR_{KOH} = -2387.71550 + 4.44851 * Temp - 2.55545 * Time + 66.61825 * KOH + 2.10000E-003 * Temp * Time - 0.054625 * Temp * KOH - 0.055417 * Time * KOH - 2.03380E-003 * Temp^2 + 0.014713 * Time^2 - 0.88425 * KOH^2$$

$$EOR_{NaOH} = -457.39300 + 0.38405 * Temp + 8.25688 * Time + 23.07700 * NaOH - 5.60000E-03 * Temp * Time - 0.011325 * Temp * NaOH - 0.079083 * Time * NaOH + 3.12000E-005 * Temp^2 - 0.015520 * Time^2 - 0.74112 * NaOH^2$$

Fig. 6.3 shows the second-order 3D response surface plot along with contour plot for extent of reduction (%) of iron ore lumps with added potassium as a function of duration of reduction and potassium hydroxide concentration; in Fig. 6.4 the second-order 3D response surface plot for extent of reduction (%) of iron ore with added potassium is shown along with the contour plot as a function of temperature of reduction and concentration of potassium hydroxide in iron ore lumps. Fig. 6.5, shows the second-order 3D response surface plot along with contour plot for extent of reduction (%) of iron ore lumps with added sodium as a function of duration of reduction and sodium hydroxide concentration; in Fig. 6.6 the second-order 3D response surface plot for extent of reduction (%) of iron ore with added sodium is shown along with the contour plot as a function of temperature of reduction and concentration of sodium hydroxide in iron ore lumps.

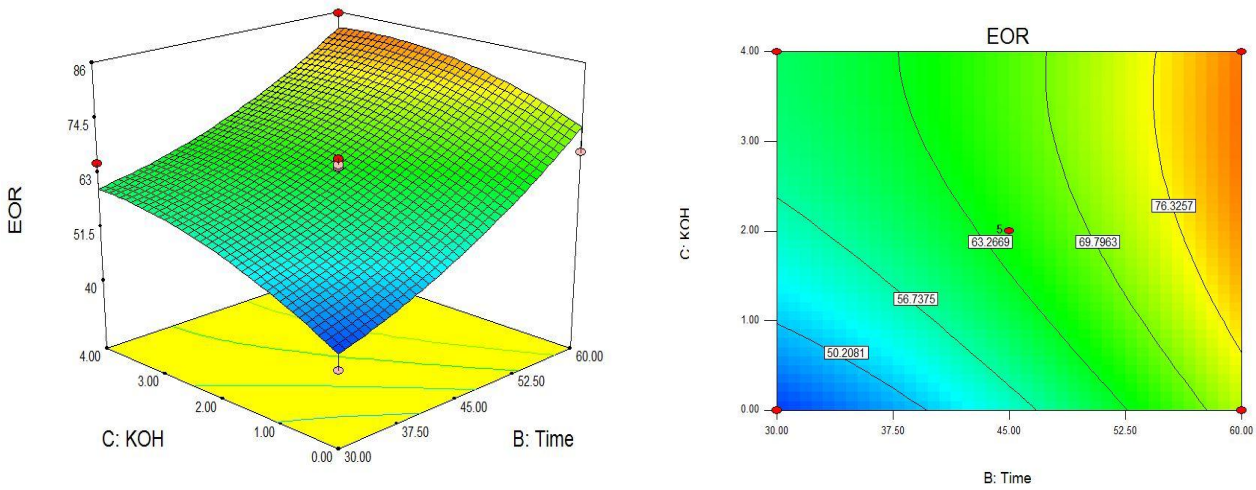

Fig. 6.3: The second-order 3D response surface plot and the contour plot for extent of reduction (%) of iron ore is shown as a function of duration of reduction and concentration of potassium hydroxide in iron ore lumps

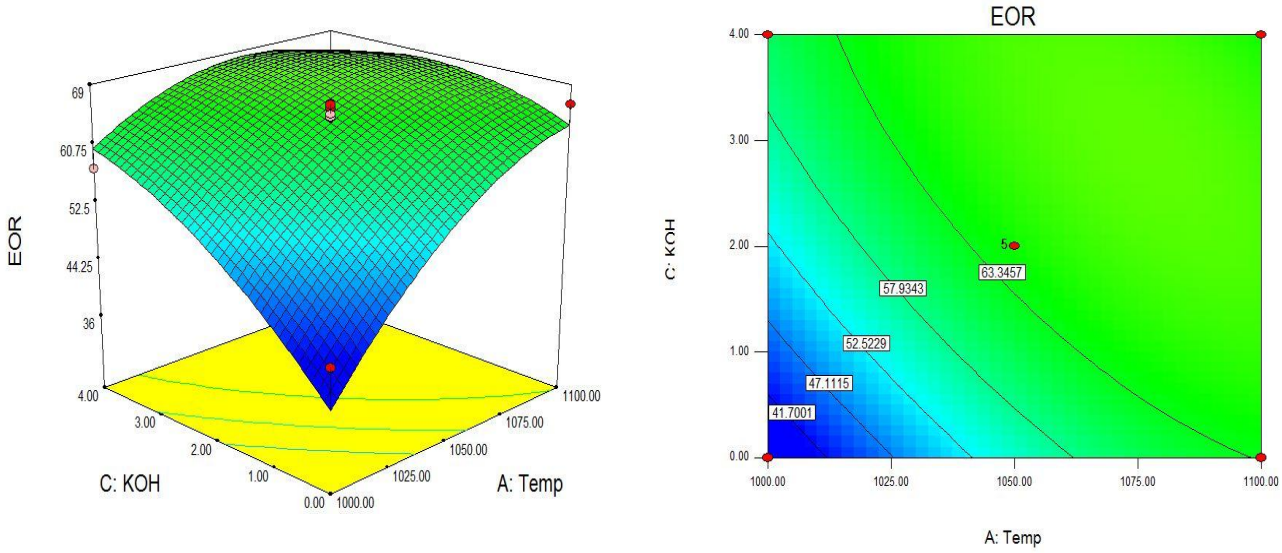

Fig. 6.4: The second-order 3D response surface plot and contour plot for extent of reduction (%) of iron ore lumps is shown as a function of temperature of reduction and concentration of Potassium Hydroxide in iron ore lumps

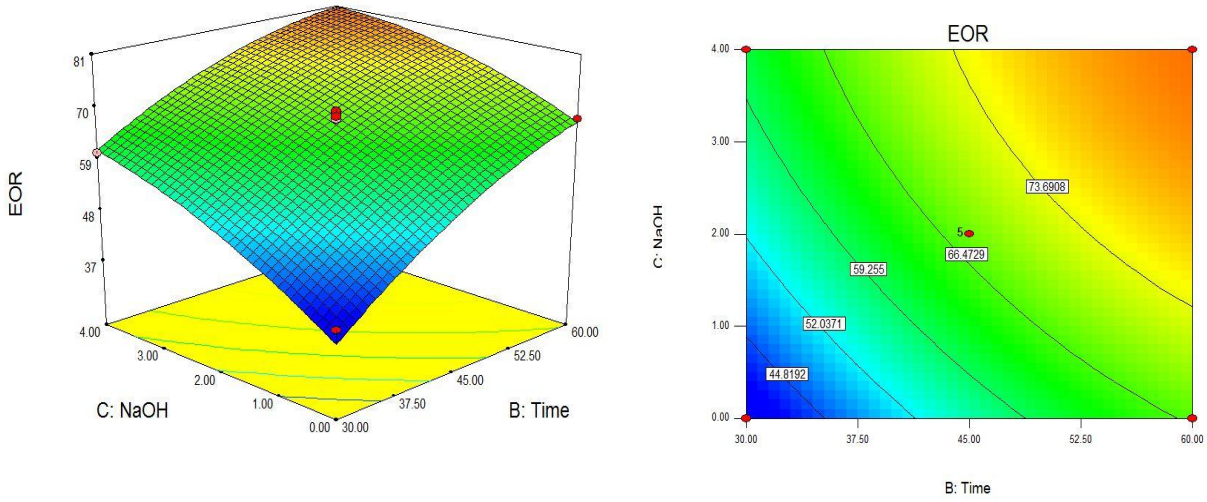

Fig. 6.5: The second-order 3D response surface plot and the contour plot for extent of reduction (%) of iron ore lump is shown as a function of duration of reduction and concentration of sodium hydroxide in iron ore lumps

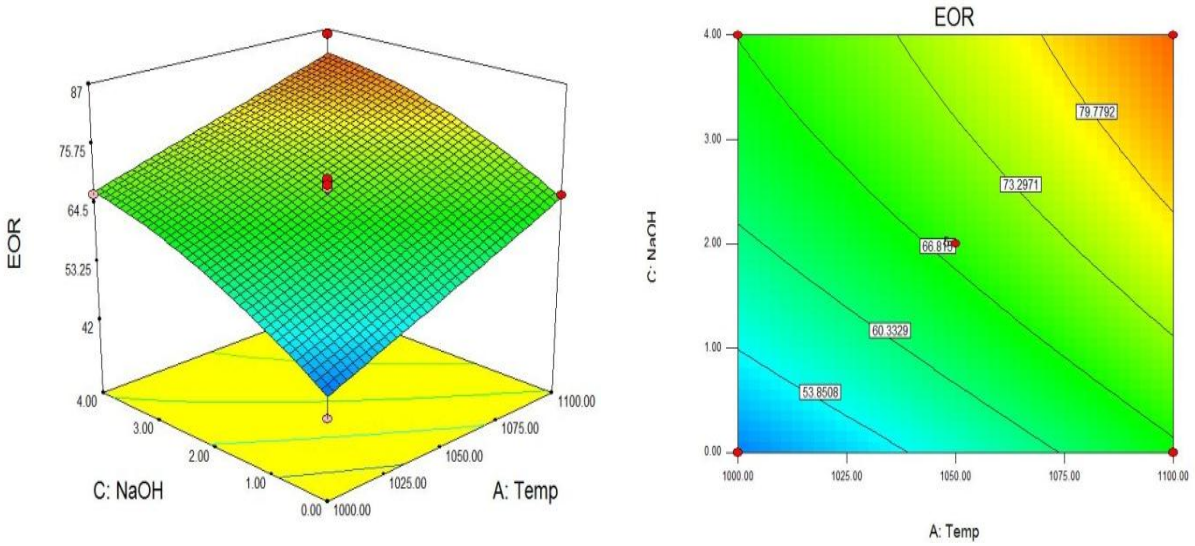

Fig. 6.6: The second-order 3D response surface plot and contour plot for extent of reduction (%) of iron ore lumps is shown as a function of temperature of reduction and concentration of Sodium Hydroxide in iron ore lump

6.4 The Effect of Alkali Content, Time and Temperature on the Iron Ore Lump Reduction.

The iron ore lumps impregnated with sodium and potassium have been reduced at three different temperatures and six different times to understand their effect on the reduction of iron ore lumps under direct reduction condition. The reduction is carried out in the same manner as described in section 6.2.

The different parameters selected for the reduction process are given below:

- Alkali Concentration (M): 0M, 2M and 4M (0M means no alkali addition)
- Time (min): 5,10,15,30,45 and 60
- Temperature (^{o}C): 1000, 1050 and 1100

The extent of reduction calculated from the final weight indicates the effect the different parameters including alkali concentration have on the reduction of iron ore lumps. The extent of reduction for the iron ore lumps under different parameters has been given in Table 6.5.

Temperature (°C)	Time (Min.)	STD EOR (%)	2M NaOH EOR (%)	4M NaOH EOR (%)	2M KOH EOR (%)	4M KOH EOR (%)
1000	5	13.37	14.06	14.56	14.10	15.17
	10	27.59	27.78	28.35	27.91	29.64
	15	31.52	36.61	38.04	38.27	42.89
	30	39.63	40.55	46.36	41.23	55.15
	45	50.03	60.47	66.35	56.47	59.76
	60	64.63	73.23	76.07	65.98	68.48
1050	5	16.78	22.20	24.44	23.45	28.79
	10	29.86	31.65	34.82	34.07	36.89
	15	32.51	39.32	43.36	39.91	43.94
	30	40.41	51.55	60.40	48.72	65.22
	45	63.13	68.67	71.69	64.91	77.69
	60	67.60	75.82	78.10	82.49	85.76
1100	5	21.86	23.25	26.61	30.84	34.68
	10	33.06	36.26	38.76	34.50	39.78
	15	39.62	40.01	45.37	41.18	42.54
	30	49.95	61.92	69.62	57.27	52.88
	45	66.31	69.85	860	70.79	57.32
	60	78.31	80.39	91.60	88.33	60.13

Table 6.5: Extent of reduction of iron ore lumps with and without added alkali under different reduction conditions

At 1000^{o}C, as time increases the EOR also increases for fixed alkali. The increase in alkali also leads to an increase of reducibility at fixed time. Sodium added lumps show higher reducibility at same time as compared to potassium added lumps after 30 minutes of reduction (for both 2M and 4M added samples). At 1050^{o}C, potassium and sodium addition increases the reducibility for same time of reduction. 2M NaOH added lumps show better reduction compared to 2M KOH added lumps after 30 minutes of reduction. Potassium (2M) is seen to have a higher effect on reduction compared to sodium for 60 minutes of reduction. 4M KOH added samples have higher reducibility compared to 4M NaOH added samples at 1050^{o}C. At 1100^{o}C, reduction of lump samples increases with time except for the 4M KOH samples. In case of 4M KOH iron ore lumps, the reducibility increases with time till 1050^{o}C. At 1100^{o}C the reducibility increases till 15 minutes but after that the rate of reducibility reduces drastically. The reducibility of the samples reduced for more than 15 minutes is even lower compared to standard iron ore lump samples. The effect of potassium is higher on the reducibility of lumps compared to sodium at 1100^{o}C. The high amount of potassium (0.3-0.4%) leads to cracking and disintegration of the lumps leading to closed of pores which impede the reducibility of the lump samples [6]. Initially the phase transformation from hematite to magnetite leads to volume expansion which in turn gives rise to cracking. Silica rich gangue along with alkali and ferrous oxide form primary liquid slag. Their formation and movement between iron oxide grains causes the binding phases to disintegrate during reduction. The increase in reduction leads to growth of large iron crystals which induces more stress resulting in a higher tendency towards cracking.

6.4.1 Effect of Sodium on the Reducibility of Iron Ore Lumps

The extent of reduction (EOR) of the iron ore lumps impregnated with sodium have been calculated as shown in Table 6.5. The plots of extent of reduction for different sodium content at different time and temperatures have been shown in Fig. 6.7, Fig. 6.8 and Fig. 6.9.

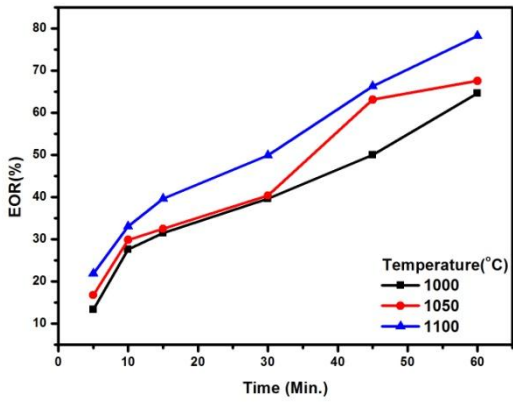

Fig.6.7: EOR of standard iron ore lumps at different time and temperature

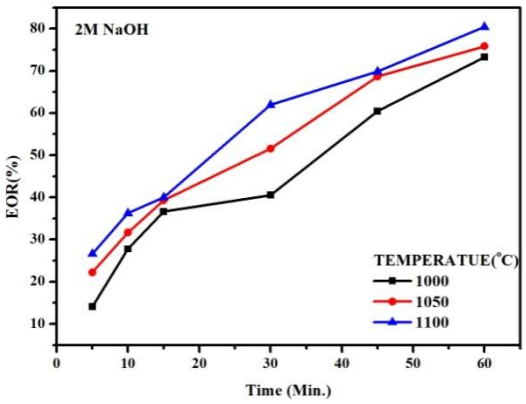

Fig.6.8: EOR of sodium (2M) added iron ore lumps at different time and temperature

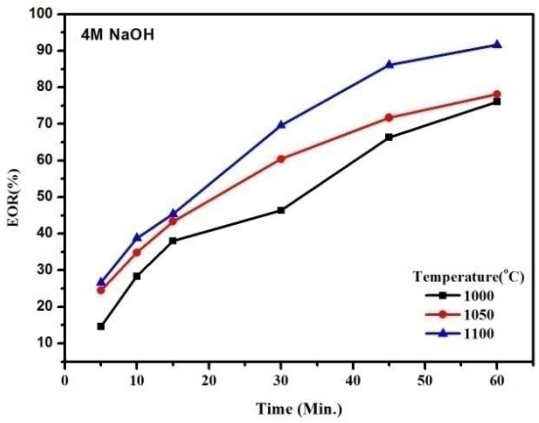

Fig.6.9: EOR of sodium (4M) added iron ore lumps at different time and temperature

It can be seen in Fig. 6.7 that the extent of reduction of the standard iron ore lumps increases with an increase in time and temperature. The highest EOR at 1000^{o}C is at the highest time i.e. 60 minutes. The highest EOR is observed at 1100^{o}C and 60 min reduction time. This

trend holds true even for the reduction of sodium added iron ore lumps. The EOR for sodium added iron ore lumps is greater than in case of standard iron ore lumps. As the content increases EOR increases further. The highest EOR is 91.60% when iron ore lumps with added sodium are reduced for 60 minutes at 1100°C as seen in Fig. 6.9.

6.4.2 Effect of Potassium on the Reducibility of Iron Ore Lumps

The extent of reduction (EOR) of the iron ore lumps impregnated with potassium have been calculated as shown in Table 6.5. The plots of extent of reduction for different potassium content at different time and temperatures have been shown in Fig. 6.10 and Fig. 6.11.

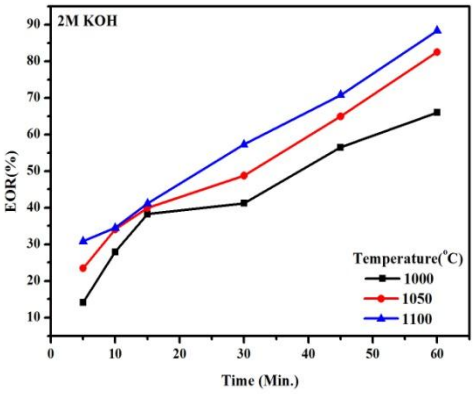

Fig.6.10: EOR of potassium (2M) added iron ore lumps at different time and temperature

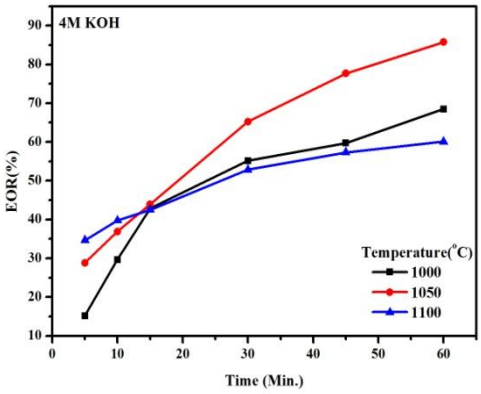

Fig.6.11: EOR of potassium (4M) added iron ore lumps at different time and temperature

The extent of reduction of the potassium added iron ore lumps also increases with time and temperature. The EOR of potassium added iron ore lumps (2M) increases with time and temperature; highest EOR of 88.33% is achieved at 1100°C and 60 minutes of reduction. The EOR at 1000°C for potassium added iron ore lumps (4M) increases with time. The EOR in case of potassium added samples (4M) increases very slowly after 30 minutes of reduction time. At 1050°C potassium added iron ore lumps (4M) have the highest rate of reduction with

EOR of 85.76%. But at 1100°C the potassium added iron ore lumps (4M) show very low rate of reduction after 15 minutes of reduction with highest EOR of 60.13%.

It can be seen from Fig. 6.7 to Fig. 6.11 that addition of alkali increases the extent of reduction with time, temperature and with the amount of sodium and potassium. The increase in EOR is higher in case of added potassium as compared to added sodium samples. In case of potassium (4M), as can be seen in Fig. 6.11 at the highest temperature the rate of reduction decreased as the duration of reduction increased more than 15 minutes. The amount of added sodium (4M) is helping with the reduction; although the strength of samples reduced at higher temperatures and for longer duration decreases and leads to breakdown into smaller pieces. In case of added potassium (4M) although cracks have been generated yet the sample did not disintegrate into smaller pieces. Thus, if the amount of sodium and potassium present in the iron ore charge material can be regulated they can help improve the reducibility of iron ore lumps even while using poor grade reductant as boiler grade coal.

6.5 XRD Analysis of Reduced Iron Ore Lumps

Fig. 6.12 depicts XRD of the reduced samples under different conditions. This confirms that in all cases iron ore lumps have been almost completely reduced to metallic iron.

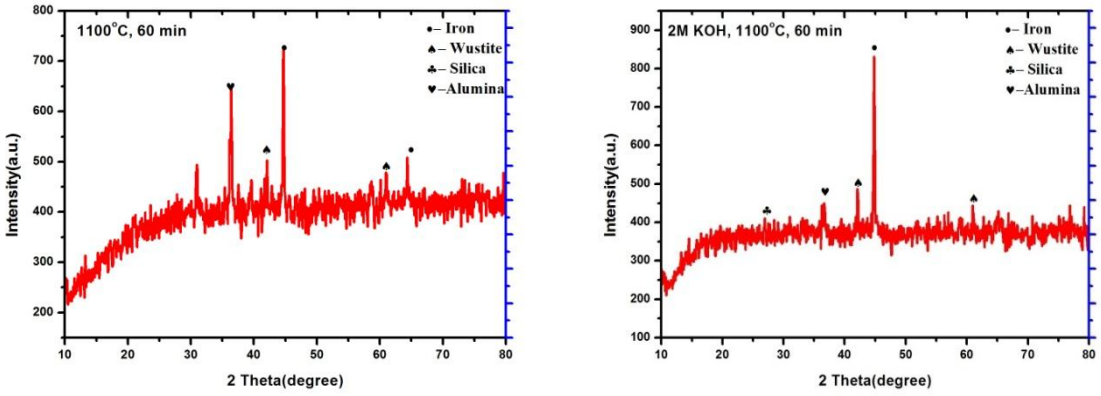

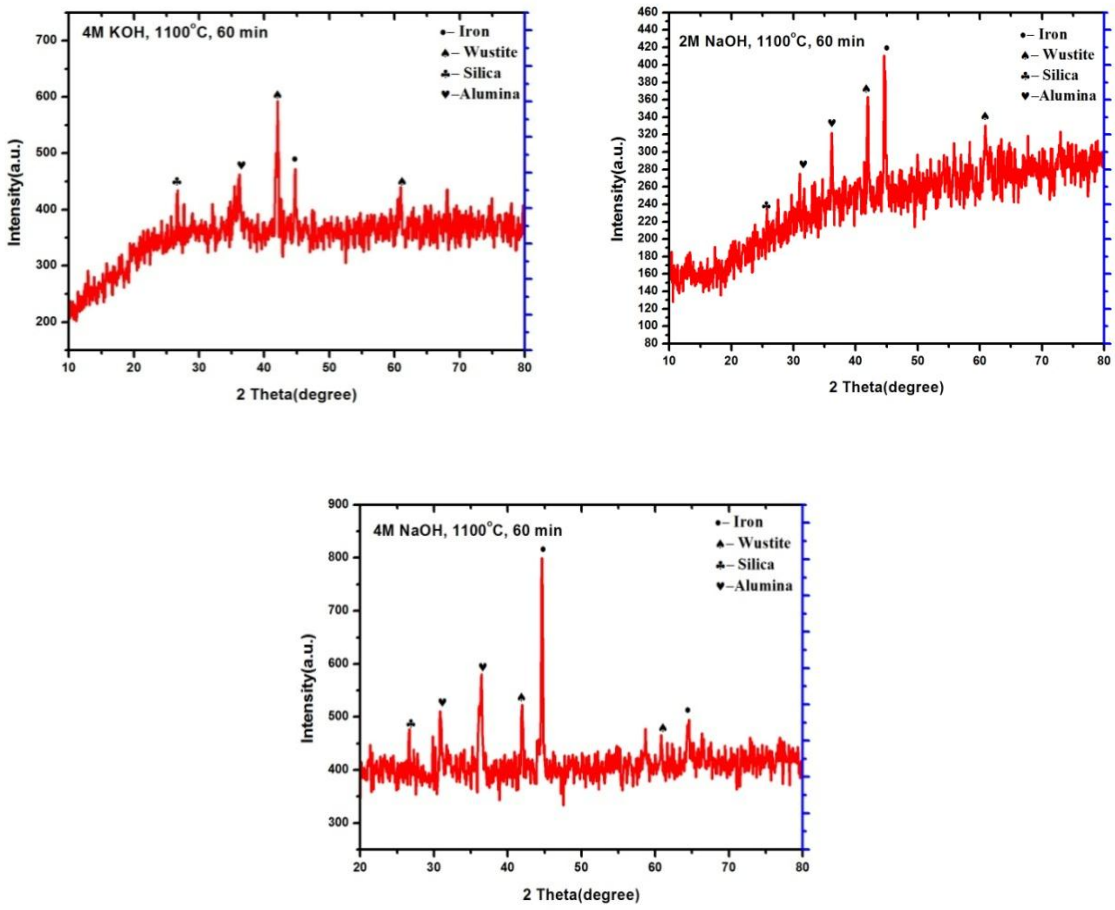

Fig. 6.12: XRD analysis of with and without alkali reduced iron ore lumps

The alkali added iron ore lumps have greater peaks of iron along with peaks of wustite and small peaks of alumina and silica. The 4M KOH lumps have highest peak of wustite which agrees with the extent of reduction. In case of all other iron ore lumps with alkali the peak of iron is highest. This indicated good reduction has taken place.

6.6 Isothermal Kinetic Study

The isothermal kinetic study of reduction of lumps using boiler grade coal has been carried out. Iron ore lumps have been reduced at 1000ºC, 1050ºC and 1100ºC for 5, 10, 15, 30, 45 and 60 minutes. The reduced time analysis as discussed in Chapter 3, section 3.5 has been carried out using experimental data to find the reaction mechanism being followed under different alkali loading at different temperatures.

6.6 Isothermal Kinetic Study of Reduction of Lumps

In the present study of the isothermal reduction kinetic, the fractional weight loss (α) is defined as:

$$\alpha = \frac{M_t}{M_0} \qquad 1$$

where, M_0 is the weight of oxygen in the iron ore lumps and M_t is the weight loss due to oxygen removal from iron ore during reduction by boiler grade coal in the tube furnace. So, α, defined by Eq. 1, gives the isothermal weight fraction loss as a function of time. These data have been graphically plotted in Fig. 6.13.

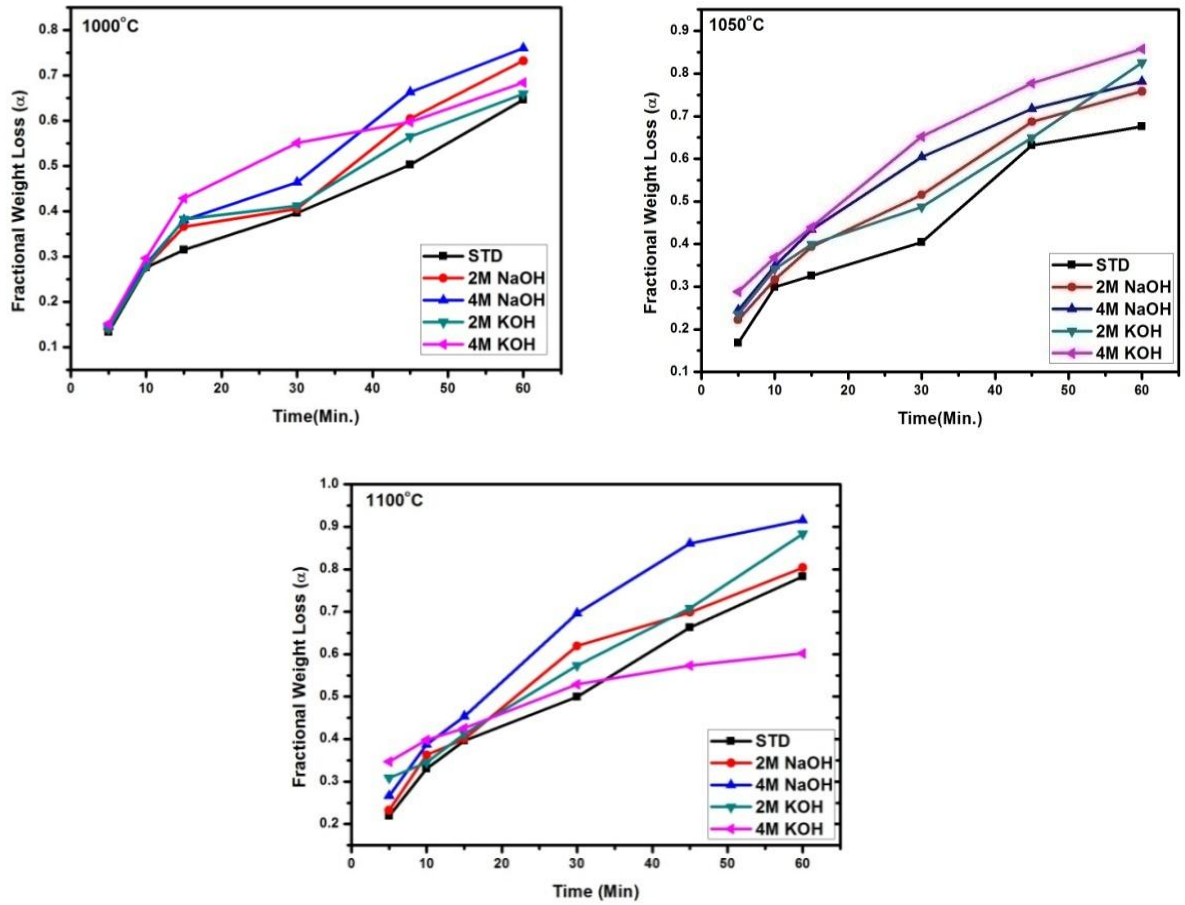

Fig. 6.13: Fractional weight loss (α) vs. time for lumps with and without alkali at different temperature and time

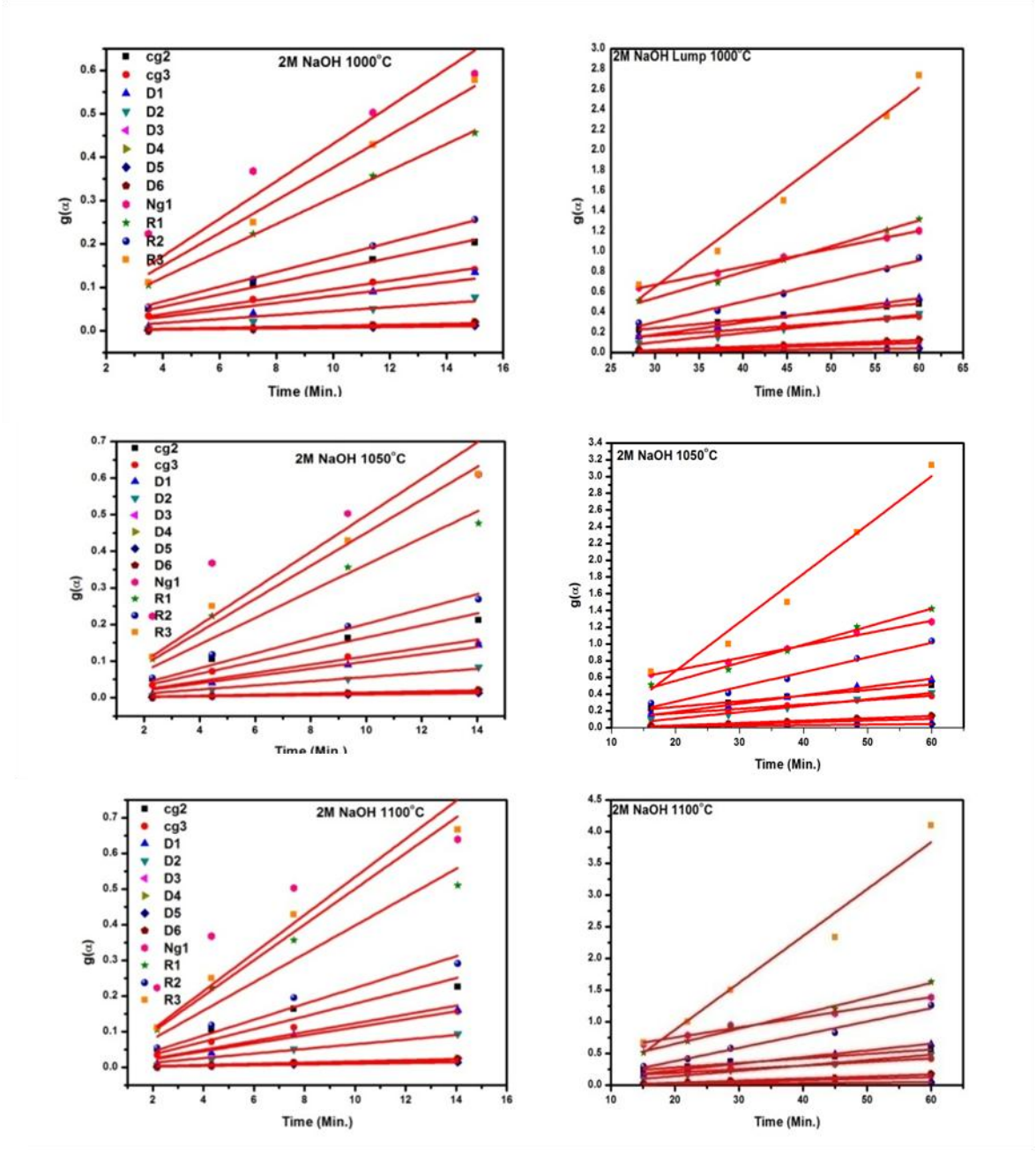

Fig. 6.14: Various mechanism models fitting showing the lump reduction vs. Time for different iron ore lump samples (Initial and final stages of reduction, respectively) (The various mechanism model fittings for the other samples has been given in Appendix-I)

Standard	CG2	CG3	D1	D2	D3	D4	D5	D6	Ng3	R1	R2	R3
1000ºC	0.989	0.990	0.985	0.982	0.981	0.978	0.989	0.978	0.962	0.993	0.995	**0.997**
	0.981	0.978	**0.971**	0.959	0.954	0.942	0.979	0.942	0.980	0.969	0.955	0.937
1050 ºC	0.939	0.942	0.966	0.966	0.966	0.966	0.965	0.966	0.900	0.946	0.953	**0.959**
	0.902	0.911	0.917	0.937	0.944	0.956	**0.902**	0.956	0.907	0.928	0.950	0.966
1100 ºC	0.969	0.973	0.991	0.988	0.986	0.983	0.994	0.983	0.923	0.979	0.987	**0.993**
	0.984	0.977	**0.976**	0.956	0.945	0.920	0.985	0.920	0.979	0.960	0.924	0.878

2M NaOH	CG2	CG3	D1	D2	D3	D4	D5	D6	Ng3	R1	R2	R3
1000 ºC	0.999	0.999	0.960	0.952	0.949	0.943	0.970	0.943	0.980	1.000	0.999	**1.000**
	0.997	0.997	**0.997**	0.994	0.991	0.984	0.996	0.984	0.998	0.996	0.988	0.974
1050 ºC	0.994	0.982	0.930	0.982	0.988	0.994	0.974	0.976	0.991	0.987	0.986	**0.982**
	0.990	0.991	**0.988**	0.985	0.982	0.973	0.988	0.973	0.992	0.989	0.978	0.959
1100 ºC	0.965	0.968	0.988	0.985	0.984	0.981	0.991	0.981	0.917	0.975	0.984	**0.991**
	0.979	0.984	**0.984**	0.991	0.991	0.984	0.974	0.984	0.984	0.989	0.981	0.956

4M NaOH	CG2	CG3	D1	D2	D3	D4	D5	D6	Ng3	R1	R2	R3
1000 ºC	0.999	0.999	0.954	0.944	0.941	0.933	0.965	0.933	0.981	1.000	0.999	**0.996**
	0.984	0.981	**0.977**	0.966	0.959	0.944	0.983	0.944	0.983	0.972	0.951	0.922
1050 ºC	0.979	0.982	0.988	0.983	0.981	0.976	0.993	0.976	0.937	0.987	0.993	**0.997**
	0.979	0.986	**0.984**	0.996	0.998	0.998	0.973	0.998	0.986	0.996	0.999	0.989
1100 ºC	0.973	0.977	0.995	0.993	0.992	0.990	0.995	0.990	0.939	0.983	0.991	**0.996**
	0.983	0.992	0.969	0.991	0.997	**1.000**	0.958	**1.000**	0.996	1.000	0.993	0.968

2M KOH	CG2	CG3	D1	D2	D3	D4	D5	D6	Ng3	R1	R2	R3
1000 ºC	1.000	1.000	0.953	0.946	0.944	0.939	0.962	0.939	0.990	**0.999**	0.998	0.995
	0.989	0.987	0.982	**0.972**	0.967	0.957	0.988	0.957	0.989	0.981	0.967	0.950
1050 ºC	0.958	0.962	0.993	0.991	0.990	0.987	0.994	0.987	0.905	0.970	0.980	**0.988**
	0.958	0.946	**0.952**	0.921	0.906	0.874	0.966	0.874	0.946	0.919	0.869	0.814
1100 ºC	0.908	0.914	0.979	0.983	0.985	0.987	0.971	0.987	0.852	0.924	0.940	**0.953**
	0.973	0.958	0.980	0.948	0.928	0.883	**0.989**	0.883	0.950	0.920	0.843	0.753

4M KOH	CG2	CG3	D1	D2	D3	D4	D5	D6	Ng3	R1	R2	R3
1000 ºC	1.000	0.947	0.939	0.936	0.930	0.958	0.930	0.991	0.999	0.997	0.993	**1.000**
	0.982	0.983	0.986	**0.986**	0.984	0.979	0.983	0.979	0.982	0.985	0.981	0.970
1050 ºC	0.949	0.953	0.991	0.992	0.992	0.992	0.988	0.992	0.904	0.961	0.971	**0.980**
	0.988	0.994	**0.984**	0.998	1.000	0.997	0.975	0.997	0.996	1.000	0.991	0.965
1100 ºC	0.999	0.999	0.953	0.947	0.944	0.940	0.961	0.940	0.992	**0.998**	0.996	0.994
	0.964	0.968	0.975	0.983	0.985	**0.990**	0.968	**0.990**	0.965	0.975	0.984	0.990

Table 6.6: Correlation coefficient calculated using different mechanism functions for the initial and final stages of iron ore lump reduction at different temperatures

According to the kinetic analysis and calculation procedures introduced in chapter 3, section 3.5, the g(α) value for each mechanism model versus the reduction time t for the reduction reaction of the iron ore lump samples have been calculated and plotted, every plot has then been subjected to linear fit through zero for initial stages of reduction whereas for later stages of reduction normal linear fitting is done. The results are shown in Fig. 6.14. (The linear fitting curve for 2M NaOH has been shown here, other plots are given in appendix) Simultaneously, the corresponding correlation coefficient for each model has been calculated, which are given in Table 6.6 for initial and final stages of reduction, respectively. Higher the correlation coefficient better is the mechanism function [7].

To determine the kinetic model and the rate controlling steps in the reaction, the experimental data have been analysed by using reduced time plots shown in Fig. 6.15, Fig. 6.16, Fig. 6.17, Fig. 6.18 and Fig. 6.19 for standard, sodium added (2M and 4M) and potassium added (2M and 4M) iron ore lump samples, respectively. From these figures and the calculated correlation coefficient given in Table 6.7, the models with the highest R squared values and those matching the experimental reduced time plots have been selected to be the governing reaction mechanism for the individual lump samples [8].

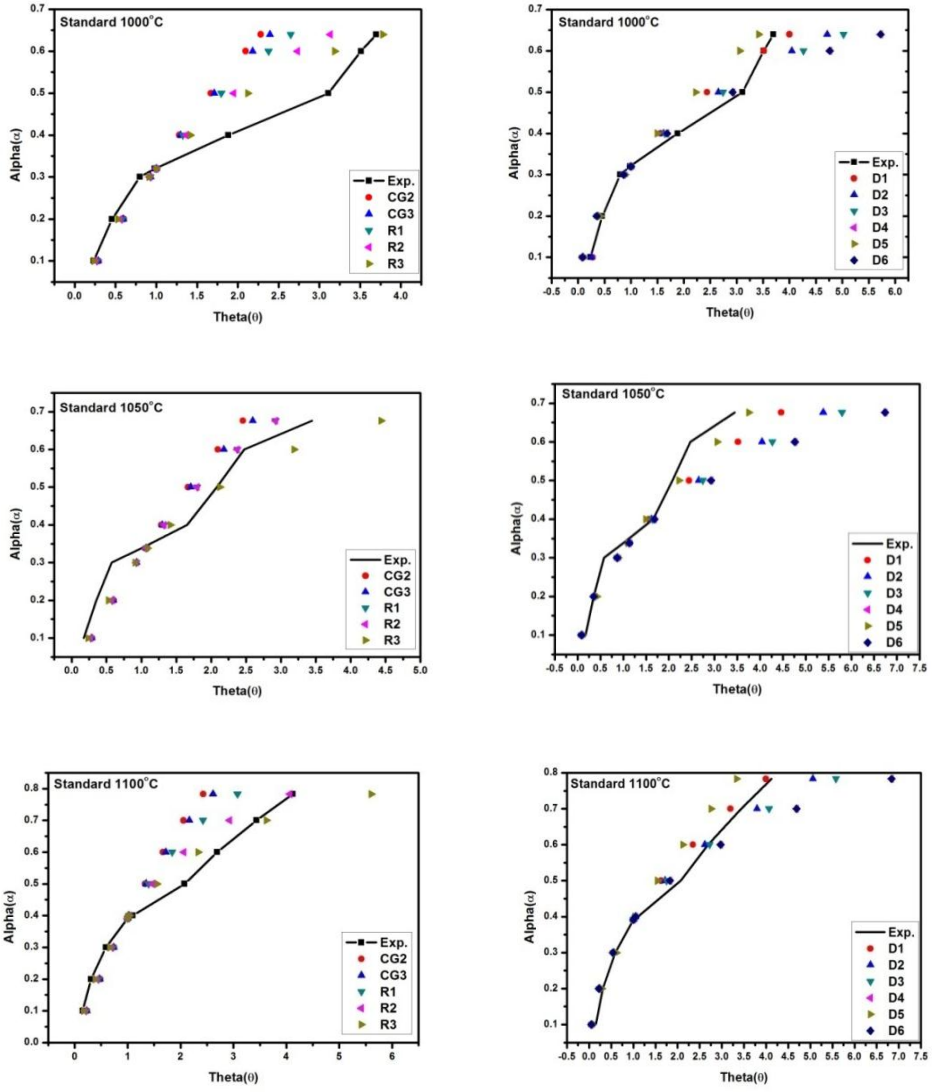

Fig. 6.15: Reduced time plot of fractional loss α along with the theoretical α vs. θ plot for different mechanism models of the standard iron ore lump samples

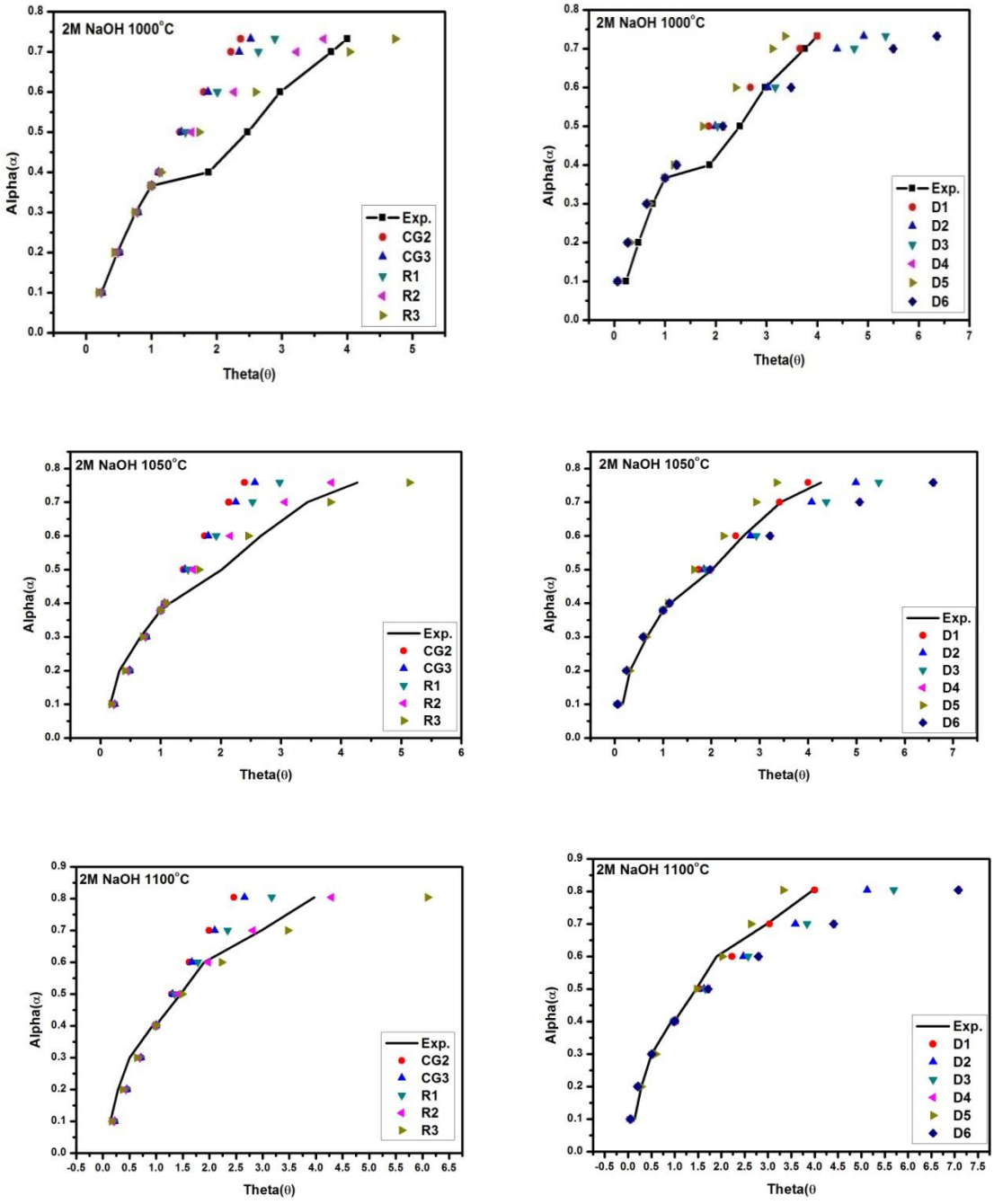

Fig. 6.16: Reduced time plot of fractional loss α along with the theoretical α vs. θ plot for different mechanism models of the 2M NaOH iron ore lump samples

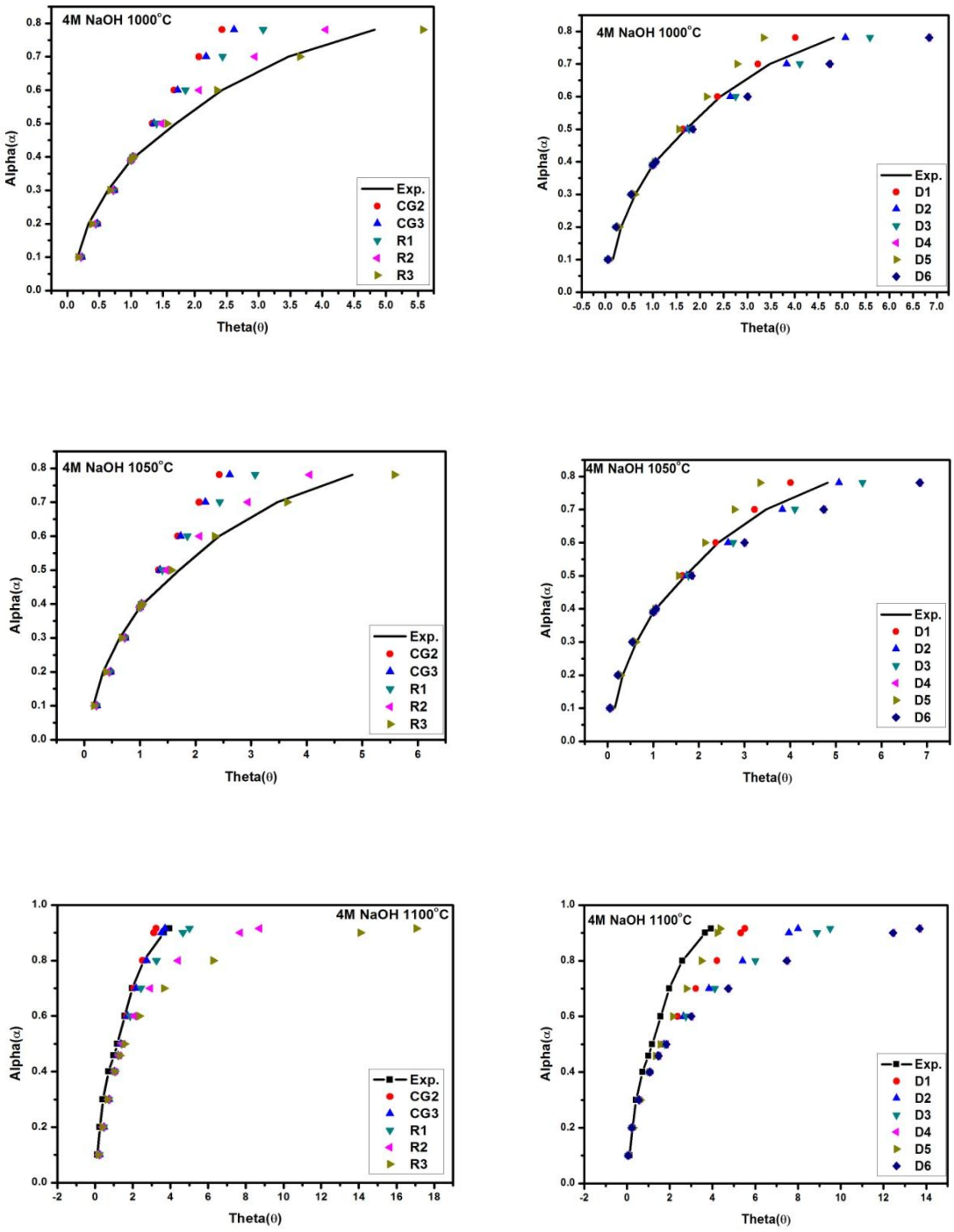

Fig. 6.17: Reduced time plot of fractional loss α along with the theoretical α vs. θ plot for different mechanism models of the 4M NaOH iron ore lump samples

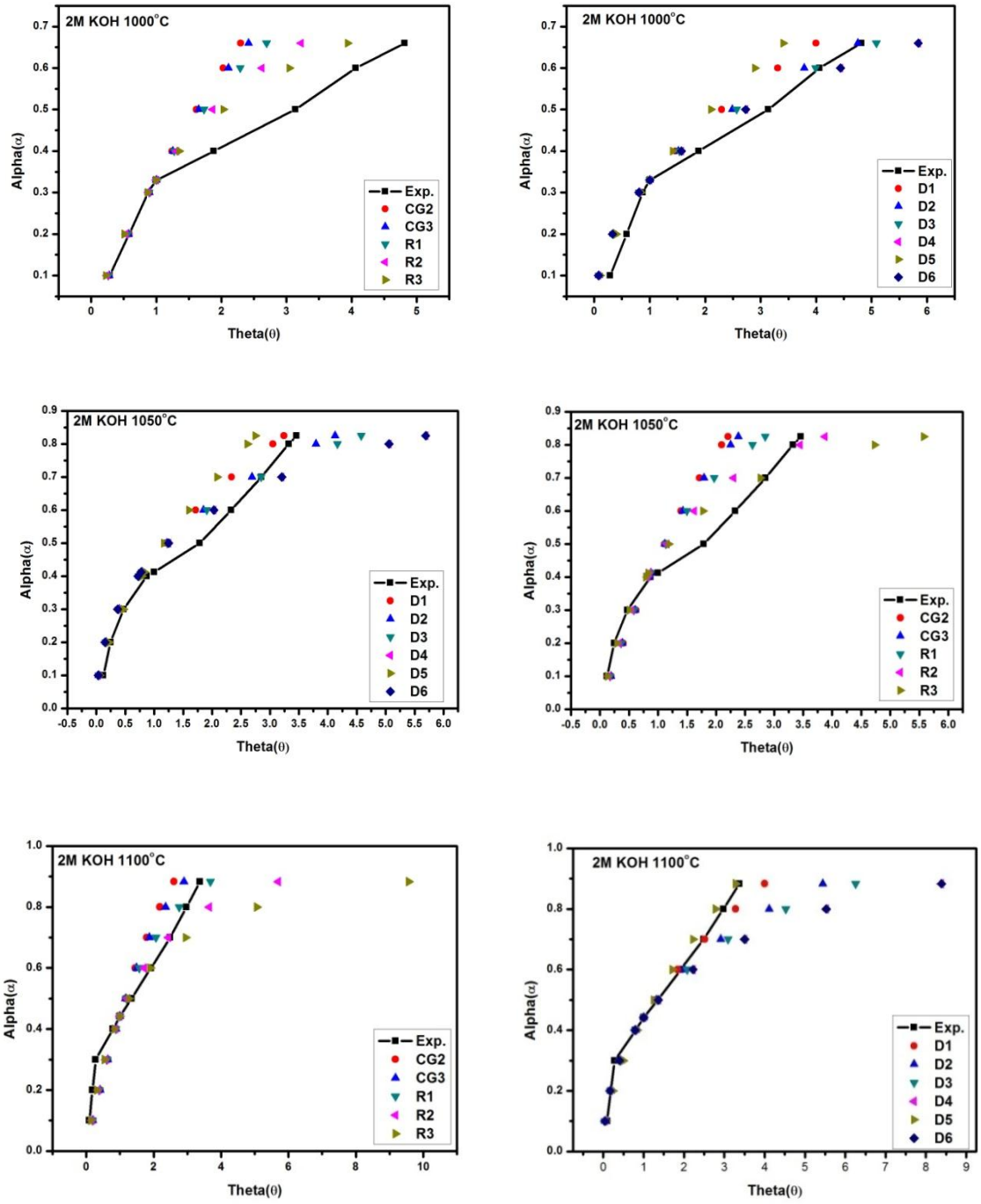

Fig. 6.18: Reduced time plot of fractional loss α along with the theoretical α vs. θ plot for different mechanism models of the 2M KOH iron ore lump samples

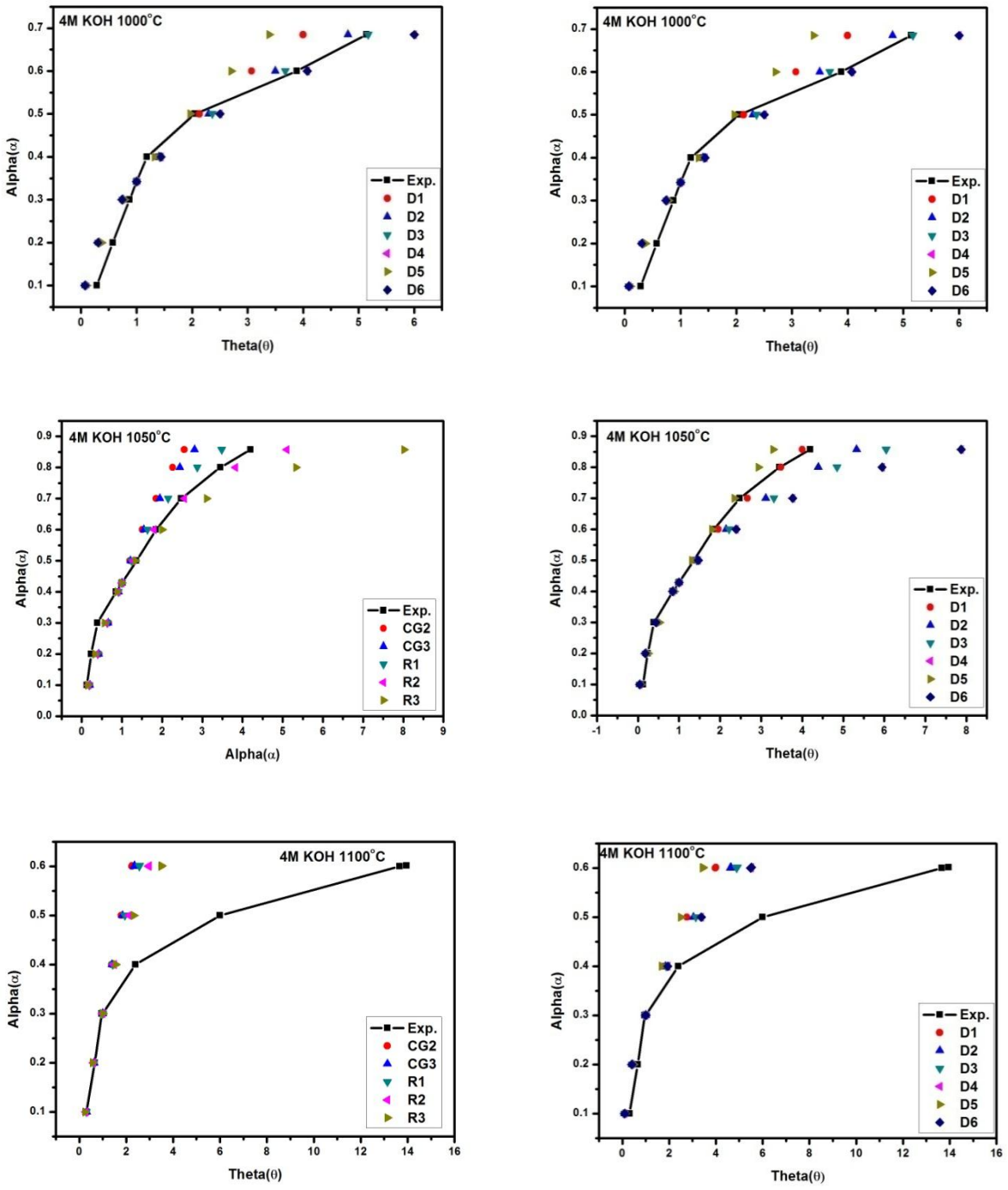

Fig. 6.19: Reduced time plot of fractional loss α along with the theoretical α vs. θ plot for different mechanism models of the 4M KOH iron ore lump samples

Standard Lumps: It can be seen that the experimental (α, θ) points coincide very well with the theoretical curve for R3 for the standard lump samples as shown in figures above in the initial stages of reduction. In the later stages of reduction, the experimental (α, θ) points coincide very well with the theoretical curve for diffusion at different temperatures. In the initial stages of reduction, the gases reduce the lumps on the surface as well as inside the pores leading to second order reaction mechanism. In the later stages of reduction as the surface is reduced the reduction carries on through diffusion mechanism.

Sodium added Lumps: It can be seen that the experimental (α, θ) points coincide very well with the theoretical curve for R3 for the sodium added lump samples as shown in figures above in the initial stages of reduction. In the later stages of reduction, the experimental (α, θ) points coincide very well with the theoretical curve for diffusion at different temperatures. In the initial stages of reduction, the gases reduce the lumps on the surface as well as inside the pores leading to second order reaction mechanism. In the later stages of reduction as the surface is reduced the reduction carries on through diffusion mechanism.

Potassium added Lumps: It can be seen that the experimental (α, θ) points coincide very well with the theoretical curve for R3 and R1 (2M KOH 1000^{o}C and 4M KOH 1100^{o}C) for the potassium added lump samples as shown in figures above in the initial stages of reduction. In the later stages of reduction, the experimental (α, θ) points coincide very well with the theoretical curve for diffusion at different temperatures. In the initial stages of reduction, the gases reduce the lumps on the surface as well as inside the pores leading to second order reaction mechanism. In the later stages of reduction as the surface is reduced the reduction carries on through diffusion mechanism.

6.7 Conclusion

- The predicted optimum combination of potassium hydroxide concentration of 1.82M, time of 60 min and temperature of 1100^{o} C for an optimized Extent of Reduction of 85.89%.
- The predicted optimum combination of sodium hydroxide concentration of 4M, time 57.34 min at a temperature of 1100^{o}C for an optimized Extent of Reduction of 84.5%.
- The extent of reduction of lumps impregnated with alkali increases as the temperature is increased but for 4M KOH the extent of reduction decreases as the temperature is increased from 1050^{o}C to 1100^{o}C.
- The predicted values of the different parameters are very close to the observed experimental values.
- The iron ore lumps reducibility under direct reduction conditions increases with time and temperature.
- The addition of alkali leads to higher rate of reduction at the same time and temperature. Sodium has higher effect on reducibility than potassium at 1000^{o}C; whereas the later has more dominant effect at higher concentrations and temperatures. At 1050^{o}C, after 60 minutes of reduction potassium's (2M) effect is more compared to that of sodium (2M).
- At 1100^{o}C, potassium has higher effect on reducibility as compared to sodium. The addition of alkali facilitates the phase transformation of hematite to magnetite which leads to crack generation leading to higher available area for reduction [9, 10, 11]. But after a certain percentage the addition of potassium hinders the reducibility of iron ore lumps at 1100^{o}C.
- Potassium is known to have a higher effect on reducibility as compared to sodium which leads to higher disintegration of the iron ore lumps which leads to blocking of

pores, which in turn leads to a lower reduction rate of iron ore lumps with high potassium content at high temperatures.

- The reduction of iron ore lumps without and with added alkali follow chemical reaction mechanisms (R3 and R1) in the initial stages of reduction whereas different diffusion mechanisms are followed in the later stages of reduction.

6.8 Reference

1. M. Cavazzuti, Optimization Methods: From Theory to Design Scientific and Technological Aspects in Mechanics (Springer Science & Business Media, 2012).
2. N. Nguyena, J.J. Borkowskib, New 3-level response surface designs constructed from incomplete block designs. J. Stat. Plan. Inference 138, 294–305 (2008).
3. N.R. Draper, H. Smith, Applied Regression Analysis (Wiley, New York, 1981).
4. G.E.P. Box, D.W. Behnken, Some new three level designs for the study of quantitative variables. Technometrics 2, 455–475 (1960).
5. D.C. Montgomery, Design and Analysis of Experiments, 8th edn. (Wiley, New Delhi, 2011).
6. Pichler, A., Schenk, J., Hanel, M., Mali, H., Thaler, C., Hauzenberger, F., & Stocker, H. (2014). Influence of alkalis on mechanical properties of lumpy iron carriers during reduction. In Conference Proceedings to the 23rd International Conference on Metallurgy and Materials (pp. 40-40).
7. Wang H, Chu M, Guo B, Bao J, Zhao W, Liu Z, et al. Investigation on Gasification Reaction Behavior and Kinetic Analysis of Iron Coke Hot Briquette under Isothermal Conditions. Steel Res Int 2019;90:1–10.
8. Sarkar BK, Kumar N, Dey R, Das GC. Optimization of Quenching Parameters for the Reduction of Titaniferous Magnetite Ore by Lean Grade Coal Using the Taguchi Method and Its Isothermal Kinetic Study. Metall Mater Trans B Process Metall Mater Process Sci 2018;49:1822–33.
9. Yu, Y.; Qi, C. Magnetizing roasting mechanism and effective ore dressing process for oolitic hematite ore. J. Wuhan Univ. Technol. Mater. Sci. Ed. 2011, 26, 176–181.

10. Feilmayr, C.; Thurnhofer, A.; Winter, F.; Mali, H.; Schenk, J. Reduction behavior of hematite to magnetite under fluidized bed conditions. ISIJ Int. 2004, 44, 1125–1133.
11. Et-Tabirou, M.; Dupre, B.; Gleitzer, C. Hematite single crystal reduction into magnetite with CO-CO2, Metall. Trans. B 1988, 19, 311–317.

Chapter-7

Optimization of the Alkali Content in Iron Ore Briquettes by the Use of Statistical Modelling via Box Behnken Design and Its Effect on Reducibility and Kinetics under Direct Reduction Conditions

7.1 Design of Experiment:

Reduction of iron ore briquettes with and without added alkali by boiler grade coal has been performed at varying time, temperature and concentration of alkali content. Response surface methodology i.e. Box Behnken design in this case has been used to determine the optimum process parameters.

7.1.1 Box Behnken Design

The Box Behnken Design modelling has been used as discussed in chapter 3, section 3.4.1. The different parameters and their range have been given in Table 7.1. The model uses these parameters and their range to provide 17 set of tests under different conditions. The 17 set of test conditions have been given in a tabulated form in Table 7.2.

Serial	Parameters	Unit		Lower	Higher	-1	0	1
1	Temperature	Deg C	C	1000	1100	1000	1050	1100
2	Time	Minutes	B	30	60	30	45	60
3	Alkali(KOH/NaOH)	M	A	0	4	0	2	4

Table 7.1: Range and coded parameter levels of experimental variables used to reduce iron ore briquettes for Box–Behnken design

Sl.No.	Temperature (Degree C)	Time (Minutes)	Concentration (M)
1	1000	30	2
2	1000	45	0
3	1000	45	4
4	1000	60	2
5	1050	30	0
6	1050	30	4
7	1050	45	2
8	1050	45	2
9	1050	45	2
10	1050	45	2
11	1050	45	2
12	1050	60	0
13	1050	60	4
14	1100	30	2
15	1100	45	0
16	1100	45	4
17	1100	60	2

Table 7.2: Details of all 17 sets of reactions as provided by BBD

7.2 Reduction of Iron ore briquettes under Direct Reduction Conditions

A tube furnace has been used for the reduction of alkali impregnated iron ore briquettes according to set of reactions given by box behnken design. An inconel tube is used to provide a closed environment for reduction of briquettes. The briquettes are placed in an inconel tube along with stoichiometric amount of coal required for reduction. During reduction the gases come out of the outlet tube. When the furnace is switched off the outlet is closed so that air does not enter leading to re-oxidation. After the inconel tube has cooled down the sample is taken out and the extent of reduction (EOR) is calculated.

7.3 Box Behnken Design model for Iron Ore Briquettes

The results of the 17 set of reductions of iron ore briquettes under direct reduction conditions according to the Box Behnken design have been given in the table below. (Calculation of extent of reduction is shown in Appendix-II)

Sl.No.	Temperature (Degree C)	Time (Minutes)	Concentration (M)	EOR of Briquettes with KOH (%)	EOR of Briquettes with NaOH (%)
1	1000	30	2	70.82	68.49
2	1000	45	0	71.44	71.44
3	1000	45	4	82.12	75.25
4	1000	60	2	81.67	81.00
5	1050	30	0	73.94	73.94
6	1050	30	4	83.98	83.07
7	1050	45	2	872	85.66
8	1050	45	2	87.78	84.79
9	1050	45	2	89.12	83.98
10	1050	45	2	85.83	86.90
11	1050	45	2	86.12	86.50
12	1050	60	0	86.71	86.71
13	1050	60	4	93.67	91.64
14	1100	30	2	80.50	77.18
15	1100	45	0	86.34	86.34
16	1100	45	4	94.11	92.78
17	1100	60	2	93.79	93.74

Table 7.3: Extent of reduction of iron ore briquette samples with added potassium and sodium for the 17 set of reactions (Box Behnken Design)

7.3.1 Statistical Analysis of Reduction of Alkali Added Iron Ore Briquettes

Optimization of the process variables (alkali concentration, time and temperature) has been carried out in order to maximize the extent of reduction (%) of the iron ore briquettes with added potassium and sodium within the framework of BBD (Table 7.3). This design predicted the optimum combination of potassium hydroxide concentration of 3.97M, time of 55.66 min and temperature of 1094.31^{o}C for an EOR of 96.2%. This design predicted the optimum combination of sodium hydroxide concentration of 3.99M, time 57.75 min at a temperature of 1093.23^{o}C for an EOR of 95.95%. Fig. 7.1, shows the Normal probability plot of the studentized residuals which confirms the normality of residuals. Fig. 7.2 shows the plot of predicted versus actual extent of reduction of iron ore briquettes with added potassium and sodium, respectively. From this figure, it can be seen that the points are lying close to the straight line and this which indicates that the experimental yield is fairly close to the yield predicted by the BBD.

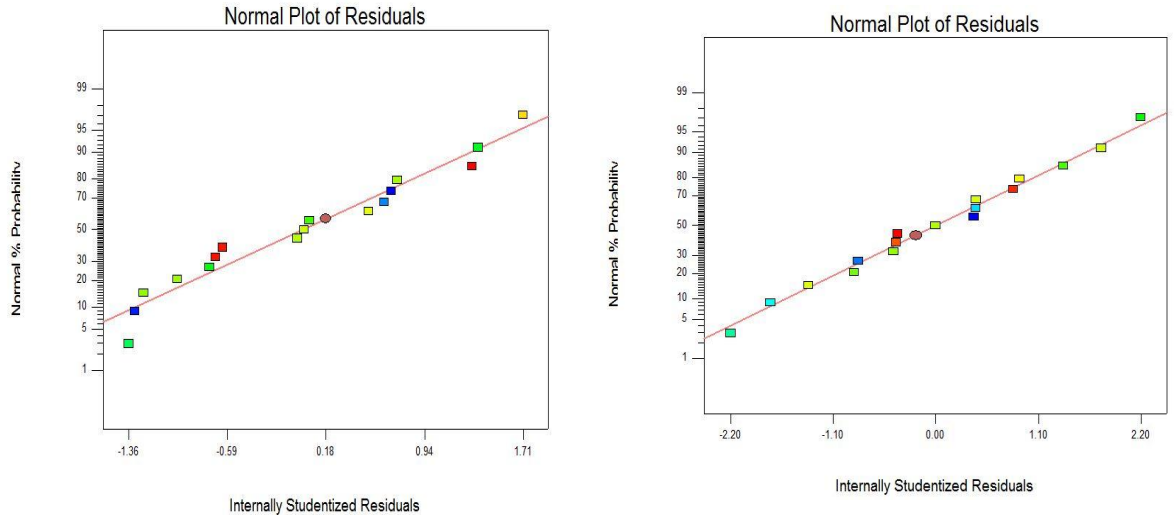

Fig 7.1: The normal plot of residuals for iron ore briquettes with added a) potassium and b) sodium

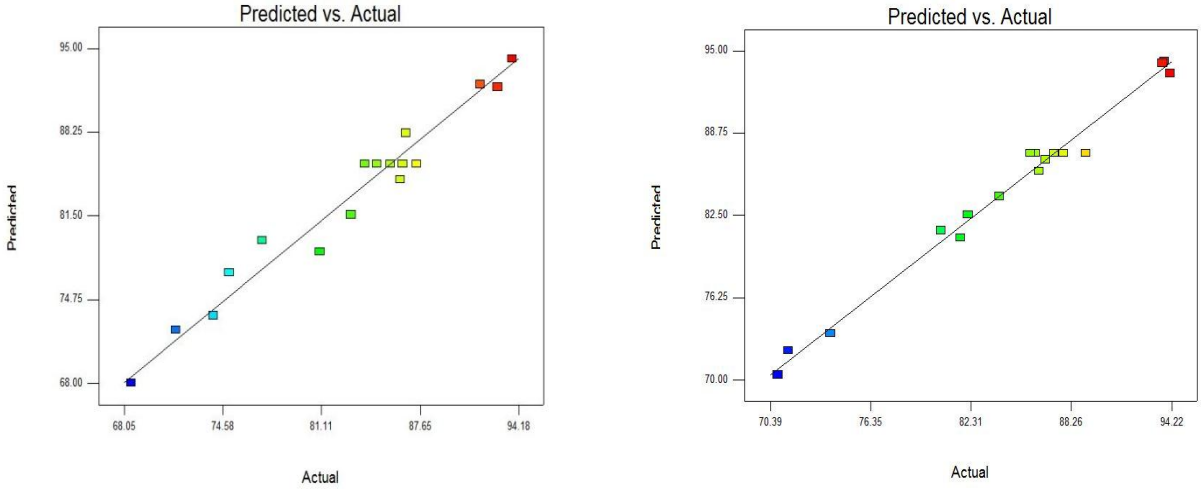

Fig. 7.2: The predicted vs. actual plots of iron ore briquettes with added a) potassium and b) sodium

7.3.2 Analysis of Variance (ANOVA)

The ANOVA of the quadratic model for the optimization of reduction of iron ore briquettes with boiler grade coal with added alkali i.e. potassium hydroxide and sodium hydroxide have been listed in the Table 7.4.

- **Model for added Potassium:**

The Model F-value of 57 implies the model is significant. There is only a 0.01% chance that a "Model F-Value" this large could occur due to noise. Values of "Prob > F" less than 0.0500 indicate model terms are significant. In this case A, B, C , A^2, B^2 and C^2 are significant model terms. Values greater than 0.1000 indicate the model terms are not significant. "Adeq Precision" measures the signal to noise ratio. A ratio greater than 4 is desirable. Here, the ratio of 24.869 indicates an adequate signal. This model can be used to navigate the design space. The R-srquared value of 0.9866 is also very good.

- **Model for added Sodium:**

The Model F-value of 20.21 implies the model is significant. There is only a 0.03% chance that a "Model F-Value" this large could occur due to noise. Values of "Prob > F" less than 0.0500 indicate model terms are significant. In this case A, B, C and A^2 are significant model terms. Values greater than 0.1000 indicate the model terms are not significant. "Adeq Precision" measures the signal to noise ratio. A ratio greater than 4 is desirable. Here, the ratio of 15.772 indicates an adequate signal. This model can be used to navigate the design space. The R-srquared value of 0.9629 is also very good.

Statistical Results	KOH Model	NaOH Model
Model *F*-value	57	20.21
Model prob.> F	<.05	<.05
R-Squared	0.9866	0.9629
CV%	1.48	2.61
Adjusted R- squared	0.9693	0.9153
Adequate precision	24.869	15.772

Table 7.4: Statistical Results of ANOVA for iron ore briquettes with added potassium and sodium

7.3.3 Extent of Reduction of Iron Ore Briquettes with Added Potassium and Sodium

Data obtained from the 17 batch runs have been analyzed using the Design Expert 7.0.0 software and the following second-order polynomial equations for extent of reduction (%) of iron ore briquettes with added potassium and sodium have been generated:

$$EOR_{KOH} = -1515.51175 + 2.86811 * Temp + 0.47497 * Time + 11.42513 * KOH + 8.13333E\text{-}004 * Temp * Time - 77500E\text{-}003 * Temp * KOH - 0.025667 * Time * KOH - 1.31830E\text{-}003 * Temp^2 - 9.88111E\text{-}003 * Time^2 - 0.10394 * KOH^2$$

$\mathbf{EOR_{NaOH}}$ =-1783.78325+3.42580 * Temp-0.30472 * Time-4.21200 * NaOH+1.35000E-03 * Temp * Time+70000E-003 * Temp * NaOH-0.035000 * Time * NaOH-1.60270E-003 * $Temp^2$-6.91889E-003 * $Time^2$-0.067313 * $NaOH^2$

Fig. 7.3 shows the second-order 3D response surface plot along with contour plot for extent of reduction (%) of iron ore briquettes with added potassium as a function of duration of reduction and potassium hydroxide concentration; in Fig. 7.4 the second-order 3D response surface plot for extent of reduction (%) of iron ore briquettes with added potassium is shown along with the contour plot as a function of temperature of reduction and concentration of potassium hydroxide in iron ore briquettes. Fig. 7.5 shows the second-order 3D response surface plot along with contour plot for extent of reduction (%) of iron ore briquettes with added sodium as a function of duration of reduction and sodium hydroxide concentration; in Fig. 7.6 the second-order 3D response surface plot for extent of reduction (%) of iron ore briquettes with added sodium is shown along with the contour plot as a function of temperature of reduction and concentration of sodium hydroxide in iron ore briquettes.

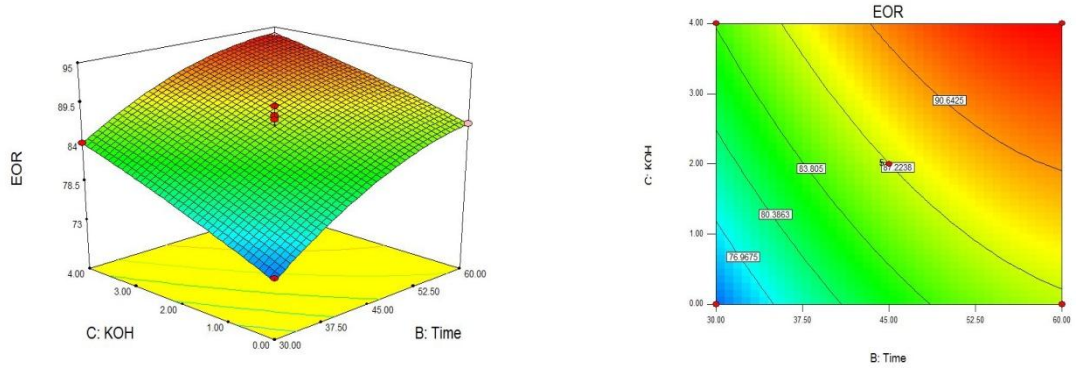

Fig 7.3: The second-order 3D response surface plot and the contour plot for extent of reduction (%) of iron ore briquettes is shown as a function of duration of reduction and concentration of potassium hydroxide in iron ore briquettes

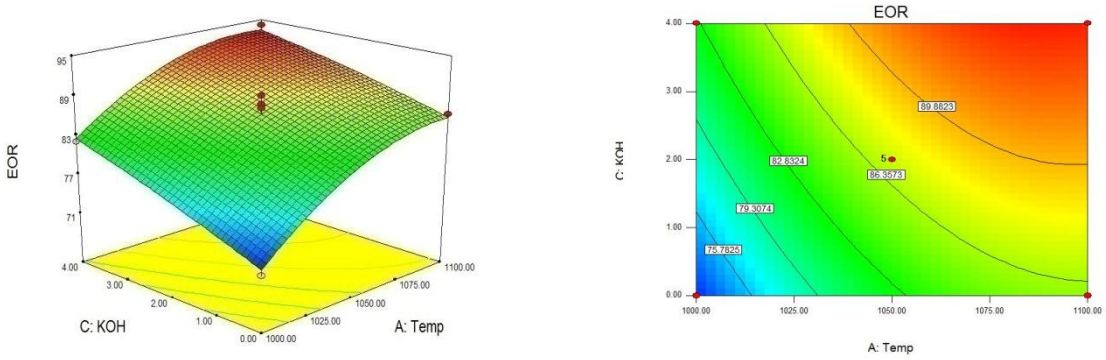

Fig. 7.4: The second-order 3D response surface plot and contour plot for extent of reduction (%) of iron ore briquettes is shown as a function of temperature of reduction and concentration of Potassium Hydroxide in iron ore briquettes

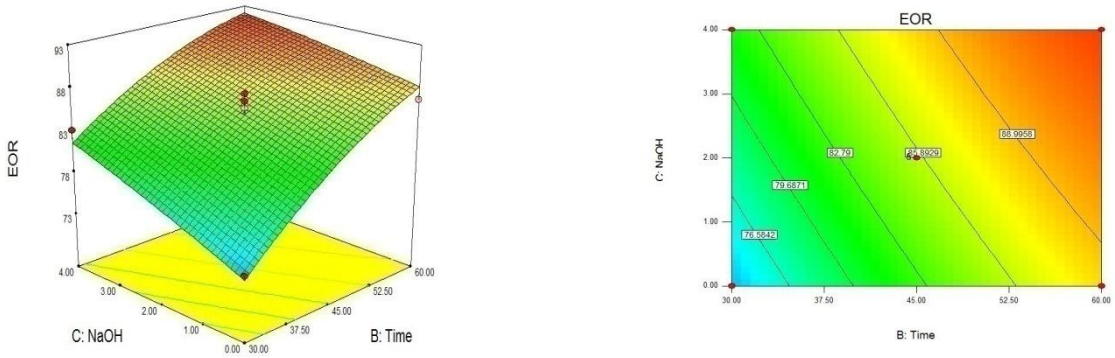

Fig. 7.5: The second-order 3D response surface plot and the contour plot for extent of reduction (%) of iron ore briquettes is shown as a function of duration of reduction and concentration of sodium hydroxide in iron ore briquettes

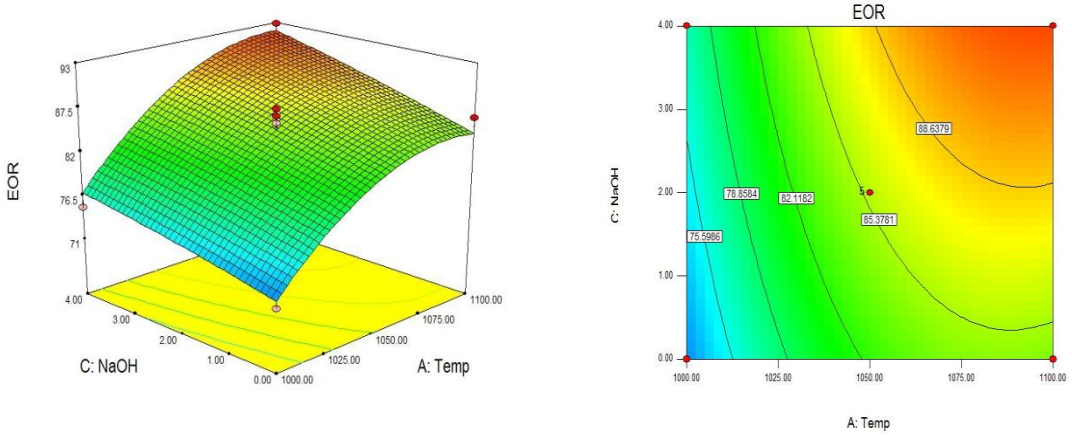

Fig.7.6: The second-order 3D response surface plot and contour plot for extent of reduction (%) of iron ore briquettes is shown as a function of temperature of reduction and concentration of Sodium Hydroxide in iron ore briquettes

7.4 Reduction of Iron Ore Briquettes Containing Sodium and Potassium under Direct Reduction Conditions

The iron ore briquettes are reduced under direct reduction conditions inside an inconel tube using boiler grade coal. The reduction is carried out in the same manner as described in section 7.2.

The different parameters of the reduction of briquettes are:

- Alkali Concentration (M): 0M, 2M and 4M
- Time (min): 5,10,15,30,45 and 60
- Temperature (^{o}C): 1000, 1050 and 1100

7.4.1 The Effect of Alkali Content, Time and Temperature on the Iron Ore Briquette Reduction

The iron ore briquettes doped with sodium and potassium have been reduced at three different temperatures and six different times to understand their effect on the reduction of briquettes under direct reduction condition. The extent of reduction calculated from the final weight indicates the effect the different parameters including alkali concentration have on the reduction of briquettes. The extent of reduction (%) for the iron ore briquettes under different parameters has been given in Table 7.5.

Temperature (ºC)	Time (Min.)	STD EOR (%)	2M KOH EOR (%)	4M KOH EOR (%)	2M NaOH EOR (%)	4M NaOH EOR (%)
1000	**5**	29.34	38.40	38.75	36.76	38.62
	10	41.05	44.70	47.37	45.32	47.65
	15	42.06	51.95	55.47	50.21	51.24
	30	53.68	70.82	73.01	68.49	69.00
	45	71.44	75.32	82.12	75.91	75.25
	60	77.05	81.67	84.05	81.01	81.53
1050	**5**	31.51	41.51	41.12	39.02	39.73
	10	44.36	49.64	54.04	48.03	48.25
	15	55.11	65.14	65.58	60.73	61.34
	30	73.94	80.50	82.18	77.18	79.44
	45	79.86	872	89.34	85.66	88.83
	60	86.71	91.79	93.67	88.38	91.64
1100	**5**	32.51	42.71	46.84	42.14	46.32
	10	49.86	58.48	63.35	53.58	57.12
	15	63.38	73.03	75.63	67.65	73.27
	30	75.30	81.24	83.98	79.55	83.07
	45	86.34	92.50	94.12	90.21	92.78
	60	92.47	93.79	97.92	93.74	96.72

Table 7.5: Extent of reduction of iron ore briquettes with and without added alkali under different reduction conditions

7.4.2 Effect of Sodium on the Reducibility of Iron Ore Briquettes

The extent of reduction (EOR) of the iron ore briquettes doped with sodium have been calculated as shown in Table 7.5. The plots of extent of reduction for different sodium content at different time and temperatures have been shown in Fig. 7.7, Fig. 7.8 and Fig. 7.9.

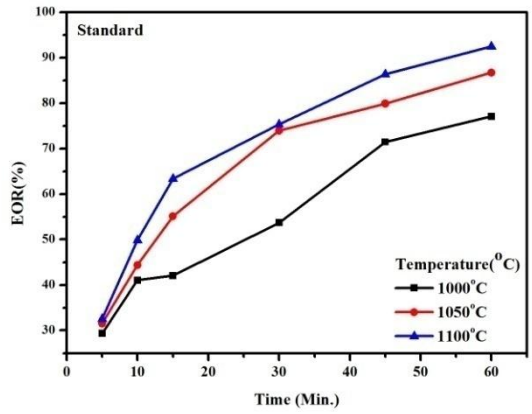

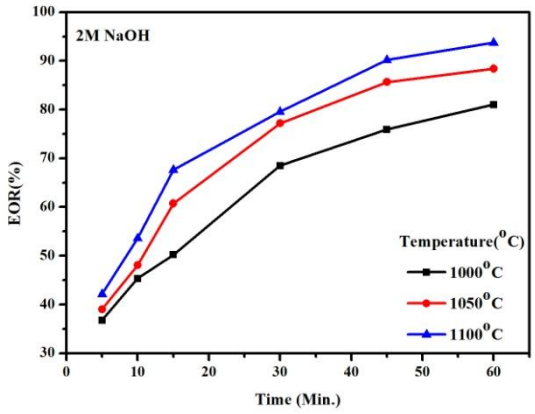

Fig.7.7: EOR of standard briquettes at different time and temperature

Fig.7.8: EOR of sodium (2M) added briquettes at different time and temperature

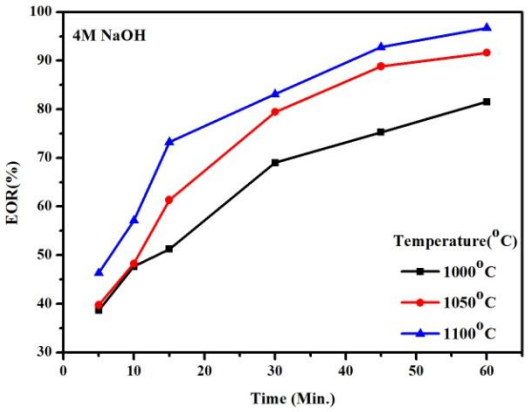

Fig.7.9: EOR of sodium (4M) added briquettes at different time and temperature

The plots of EOR vs. time for different reduction temperatures at different sodium concentrations are shown in Fig. 7.7, Fig. 7.8 and Fig. 7.9. It can be seen that the EOR increases with time at a particular temperature. The EOR also increases with the increase in temperature. The EOR for added sodium is higher than that of briquettes with no added sodium. It can be seen the highest EOR for standard briquettes is at 1100^{o}C and 60 minutes reduction, which is 92.47%. The highest EOR of briquettes with added sodium is achieved at 1100^{o}C, 60 minutes of reduction and 4M NaOH concentration, which is 96.72%. Under the same conditions and 2M NaOH concentration the EOR is 93.74%. The addition of sodium increases the EOR with increasing temperatures and time.

7.4.3 Effect of Potassium on the Reducibility of Iron Ore Briquettes

The extent of reduction (EOR) of the iron ore briquettes doped with potassium have been calculated as shown in Table 7.5. The plots of extent of reduction for different potassium content at different time and temperatures have been shown in Fig. 7.10 and 7.11.

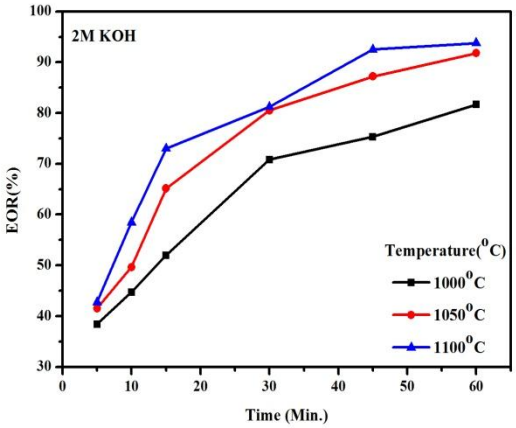

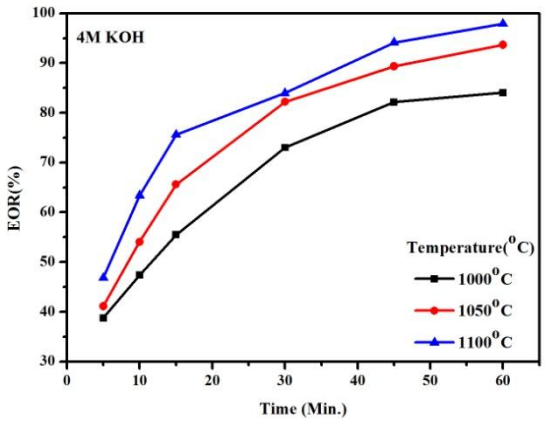

Fig. 7.10: EOR of potassium (2M) added briquettes at different time and temperature

Fig. 7.11: EOR of potassium (4M) added briquettes at different time and temperature

The EOR plots for potassium added briquettes are shown in Fig. 7.10 and Fig. 7.11. The EOR of potassium added briquettes is higher compared to the standard briquettes at any temperature for any duration of time. The EOR keeps on increasing with the amount of potassium, the temperature and duration of reduction. The highest EOR is obtained at 1100^{o}C, 60 minutes and 4M KOH, which is 97.92%. The EOR for 2M KOH under the same conditions is 93.79%. Increase in amount of alkali is a bigger factor than the type of alkali. All the alkali added briquettes have higher EOR as compared to the standard briquettes.

The EOR of potassium added briquettes is higher than that of sodium added briquettes which implies that potassium has more predominant positive effect on the reducibility of iron ore briquettes. In case of briquettes some swelling is observed but the strength did not reduce as drastically as in case of briquettes. Some cracks and swelling has been observed in the reduced briquettes but still the strength of briquettes did not reduce drastically.

7.5 XRD Analysis of Reduced Iron Ore Briquettes: Fig. 7.12 depicts the XRD of the reduced briquettes under different conditions. This confirms that in all cases iron ore briquettes have been almost completely reduced to metallic iron.

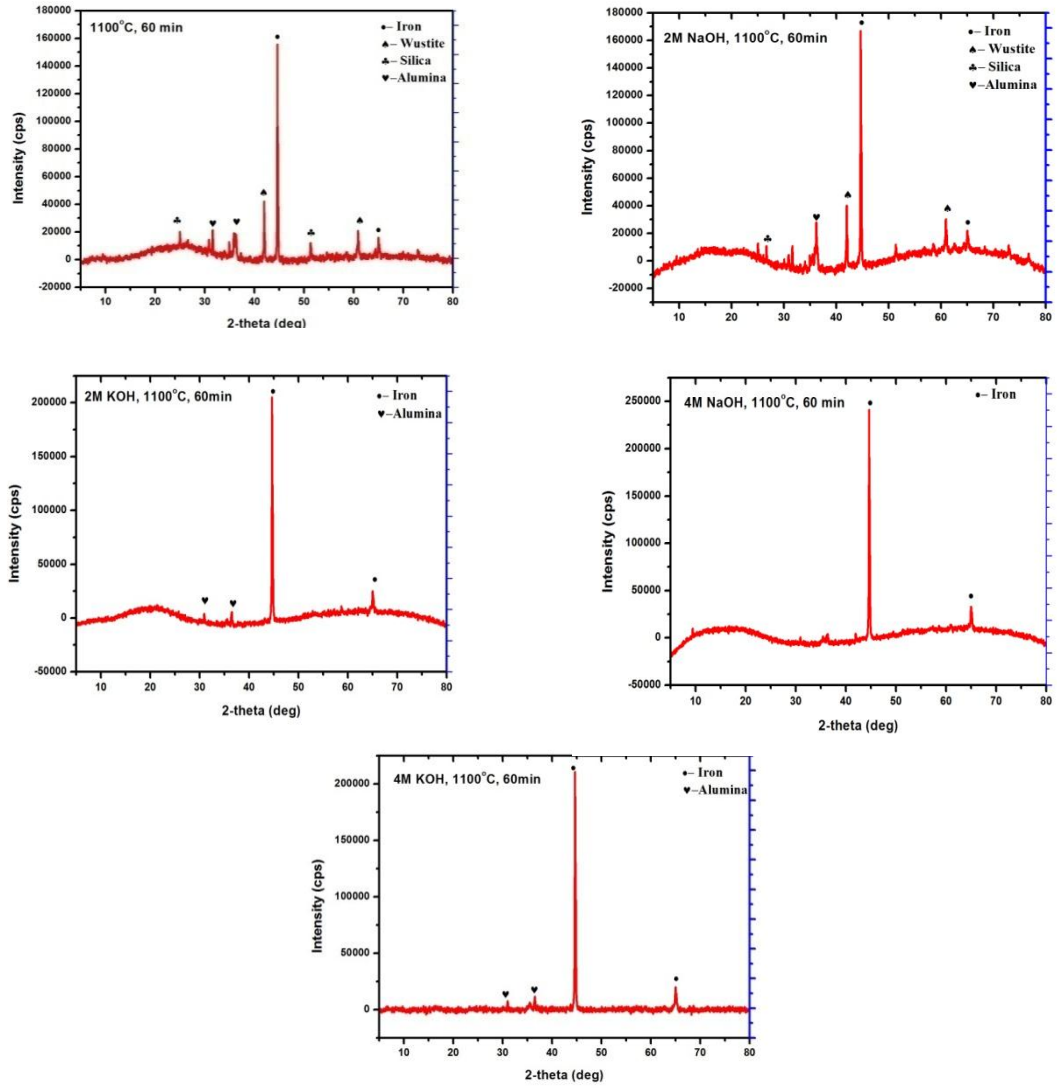

Fig. 7.12: XRD analysis of standard and alkali added reduced briquettes

It can be seen from the XRD plots that the main phase present is iron. This indicates that very good reduction has taken place and it is also in agreement with the extent of reduction values. The intensity of iron phase increases as alkali added samples are considered. The higher the alkali content higher is the intensity of the iron peak. Some amount of wustite is also present in normal briquettes and low alkali briquettes. High alkali briquettes have very small peak of wustite. The increase in alkali leads to complete conversion of hematite to iron.

7.6 Isothermal Kinetic Study

The isothermal kinetic study of reduction of briquettes using boiler grade coal has been carried out. Briquettes have been reduced at 1000°C, 1050°C and 1100°C for 5, 10, 15, 30, 45 and 60 minutes. The reduced time analysis as discussed in Chapter 3, section 3.5 has been carried out using experimental data to find the reaction mechanism being followed under different alkali loading at different temperatures. Many kinetic studies of briquettes reduction have been carried out [5, 6, 7, 8, 9, 10].

7.6.1 Isothermal Kinetic Study of Reduction of Briquettes

In the present study of the isothermal reduction kinetic, the fractional weight loss (α) is defined as:

$$\alpha = \frac{M_t}{M_0} \qquad 1$$

where, M_0 is the weight of oxygen in the iron ore briquettes and M_t is the weight loss due to oxygen removal from iron ore briquettes during reduction by boiler grade coal in the tube furnace. So, α, defined by Eq. 1, gives the isothermal weight fraction loss as a function of time. These data have been graphically plotted in Fig. 7.13.

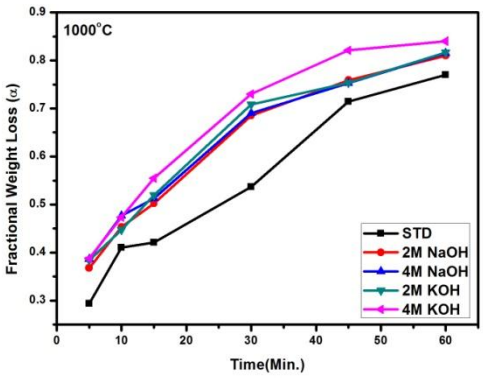

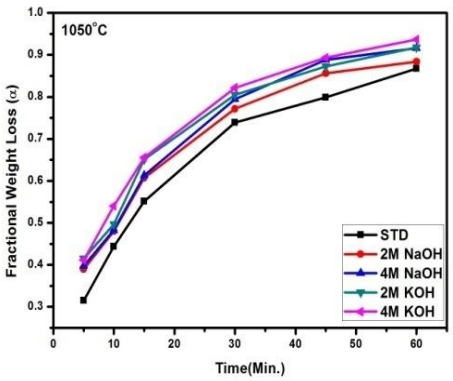

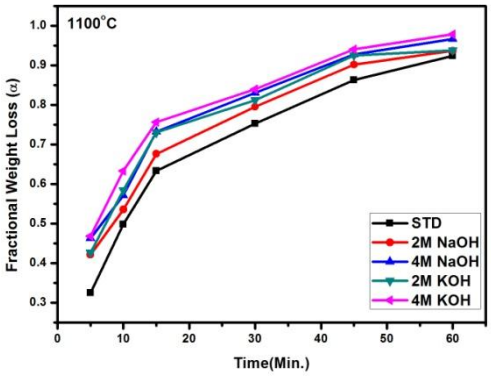

Fig. 7.13: Fractional weight loss (α) vs. time for briquette with and without alkali at different temperature and time

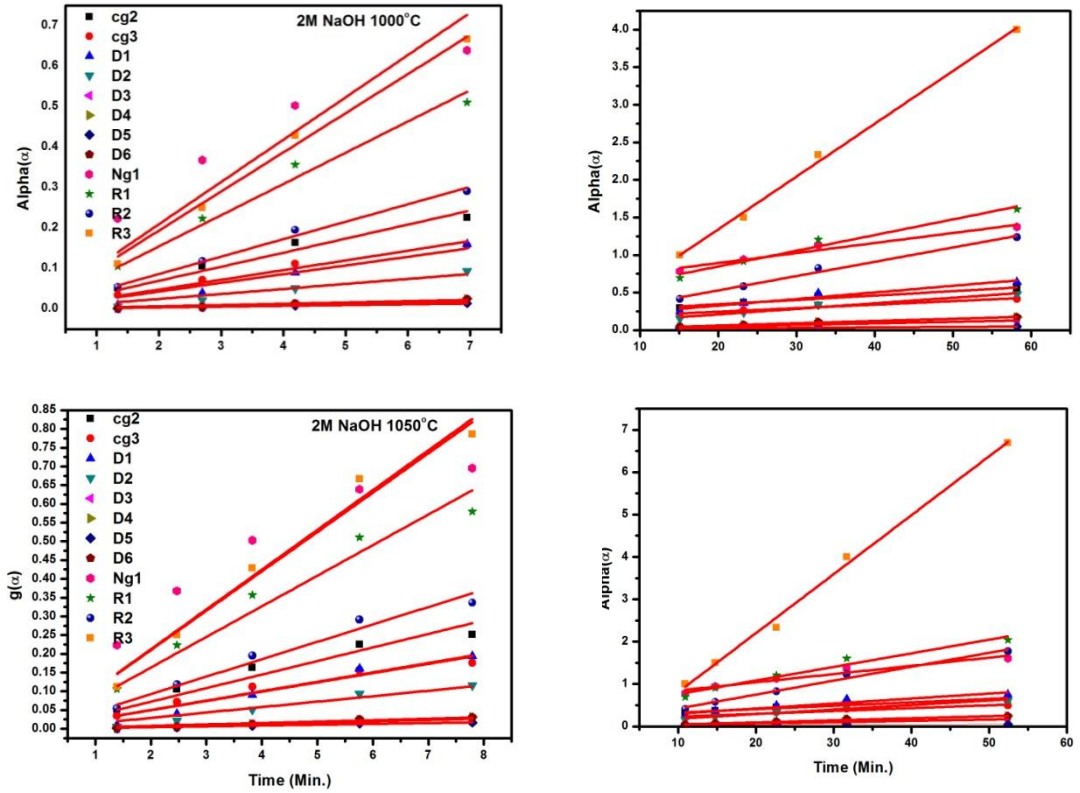

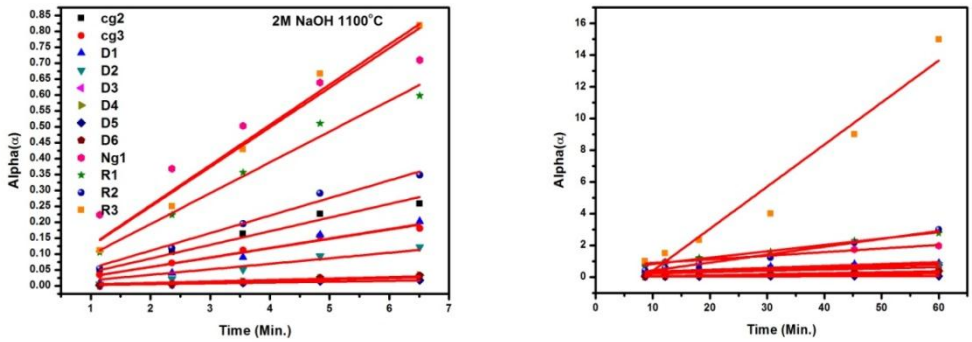

Fig. 7.14: Various mechanism models fitting showing the briquette reduction vs. Time for different iron ore briquette samples with added sodium (2M NaOH) (1st part and last part of reduction, respectively) (The various mechanism model fittings for the other samples has been given in Appendix-II)

Standard	cg2	cg3	D1	D2	D3	D4	D5	D6	Ng1	R1	R2	R3
1000ºC	0.981	0.983	0.973	0.969	0.967	0.962	0.979	0.962	0.949	0.986	0.991	**0.993**
	0.971	0.968	0.964	0.953	0.947	**0.933**	0.969	**0.933**	0.970	0.960	0.941	0.915
1050ºC	0.987	0.988	0.980	0.975	0.973	0.969	0.985	0.969	0.962	0.991	0.995	**0.996**
	0.964	0.975	0.959	0.983	**0.990**	0.995	0.945	0.995	0.978	0.989	0.993	0.975
1100ºC	0.996	0.997	0.972	0.964	0.960	0.953	0.980	0.953	0.976	0.999	**0.999**	0.997
	0.976	0.980	0.973	**0.985**	0.983	0.966	0.961	0.966	0.979	0.975	0.935	0.869

2M NaOH	cg2	cg3	D1	D2	D3	D4	D5	D6	Ng1	R1	R2	R3
1000ºC	0.989	0.991	0.970	0.963	0.960	0.953	0.979	0.953	0.959	0.994	0.997	**0.998**
	0.926	0.939	0.925	0.955	**0.965**	0.981	0.908	0.981	0.942	0.962	0.985	0.996
1050ºC	0.983	0.985	0.977	0.972	0.970	0.966	0.981	0.966	0.959	0.988	0.992	**0.994**
	0.901	0.920	0.887	0.930	0.946	**0.971**	0.865	**0.971**	0.929	0.953	0.985	0.994
1100ºC	0.993	0.994	0.966	0.958	0.955	0.949	0.975	0.949	0.975	0.995	**0.996**	0.994
	0.956	0.973	0.931	0.972	**0.985**	0.995	0.912	0.995	0.982	0.993	0.986	0.942

4M NaOH	cg2	cg3	D1	D2	D3	D4	D5	D6	Ng1	R1	R2	R3
1000ºC	0.998	0.999	0.945	0.934	0.929	0.920	0.958	0.920	0.982	**0.999**	0.997	0.993
	0.949	0.960	0.948	0.972	0.980	**0.991**	0.934	**0.991**	0.962	0.978	0.994	0.997
1050ºC	0.973	0.975	0.968	0.964	0.962	0.958	0.972	0.958	0.947	0.979	0.983	**0.985**
	0.914	0.937	0.890	0.942	0.961	0.985	**0.866**	0.985	0.948	0.972	0.996	0.989
1100ºC	0.997	0.997	0.947	0.935	0.930	0.919	0.960	0.919	0.988	**0.997**	0.993	0.986
	0.969	0.978	0.948	0.979	0.983	0.965	**0.930**	0.965	0.977	0.969	0.894	0.780

2M KOH	cg2	cg3	D1	D2	D3	D4	D5	D6	Ng1	R1	R2	R3
1000ºC	0.996	0.996	0.956	0.946	0.942	0.934	0.967	0.934	0.974	0.998	**0.998**	0.996
	0.895	0.911	0.894	0.929	0.942	**0.963**	0.874	**0.963**	0.914	0.938	0.969	0.988
1050ºC	0.983	0.985	0.963	0.957	0.954	0.949	0.970	0.949	0.963	0.987	**0.988**	0.988
	0.900	0.925	0.875	0.932	**0.954**	0.983	0.848	0.983	0.938	0.966	0.997	0.995
1100ºC	0.999	0.999	0.953	0.942	0.938	0.929	0.965	0.929	0.989	**0.998**	0.995	0.990
	0.925	0.947	0.896	0.945	**0.963**	0.982	0.873	0.982	0.960	0.977	0.984	0.953

4M KOH	cg2	cg3	D1	D2	D3	D4	D5	D6	Ng1	R1	R2	R3
1000ºC	0.999	0.999	0.945	0.933	0.929	0.920	0.958	0.920	0.983	**0.999**	0.997	0.993
	0.960	0.969	0.957	0.976	0.982	**0.990**	0.946	**0.990**	0.972	0.983	0.993	0.993
1050ºC	0.994	0.995	0.961	0.952	0.949	0.942	0.970	0.942	0.979	**0.996**	0.995	0.992
	0.945	0.964	0.919	0.964	**0.980**	0.996	0.898	0.996	0.975	0.990	0.997	0.970
1100ºC	0.999	0.999	0.939	0.924	0.918	0.906	0.955	0.906	0.992	**0.996**	0.990	0.981
	0.969	0.984	0.933	0.982	**0.992**	0.980	0.910	0.980	0.986	0.980	0.893	0.769

Table 7.6: Correlation coefficient calculated using different mechanism functions for the initial and final stages of iron ore briquette reduction at different temperatures

According to the kinetic analysis and calculation procedures introduced in chapter 3, section 3.5, the g(α) value for each mechanism model versus the reduction time t for the reduction reaction of the iron ore briquette samples have been calculated and plotted, every plot has then been subjected to linear fit through zero for initial stages of reduction whereas for later stages of reduction normal linear fitting is done. The results are shown in Fig. 7.14. (The linear fitting curve for 2M NaOH has been shown here, other plots are given in appendix) Simultaneously, the corresponding correlation coefficient for each model have been calculated, which is given in Table 7.6 for initial and final stages of reduction, respectively. Higher the correlation coefficient, better is the mechanism function [11].

To determine the kinetic model and the rate controlling steps in the reaction, the experimental data has been analysed by using reduced time plots shown in Fig. 7.15, Fig. 7.16 Fig. 7.17, Fig. 7.18 and Fig. 7.19 for standard, sodium added (2M and 4M) and potassium added (2M and 4M) iron ore briquette samples, respectively. From these figures and the calculated correlation coefficient given in Table 7.6, the models with the highest R squared values and those matching the experimental reduced time plots have been selected to be the governing reaction mechanism for the individual briquette samples [12].

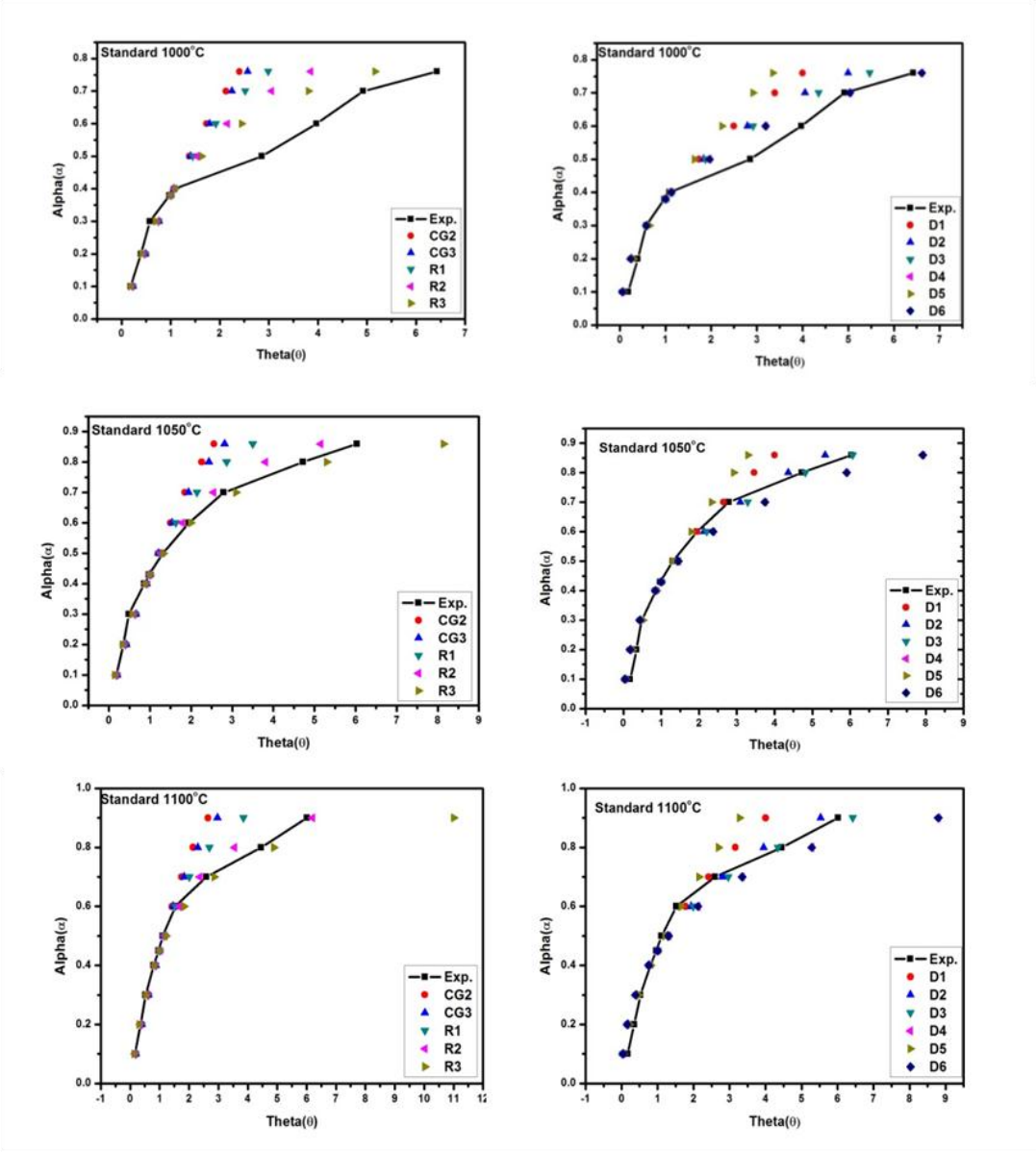

Fig. 7.15: Reduced time plot of fractional loss α along with the theoretical α vs. θ plot for different mechanism models of the standard iron ore briquettes samples

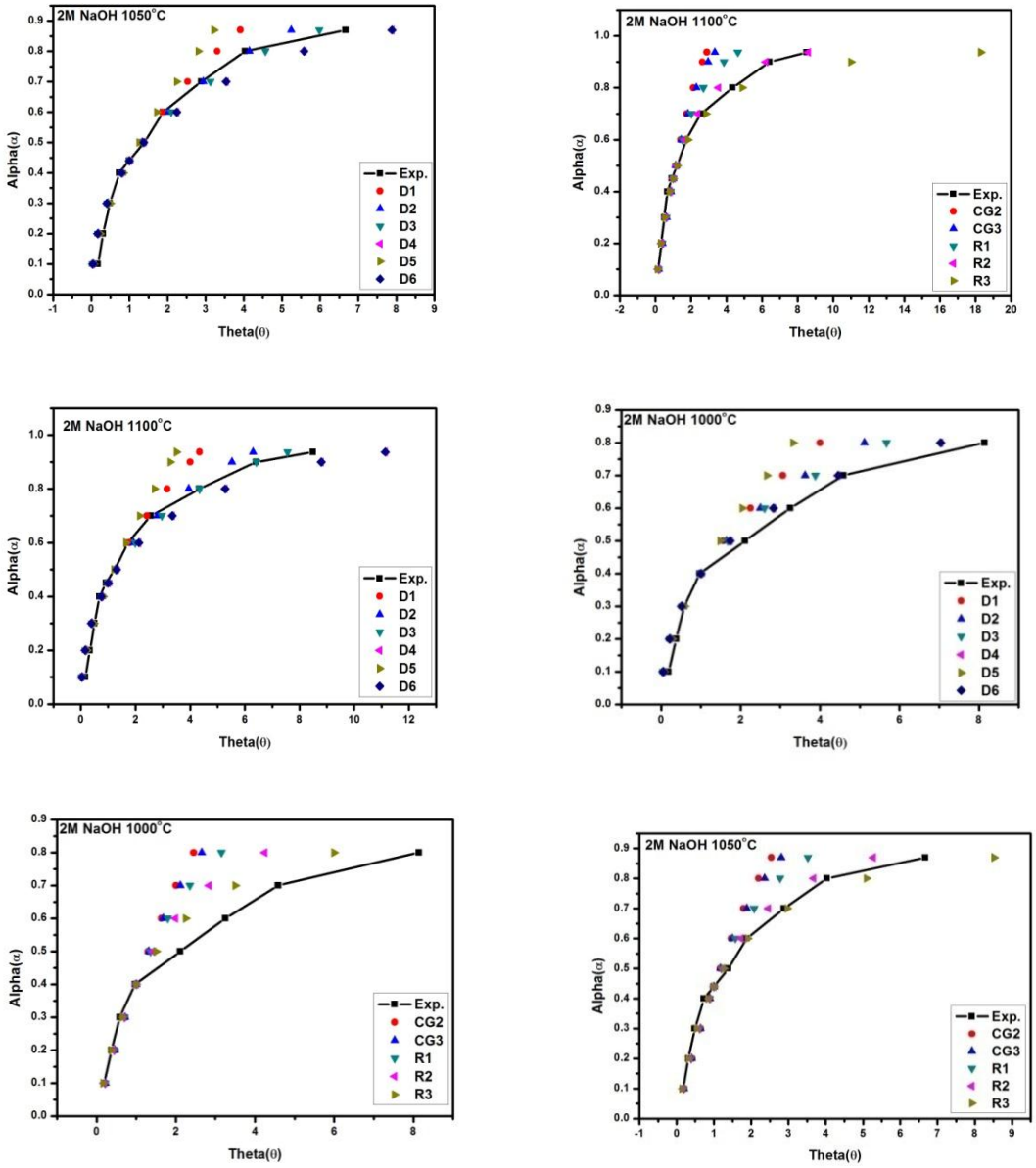

Fig. 7.16: Reduced time plot of fractional loss α along with the theoretical α vs. θ plot for different mechanism models of the 2M NaOH iron ore briquette samples

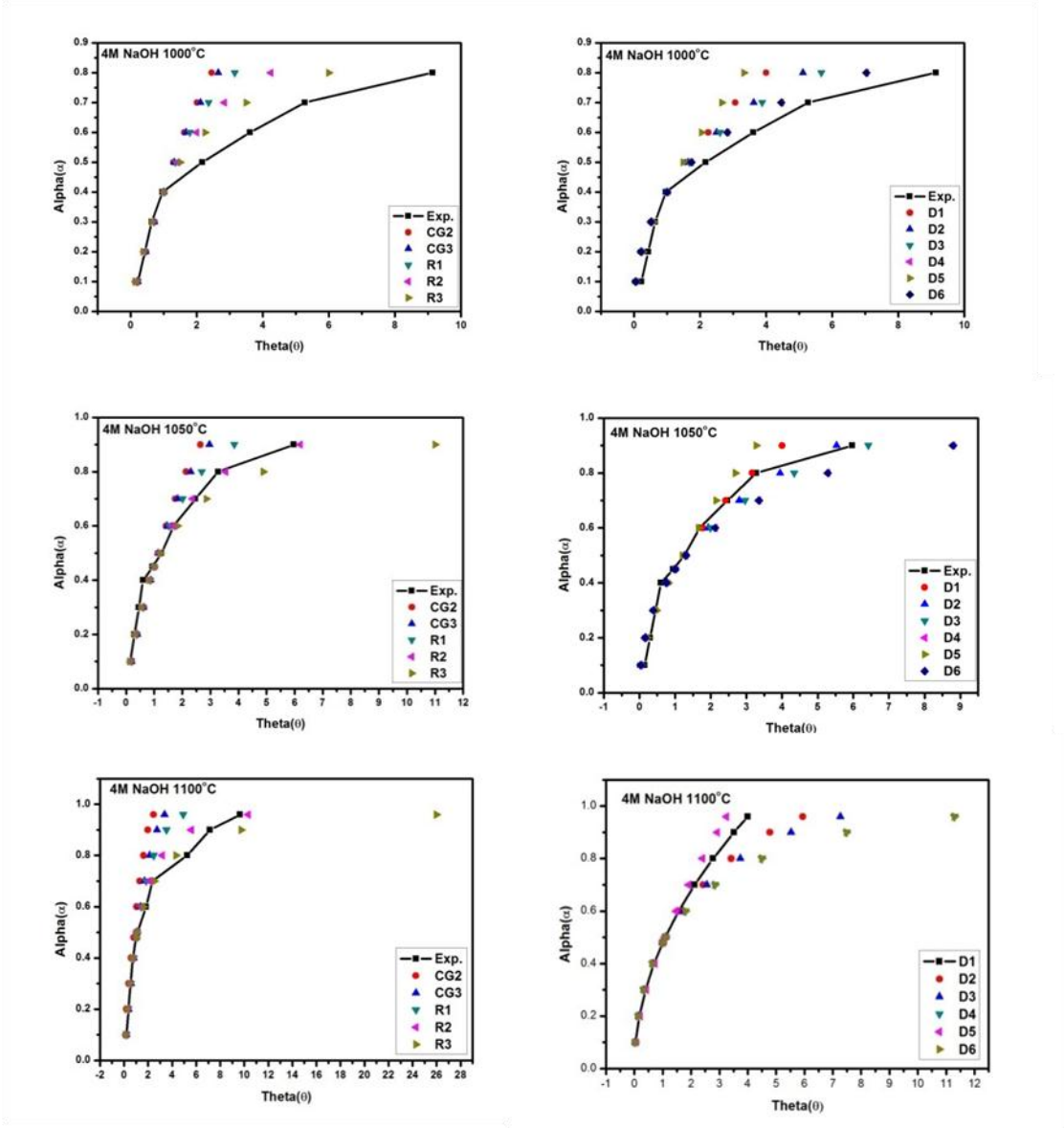

Fig. 7.17: Reduced time plot of fractional loss α along with the theoretical α vs. θ plot for different mechanism models of the 4M NaOH iron ore briquette samples

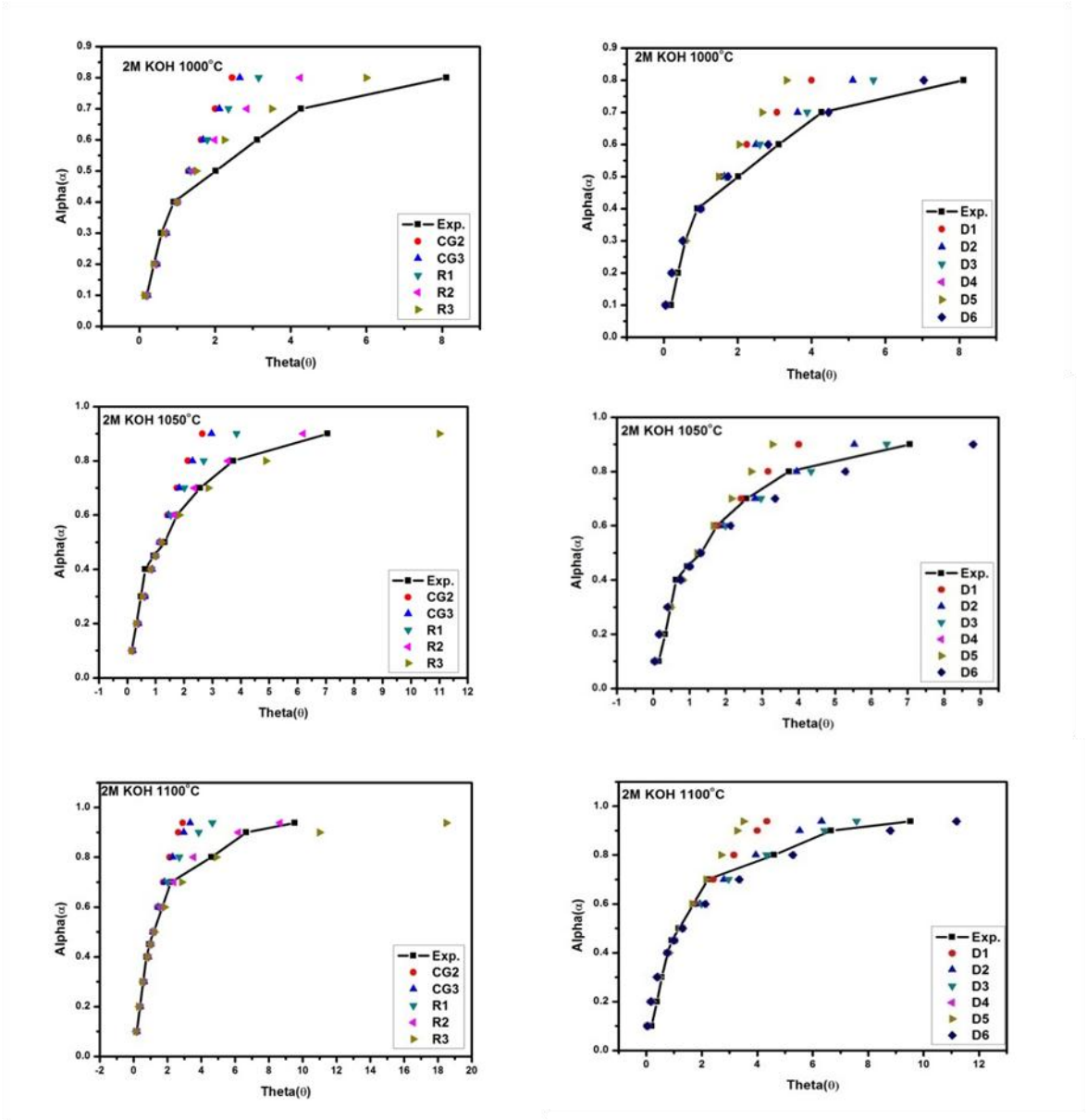

Fig. 7.18: Reduced time plot of fractional loss α along with the theoretical α vs. θ plot for different mechanism models of the 2M KOH iron ore briquette samples

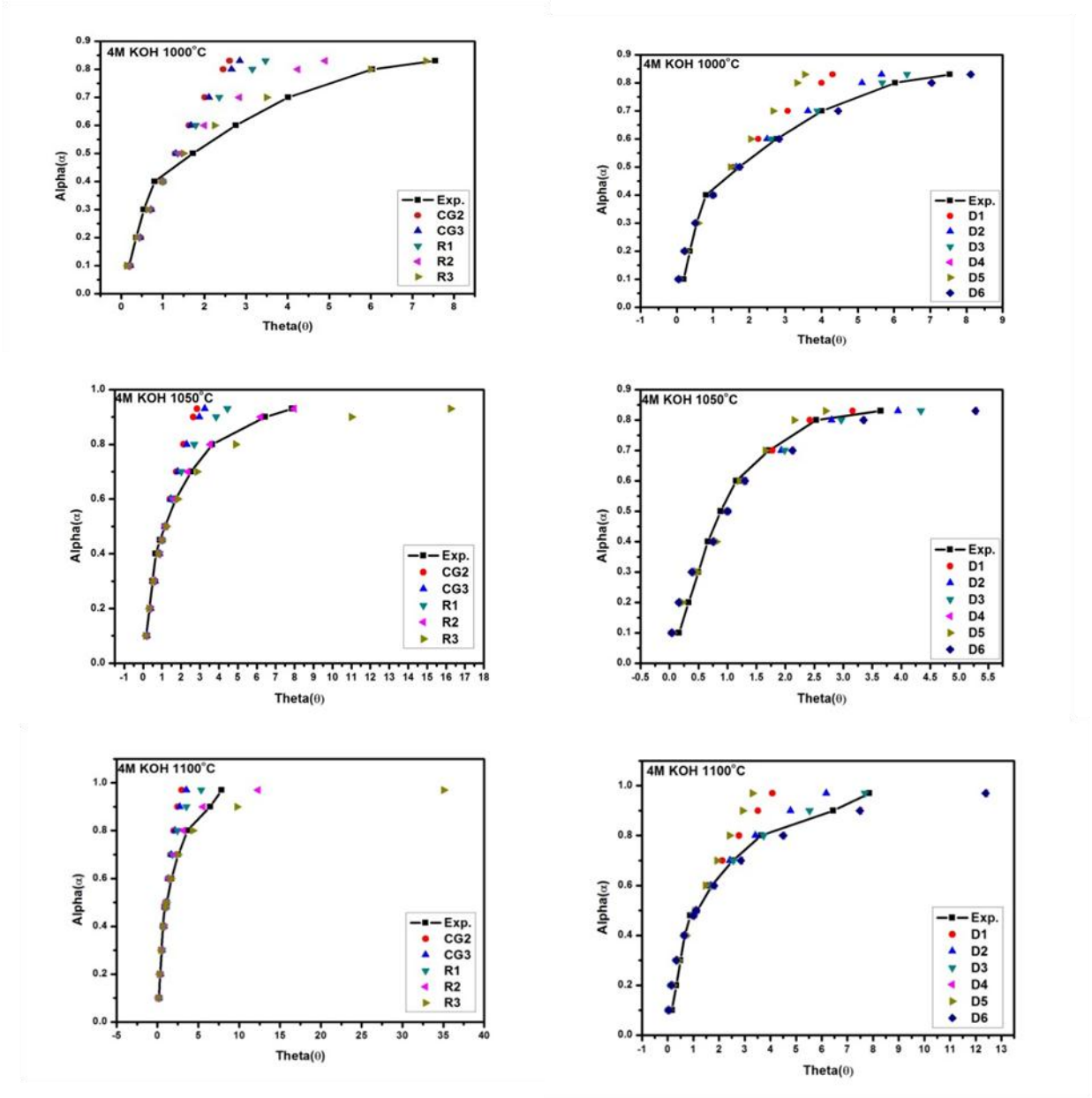

Fig. 7.19: Reduced time plot of fractional loss α along with the theoretical α vs. θ plot for different mechanism models of the 4M KOH iron ore briquette samples

Standard Briquettes: It can be seen that the experimental (α, θ) points coincide very well with the theoretical curve for R3 and R2 for the standard briquette samples as shown in figures above in the initial stages of reduction. In the later stages of reduction, the experimental (α, θ) points coincide very well with the theoretical curve for different diffusion mechanisms at different temperatures. In the initial stages of reduction, the gases reduce the briquettes on the surface as well as inside the pores leading to second order reaction mechanism. In the later stages of reduction as the surface is reduced the reduction carries on through diffusion mechanism.

Sodium added Briquettes: It can be seen that the experimental (α, θ) points coincide very well with the theoretical curve for R3 and R1 for the 2M NaOH (sodium added) briquette samples whereas they follow R3 and R2 for 4M NaOH (sodium added) briquette samples as shown in figures above in the initial stages of reduction. In the later stages of reduction, the experimental (α, θ) points coincide very well with the theoretical curves for different diffusion mechanisms at different temperatures. In the initial stages of reduction, the gases reduce the briquette s on the surface as well as inside the pores leading to second order reaction mechanism. In the later stages of reduction as the surface is reduced the reduction carries on through diffusion mechanism.

Potassium added Briquettes: It can be seen that the experimental (α, θ) points coincide very well with the theoretical curve for R2 and R1 for the 2M KOH (potassium added) briquette samples whereas for 4M KOH (potassium added) briquette samples the experimental (α, θ) points coincide very well with the theoretical curve for R1 the as shown in figures above in the initial stages of reduction. In the later stages of reduction, the experimental (α, θ) points coincide very well with the theoretical curves for different diffusion mechanisms at different

temperatures. In the initial stages of reduction, the gases reduce the briquettes on the surface as well as inside the pores leading to second order reaction mechanism. In the later stages of reduction as the surface is reduced the reduction carries on through diffusion mechanism.

7.7 Conclusion

- The predicted optimum combination of potassium hydroxide concentration of 3.97M, time of 55.66 min and temperature of 1094.31^{O}C for an Extent of Reduction of 96.2%.
- The predicted optimum combination of sodium hydroxide concentration of 3.99M, time 57.75 min at a temperature of 1093.23^{O}C for an Extent of Reduction of 95.95%.
- The extent of reduction of briquettes increases with alkali content, time of reduction and the temperature of reduction. The predicted values of the different parameters are very close to the observed experimental values.
- Addition of alkali to iron ore briquettes increases their reducibility with time as well as temperature.
- Potassium has a higher effect on briquette reduction than sodium for all times and temperatures.
- Briquettes show higher resistance to cracking with respect to lumps in presence of alkali; although the alkali percentage in briquettes is higher than in case of lumps.
- There is swelling and cracking in some briquettes samples which have been reduced at 1100^{o}C for 60 minutes [13].

7.8 Reference

1. M. Cavazzuti, Optimization Methods: From Theory to Design Scientific and Technological Aspects in Mechanics (Springer Science & Business Media, 2012).
2. N. Nguyena, J.J. Borkowskib, New 3-level response surface designs constructed from incomplete block designs. J. Stat. Plan. Inference 138, 294–305 (2008).
3. N.R. Draper, H. Smith, Applied Regression Analysis (Wiley, New York, 1981).
4. G.E.P. Box, D.W. Behnken, Some new three level designs for the study of quantitative variables. Technometrics 2, 455–475 (1960).
5. D.C. Montgomery, Design and Analysis of Experiments, 8th edn. (Wiley, New Delhi, 2011).
6. Sarkar, B. K., Samanta, S., Dey, R., & Das, G. C. (2016). A study on reduction kinetics of titaniferous magnetite ore using lean grade coal. International Journal of Mineral Processing, 152, 36-45.
7. Xu, R., Dai, B., Wang, W., Schenk, J., & Xue, Z. (2018). Effect of iron ore type on the thermal behaviour and kinetics of coal-iron ore briquettes during coking. Fuel Processing Technology, 173, 11-20.
8. Zheng, H., Wang, W., Xu, R., Zan, R., Schenk, J., & Xue, Z. (2018). Effect of the particle size of iron ore on the pyrolysis kinetic behaviour of coal-iron ore briquettes. Energies, 11(10), 2595.
9. Sarkar, B. K., Dastidar, M. G., Dey, R., & Das, G. C. (2019). A study on isothermal reduction kinetics of titaniferous magnetite ore using coke dust, an industrial waste. Canadian Metallurgical Quarterly, 58(3), 299-307.

10. Biswas, C., Gupta, P., De, A., Chaudhuri, M. G., & Dey, R. (2016). Kinetic studies on the reduction of iron ore nuggets by devolatilization of lean-grade coal. International Journal of Minerals, Metallurgy, and Materials, 23(12), 1360-1368.
11. Wang H, Chu M, Guo B, Bao J, Zhao W, Liu Z, et al. Investigation on Gasification Reaction Behavior and Kinetic Analysis of Iron Coke Hot Briquette under Isothermal Conditions. Steel Res Int 2019;90:1–10.
12. Sarkar BK, Kumar N, Dey R, Das GC. Optimization of Quenching Parameters for the Reduction of Titaniferous Magnetite Ore by Lean Grade Coal Using the Taguchi Method and Its Isothermal Kinetic Study. Metall Mater Trans B Process Metall Mater Process Sci 2018;49:1822–33.
13. Song, Wei, Luo, Guo-Ping, Sun, Chen-Chen, Zhang, Jing and Zhu, Jian-Guo. "Effect of K and Na on reduction swelling performance of oxidized roasted briquettes" High Temperature Materials and Processes, vol. 40, no. 1, 2021, pp. 241-252.

Chapter-8

Study of the Effect of Alkali on the Reducibility and Kinetics of Pellets under Blast Furnace Conditions

8.1 Alkali Impregnation of Iron Ore Pellets

Iron ore pellets have been collected from Tasmania, Australia. The composition and XRD analysis of the pellets have been given in chapter 5. The pellets contain mainly hematite phase. The pellets have been impregnated with sodium and potassium. Two solutions of 2M and 4M concentration have been made using sodium hydroxide and potassium hydroxide. 500gms of pellets have been weighed. The samples are then put in a beaker containing the alkali solution. The beaker is then put in a desiccator attached to a vacuum pump. The desiccator is closed and the pump is switched on. There is bubbling due to alkali entering the pores; the pump is switched off when the bubbling ends. The pellets are taken out and heated at 120^{o}C for 1 hour. The final weight of the pellets is taken to find out the alkali gain.

Pellet	Alkali (%)
Standard	0
2M NaOH	0-0.15%
4M NaOH	0.15-0.30%
2M KOH	0-0.15%
4M KOH	0.15-0.30%

Table 8.1: Alkali gain by iron ore pellets

8.2 Reduction of Pellets under Blast Furnace Conditions

The pellets with and without alkali are reduced under the reduction conditions of a blast furnace. Pellets have been selected in the size range of -12.5mm to +10mm. The pellets are put inside the reduction tube. There is a perforated plate at the bottom which allows the gases to flow from below and reduce the pellets. A layer of porcelain balls is put in between the pellets and the perforated plate to allow uniform gas flow. A thermocouple has been placed at the centre of the test sample. The reduction tube is closed and placed inside the furnace. The tube is suspended through the weighing device. It should be made sure that the tube does not touch the furnace walls or the heating elements. The conditions are set and the furnace is

started. Initially nitrogen is passed through the tube but as soon as the temperature reaches 950^{o}C (blast furnace lower stack), carbon monoxide gas (40% CO, 60% N_2) is passed through the tube for reduction [1]. The testing is continued till 65% reduction is achieved. Again nitrogen is passed through the system as the sample cools down. The weight loss throughout the process is recorded in the computer. The sample is taken out and weighed to find out the final weight of the sample. The degree of reduction and the reducibility index have been calculated to understand the effect of alkali on pellet reduction [1]. (Calculation has been shown in Appendix-III)

- **Degree of Reduction**

$$R_t = \left(\frac{0.111\, w_1}{0.430\, w_2} + \frac{m_1 - m_t}{m_0 \times 0.430\, w_2} \times 100 \right) \times 100 \qquad 1$$

where; w_1 is the FeO content in the sample

w_2 is the total Fe in the sample

m_0 is the weight of sample

m_1 is the weight of sample just before testing

m_t is the weight of sample after reduction time t

(m_0 and m_1 are the same in lab scale but in industrial tests these values differ from each other) The different pellets, i.e. with and without alkali are reduced in the vertical retort furnace and their degree of reduction has been calculated. The degree of reduction has been plotted against time to understand the effect alkali have on the degree of reduction of iron ore pellets.

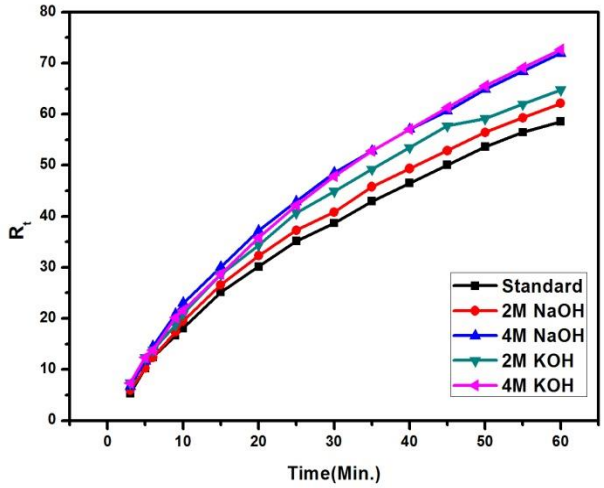

Fig. 8.1: The reducibility degree of pellet under different alkali loadings

The degree of reduction increases as the alkali content of the pellets increases. The highest degree of reduction has been achieved in case of potassium (4M). The effect of potassium is much more dominant as compared to sodium.

- **Reducibility Index:**

$$\frac{dR}{dt} = \frac{33.6}{t_{60} - t_{30}} \qquad 2$$

where; t_{60}= time taken to attain 60% degree of reduction

t_{30}= time taken to attain 30% degree of reduction

The reducibility index for different alkali loaded iron ore pellets has been calculated and is given in the Table 8.2.

Pellet	Reducibility Index
Standard	0.78
2M NaOH	0.88
4M NaOH	0.93
2M KOH	1.20
4M KOH	1.24

Table 8.2: Reducibility index of Iron ore pellets at different alkali loading

It can be observed from the table above that the reducibility index of the iron ore pellets increases with the amount of alkali. The effect of potassium on the reducibility index is higher than that of sodium. But swelling and sticking takes place during reduction due to the presence of alkali [2, 3, 4, 5]. This makes it difficult to take out the samples out of the reduction tube without damaging the samples. Due to this reason the degradation tendency and abrasion tendency of pellets could not be evaluated.

8.3 XRD Analysis of the Iron Ore Pellets

These crushed reduced samples have been subjected to XRD analysis to find out the main phases present in the reduced pellets.

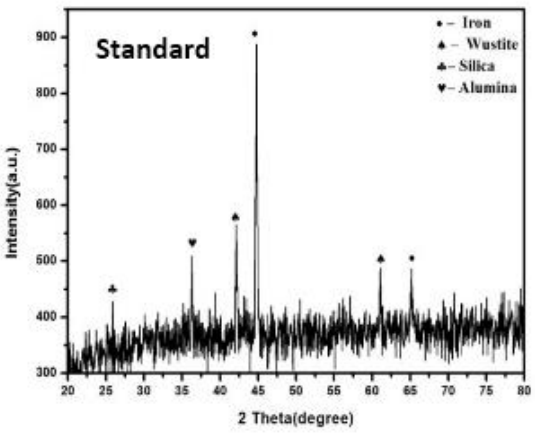

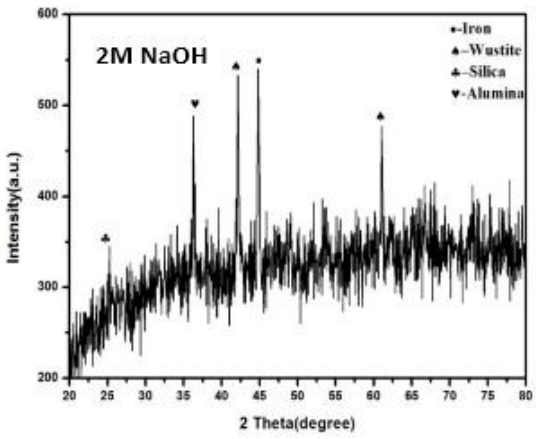

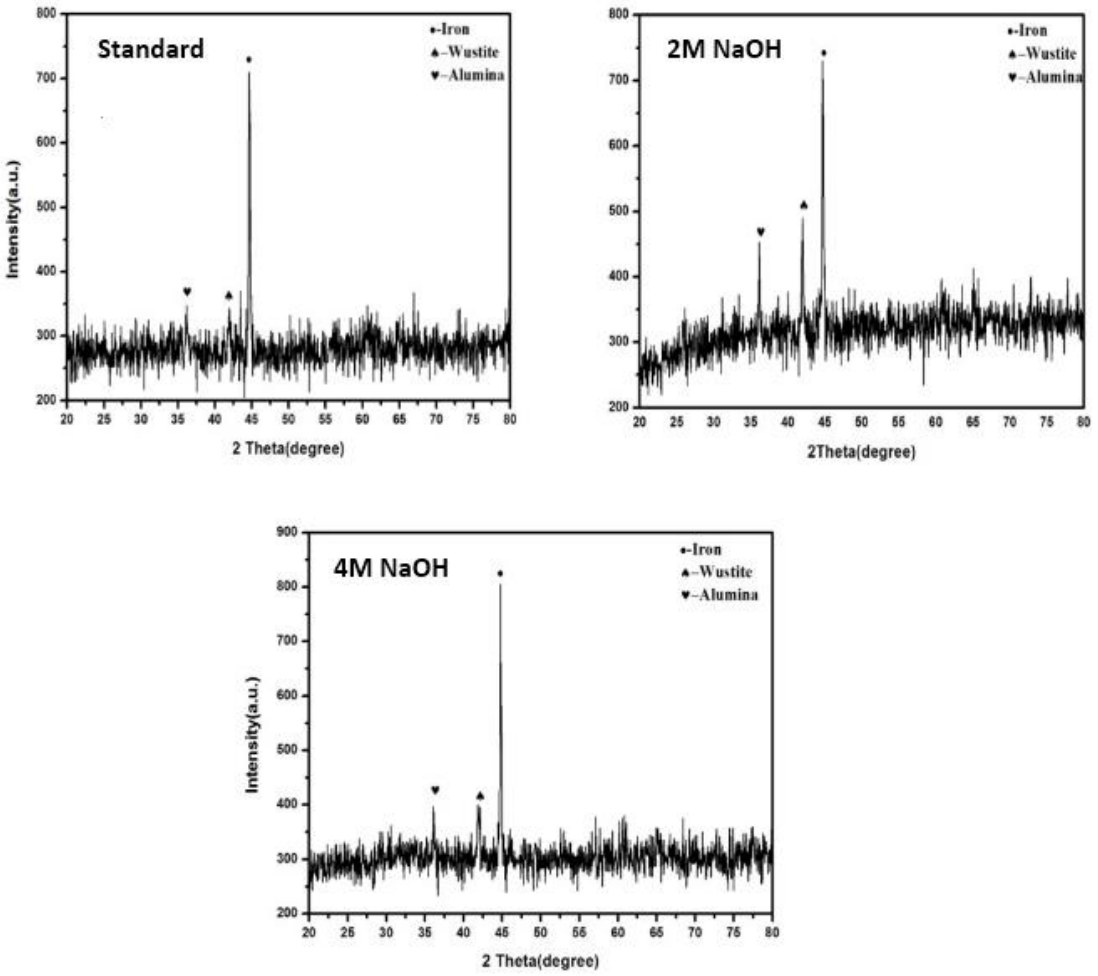

Fig. 8.2: XRD plots of pellets with and without alkali

It can be observed from the XRD plots that the main phase present is iron in all the cases. The amount of wustite increases as the alkali content of the pellets increases. Potassium has the lowest intensity peak of iron with wustite as the other major phase. Due to the presence of alkali the reduction step of wustite to iron is impeded which leads to high intensity peaks of wustite along with iron [2].

8.4 Isothermal Kinetic Study

The isothermal kinetic study of reduction of pellets using carbon monoxide has been carried out. Pellets have been reduced at 950°C for 5, 10, 15, 20, 30, 40, 50 and 60 minutes. The reduced time analysis as discussed in Chapter 3, section 3.5 has been carried out using experimental data to find the reaction mechanism being followed under different alkali loadings. Many isothermal kinetic study of iron ore pellets have been conducted [6, 7, 8, 9, 10].

8.4.1 Effect of Alkali and Time on Pellet Reduction:

The loss of weight percentage as a function of time at 950°C has been plotted in fig. 8.3.

The weight loss percentage has been calculated using the following formulae:

$$\% \text{ of Weight Loss} = \frac{W_0 - W_t}{W_0} \quad 3$$

Where w_o and w_t are the weight of the pellets before and after reduction.

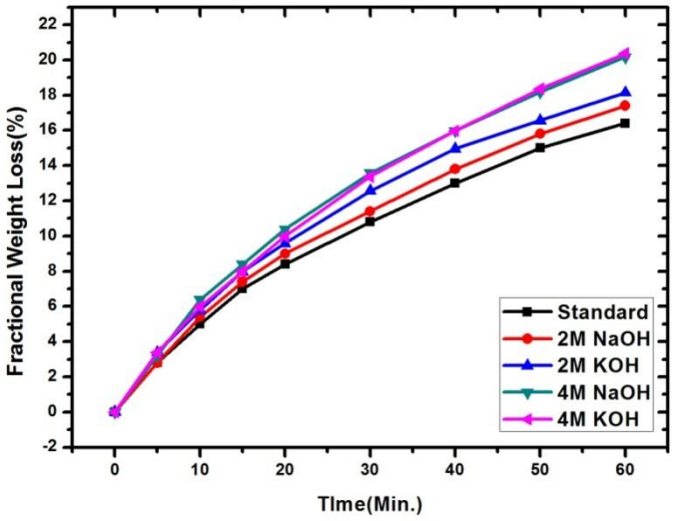

Fig. 8.3: Fractional weight loss (%) vs. time for pellets with and without alkali

It can be observed from the above figure that the alkali increases the fractional weight loss (%) of pellets during reduction. Sodium has higher effect than standard pellets and potassium has higher effect compared to the effect of sodium.

8.4.2 Isothermal Kinetic Study of Reduction of Pellets

In the present study of the isothermal reduction kinetic, the fractional weight loss (α) is defined as:

$$\alpha = \frac{M_t}{M_0} \qquad 4$$

where, M_0 is the initial weight of the iron ore pellets and M_t is the weight loss due to iron ore reduction by carbon monoxide in the vertical retort. So, α, defined by Eq. 4, gives the isothermal weight fraction loss as a function of time. These data have been graphically plotted in Fig. 8.4.

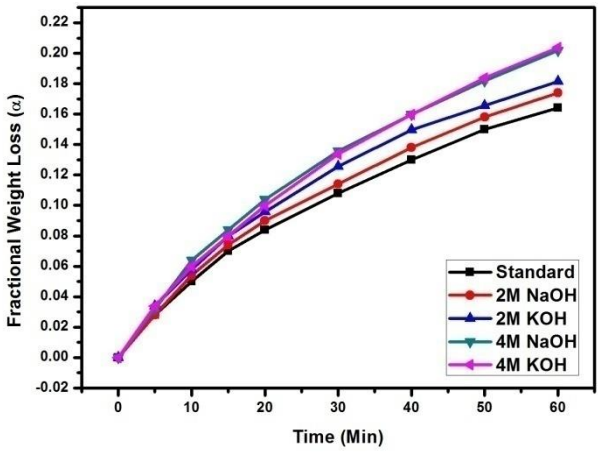

Fig. 8.4: Fractional weight loss (%) vs. time for pellets with and without alkali

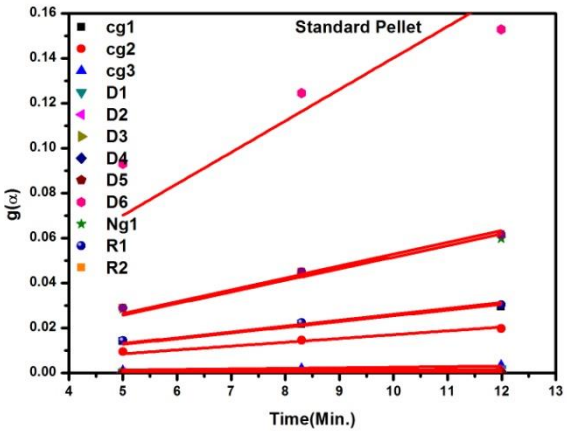

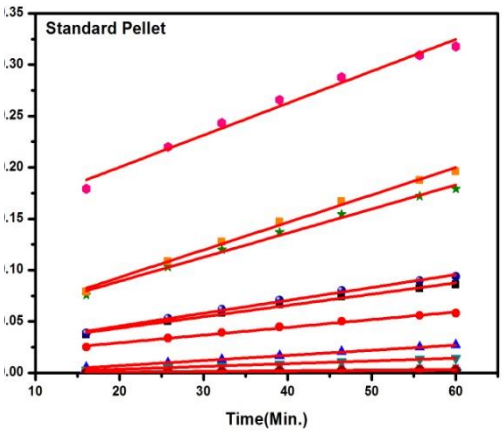

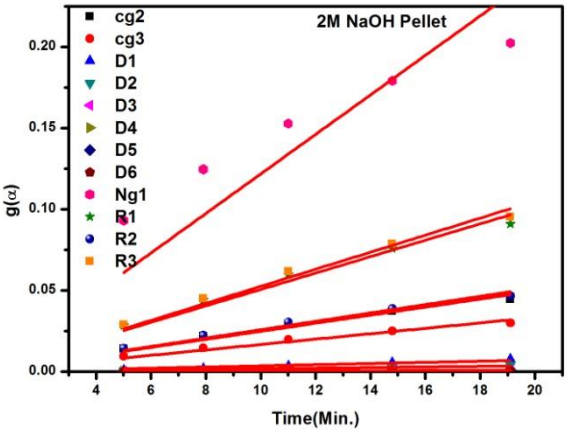
2M NaOH Pellet
cg2
cg3
D1
D2
D3
D4
D5
D6
Ng1
R1
R2
R3
g(α)
Time(Min.)

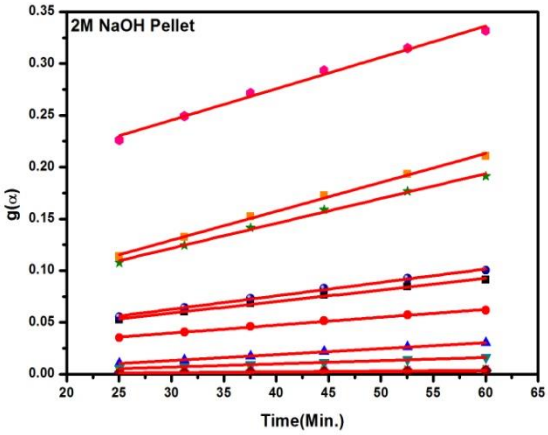
2M NaOH Pellet
g(α)
Time(Min.)

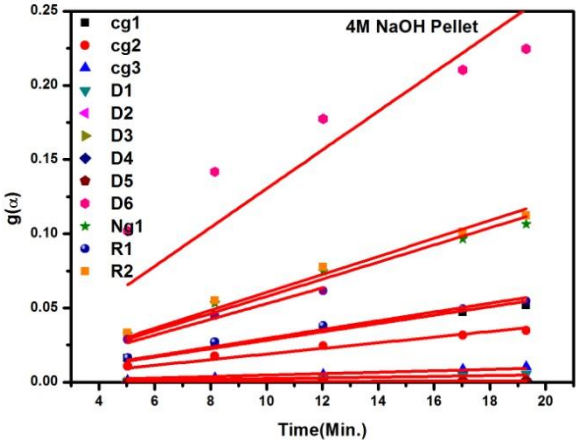
4M NaOH Pellet
cg1
cg2
cg3
D1
D2
D3
D4
D5
D6
Ng1
R1
R2
g(α)
Time(Min.)

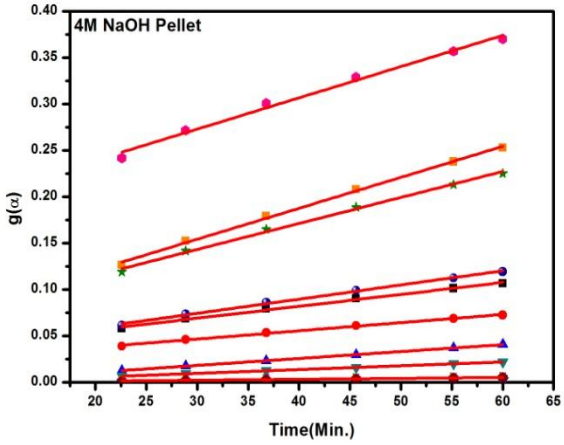
4M NaOH Pellet
g(α)
Time(Min.)

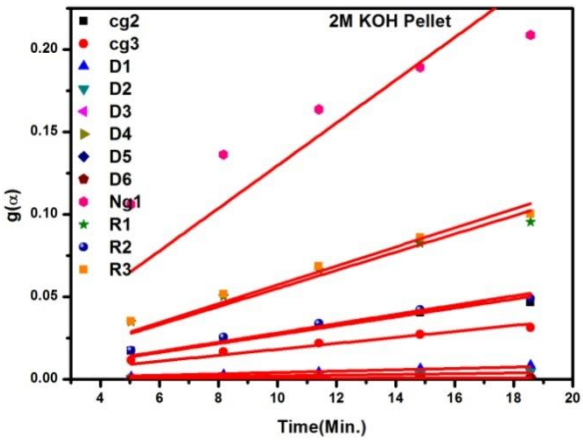
2M KOH Pellet
cg2
cg3
D1
D2
D3
D4
D5
D6
Ng1
R1
R2
R3
g(α)
Time(Min.)

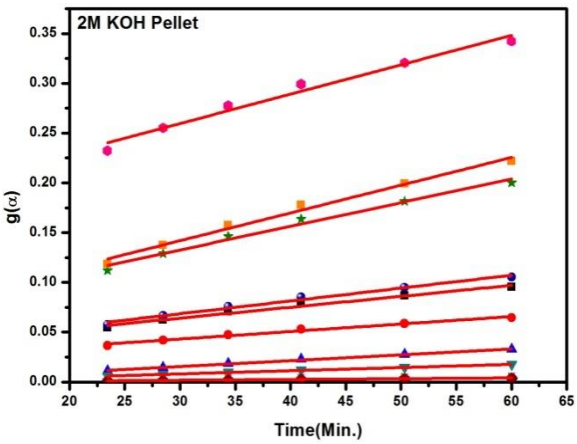
2M KOH Pellet
g(α)
Time(Min.)

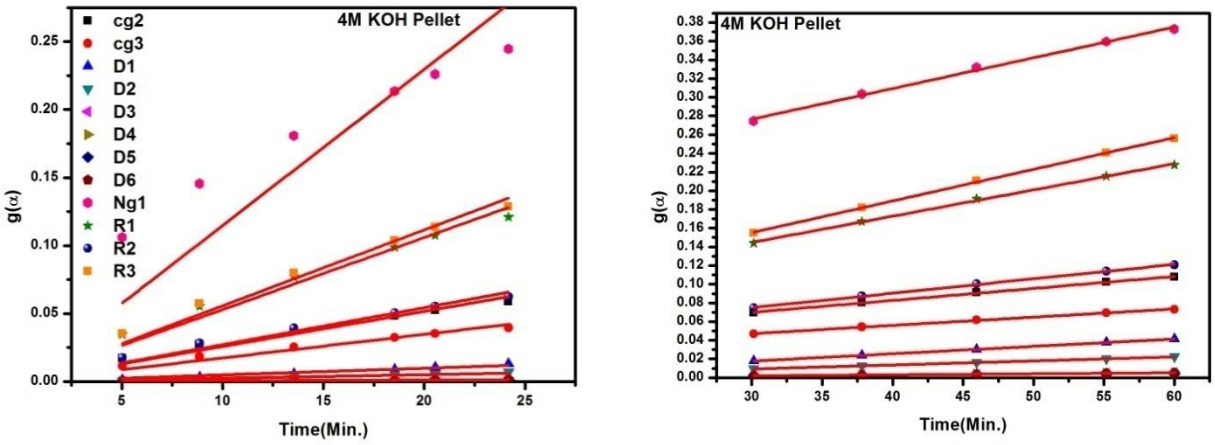

Fig. 8.5: Various mechanism models fitting showing the pellet reduction vs. Time for different pellet samples (Initial and last part of reduction, respectively)

	CG2	CG3	D1	D2	D3	D4	D5	D6	Ng1	R1	R2	R3
Standard	0.9967	0.9968	0.9607	0.9594	0.9589	0.9580	0.9631	0.9580	0.9739	0.9970	0.9974	**0.9977**
2M NaOH	0.9948	0.9950	0.9650	0.9634	0.9629	0.9617	0.9679	0.9617	0.9679	0.9955	0.9961	**0.9967**
2M KOH	0.9922	0.9925	0.9761	0.9747	0.9742	0.9732	0.9786	0.9732	0.9645	0.9931	0.9939	**0.9946**
4M NaOH	0.9950	0.9721	0.9706	0.9701	0.9690	0.9748	0.9690	0.9691	0.9955	0.9962	**0.9969**	0.9939
4MKOH	0.9935	0.9938	0.9801	0.9786	0.9781	0.9770	0.9825	0.9770	0.9671	0.9944	0.9953	**0.9960**

Table 8.3: Correlation coefficient calculated using different mechanism functions for the initial stages of pellet reduction

	CG2	CG3	D1	D2	D3	D4	D5	D6	Ng1	R1	R2	R3
Standard	0.9902	0.9908	0.9989	0.9986	0.9984	0.9982	0.9991	**0.9982**	0.9819	0.9918	0.9932	0.9944
2M NaOH	0.9939	0.9942	0.9996	0.9996	0.9996	0.9995	**0.9995**	0.9995	0.9898	0.9948	0.9957	0.9965
2M KOH	0.9811	0.9817	0.9961	0.9969	0.9971	0.9975	**0.9948**	0.9975	0.9740	0.9830	0.9848	0.9865
4M NaOH	0.9944	0.9948	0.9998	0.9996	0.9995	0.9993	**0.9998**	0.9993	0.9901	0.9955	0.9965	0.9974
4MKOH	0.9940	0.9944	0.9999	0.9998	0.9997	0.9995	**0.9998**	0.9995	0.9897	0.9952	0.9963	0.9972

Table 8.4: Correlation coefficient calculated using different mechanism functions for the final stages of pellet reduction

According to the kinetic analysis and calculation procedures introduced in chapter 3, section 3.5, the g(α) value for each mechanism model versus the reduction time t for the gasification reaction of the pellet samples have been calculated and plotted, every plot is then subjected to linear fit through zero for initial stages of reduction whereas for later stages of reduction normal linear fitting is done. The results are shown in figure 8.5. Simultaneously, the corresponding correlation coefficient for each model has been calculated, which is given in Table 8.3 and 8.4 for initial and final stages of reduction, respectively. The higher the correlation coefficient the better is the mechanism function [12].

To determine the kinetic model and the rate controlling steps in the reaction, the experimental data are analysed by using reduced time plots shown in figure 8.6, 8.7, 8.8, 8.9 and 8.10 for standard, sodium added (2M and 4M) and potassium added (2M and 4M) pellet samples, respectively. From these figures and the calculated correlation coefficient given in table 8.3 and 8.4, the models with the highest R squared values and those matching the experimental reduced time plots have been selected to be the governing reaction mechanism for the individual pellet samples [13].

Standard Pellet: It has been found that the experimental (α, θ) points coincide very well with the theoretical curve for R3 for the standard pellet samples as shown in figures below in the initial stages of reduction. In the later stages of pellet reduction, the experimental (α, θ) points coincide very well with the theoretical curve for D6. In the initial stages of reduction, the gases reduce the pellets on the surface as well as inside the pores leading to second order reaction mechanism. In the later stages of reduction as the surface is reduced the reduction carries on through diffusion mechanism.

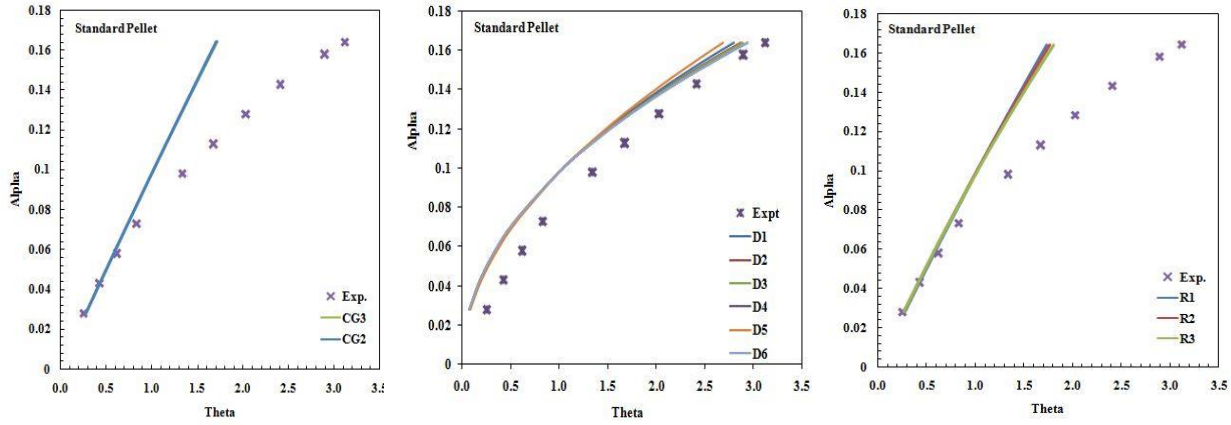

Fig. 8.6: Reduced time plot of fractional loss α along with the theoretical α vs. θ plot for different mechanism models of the standard pellet samples

Sodium added Pellets: It can be seen that the experimental (α, θ) points coincide very well with the theoretical curve for R3 for the sodium added pellet samples as shown in figures below in the initial stages of reduction, only 4M NaOH added pellets follow R2 reaction mechanism. In the later stages of pellet reduction, the experimental (α, θ) points coincide very well with the theoretical curve for D5. In the initial stages of reduction, the gases reduce the pellets on the surface as well as inside the pores leading to second order reaction mechanism. In the later stages of reduction as the surface is reduced the reduction carries on through diffusion mechanism. Due to the presence of sodium the reduction of pellets follow a much faster reaction mechanism compared to standard pellets which follow the much slower D6 reaction mechanism.

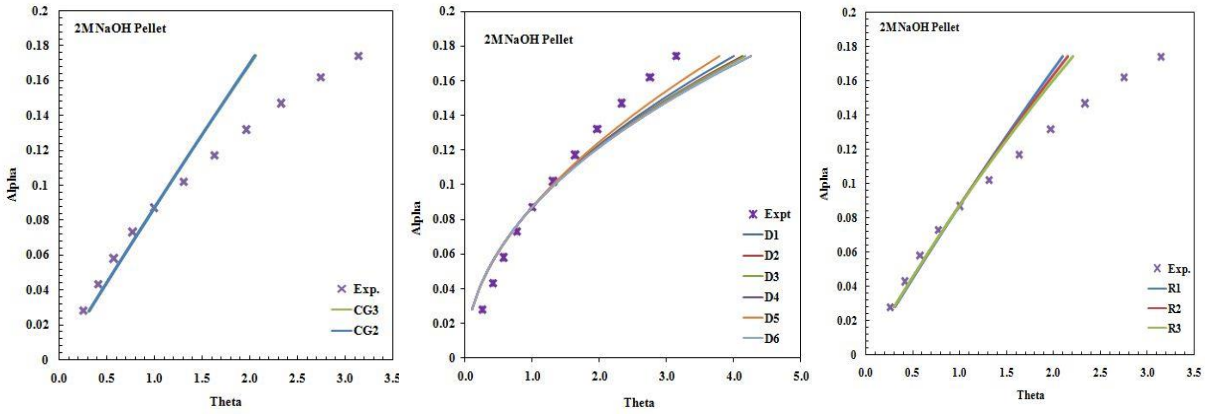

Fig. 8.7: Reduced time plot of fractional loss α along with the theoretical α vs. θ plot for different mechanism models of the 2M NaOH pellet samples

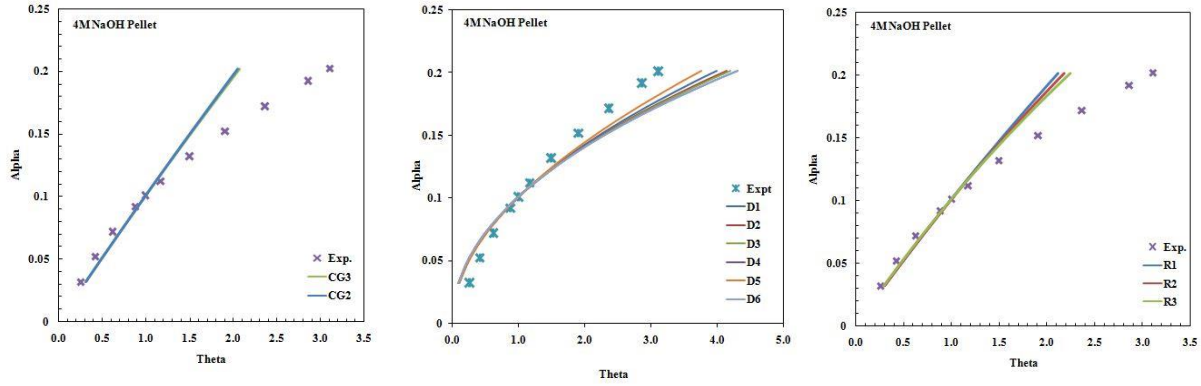

Fig. 8.8: Reduced time plot of fractional loss α along with the theoretical α vs. θ plot for different mechanism models of the 4M NaOH pellet samples

Potassium added Pellets: It has been found that the experimental (α, θ) points coincide very well with the theoretical curve for R3 for the sodium added pellet samples as shown in figures below in the initial stages of reduction. In the later stages of pellet reduction, the experimental (α, θ) points coincide very well with the theoretical curve for D5. In the initial stages of reduction, the gases reduce the pellets on the surface as well as inside the pores

leading to second order reaction mechanism. In the later stages of reduction as the surface is reduced the reduction carries on through diffusion mechanism. Due to the presence of potassium the reduction of pellets follow a much faster reaction mechanism compared to standard pellets and sodium loaded pellets which follow the much slower D6 reaction mechanism. It can be seen from the plots of degree of reduction and fractional weight loss vs. time shows that in case of reduction of pellets loaded with 4M NaOH follows faster reduction than 4M loaded KOH in the initial stages whereas in the later stages the effect of potassium becomes more dominant.

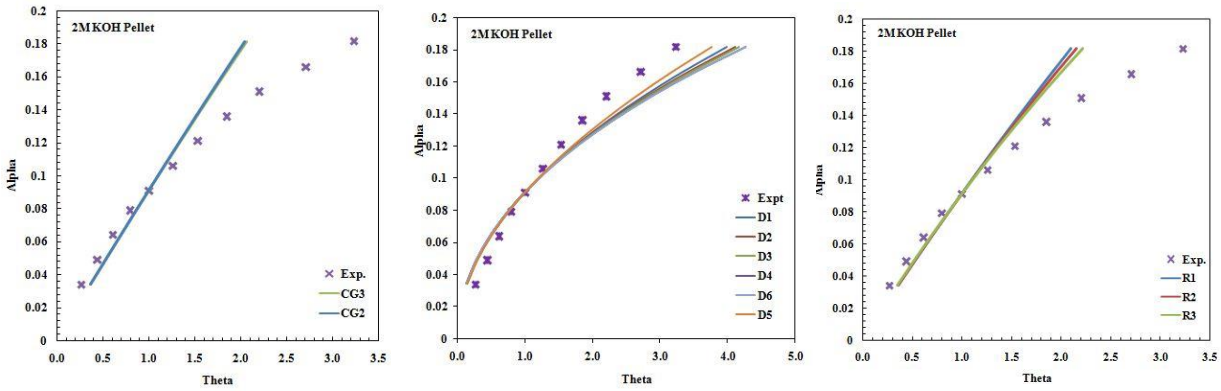

Fig. 8.9: Reduced time plot of fractional loss α along with the theoretical α vs. θ plot for different mechanism models of the 2M KOH pellet samples

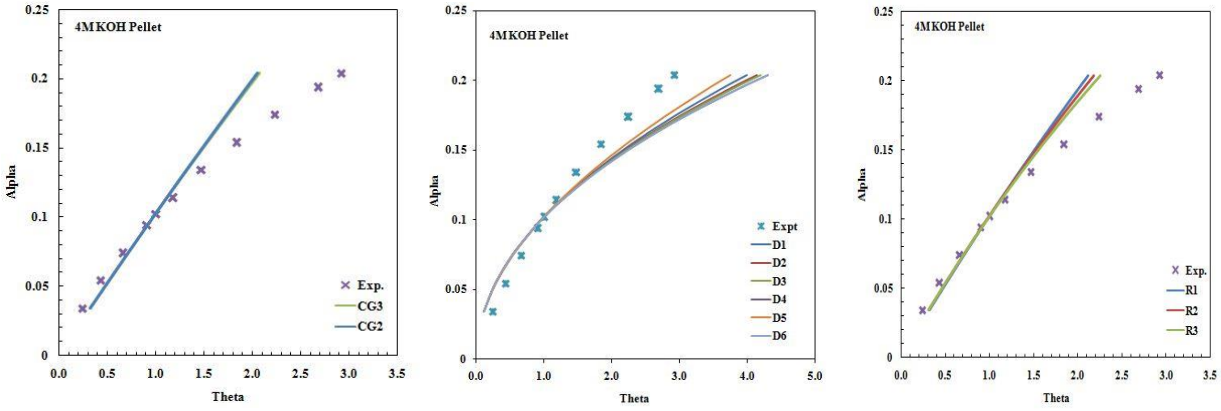

Fig. 8.10: Reduced time plot of fractional loss α along with the theoretical α vs. θ plot for different mechanism models of the 4M KOH pellet samples

8.5 Conclusion

- Iron ore pellets reducibility in the reduction zone of blast furnace increases with time, temperature and alkali content.
- Alkali loaded pellets have higher reducibility compared to standard pellets. Potassium has much higher effect on degree of reduction and reduction index compared to sodium.
- The reduction of pellet follows second order reaction mechanism (R3) in all the cases except for 4M NaOH added pellets which follows one and half order chemical reaction (R2) during initial stages of reduction.
- In the later stages of reduction, the reaction mechanism shifts from D6 (diffusion mechanism) in case of standard pellets to D5 (diffusion mechanism) in case of alkali loaded pellets.
- Although pellets reducibility increases due to alkali, a lot of swelling and sticking takes place in alkali loaded pellets [2, 5].
- These cause many process irregularities in the blast furnace. Pellets with alkali should be avoided from being used in a blast furnace.

8.6 Reference

1. International Organization for Standardization: ISO 4695 Iron ores - Determination of reducibility (1995).
2. Taymour ELKASABGY, Effect of Alkalis on Reduction Behavior of Acid Iron Ore Pellets, Transactions of the Iron and Steel Institute of Japan, 1984, 24: 8, p. 612-621.
3. Mikko Iljana, Olli Mattila, Tuomas Alatarvas, Jari Kurikkala, Timo Paananen, Timo Fabritius, Effect of Circulating Elements on the Dynamic Reduction Swelling Behaviour of Olivine and Acid Iron Ore Pellets under Simulated Blast Furnace Shaft Conditions, ISIJ International, 2013, 53:3, p. 419-426.
4. E. T. Turkdogan & J. V. Vinters (1973) Reducibility of iron ore pellets and effect of additions, Canadian Metallurgical Quarterly, 12:1, 9-21.
5. Pichler, A., Schenk, J., Hanel, M., Mali, H., Thaler, C., Hauzenberger, F., & Stocker, H. (2014). Influence of alkalis on mechanical properties of lumpy iron carriers during reduction. In Conference Proceedings to the 23rd International Conference on Metallurgy and Materials (pp. 40-40).
6. Sah, R., & Dutta, S. K. (2011). Kinetic studies of iron ore–coal composite pellet reduction by TG–DTA. Transactions of the Indian Institute of Metals, 64(6), 583-591.
7. Valipour, M. S., Hashemi, M. M., & Saboohi, Y. (2006). Mathematical modeling of the reaction in an iron ore pellet using a mixture of hydrogen, water vapor, carbon monoxide and carbon dioxide: an isothermal study. Advanced Powder Technology, 17(3), 277-295.
8. Hammam, A., Li, Y., Nie, H., Zan, L., Ding, W., Ge, Y., ... & Yu, Y. (2021). Isothermal and non-isothermal reduction behaviors of iron ore compacts in pure hydrogen atmosphere and kinetic analysis. Mining, Metallurgy & Exploration, 38(1), 81-93.

9. Junca, E., Restivo, T. A. G., Espinosa, D. C. R., & Tenório, J. A. S. (2015). Application of stepwise isothermal analysis method in the kinetic study of reduction of basic oxygen furnace dust. Journal of Thermal Analysis and Calorimetry, 120(3), 1913-1919.
10. Kowitwarangkul, P., Babich, A., & Senk, D. (2014). Reduction kinetics of self-reducing pellets of iron ore. AISTech Proc, 1, 611-622.
11. Sarkar, B. K., Samanta, S., Dey, R., & Das, G. C. (2016). A study on reduction kinetics of titaniferous magnetite ore using lean grade coal. International Journal of Mineral Processing, *152*, 36-45.
12. Wang H, Chu M, Guo B, Bao J, Zhao W, Liu Z, et al. Investigation on Gasification Reaction Behavior and Kinetic Analysis of Iron Coke Hot Briquette under Isothermal Conditions. Steel Res Int 2019;90:1–10.
13. Sarkar BK, Kumar N, Dey R, Das GC. Optimization of Quenching Parameters for the Reduction of Titaniferous Magnetite Ore by Lean Grade Coal Using the Taguchi Method and Its Isothermal Kinetic Study. Metall Mater Trans B Process Metall Mater Process Sci 2018;49:1822–33.

Chapter-9

Study of the Effect of Alkali on the Reducibility and Kinetics of Sinters under Blast Furnace Conditions

9.1 Alkali Impregnation and Selection of Iron Ore Sinters

Iron ore sinters have been collected from Tata Steel, Jamshedpur, India; Vizag Steel Plant, Vishakapattanam, India and Donawitz, Austria. The composition and XRD analysis of the sinters have been given in chapter 5. The WDXRF analysis of sinters collected from India has been done and the results are given in table 9.1.

- The XRD analysis of sinter from Austria has high intensity peak of magnetite. We have collected hematite as well as magnetite sinters.
- The sinter collected from Donawitz innately has high percentage of potassium as seen from the WDXRF data of the sinter as given in chapter 5.
- The sinters with low potassium percentage have been impregnated with potassium initially.

A solution of 2M concentration has been made using potassium hydroxide. 500gms of sinter has been weighed. The samples are then put in a beaker containing the alkali solution. The beaker is then put in a desiccator attached to a vacuum pump. The desiccator is closed and the pump is switched on. There is bubbling due to alkali entering the pores; the pump is switched off when the bubbling ends. The sinters are taken out and heated at 120^{o}C for 1 hour. The final weight of the sinters is taken to find out the alkali gain. For the selection of sinter LTD test has been carried out for all the three sinter samples (hematite and magnetite sinters). Sinter with the best LTD properties has been selected for further testing.

Composotion	T Fe	FeO	CaO	MgO	SiO_2	Al_2O_3	MnO	TiO_2	P	K_2O	Na_2O
Vizag Steel	57.7	10.97	9.2	2.1	4.5	2.2	0.08	0.15	0.045	0.06	0.02
Tata Steel		10.5	11.6	1.803	4.26	2.2	0.068	0.14	0.01	0.032	0.07

Table 9.1: WDXRF analysis of sinters from India

Sinter	Potassium (%)
Tata Steel	0.15%
Vizag Steel Plant	0-0.20%
Donawitz	0.40%

Table 9.2: Alkali gain by iron ore sinter

9.1.1 Low Temperature Reduction Degradation (LTD) Indices for Blast Furnace Feedstock:

The sinters have been selected in the size range of -12.5mm to +10mm. 500 grams of sinter is weighed for the test. The sinters are then put inside the reduction tube after the perforated plates and porcelain balls to ensure uniform gas flow. The thermocouple is placed into the centre of the sample holder. The tube is then closed and hung via the weighing device. The tube should not touch the furnace walls or the heating elements. The furnace is closed and the program is run for the LTD test. The sinters are reduced at 500^{o}C (upper stack region) with the help of CO, CO_2, N_2 and H_2 (20%, 20%, 58% and 2% respectively) for 60 minutes [1]. The tube is allowed to cool down after which the sample is taken out and weighed to find out the weight lost. The samples are then taken for evaluating RDI-$1_{6.3,}$ RDI-$1_{3.15}$ and RDI-$1_{0.5}$ values of sinters, as given in section 4.3.1 of chapter 4[2]. The results have been given in the table below.

Sample	RDI-$1_{6.3}$	RDI-$1_{3.15}$	RDI-$1_{0.5}$
Tata Steel	39.53	27.56	3.50
Vizag Steel Plant	25.60	40.41	9.17
Donawitz	55.03	17.06	3.00

Table 9.3: The low temperature reduction degradation indices for different sinters with added potassium

It can be seen from the table that hematite sinters with added potassium have very poor LTD properties. The magnetite sinter on the other hand showed much better LTD properties even though it contains the higher amount of potassium as can be seen in table 9.1 [3]. The phase transformation during hematite to magnetite leads to stress generation which in turn results in crack formation and loss of strength whereas; the transformation from magnetite to wustite does not lead to such loss of strength [4, 5, 6, 7, 8]. The magnetite sinter collected from Donawitz, Austria has been selected for further testing of effects of alkali on the reducibility of sinters under direct reduction zone of blast furnace.

9.1.2 Sodium Impregnation of Magnetite Sinters:

The sinters collected from Donawitz innately contain high percentage of potassium (0.4%); that is why no extra potassium has been added. Only sodium addition has been done in the same manner as described in section 9.1, with the help of sodium hydroxide solutions. The alkali gain has been calculated and given in the table below.

Donawitz Sinter	Alkali (%)
Standard	0.40% K
2M NaOH	0.40% K, 0.15% Na
4M NaOH	0.40%K, 0.30% Na

Table 9.4: Alkali gain by iron ore sinter

9.2 Reduction of Sinters under Blast Furnace Condition

The sinters with alkali are reduced under the reduction conditions of a blast furnace. Sinters have been selected in the size range of -12.5mm to +10mm. The sinters are put inside the reduction tube. There is a perforated plate at the bottom which allows the gases to flow from below and reduce the sinters. A layer of porcelain balls is put in between the sinters and the perforated plate to allow uniform gas flow. A thermocouple has been placed at the centre of

the test sample. The reduction tube is closed and placed inside the furnace. The tube is suspended through the weighing device. It should be made sure that the tube does not touch the furnace walls or the heating elements. The conditions are set and the furnace is started. Initially nitrogen is passed through the tube but as soon as the temperature reaches 950^{o}C (blast furnace lower stack), carbon monoxide gas (40% CO, 60% N_2) is passed through the tube for reduction. The testing is continued till 65% reduction is achieved. Again nitrogen is passed through the system as the sample cools down. The weight loss throughout the process is recorded in the computer. The sample is taken out and weighed to find out the final weight of the sample. The degree of reduction and the reducibility index have been calculated to understand the effect of alkali on sinters reduction.

- **Degree of Reduction**

$$R_t = \left(\frac{0.111\, w_1}{0.430\, w_2} + \frac{m_1 - m_t}{m_0 \times 0.430\, w_2} \times 100 \right) \times 100 \qquad 1$$

where; w_1 is the FeO content in the sample

w_2 is the total Fe in the sample

m_0 is the weight of sample

m_1 is the weight of sample just before testing

m_t is the weight of sample after reduction time t

(m_0 and m_1 are the same in lab scale but in industrial tests these values differ from each other)

The different sinters, i.e. with and without alkali are reduced in the vertical retort furnace and their degree of reduction has been calculated. The degree of reduction has been plotted against time to understand the effect alkali have on the degree of reduction of iron ore sinters.

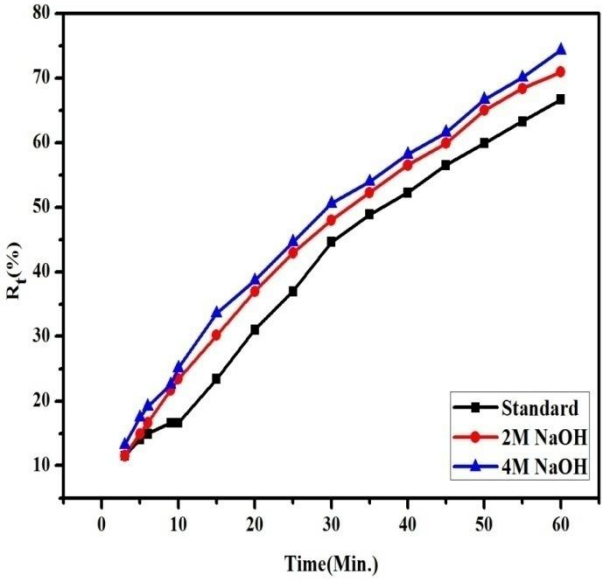

Fig. 9.1: The reducibility degree of sinter under different alkali loadings

The degree of reduction of sinters increases with time as well as the alkali content. The reducibility degree of sinters keeps on increasing with increase in amount of alkali in the sinter.

- **Reducibility Index:**

$$\frac{dR}{dt} = \frac{33.6}{t_{60} - t_{30}} \qquad 2$$

Where; t_{60}= time taken to attain 60% degree of reduction

t_{30}= time taken to attain 30% degree of reduction

The reducibility index for different alkali loaded iron ore sinters has been calculated and is given in the table 9.5.

Sinter	Reducibility Index
Standard	1.29
2M NaOH	1.34
4M NaOH	1.46

Table 9.5: Reducibility index of Iron ore sinters at different alkali loading

The reducibility index of the sinters increases as the amount of alkali increases. The reducibility index of sinter with innate alkali content (0.4% K) is in itself very high. The addition of alkali to magnetite sinters increases both the degree of reduction as well as the reducibility index. It is very important that we study the effect alkali have on the strength of the sinters.

9.3 Alkali Effect on the Strength of Sinters

The strength of the sinter samples after reduction has been evaluated. The sinters are rotated for 30 minutes in a tumbler at 30r.p.m [9]. The samples have been taken out and the degradation tendency (DT) and abrasion tendency (AT) have been calculated.

$$DT = (m_1/m_0)*100 \quad 3$$

$$AT = (m_2/m_0)*100 \quad 4$$

Where; m_0= initial weight of sample before tumbling

m_1= weight of sample greater than 6.3mm in size

m_2= weight of sample less than 0.5mm

Sample	DT	AT
Standard (0.4% K)	82.54	3.75
2M NaOH	87.90	2.51
4M NaOH	89.42	2.37

Table 9.6: Degradation and abrasion tendency of sinters under different alkali loadings

Both the degradation as well as the abrasion properties of the magnetite sinters have improved with increase in alkali percentage. The strength of sinters has increased drastically with the addition of sodium. The increase in sodium percentage further improves the DT and AT of the sinters as shown in table 9.6.

9.4 Alkali Effect on the Low Temperature Reduction Degradation Indices of Sinter

The sinter samples with different alkali loading have been subjected to LTD test as explained in section 9.1.1.

Sample	RDI-$1_{6.3}$	RDI-$1_{3.15}$	RDI-$1_{0.5}$
Standard (0.4% K)	55.03	17.06	3.00
2M NaOH	61.29	12.58	2.80
4M NaOH	45.83	25.20	3.10

Table 9.7: The low temperature reduction degradation indices for sinters with different alkali loading

The low temperature degradation properties of sinters have improved with the addition of sodium but as the percentage of sodium is increased further the LTD properties of the sinter deteriorates. This means that at high alkali loading, even magnetite sinters lose their strength which leads to fines generation.

9.5: XRD Analysis of Reduced Sinter

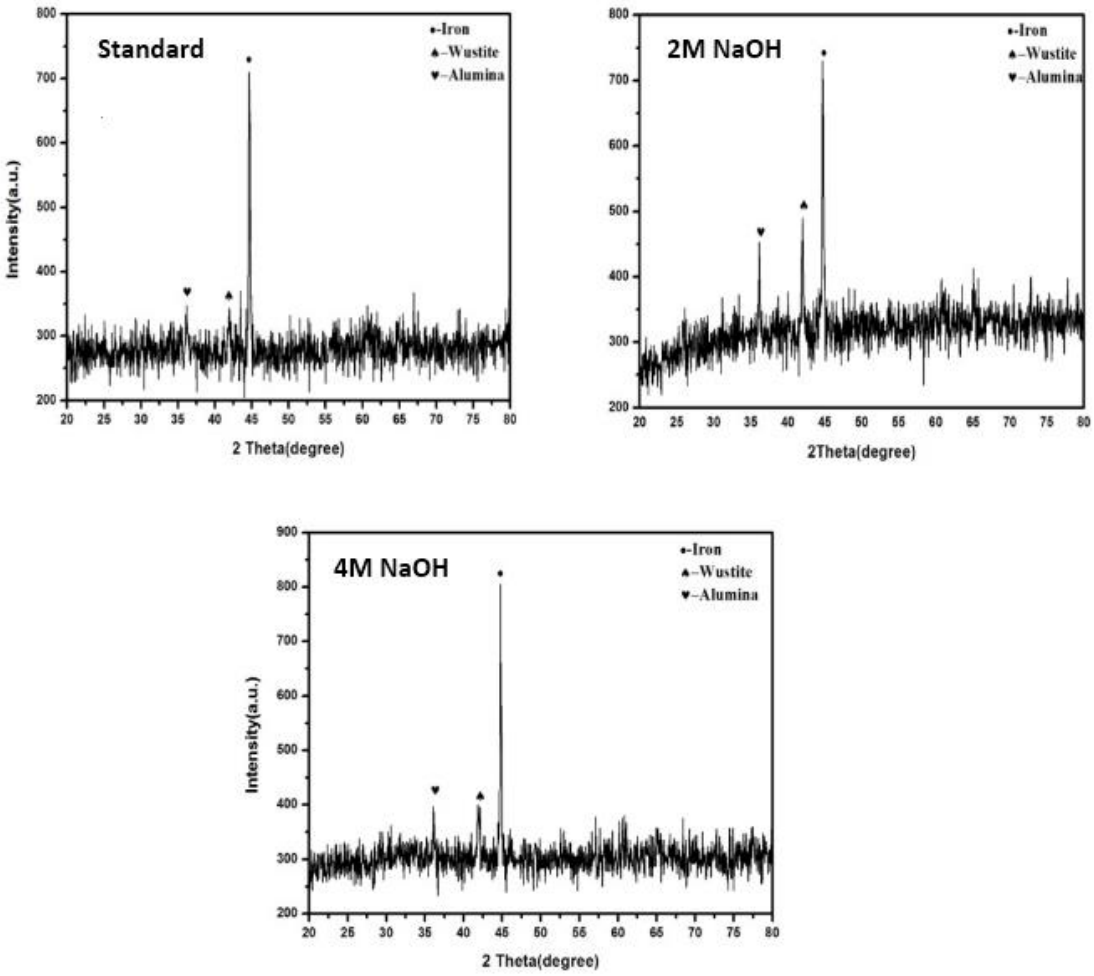

Fig. 9.2: XRD plots of sinters with alkali.

It can be seen from the XRD plots that the reduced iron ore sinters have high intensity peaks of iron, wustite and alumina. It can be seen that with increasing amount of alkali the intensity of the iron peak also increases which is in agreement with the degree of reduction results for the same sinters.

9.6 Isothermal Kinetic Study

The isothermal kinetic study of reduction of sinter using carbon monoxide has been carried out. Sinters have been reduced at 950°C for 5, 10, 15, 20, 30, 40, 50 and 60 minutes. The reduced time analysis as discussed in Chapter 3, section 3.5 has been carried out using experimental data to find the reaction mechanism being followed under different alkali loadings.

9.6.1 Effect of Alkali and Time on Sinter Reduction:

The loss of weight percentage as a function of time at 950°C has been plotted in fig. 9.3.

The weight loss percentage has been calculated using the following formulae:

$$\% \text{ of Weight Loss} = \frac{W_0 - W_t}{W_0} \qquad 5$$

where; w_o and w_t are the weight of the sinters before and after reduction.

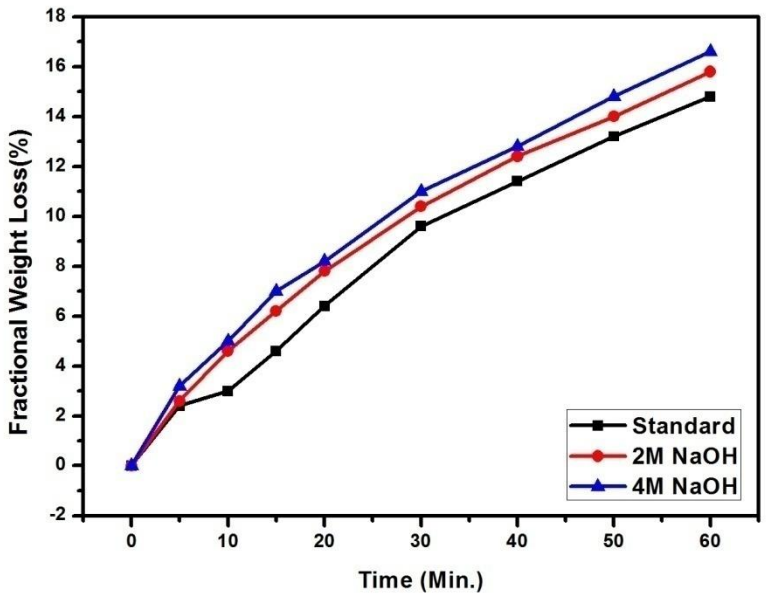

Fig. 9.3: Fractional weight loss (%) vs. time for sinter with alkali.

It can be observed from the above figure that the alkali increases the fractional weight loss (%) of sinters during reduction. Sodium addition drastically increases the weight loss percentage.

9.6.2 Isothermal Kinetic Study of Reduction of Sinters

In the present study of the isothermal reduction kinetic, the fractional weight loss (α) is defined as:

$$\alpha = \frac{M_t}{M_0} \qquad 6$$

where, M_0 is the initial weight of the iron ore sinters and M_t is the weight loss due to iron ore reduction by carbon monoxide in the vertical retort. So, α, defined by Eq. 6, gives the isothermal weight fraction loss as a function of time. These data have been graphically plotted in Fig. 9.4.

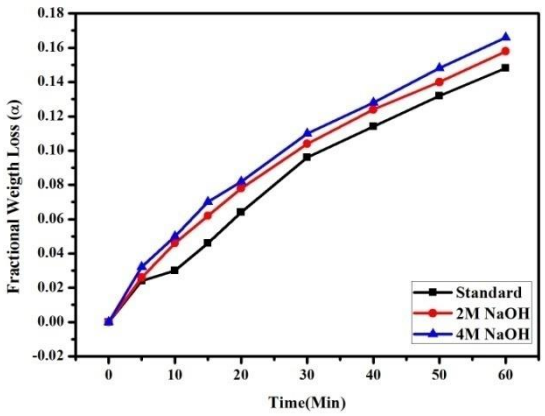

Fig. 9.4: Fractional weight loss (α) vs. time for sinters with alkali

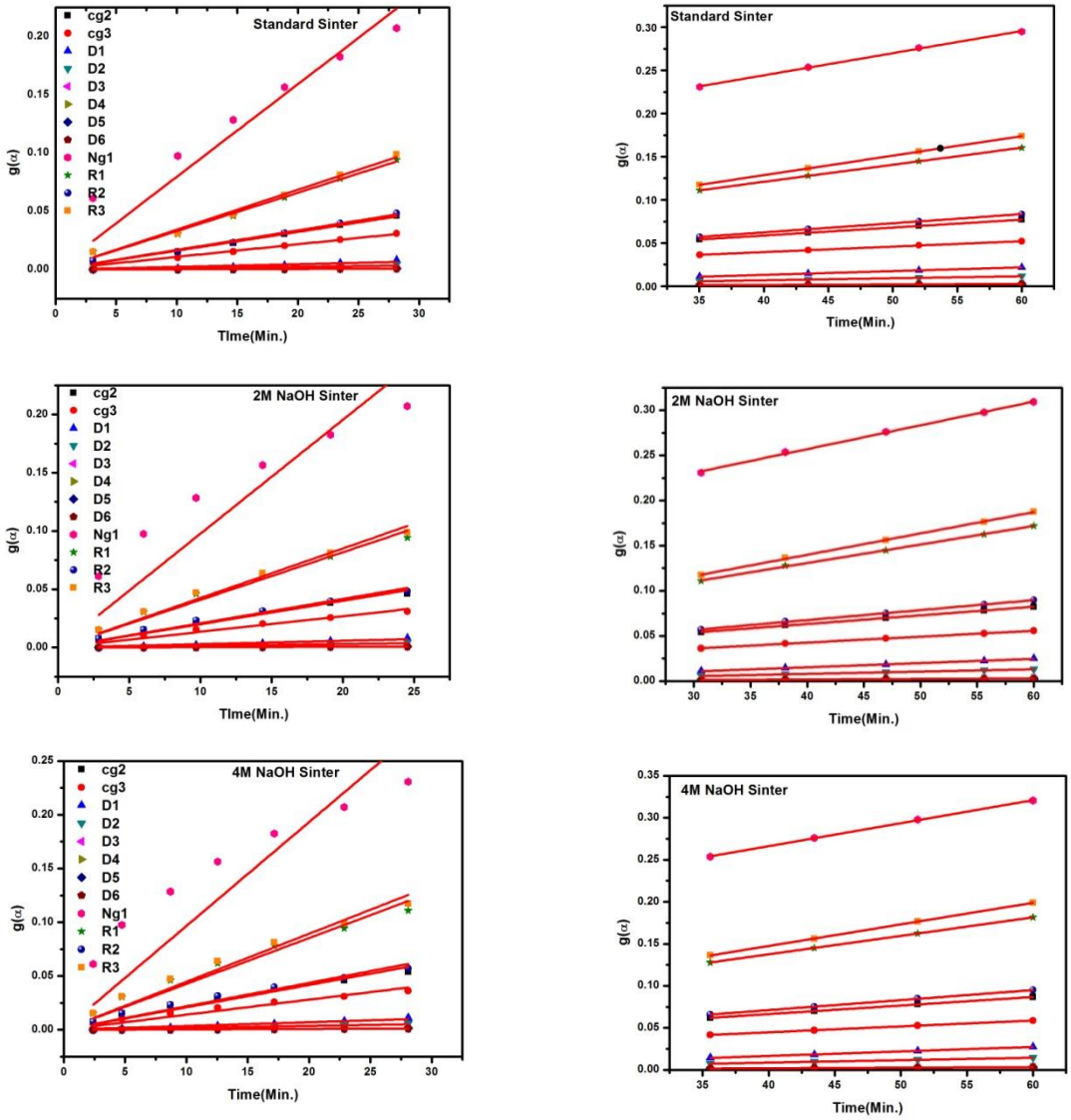

Fig. 9.5: Various mechanism models fitting showing the sinter reduction vs. Time for different sinter samples (Initial part and last part of reduction, respectively)

	cg2	cg3	D1	D2	D3	D4	D5	D6	Ng1	R1	R2	R3
STD	0.998	0.998	0.924	0.921	0.920	0.919	0.928	0.919	0.981	0.998	0.998	**0.997**
2M NaOH	0.992	0.992	0.969	0.967	0.967	0.966	0.972	0.966	0.953	0.993	0.994	**0.995**
4M NaOH	0.985	0.986	0.979	0.978	0.977	0.976	0.982	0.976	0.940	0.987	0.988	**0.989**

Table 9.8: Correlation coefficient calculated using different mechanism functions for the initial stages of sinter reduction

	cg2	cg3	D1	D2	D3	D4	D5	D6	Ng1	R1	R2	R3
STD	0.99958	0.99964	0.99856	0.99823	0.99811	0.99785	0.99902	0.99785	0.99862	0.99974	0.99985	**0.99992**
2M NaOH	0.99901	0.99906	0.99774	0.99733	0.99718	0.99686	0.99831	0.99686	0.99791	0.99917	0.99928	**0.99934**
4M NaOH	0.99992	0.99994	0.99768	0.99720	0.99703	0.99667	0.99832	0.99667	0.99945	0.99996	0.99995	**0.99989**

Table 9.9: Correlation coefficient calculated using different mechanism functions for the final stages of sinter reduction

According to the kinetic analysis and calculation procedures introduced in chapter 3, section 3.5, the g(α) value for each mechanism model versus the reduction time t for the gasification reaction of the sinter samples have been calculated and plotted, every plot has then been subjected to linear fit through zero for initial stages of reduction whereas for later stages of reduction normal linear fitting is done. The results are shown in figure 9.5. Simultaneously, the corresponding correlation coefficient for each model has been calculated, which is given in Table 9.7 and 9.8 for initial and final stages of reduction, respectively. The higher the correlation coefficient the better is the mechanism function [11]. To determine the kinetic model and the rate controlling steps in the reaction, the experimental data are analysed by using reduced time plots shown in figure 9.6, 9.7 and 9.8 for standard, sodium added and potassium added sinter samples, respectively. From these figures and the calculated correlation coefficient given in table 9.8 and 9.9, the models with the highest R squared values and those matching the experimental reduced time plots have been selected to be the governing reaction mechanism for the individual sinter samples [12].

Potassium effect on Sinter: In case of standard sinter samples (0.3% K) reduction the experimental (α, θ) points coincide very well with the theoretical curve for R3 as shown in figures below. During reduction, the gases initiate reduction on surface and the pores of dense magnetite sinter. The reaction in the pores is accelerated by alkali leading to second order chemical reaction mechanism (R3) in both initial as well as last stage of reduction.

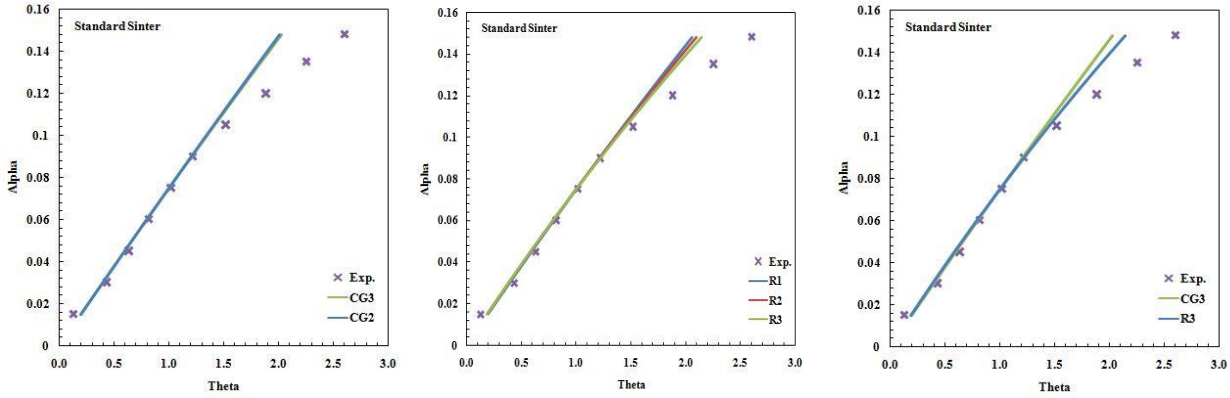

Fig. 9.6: Reduced time plot of fractional loss α along with the theoretical α vs. θ plot for different mechanism models of the standard sinter samples

Sodium effect on sinters: It has been found that the experimental (α, θ) points coincide very well with the theoretical curve for R3 for the sodium added sinter samples (with extra 0.4% K) as shown in figures below in the initial as well as later stages of reduction. The high alkali content of potassium and sodium accelerates the reactions taking place inside the pores along with surface reduction leading to second order reaction mechanism.

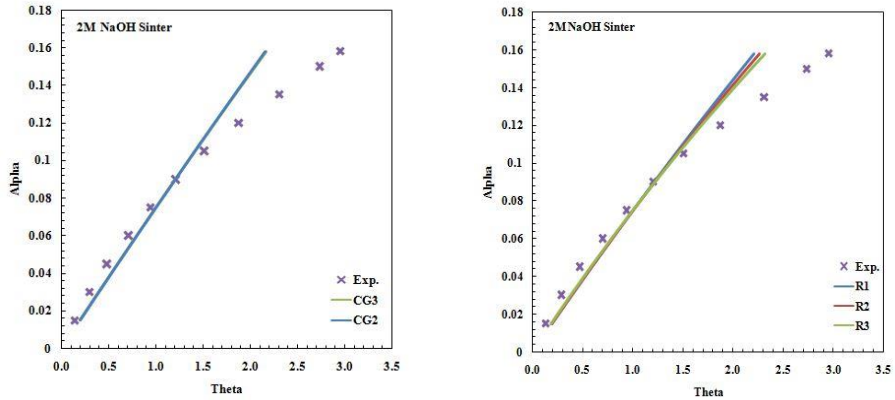

Fig. 9.7: Reduced time plot of fractional loss α along with the theoretical α vs. θ plot for different mechanism models of the 2M NaOH sinter samples

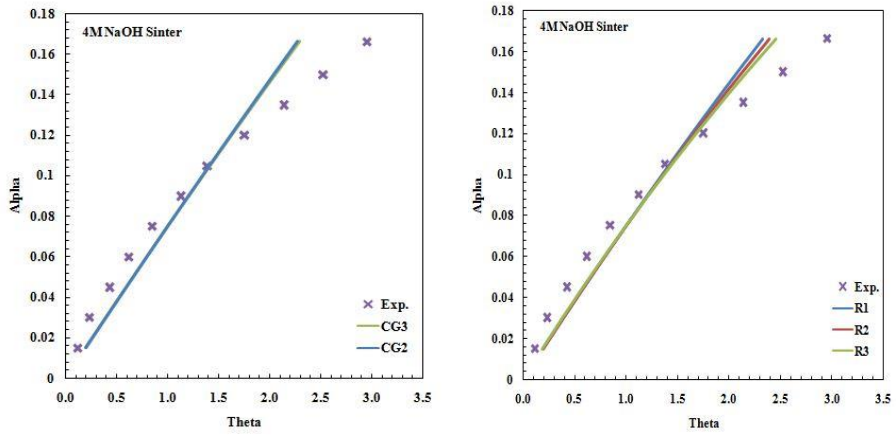

Fig. 9.8: Reduced time plot of fractional loss α along with the theoretical α vs. θ plot for different mechanism models of the 4M NaOH sinter samples

9.7 Conclusion

- Hematite sinters have very poor low temperature reduction degradation (LTD) indices compared to magnetite sinters although the potassium content of hematite sinters is lower.
- The degradation tendency and abrasion tendency of magnetite sinters improves with alkali increase even upto 0.4% K and 0.3% Na.
- The low temperature reduction degradation (LTD) indices of magnetite sinters improve up to 0.4% K and 0.15% Na but start to deteriorate after alkali is increased to 0.4%K and 0.3% Na.

9.8 Reference

1. International Organization for Standardization: ISO 4695 Iron ores - Determination of reducibility (1995).
2. International Organization for Standardization: ISO 4696-1 Iron ores for blast furnace feedstocks — Determination of low-temperature reduction-disintegration indices by static method — Part 1: Reduction with CO, CO2, H2 and N2 (2007).
3. L. X. YANG, Sintering Fundamentals of Magnetite Alone and Blended with Hematite and Hematite/Goethite Ores, ISIJ International, 2005, 45:4, p. 469-476.
4. Yu, Y.; Qi, C. Magnetizing roasting mechanism and effective ore dressing process for oolitic hematite ore. J. Wuhan Univ. Technol. Mater. Sci. Ed. 2011, 26, 176–181.
5. Feilmayr, C.; Thurnhofer, A.; Winter, F.; Mali, H.; Schenk, J. Reduction behavior of hematite to magnetite under fluidized bed conditions. ISIJ Int. 2004, 44, 1125–1133.
6. Et-Tabirou, M.; Dupre, B.; Gleitzer, C. Hematite single crystal reduction into magnetite with CO-CO2. Metall. Trans. B 1988, 19, 311–317.
7. Guo, Xingmin & Sasaki, Yasushi & Kashiwaya, Yoshiaki & Ishii, Kuniyoshi. (2004). Microreaction mechanism in reduction of magnetite to wustite. Metallurgical and Materials Transactions B. 35. 517-522. 10.1007/s11663-004-0052-2.
8. Weiss, B., Sturn, J., Voglsam, S., Strobl, S., Mali, H., Winter, F., & Schenk, J. (2011). Structural and morphological changes during reduction of hematite to magnetite and wustite in hydrogen rich reduction gases under fluidised bed conditions. *Ironmaking & Steelmaking*, *38*(1), 65-73.
9. Pichler, A., Schenk, J., Hanel, M., Mali, H., Thaler, C., Hauzenberger, F., & Stocker, H. (2014). Influence of alkalis on mechanical properties of lumpy iron carriers during reduction. In Conference Proceedings to the 23rd International Conference on Metallurgy and Materials (pp. 40-40).

10. Sarkar, B. K., Samanta, S., Dey, R., & Das, G. C. (2016). A study on reduction kinetics of titaniferous magnetite ore using lean grade coal. International Journal of Mineral Processing, 152, 36-45.
11. Wang H, Chu M, Guo B, Bao J, Zhao W, Liu Z, et al. Investigation on Gasification Reaction Behavior and Kinetic Analysis of Iron Coke Hot Briquette under Isothermal Conditions. Steel Res Int 2019;90:1–10.
12. Sarkar BK, Kumar N, Dey R, Das GC. Optimization of Quenching Parameters for the Reduction of Titaniferous Magnetite Ore by Lean Grade Coal Using the Taguchi Method and Its Isothermal Kinetic Study. Metall Mater Trans B Process Metall Mater Process Sci 2018;49:1822–33.

Chapter-10

Effect of Alkali on the Reactivity, Strength and Reaction Mechanism of Coke under Blast Furnace Conditions

10.1 Analysis of Coke Samples

Coke samples have been collected from two different plants: Tata Steel and Vizag Steel Plant (C1 and C2, respectively). The proximate analysis and TG/DTA of the coke samples have been carried out as shown in section 5.1.2.2.

10.2 Impregnation of Coke Samples

These coke samples have been sieved in the range of 19.00 mm to 22.4 mm. The samples have been weighed. These samples are impregnated with sodium and potassium by putting them in solutions of sodium hydroxide (NaOH) and potassium hydroxide (KOH) in a beaker. The beaker is put inside a desiccator; a vacuum pump is attached to the desiccator. The pump is switched off as the bubbling ends. After some time, the samples are taken out and heated in a hot air oven at 110^0C (383K) for about 2 hours. The dried samples are weighed to calculate the amount of weight gained as shown in Table 10.1 and Table 10.2.

Coke initial weight	200.2	Coke initial weight	198
Final Weight	201.9	Final Weight	199.4
Gain	1.7	Gain	1.4
Weight of K	39	Weight of Na	23
Weight KOH	56	Weight NaOH	40
Amount of K Gain	1.183	Amount of Na Gain	0.805
Gain %	0.586	Gain %	0.403

Table 10.1: Alkali weight gain for Tata Steel coke samples (wt. in gm)

Coke initial weight	198.7	Coke initial weight	201
Final Weight	201.3	Final Weight	202.8
Gain	2.6	Gain	1.8
Weight of K	39	Weight of Na	23
Weight KOH	56	Weight NaOH	40
Amount of K Gain	1.810	Amount of Na Gain	1.035
Gain %	0.899	Gain %	0.510

Table 10.1.2: Alkali weight gain for Vizag Steel plant coke samples (wt. in gm)

Both the coke samples have been impregnated using same solutions under same conditions (end of bubbling), it can be observed from the table that the alkali pickup is more in case of Vizag Steel compared to alkali pickup by the Tata Steel coke samples. The available surface area of has been found to be 6.88m^2/gm for Tata Steel coke samples and 13.99m^2/gm for Vizag Steel Plant coke samples.

10.3 Experimental Procedure

CRI and CSR Tests: Coke Reactivity Index (CRI) and Coke Strength after Reaction (CSR) are internationally accepted testing standards for blast furnace cokes, described under ISO 18894 (2006) [1]. All the coke samples (with and without added alkali) are tested under standard conditions. For CRI, a test portion of the dried coke sample (200 ± 3 g) having a size range from 19.0 mm to 22.4 mm is heated in a reaction vessel to 1100°C (1373K) in nitrogen atmosphere. The gas composition and temperature inside the vertical retort have been set to replicate the conditions in a blast furnace. For the test, the atmosphere is changed to carbon dioxide for exactly 2 hours. During this treatment, the carbon part of the coke sample is gasified by forming carbon monoxide. This is an endothermic reaction and known as Boudouard Reaction.

$$C\ (solid) + CO2\ (gas) = 2CO\ (gas)\ with\ \Delta H_{orxn} = = +172{,}67\ kJ/mol\ [2] \quad 1$$

After the test, the reaction vessel is cooled down to about 50 °C in a nitrogen atmosphere. The comparison of the sample weight before and after the reaction determines the CRI. The reacted mass is tumbled in a specially designed tumbler for 30 minutes at 20 r.p.m. After tumbling, the percentage of the mass of coke having a particle size greater than 10 mm to the mass of reacted coke is defined as CSR. The weight of coke below the size of 5mm to the final weight gives the abrasion value (AV). The samples are then characterised using XRD.

10.4. Isothermal Reduction Kinetic Study of Bouduard Reaction

The reaction of dried coke samples with carbon dioxide is carried out isothermally in reaction vessel at 1373K in nitrogen atmosphere for a period of two hours. The conventional gas-solid reaction mechanisms for isothermal kinetic study and reduced time analysis has been carried out as discussed in Chapter 3, section 3.5.

10.5. CRI, CSR and AV of the Coke Samples

The CRI, CSR and Abrasion values for the coke samples have been found as shown in Table 10.3 and Table 10.4. The CRI and CSR values of the coke samples are close to the industrial values. The addition of alkali however, increased the CRI and abrasion values while decreasing the CSR values.

Normal		**KOH Trial**		**NaOH TRIAL**	
Initial Weight	200.8	Initial Weight	201.9	Initial Weight	199.4
Final Weight	145.6	Final Weight	123.7	Final Weight	130.4
Loss of weight	55.2	Loss of weight	78.2	Loss of weight	69
CRI	**27.49**	**CRI**	**38.73**	**CRI**	**34.60**
Weight > 10mm	95.5	Weight > 10mm	71.8	Weight > 10mm	76.2
Weight< .5mm	40.5	Weight< .5mm	42.7	Weight< .5mm	44.6
CSR Value	**65.59**	**CSR Value**	**58.04**	**CSR Value**	**58.43**
AV	**27.81**	**AV**	**34.51**	**AV**	**34.20**

Table 10.3: Test results of Tata Steel coke samples

Normal		KOH Trial		NaOH TRIAL	
Initial Weight	200.4	Initial Weight	201.3	Initial Weight	202.8
Final Weight	141	Final Weight	109.8	Final Weight	119.9
Loss of weight	59.4	Loss of weight	91.5	Loss of weight	82.9
CRI	**29.64**	**CRI**	**45.45**	**CRI**	**40.87**
Weight > 10mm	86.4	Weight > 10mm	53.4	Weight > 10mm	57.1
Weight< .5mm	43.9	Weight< .5mm	46.1	Weight< .5mm	48.6
CSR Value	**61.27**	**CSR Value**	**48.63**	**CSR Value**	**47.62**
AV	**31.13**	**AV**	**41.98**	**AV**	**40.53**

Table 10.4: Test results for Vizag Steel coke samples

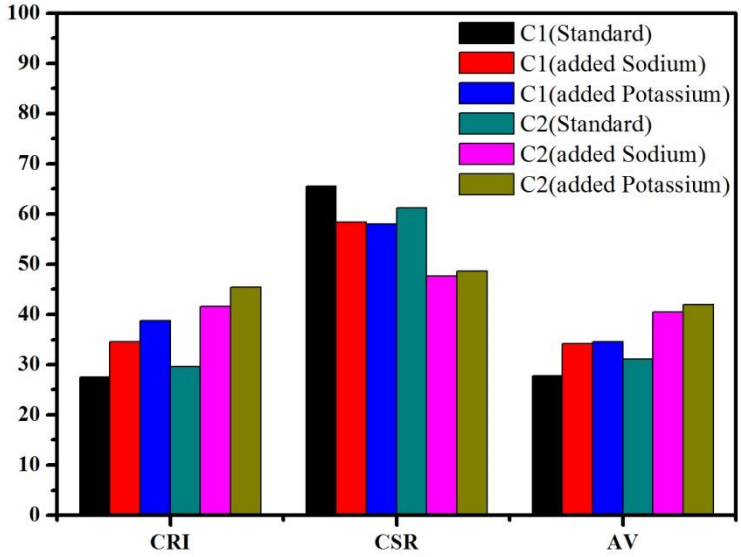

Fig10.1: Graphs depicting the alkali effect on CRI/CSR/AV of Vizag Steel and Tata Steel coke

It can be seen that the alkali effect is much more pronounced on Vizag Steel Coke than Tata Steel Coke samples. The coke strength after reaction decreases as the alkali percentage is increased [3]. The abrasion values increase as the alkali percentage is increased. The coke reactivity index also increases with the alkali percentage [4]. Potassium has greater effect on coke reactivity index as compared to sodium on the coke samples. The effect of alkali is very high on the coke strength after reaction as shown in Fig. 10.1.

10.6 XRD analysis of Tata Steel and Vizag Steel Coke samples

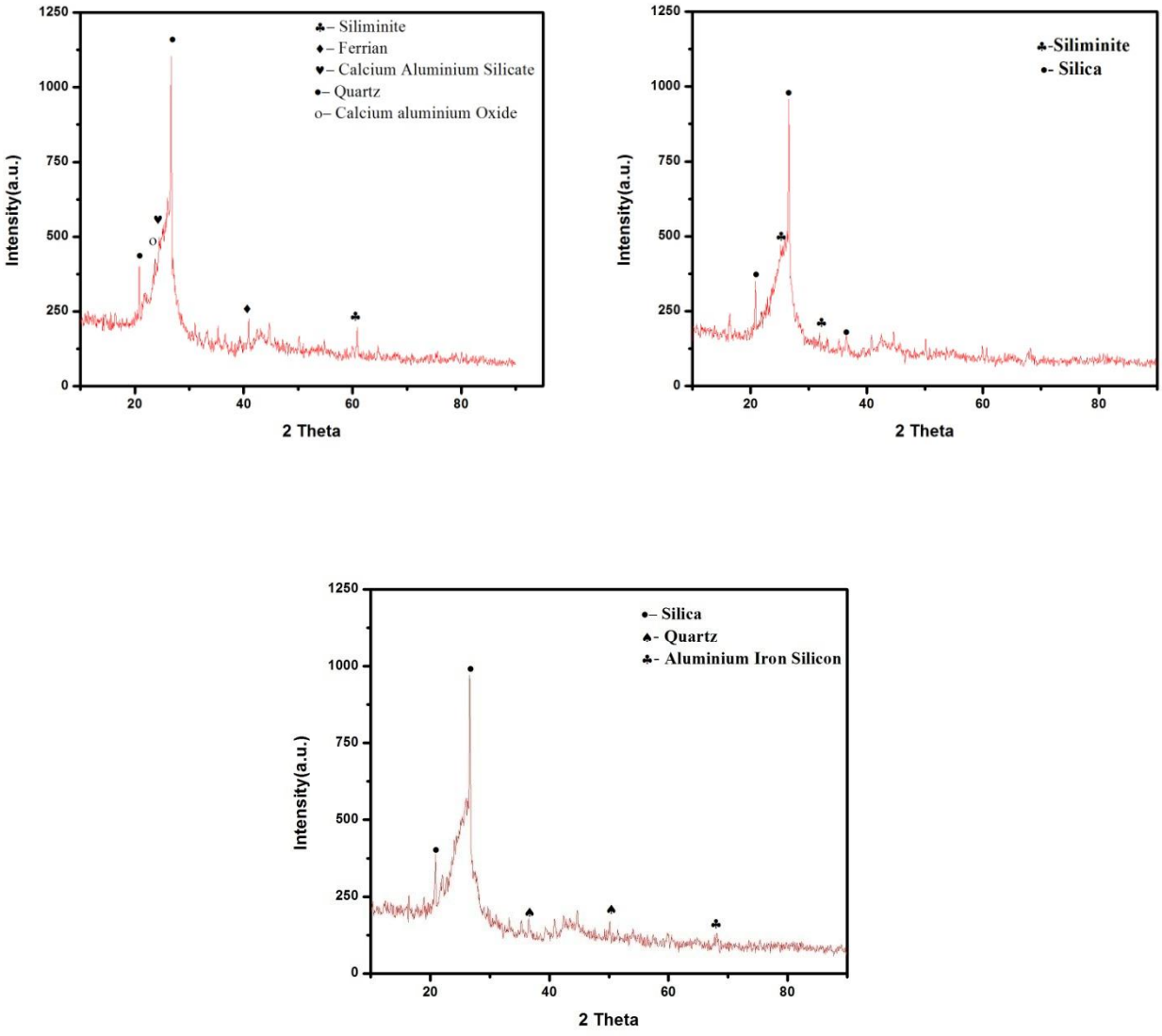

Fig. 10.2: XRD pattern of Tata steel coke a) Standard sample, b) Potassium impregnated and c) Sodium impregnated

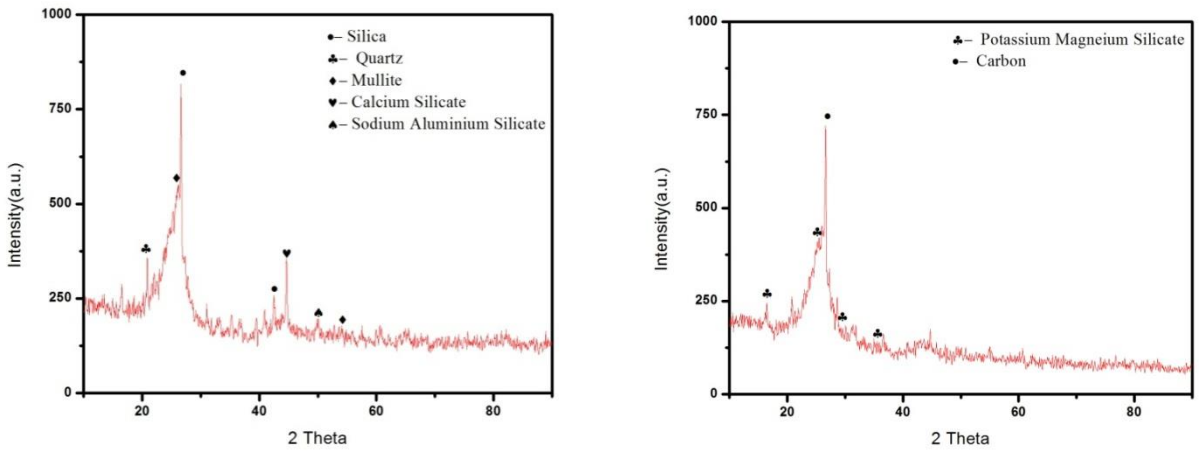

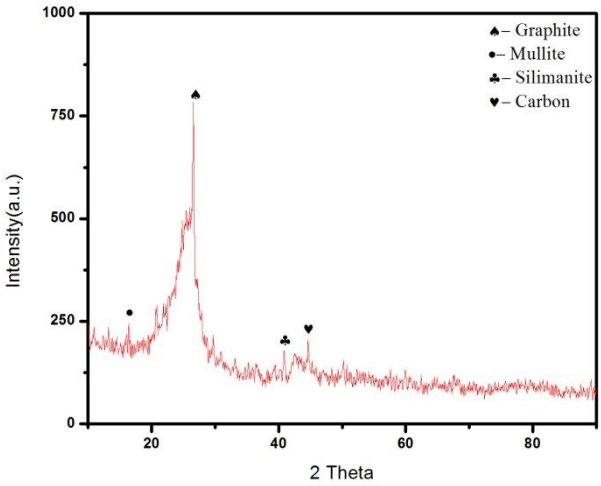

Fig 10.3: XRD pattern of Vizag steel coke a) Standard sample, b) Potassium impregnated and c) Sodium impregnated

The XRD plots of the coke samples after bouduard reaction shows major peaks of silica along with some minor peaks of mullite and siliminite (alumina silicate). In case of coke samples with added potassium and sodium it can be seen that there are some minor peaks of potassium aluminium silicates and sodium aluminium silicates, respectively.

10.7 Effect of Time on Coke Reaction in Blast Furnace conditions

Loss of weights as a function of time at different temperatures is plotted in Fig. 10.4.

Percentage of loss of weights is calculated by the following equation-

$$\% \text{ of Weight Loss} = \frac{W_0 - W_t}{W_0} * 100 \qquad 2$$

Where, W_0 and W_t are the weight of coke samples before and after the reaction for time t minutes, respectively.

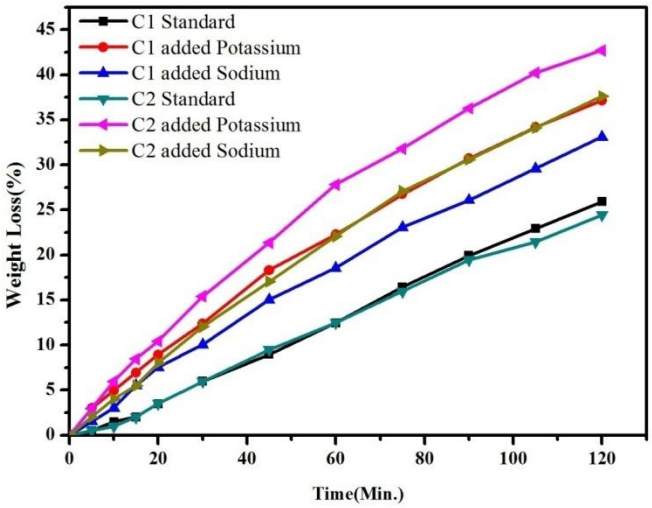

Fig. 10.4: Weight loss (%) vs. time for standard and alkali impregnated coke samples

It is clear that with time the weight loss increases as more carbon from the coke reacts with carbon dioxide gas to form carbon monoxide. It can be seen in Fig. 10.4 that the maximum weight loss is observed for potassium impregnated C2 samples followed by potassium impregnated C1 samples. The weight loss for the standard coke samples is almost the same. The addition of alkali (Sodium and Potassium) increases the weight loss with time at a higher rate [5]. It can also be seen that for the coke samples from same source, potassium addition leads to higher weight loss compared to sodium addition [6]. But this can be due to the reason that potassium gain percentage is more that sodium for both the coke samples.

10.8 Isothermal Kinetic Study of Bouduard Reaction

In the present study of the isothermal reduction kinetic, the fractional weight loss (α) is defined as:

$$\alpha = \frac{M_t}{M_0} \qquad 3$$

where, M_0 is the initial weight of the coke samples and M_t is the weight loss due to carbon reacting with carbon dioxide gas in the vertical retort. So, α as defined by Eq. 3, gives the isothermal weight fraction loss as a function of time. These data have been graphically plotted in Fig. 10.5.

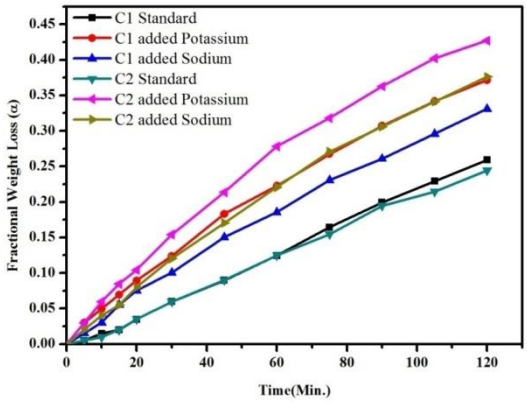

Fig. 10.5: Fractional weight loss (α) vs. time for standard and alkali impregnated coke

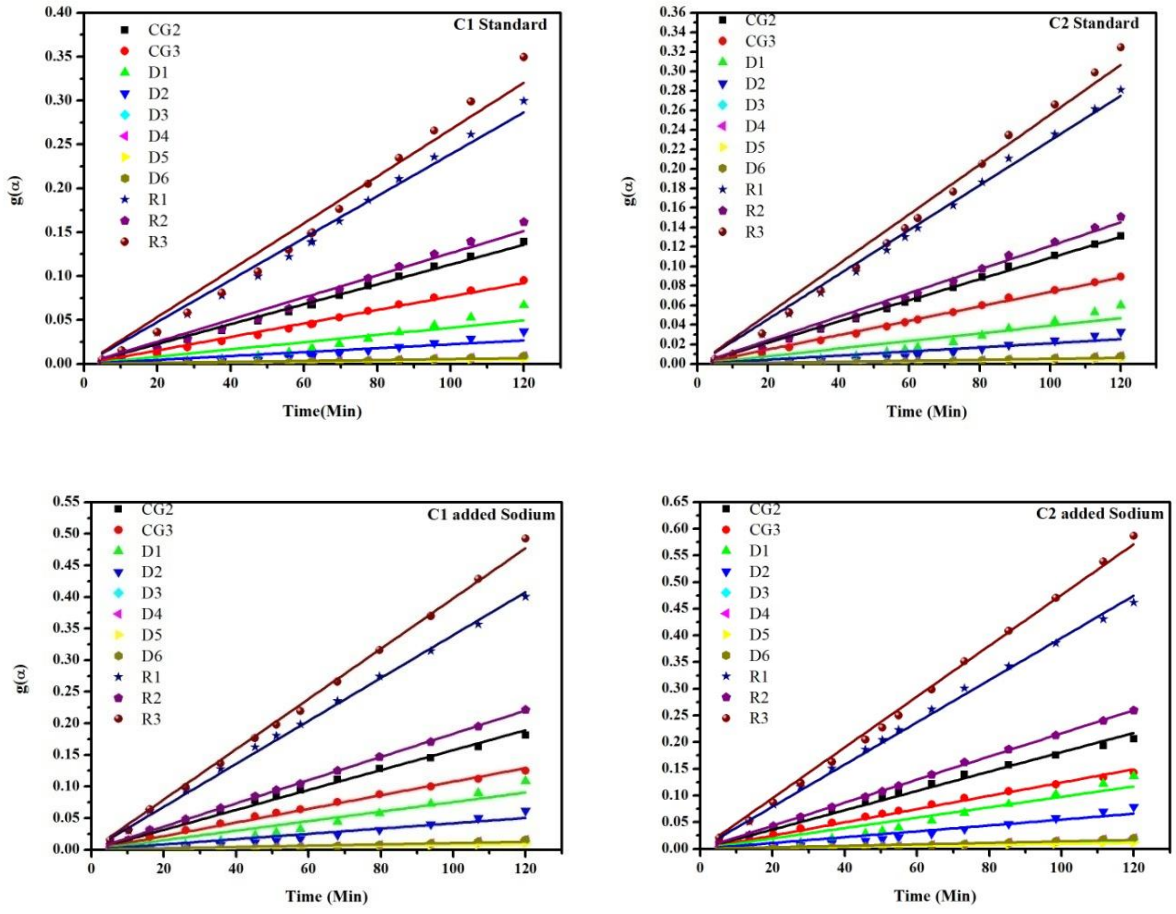

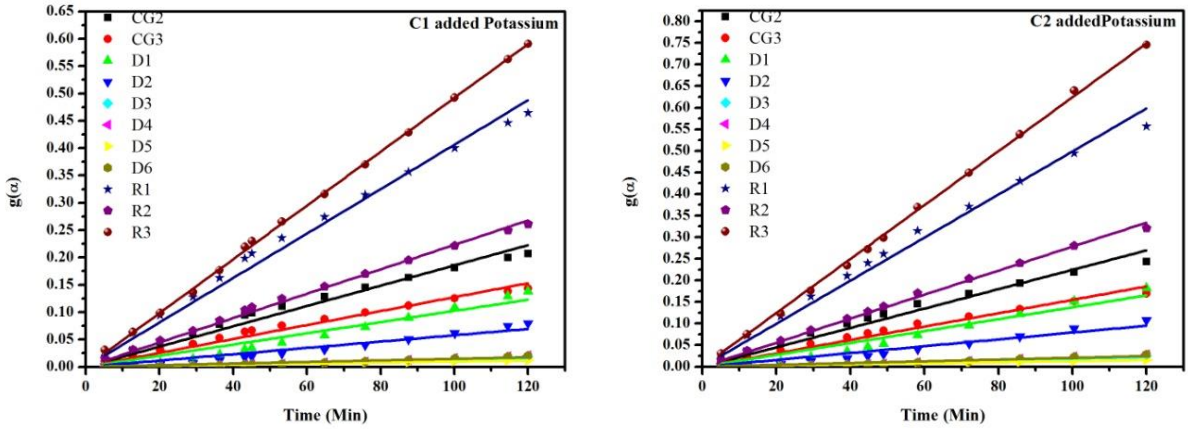

Fig. 10.6: Various mechanism models fitting showing the carbon conversion rate of bouduard reaction vs. time for different coke samples

	C1 Standard	C1 added Sodium	C1 added Potassium	C2 Standard	C2 added Sodium	C2 added Potassium
Cg2	0.99774	0.99775	0.99317	0.99857	0.99734	0.99187
Cg3	**0.99731**	0.99836	0.99447	**0.99837**	0.9981	0.99357
D1	0.91007	0.95755	0.97513	0.92711	0.96278	0.97498
D2	0.90156	0.94943	0.96818	0.92034	0.95445	0.96655
D3	0.89856	0.94643	0.96553	0.91796	0.95732	0.96322
D4	0.89236	0.94015	0.95987	0.91306	0.94473	0.95601
D5	0.92253	0.96797	0.98323	0.93716	0.97287	0.98393
D6	0.89236	0.94015	0.95987	0.91306	0.94473	0.95601
R1	0.99624	0.99928	0.99668	0.99781	0.99922	0.99642
R2	0.99416	**0.99981**	0.99894	0.99658	**0.99984**	0.99912
R3	0.99146	0.99927	**0.99982**	0.99484	0.99906	**0.99969**

Table 10.5: Correlation coefficient calculated using different mechanism functions

According to the kinetic analysis and calculation procedures introduced in chapter 3, section 3.5, the g(α) values for each mechanism model versus the reaction time t for the gasification reaction of the carbon samples have been calculated and plotted, every plot is then subjected to linear fit through zero. The results are shown in Fig. 10.6. Simultaneously, the corresponding correlation coefficient for each model is calculated, which is given in Table 10.5. The higher the correlation coefficient the better is the mechanism function [7].

To determine the kinetic model and the rate controlling steps in the reaction, the experimental data are analysed by using reduced time plots shown in Fig. 10.7 and Fig. 10.8 for C1 and C2 coke samples, respectively. From these figures and the calculated correlation coefficient given in table 6, the models with the highest R squared values and those matching the experimental reduced time plots are selected to be the governing reaction mechanism for the individual coke samples [8]. It has been found that the experimental (α, θ) points coincide very well with the theoretical curve for CG3 for both the standard coke samples as shown in figures below. It can also be seen that after addition of alkali the experimental points coincide well with the theoretical curve for R2 mechanism in case of both the coke samples with added sodium whereas the potassium added samples follow R3 mechanism as shown in figures below. In case of standard Coke samples, the gasses react with the surface. The surface of the coke is connected to the inside through pores but the concentration of carbon dioxide inside the pores decreases as the distance from the surface increases [9]. The surface reaction dominates and it follows a CG3 mechanism. As the reacted surface increases and the distance to be travelled by carbon dioxide for reaction inside the pores decreases. The diffusion of gases leads to reaction inside the pores but in case of no added catalyst the surface reaction predominates and a CG3 mechanism is followed. In sodium or potassium added coke samples when the gas diffuses inside the pores the reaction is activated by the alkali. The alkali activate the reaction inside the pores at a high rate which widens the pores

leading to greater diffusion of gasses inside the pores [9]. After this a mixed mode of reaction takes place. Potassium has higher catalytic effect on carbon gasification compared to sodium [6]. So, after a certain time when diffused gases react inside the pores the rate of reaction and fractional weight loss increases. It is observed that in case of sodium added coke the reaction mechanism being followed is one-half order reaction (R2) where as in case of added potassium the reaction mechanism being followed is second order reaction (R3) in both cases.

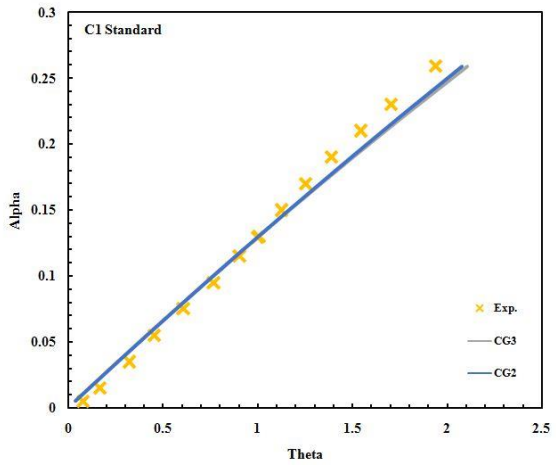

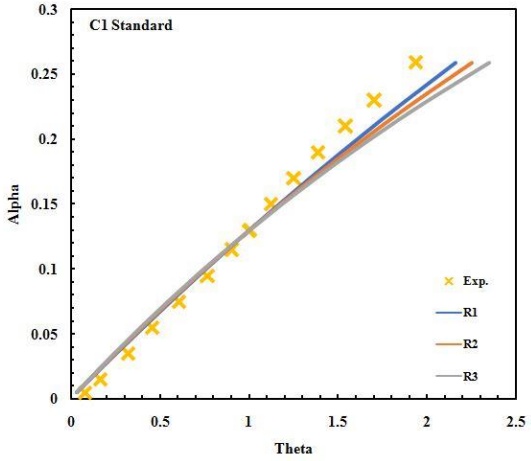

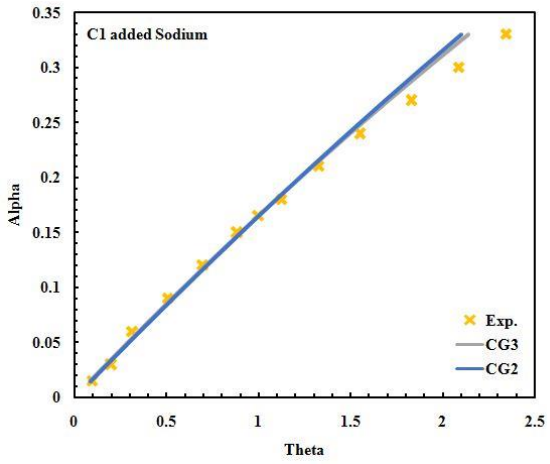

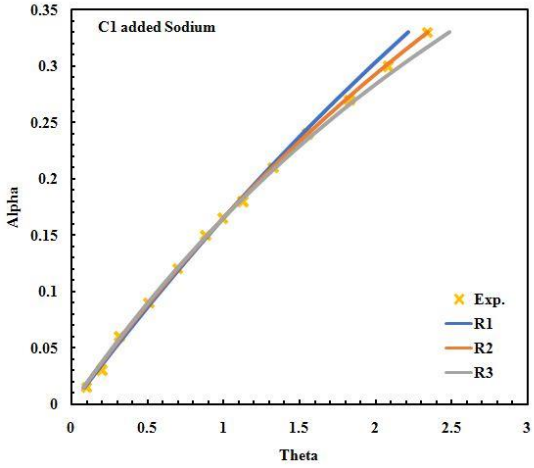

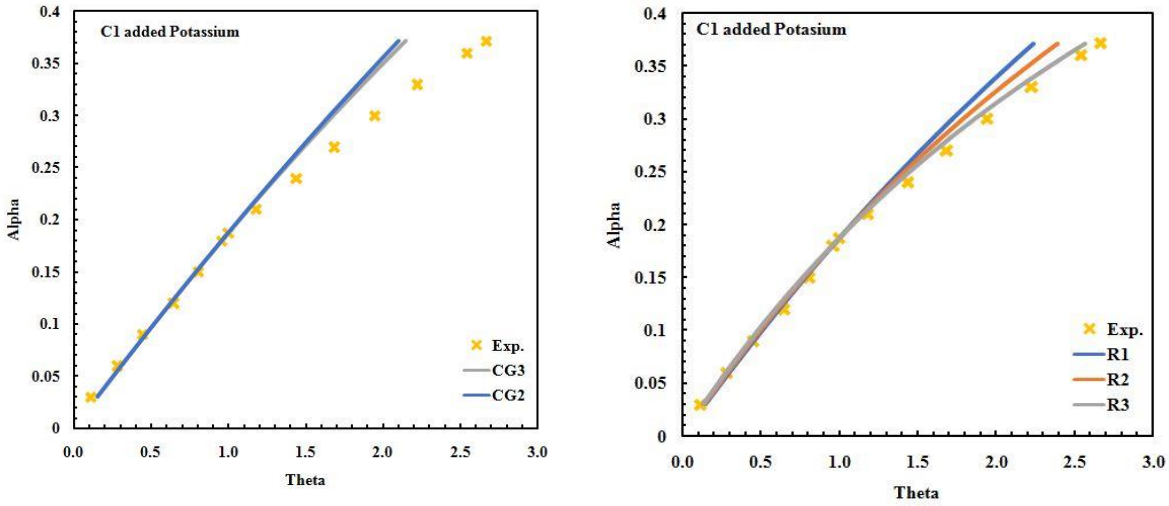

Fig. 10.7: Reduced time plot of fractional loss α along with the theoretical α vs. θ plot for different mechanism models of the C1

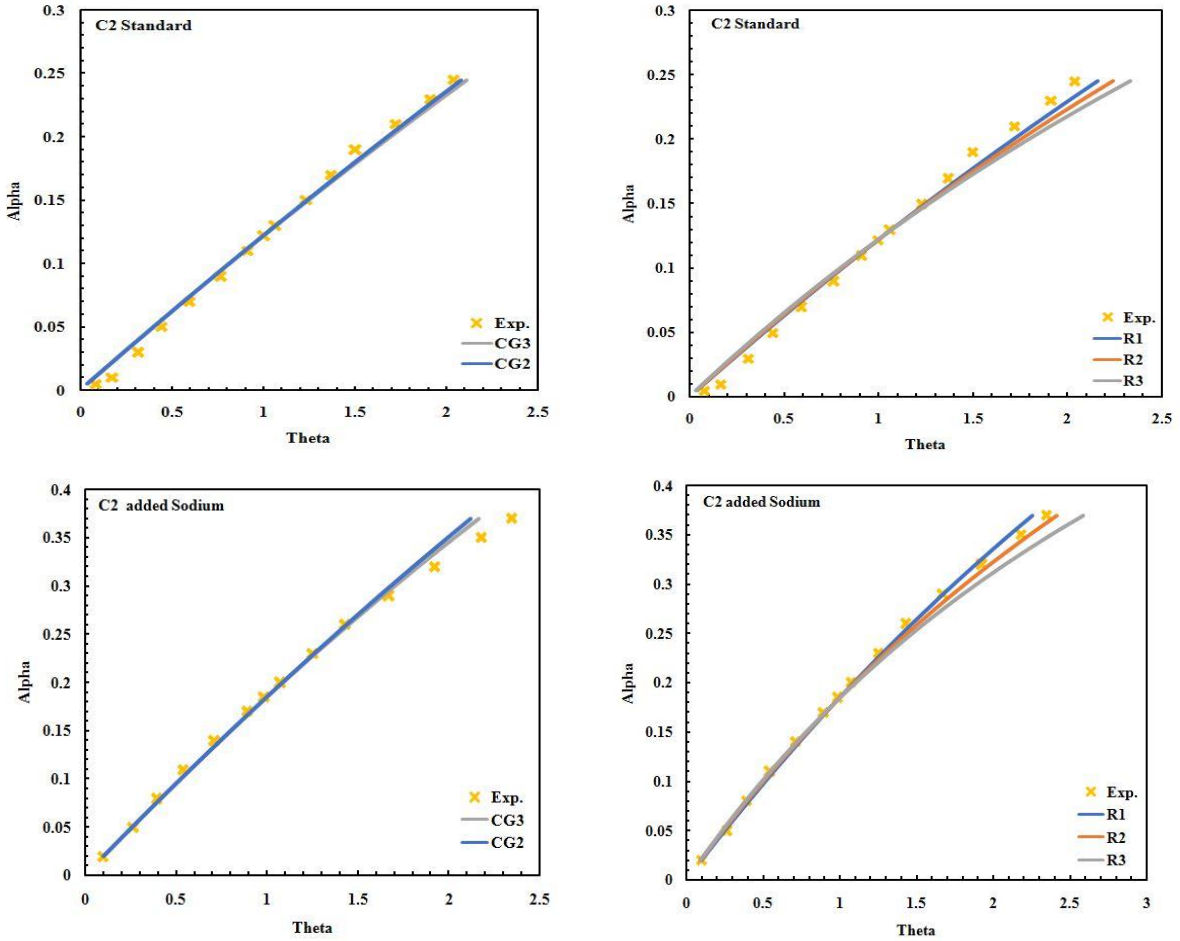

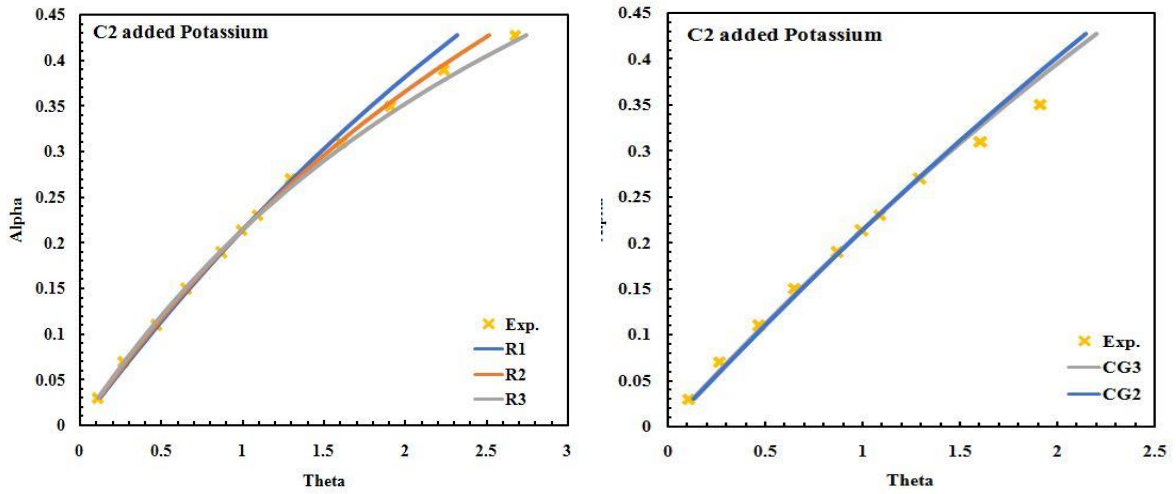

Fig.10.8: Reduced time plot of fractional loss α along with the theoretical α vs. θ plot for different mechanism models of C2

10.9 Rate of Carbon Gasification

The rate of carbon gasification at 1100°C has been calculated using the following equation for the different set of samples to get a better understanding of the alkali effect on the reaction. The rate of gasification of carbon has been calculated using the following formula:

$$-dN_C/dt = (M_c \text{ X } \alpha)/dt \qquad 4$$

M_c is the moles of carbon present in coke sample, α is the fractional weight loss and dt is the time from the start of weight loss till the end of test. The different rates have been listed in Table 10.7. (Calculation has been shown in Appendix-IV)

Sample	Rate of reaction (mol/min)
C1 (Standard)	0.0284
C1 (added Na)	0.0358
C1 (added K)	0.0406
C2 (Standard)	0.0262
C2 (added Na)	0.0379
C2 (added K)	0.0436

Table 10.7: The rate of carbon gasification for different coke samples

It can be seen from the data in Table 10.7 that the rate of carbon gasification increased gradually with the addition of alkali [10, 11, 12, 13]. The reaction rate for coke samples with added sodium is higher than that for the standard coke samples, whereas the coke samples with added potassium have higher reaction rate than the coke samples with added sodium. It has been reported previously that potassium has the highest catalytic effect on bouduard reaction compared to other alkali [6]. It has been reported earlier that lattice disturbance is caused in graphite crystal stem which have much lower atomic radii as compared to the alkali [14]. The rapid diffusion of alkali inside the graphite crystal system causes subsequent expansion and distortion of the unit cells. The reaction rate of coke gasification in presence of alkali also helps back this claim of ionic radii of alkali being the reason behind the detriment of the coke properties.

10.10 Effect of Sodium and Potassium on the Activation Energy of Bouduard Reaction

The effect of sodium and potassium on the activation energy of the Bouduard reaction has been carried out for the coke sample with higher rate of carbon gasification. In this case C1 coke samples have been used.

10.11 CRI, CSR Tests of the Coke Samples

The CRI, CSR and Abrasion values for the coke samples are measured. The CRI and CSR values of the coke samples show standard values in the context of Indian steel industry. The addition of alkali however, increased the CRI and abrasion values while decreasing the CSR values. The results of the CRI, CSR and AV of C1 samples have been given in Table 10.8and Table 10.9 along with a graphical representation in Fig. 10.9.

	Na 900ºC	Na1000ºC	Na 1100ºC
CRI (%)	12.98	26.22	34.60
CSR (%)	77.34	65.58	58.40
AV (%)	18.17	29.09	34.20

Table 10.8: Test results of sodium added coke samples at different temperatures

	K 900ºC	K 1000ºC	K 1100ºC
CRI (%)	10.73	29.42	38.73
CSR (%)	80.19	65.85	58.04
AV (%)	17.20	26.81	34.52

Table 10.9: Test results of potassium added coke samples at different temperatures

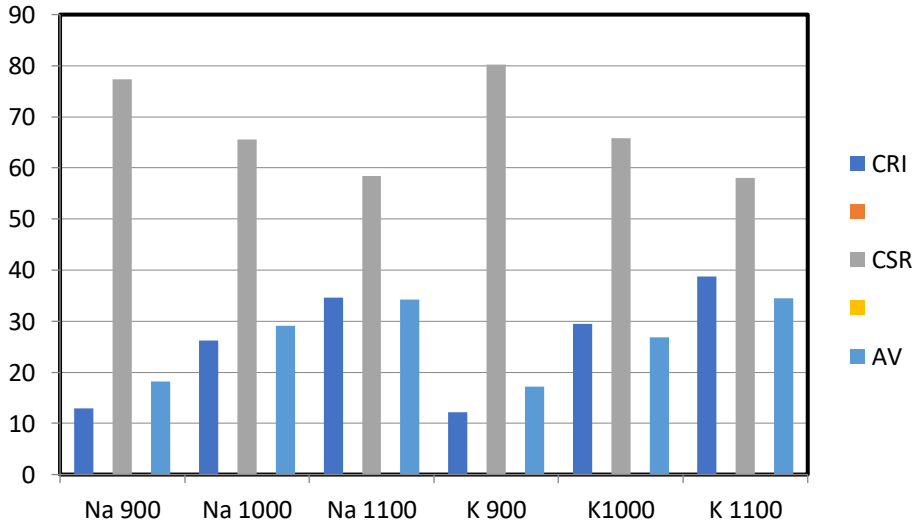

Fig.10.9: Graphs depicting the sodium and potassium effect on CRI/CSR/AV of the coke sample at different temperatures

The CSR values for alkali impregnated coke decrease with increasing temperature for both cases. The CRI vales also increase with the temperature and the abrasion value of the coke sample also follows the same trend as it can be seen from the graph. The effect of sodium on the strength and reactivity of the coke samples is more compared to that of potassium at lower temperature. The CRI and AV values for sodium impregnated samples is more compared to potassium ones. But on the other hand as the temperature increases to 1000^0C the effect of potassium is higher on the coke reactivity yet the effect on strength is lower compared to that of sodium. At 1100^0C the potassium effect on coke strength and reactivity is higher compared to sodium.

10.12. Alkali Effect on Bouduard Reaction at Different Temperatures

Loss of weights as a function of time at different temperatures is plotted in Fig. 10.10. Percentage of loss of weights is calculated by the following equation-

$$\% \text{ of Weight Loss} = \frac{W_0 - W_t}{W_0} * 100 \qquad 5$$

Where, W_0 and W_t are the weight of coke samples before and after the reaction for time t minutes, respectively.

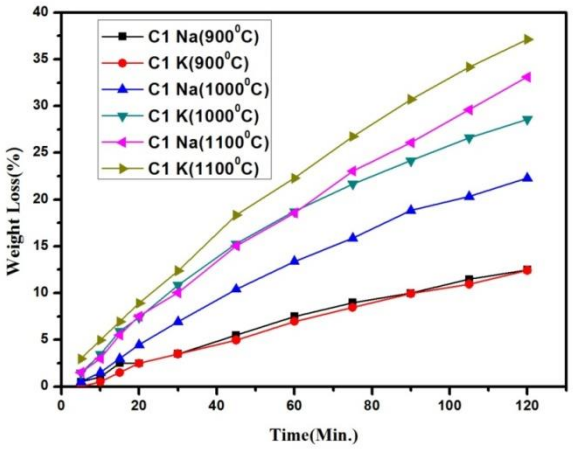

Fig. 10.10: Weight loss (%) vs. time for standard and alkali impregnated coke samples

It is clear that with time the weight loss increases as more carbon from the coke reacts with carbon dioxide gas to form carbon monoxide. It can be seen in Fig. 10.10 that the maximum weight loss is observed for potassium impregnated Coke sample at 1100^0C. The addition of alkali (Sodium and Potassium) increases the weight loss with temperature at a higher rate. It can also be seen that for the coke samples, potassium addition leads to higher weight loss compared to sodium addition except for at 900^0C, where sodium has greater effect on weight loss.

10.13 Isothermal Kinetic Study of Bouduard Reaction

In the present study of the isothermal reduction kinetic, the fractional weight loss (α) is defined as:

$$\alpha = \frac{M_t}{M_0} \qquad 6$$

where, M_0 is the initial weight of the coke samples and M_t is the weight loss due to carbon reacting with carbon dioxide gas in the vertical retort. So, α, defined by Eq. 6, gives the isothermal weight fraction loss as a function of time. These data has been graphically plotted in Fig. 10.11.

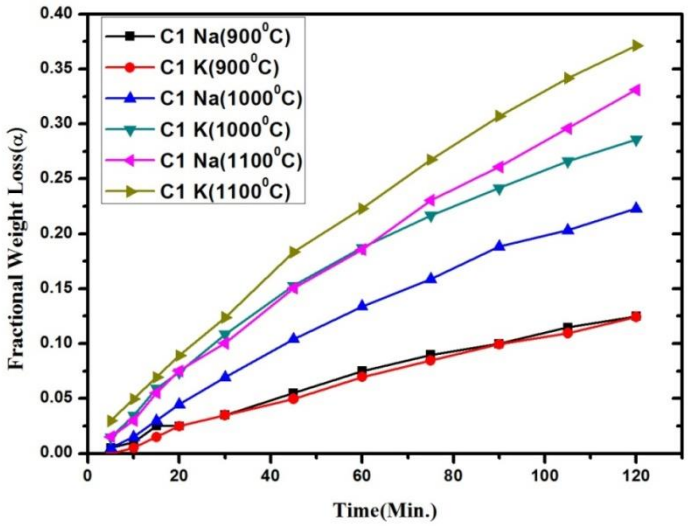

Fig. 10.11: Fractional weight loss (α) vs. time for standard and alkali impregnated coke

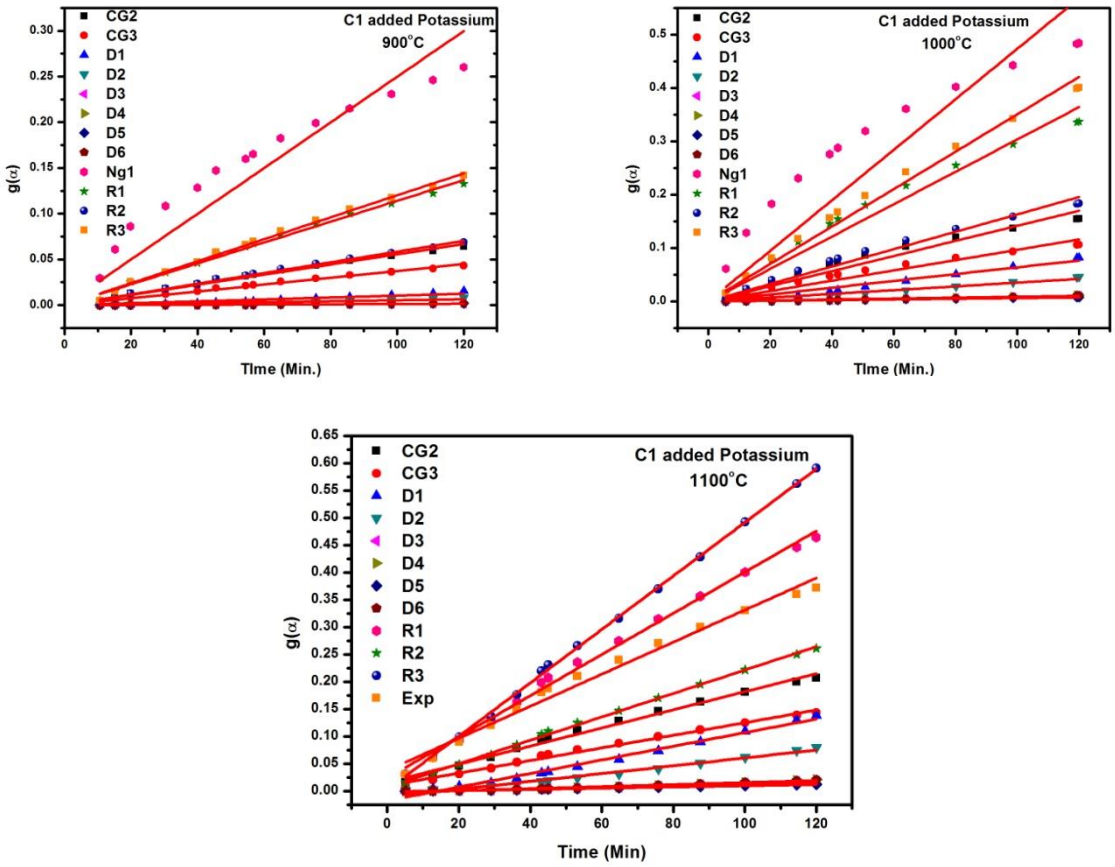

Fig. 10.12: Various mechanism model fittings showing the potassium effect on carbon conversion rate of bouduard reaction vs. time for coke sample at different temperatures

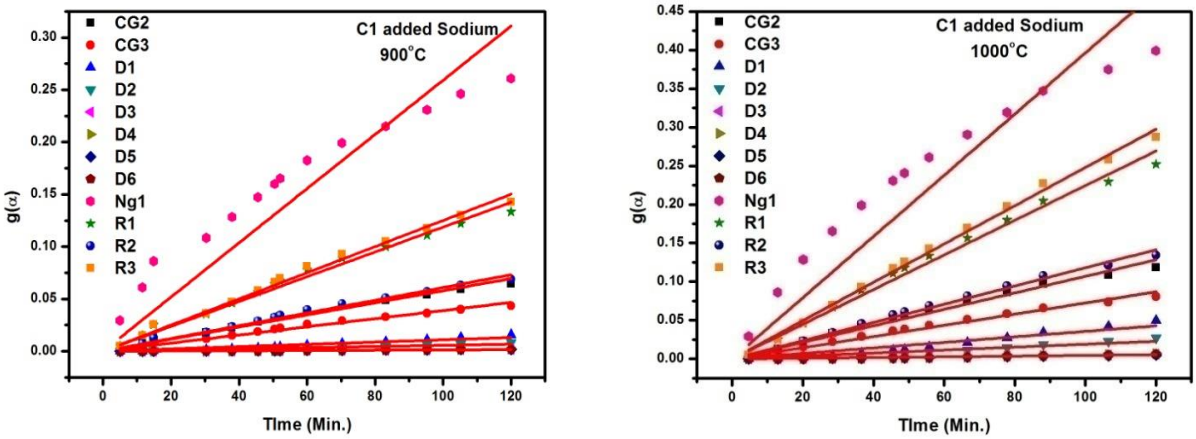

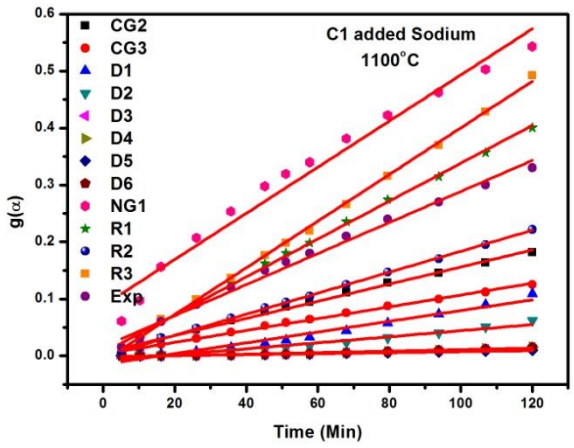

Fig. 10.13: Various mechanism model fittings showing the sodium effect on carbon conversion rate of bouduard reaction vs. time for coke sample at different temperatures

	Na 900°C	Na 1000 °C	Na 1100 °C	K 900 °C	K 1000 °C	K 1100 °C
Cg2	0.99564	0.94338	0.99775	0.99756	0.86229	0.99317
Cg3	0.9959	0.94329	0.99836	0.99772	0.86141	0.99447
D1	0.95626	0.87646	0.95755	0.94755	0.76724	0.97513
D2	0.9537	0.86998	0.94943	0.94477	0.75863	0.96818
D3	0.95283	0.86772	0.94643	0.94382	0.75561	0.96553
D4	0.95103	0.86304	0.94015	0.94187	0.74946	0.95987
D5	0.96061	0.8863	0.96797	0.9523	0.77996	0.98323
D6	0.95103	0.86304	0.94015	0.94187	0.74946	0.95987
R1	0.96799	0.93042	0.99928	0.97606	0.86672	0.99668
R2	0.9964	0.943	**0.99981**	0.99801	0.85943	0.99894
R3	**0.99706**	**0.94223**	0.99927	**0.99836**	**0.85585**	**0.99982**

Table 10.10: Correlation coefficient calculated using different mechanism functions

According to the kinetic analysis and calculation procedures introduced in chapter 3, section 3.5, the g(α) value for each mechanism model versus the reaction time t for the gasification reaction of the carbon samples are calculated and plotted, every plot is then subjected to linear fit through zero. The results are shown in Fig. 10.12 and Fig. 10.13. Simultaneously, the corresponding correlation coefficient for each model has been calculated, which is given

in Table 10.10. The higher the correlation coefficient the better is the mechanism function [6].

To determine the kinetic model and the rate controlling steps in the reaction, the experimental data are analysed by using reduced time plots shown in Fig. 10.14 and Fig. 10.15 for Potassium and Sodium added coke samples at different temperatures, respectively. From these figures and the calculated correlation coefficient given in Table 10.10 , the models with the highest R squared values and those matching the experimental reduced time plots are selected to be the governing reaction mechanism for the individual coke samples at different temperatures [7]. It can also be seen that after addition of alkali the experimental points (α, θ) coincide well with the theoretical curve for R2 mechanism only in case of sodium added coke samples at 1100^{o}C other than that all the coke samples with added sodium or potassium follow R3 mechanism as shown in figures below. In case of sodium or potassium added coke samples when the gas diffuses inside the pores the catalysts activate the reaction inside the pores at a high rate which widens the pores leading to greater diffusion of gasses inside the pores. After this a mixed mode of reaction takes place. Potassium has higher catalytic effect on carbon gasification compared to sodium [8]. So, after a certain time when diffused gases react inside the pores the rate of reaction and fractional weight loss increases. It can be seen that sodium added coke samples also follow higher rate mechanism i.e. R3 from 900^{o}C to 1000^{o}C but at 1100^{o}C it follows the slower R2 reaction mechanism. It is observed that in case of sodium added coke the reaction mechanism being followed is one-half order reaction (R2) in case of added sodium at 1100^{o}C where as in case of all other samples at different temperatures the reaction mechanism being followed is second order reaction (R3) in both cases.

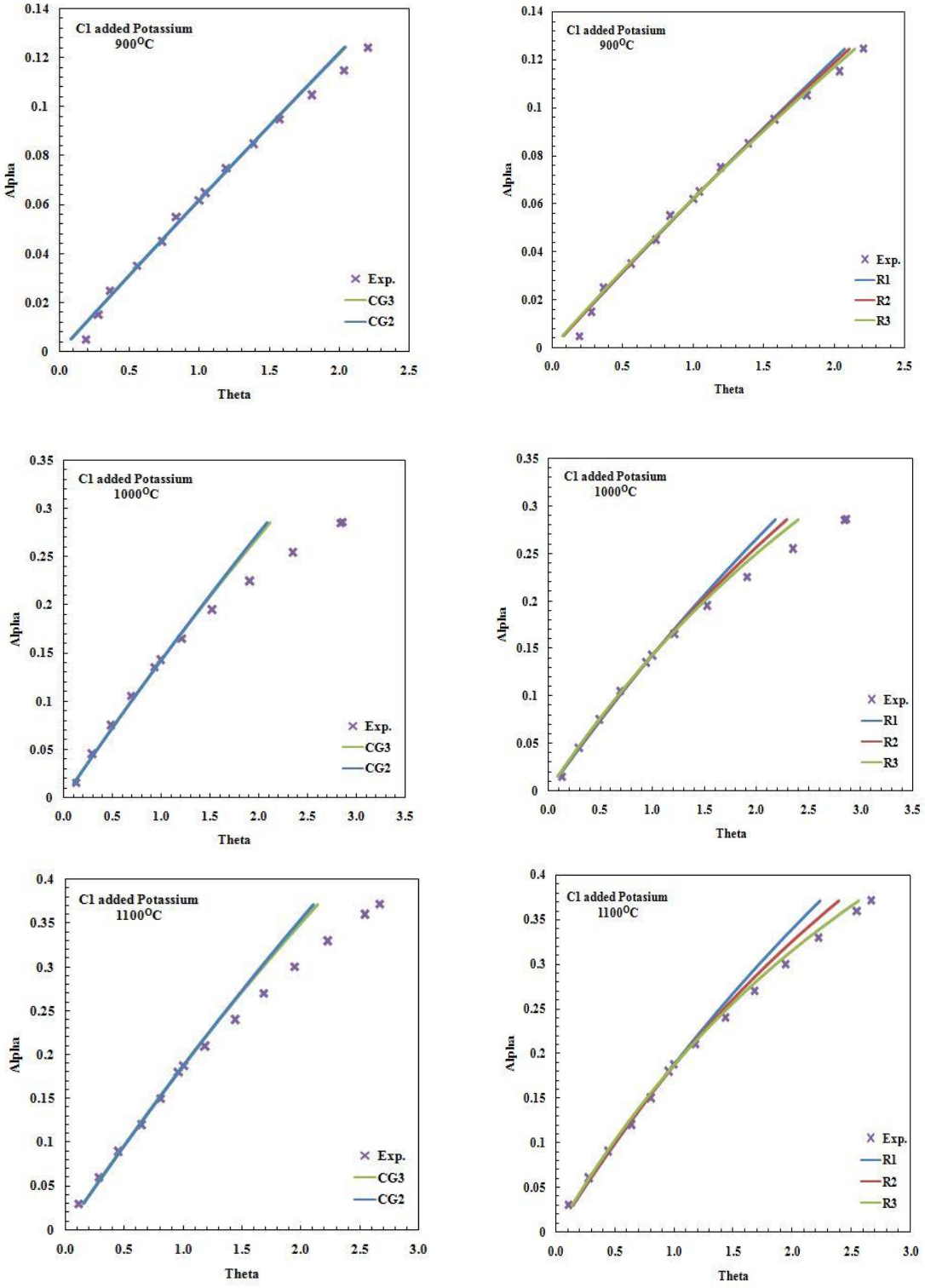

Fig. 10.14: Reduced time plot of fractional loss α along with the theoretical α vs. θ plot for different mechanism models of the coke samples with potassium at different temperatures

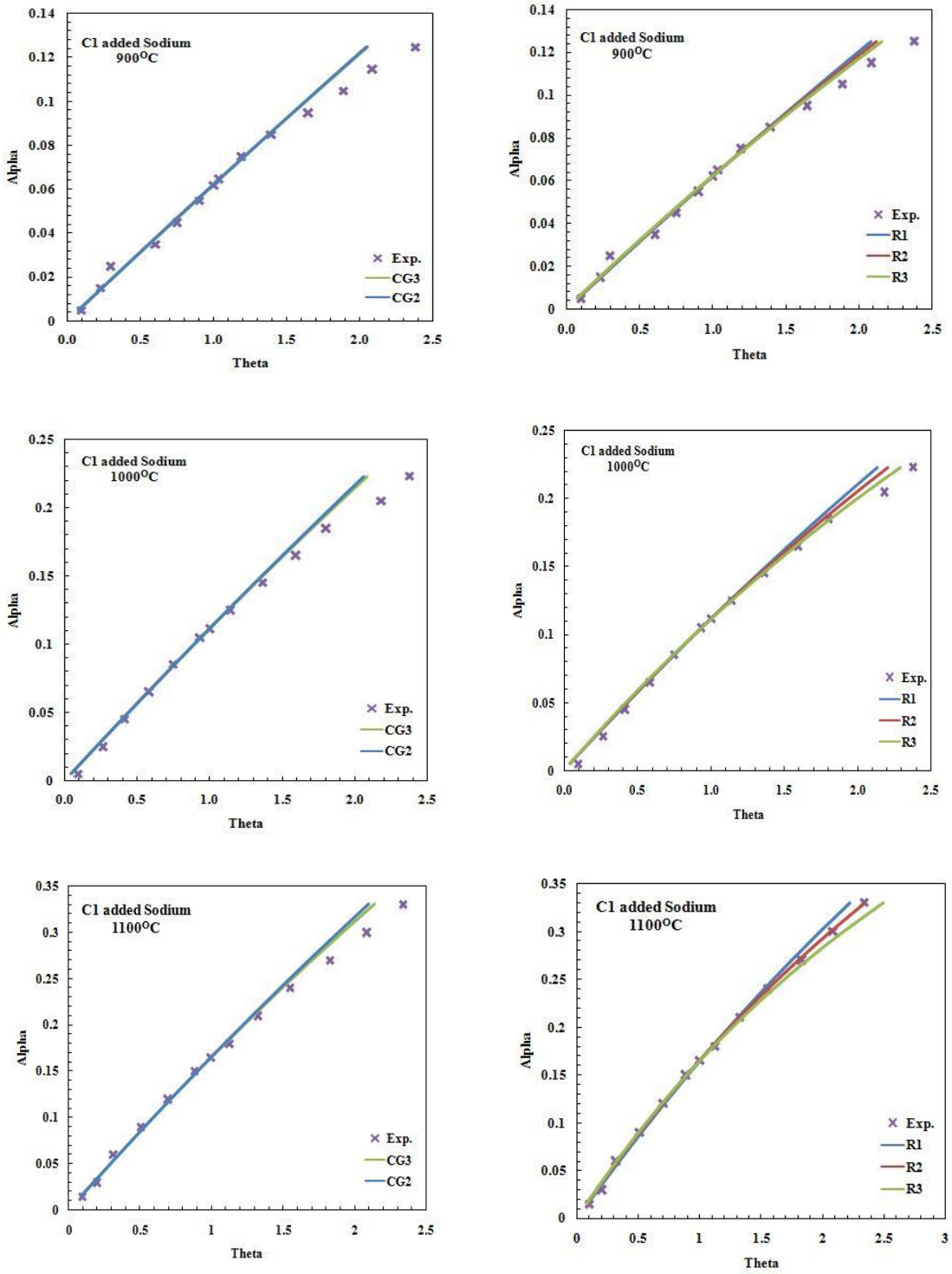

Fig. 10.15: Reduced time plot of fractional loss α along with the theoretical α vs. θ plot for different mechanism models of the coke samples with sodium at different temperatures

10.14 Activation Energy

According to Arrhenius equation, the rate constant (k) of a reaction can be expressed as follows:

$$k = A \cdot \exp(-Ea/RT) \quad (7)$$

where;

A – pre-exponential factor,

Ea – activation energy (kJ mol^{-1}),

R – universal gas constant,

T – temperature (K).

The activation energy can be calculated using the data obtained from the graphs of g (α) vs. time plots for different alkali added coke samples at different temperatures as given in the table. The carbon gasification follows contracting geometry (CG3) reaction mechanism in the beginning for both the coke samples i.e. with added sodium and potassium. In the later parts of the reaction for all three temperatures second order reaction mechanism is followed in case of potassium added coke samples and it is the same for sodium added coke samples except for at 1100°C where it follows one and half order reaction mechanism. The k values have been found out using the g (α) vs. time plots and they have been used to calculate the activation energy.

Kinetic parameters for CG3 reaction mechanism for different coke samples obtained from different g (α) vs. time plots:

	Na 900°C (1173K)	Na 1000°C (1273K)	Na 1100°C (1373K)	K 900°C (1173K)	K 1000°C (1273K)	K 1100°C (1373K)
Slope(k)	0.000419278	0.000778	0.00113347	0.00039094	0.0011538	0.00142757

The data from the above table is used to plot lnk vs. $10^4/T$ graph shown in Fig. 10.16 and from the best fitted line the activation energy is calculated. In this case the activation energy for sodium added coke sample came out to be 66.87kJ mol^{-1} and for potassium added coke

sample it is 88.05kJ mol^{-1} for the initial portion of the reaction where CG3 reaction mechanism is followed.

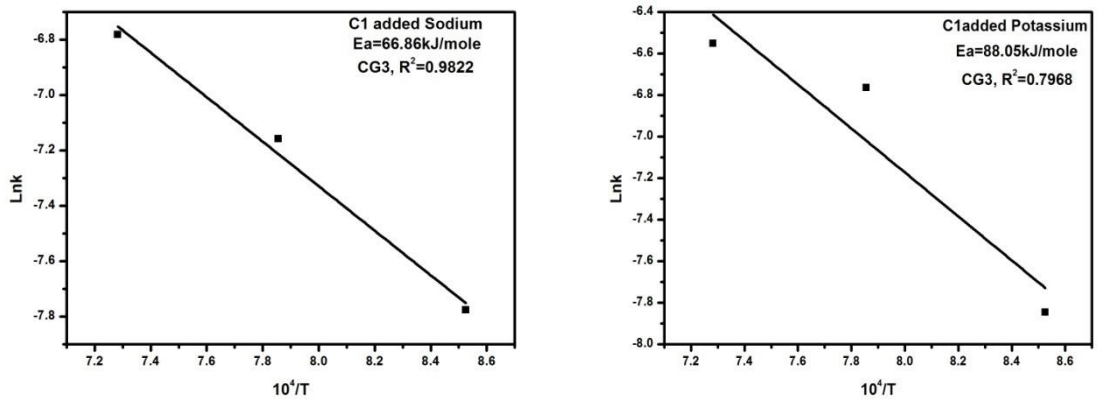

Fig. 10.16: Arrhenius plot of lnk vs. 10^4/T for sodium and potassium added coke samples following CG3 reaction mechanism

In case of added sodium at 1100°C the carbon gasification follows one and half order reaction whereas for 900°C and 1000°C it follows second order reaction due to this reason it is difficult to find out the activation energy of the later portion of the carbon gasification reaction of sodium added coke samples. The potassium added coke samples follow the second order reaction mechanism for all the three temperatures and the activation energy is 102.48kJ mol^{-1}.

Kinetic parameters for R3 reaction mechanism obtained from different g (α) vs. time plots for potassium added coke samples:

	K 900 °C (1173K)	**K 1000 °C (1273K)**	**K 1100 °C (1373K)**
Slope(k)	0.0010857	0.002812	0.004983

The data from the above table is used to plot lnk vs. 10^4/T plot given below and from the best fitted line the activation energy is calculated. In this case the activation energy for potassium

added coke sample it is 102.48 kJ mol^{-1} for the later portion of the reaction where R3 reaction mechanism is followed.

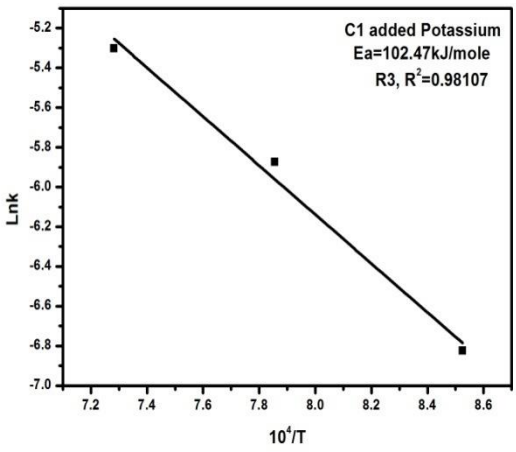

Fig. 10.17: Arrhenius plot of lnk vs. $10^4/T$ for potassium added coke samples following R3 reaction mechanism

10.15 Conclusion:

- Although, potassium has greater effect on the coke reactivity and strength as the temperature increases but sodium has a more profound effect at 900°C. The effect of potassium becomes more evident from the data at higher temperatures.
- Sodium has lowered the activation energy of bouduard reaction to 66.87kJ mol^{-1}, which is even lower compared to the activation in presence of potassium, which came out to be 88.05 kJ mol^{-1}; for the initial part of the bouduard reaction. The sodium added coke samples follow different reaction mechanisms at the end which makes difficult to find the activation energy with high accuracy (high R^2 value).
- The potassium added coke samples on the other hand follow the second order reaction mechanism at all the three temperatures in the end part. The activation energy for the R3 reaction mechanism is 102.48 kJ mol^{-1}.

- The low activation energy is the reason behind the high reactivity of the sodium and potassium added coke samples. The activation energy of blast furnace coke samples is round 138.7 kJ mol^{-1} [15]; which is much higher as compared to the sodium and potassium added coke samples.

10.16 Reference

1. International Organization for Standardization: ISO 18894, 2006. Coke – Determination of Coke Reactivity Index (CRI) and Coke Strength after Reaction (CSR).
2. Yamazaki, Y. (2012). Gasification reactions of metallurgical coke and its application–improvement of carbon use efficiency in blast furnace. Gasification for Practical Applications, 51-84.
3. Bhattacharyya, A., Schenk, J., Rantitsch, G., Thaler, C., & Stocker, H. (2015). Effect of alkaline elements on the reactivity, strength and structural properties of blast furnace cokes. Metalurgija, 54(3), 503-506.
4. Dongsheng Yu, Rui Guo, Yinghua Liang, Lianji Liu and Peng Chen, Effects of alkali metal on solution loss and coke degradation, Metall. Res. Technol., 116 6 (2019) 609
5. Lundgren, M., Sundqvist Ökvist, L., & Björkman, B. (2009). Coke reactivity under blast furnace conditions and in the CSR/CRI test. Steel Research International, 80(6), 396-401.
6. Rao YK, Adjorlolo A, Haberman JH. On the mechanism of catalysis of the Boudouard reaction by alkali-metal compounds. Carbon N Y 1982;20:207–12.
7. Wang H, Chu M, Guo B, Bao J, Zhao W, Liu Z, et al. Investigation on Gasification Reaction Behavior and Kinetic Analysis of Iron Coke Hot Briquette under Isothermal Conditions. Steel Res Int 2019; 90:1–10.
8. Sarkar BK, Kumar N, Dey R, Das GC. Optimization of Quenching Parameters for the Reduction of Titaniferous Magnetite Ore by Lean Grade Coal Using the Taguchi Method and Its Isothermal Kinetic Study. Metall Mater Trans B Process Metall Mater Process Sci 2018; 49:1822–33.

9. Nomura S, Naito M, Yamaguchi K. Post-reaction strength of catalyst-added highly reactive coke. ISIJ Int 2007; 47:831–9.
10. Adjorlolo AA, Rao YK. Effect of potassium and sodium carbonate catalysts on the rate of gasification of metallurgical coke. Carbon N Y 1984; 22:173–6. doi:10.1016/0008-6223(84)90207-0.
11. Sahajwalla V, Hilding T, Oelreich A, Gupta S, Björkman B, Wikström J-O, et al. Structure and Alkali Content of Coke in an Experimental Blast Furnace and their Gasification Reaction. AISTech 2004- Iron Steel Technol. Conf. Proc., vol. 1, Nashville, Tennessee, USA: 2004, p. 491–502.
12. Lindstad T, Syvertsen M, Ishak RJ, Arntzen HB, Grøntvedt PO. The influence of alkalis on the Boudouard reaction. InProceedings: Tenth International Ferroalloys Congress 2004 Feb 1 (Vol. 1, p. 4).
13. Li K, Zhang J, Barati M, Khanna R, Liu Z, Zhong J, et al. Influence of alkaline (Na, K) vapors on carbon and mineral behavior in blast furnace cokes. Fuel 2015; 145:202–213.
14. Bhattacharyya A, Albering J, Letofsky-Papst I. Effect of Alkaline Elements on Coke Structure under Blast Furnace Process Conditions. 25th Anniv. Int. Conf. Metall. Mater., Brno, Czech Republic, EU: 2016, p. 78–83.
15. Mianowski, A., Radko, T., & Siudyga, T. (2015). The reactivity of cokes in Boudouard–Bell reactions in the context of an Ergun model. Journal of Thermal Analysis and Calorimetry, 122(2), 1013-1021.

Chapter-11

Comparative Study of the Effect of Different Percentages of Sodium and Potassium on the Reactivity and Reaction Kinetics of Coke under Blast Furnace Conditions

11.1 Analysis of Coke Samples

Coke samples have been collected from two different areas: Germany and Linz, Austria (C3 and C4). The proximate analysis of the coke samples has been carried out and the results have been given in Table 11.1 [1].

	C3	C4
Ash	10.7	10.1
Volatile Matter	0.19	0.37
Moisture	3.40	3.15
Fixed Carbon	85.71	86.38

Table 11.1: Proximate analysis of coke samples

The coke samples have been impregnated in the same way as mentioned in section 10.2. The samples have been divided into three categories as follows: no added alkali, medium alkali content (0.4-1.0%) and high alkali content (1.0-2.0%).

11.2 Effect of Time on Coke Reaction in Blast Furnace Conditions

Loss of weights as a function of time at different temperatures is plotted in Fig. 11.1 and 11.2. Percentage of loss of weights is calculated by the following equation-

$$\% \text{ of Weight Loss} = \frac{W_0 - W_t}{W_0} * 100 \qquad 1$$

Where, W_0 and W_t are the weight of coke samples before and after the reaction for time t minutes, respectively.

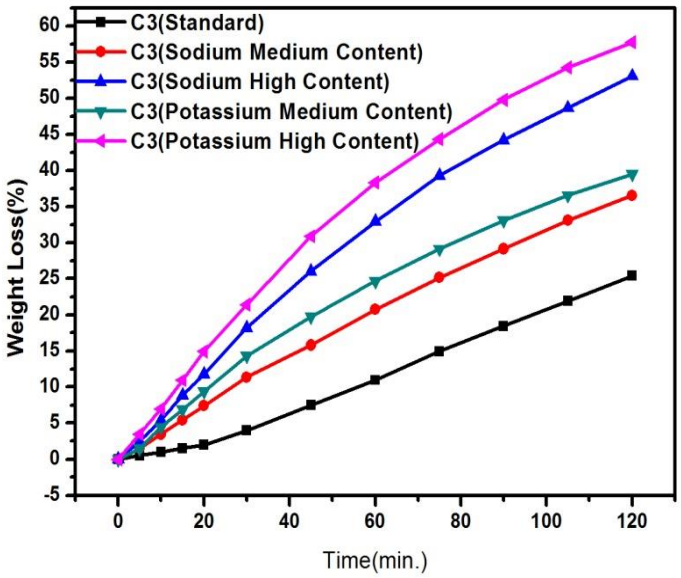

Fig. 11.1: Weight loss (%) vs. time for standard and alkali impregnated coke samples (C3)

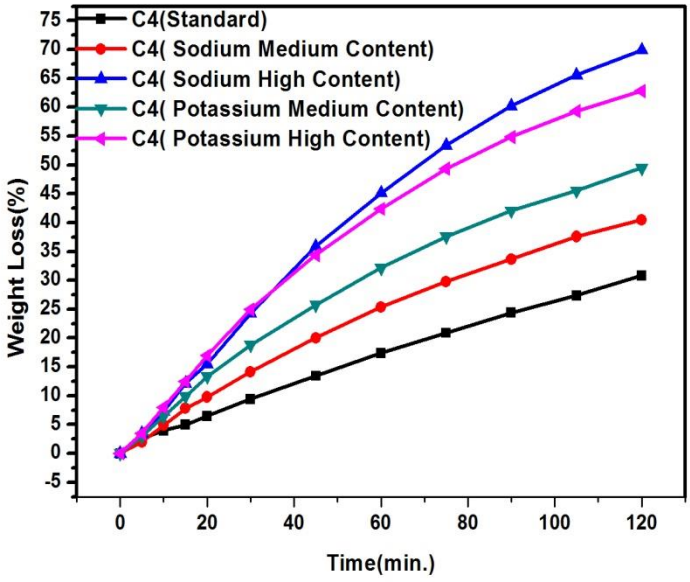

Fig. 11.2: Weight loss (%) vs. time for standard and alkali impregnated coke samples (C4)

It is clear that with time the weight loss increases as more carbon from the coke reacts with carbon dioxide gas to form carbon monoxide. It can be seen in Fig. 11.2 that the maximum weight loss is observed for high sodium impregnated C4 samples followed by high potassium impregnated C4 samples. The weight loss for the standard coke samples is almost the same. The addition of alkali (Sodium and Potassium) increases the weight loss with time at a higher rate [2, 3, 4]. It can also be seen that for the coke samples from same source, potassium addition leads to higher weight loss compared to sodium addition except for C4 samples. In case of C3 the weight loss increases with increase of alkali; with high potassium content coke having the maximum loss in weight followed by high sodium content.

11.3 Isothermal Kinetic Study of Bouduard Reaction

In the present study of the isothermal reduction kinetic, the fractional weight loss (α) is defined as:

$$\alpha = \frac{M_t}{M_0} \qquad 2$$

where, M_0 is the initial weight of the coke samples and M_t is the weight loss due to carbon reacting with carbon dioxide gas in the vertical retort. So, α, defined by Eq. 2, gives the isothermal weight fraction loss as a function of time. These data have been graphically plotted in Fig. 11.3 and 11.4.

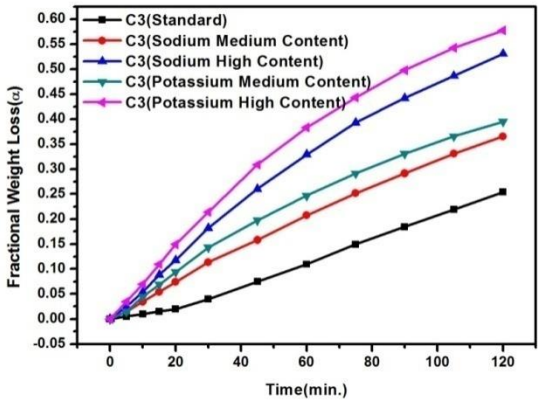

Fig. 11.3: Fractional weight loss (α) vs. time for standard and alkali impregnated coke (C3)

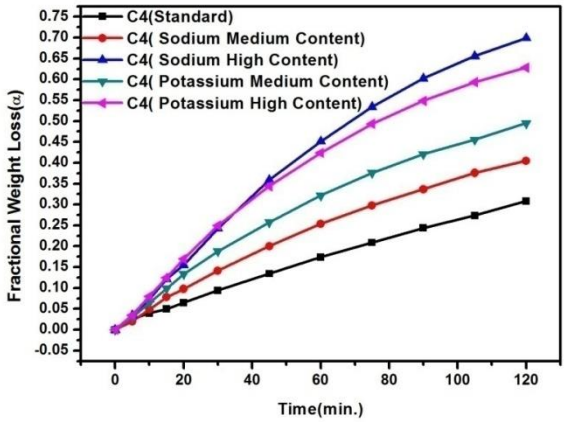

Fig. 11.4: Fractional weight loss (α) vs. time for standard and alkali impregnated coke (C4)

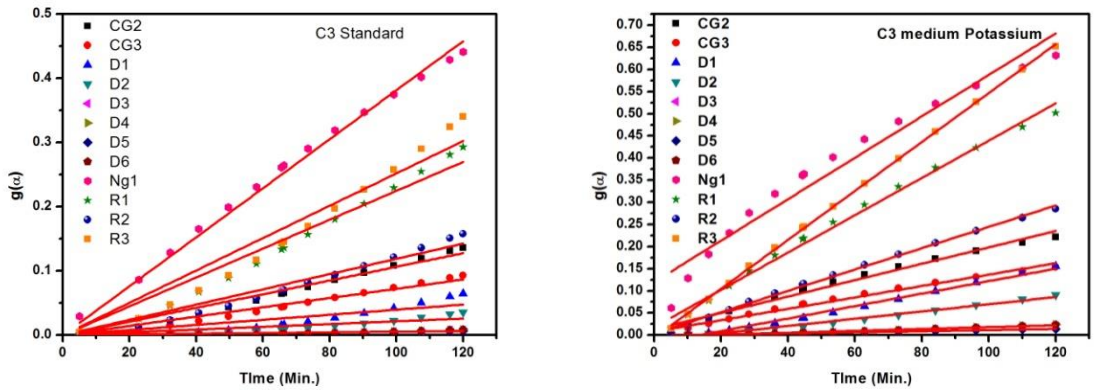

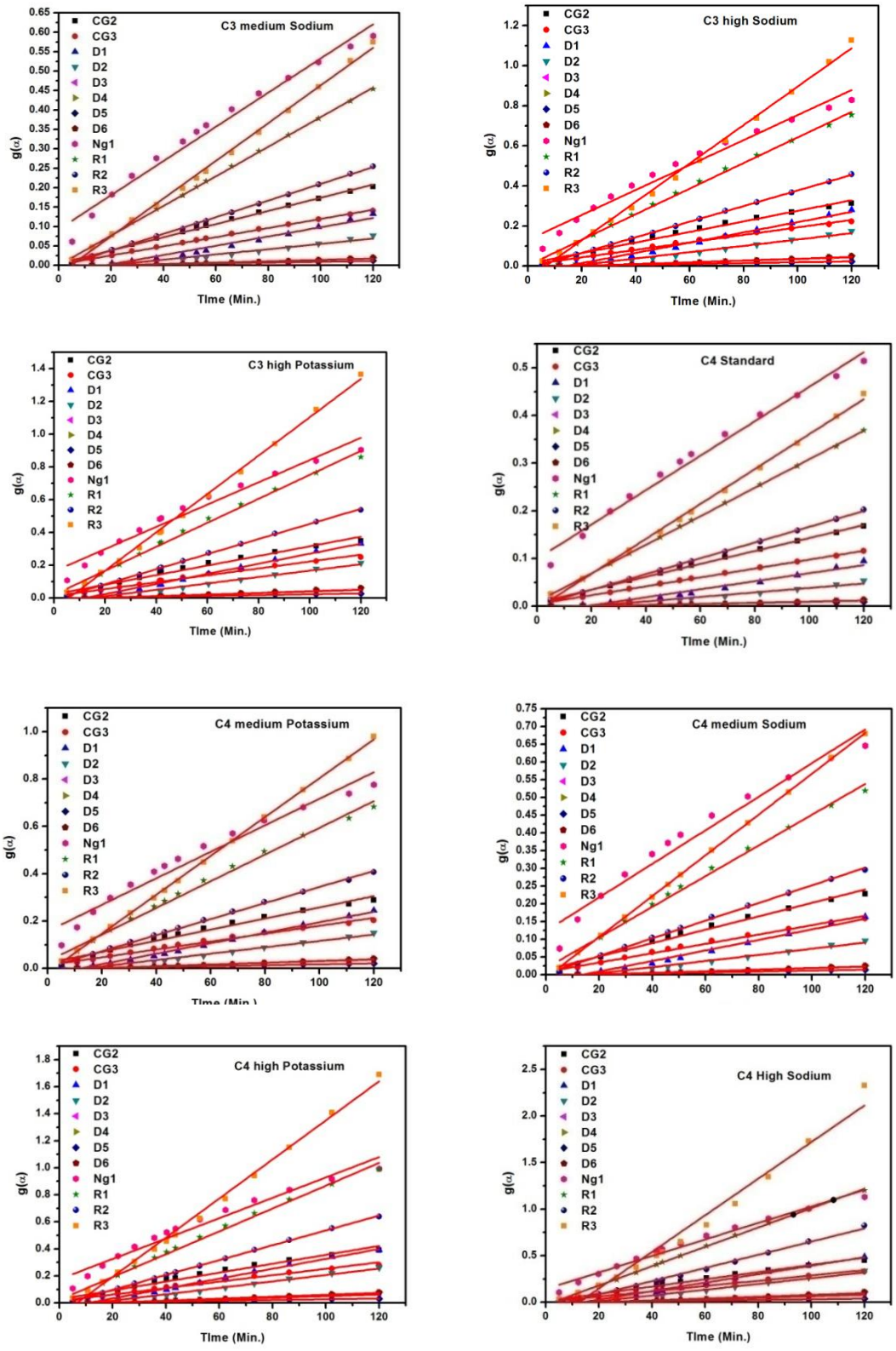

Fig.11.5: Various mechanism models fitting showing the carbon conversion rate of bouduard reaction vs. time for different coke samples

	C3 Standard	C3 Medium Sodium	C3 High Sodium	C3 Medium Potassium	C3 High Potassium
Cg2	0.99182	0.99744	0.99062	0.98483	0.9822
Cg3	**0.99099**	0.9984	0.99363	0.98762	0.98716
D1	0.89454	0.96651	0.98792	0.98831	0.99224
D2	0.88645	0.95761	0.97947	0.98248	0.98567
D3	0.88362	0.95428	0.97571	0.98012	0.98228
D4	0.87782	0.94727	0.96717	0.97493	0.97407
D5	0.90661	0.97709	0.99417	0.994	0.99525
D6	0.87782	0.94727	0.96717	0.97493	0.97407
NG1	0.99884	0.97813	0.97238	0.95385	0.9624
R1	0.98914	**0.99961**	**0.9979**	0.99235	0.99464
R2	0.98592	0.99964	0.99982	0.99731	**0.99963**
R3	0.98213	0.99756	0.99637	**0.99968**	0.99717

Table 11.2: Correlation coefficient calculated using different mechanism functions for C3

	C4 Standard	C4 Medium Sodium	C4 High Sodium	C4 Medium Potassium	C4 High Potassium
Cg2	0.99886	0.9877	0.98999	0.98294	0.979
Cg3	0.99932	0.99032	0.99478	0.98684	0.98513
D1	0.96288	0.98546	0.98737	0.99287	0.99411
D2	0.95535	0.97879	0.97516	0.98687	0.98847
D3	0.95259	0.97612	0.96852	0.98413	0.98507
D4	0.94685	0.97028	0.95239	0.97777	0.97631
D5	0.97264	0.99212	0.99266	0.99687	0.99506
D6	0.94685	0.97028	0.95239	0.97777	0.97631
NG1	0.98555	0.95982	0.97935	0.95886	0.96026
R1	0.9998	0.99461	**0.99938**	0.99312	0.99426
R2	**0.99939**	0.99868	0.99339	0.99868	**0.99976**
R3	0.99766	**0.99991**	0.97249	**0.99961**	0.99549

Table 11.3: Correlation coefficient calculated using different mechanism functions for C4

According to the kinetic analysis and calculation procedures discussed in chapter 3, section 3.5, the g(α) value for each mechanism model versus the reaction time t for the gasification reaction of the carbon samples have been calculated and plotted, every plot is then subjected to linear fit through zero. The results are shown in Fig. 11.5. Simultaneously, the corresponding correlation coefficient for each model has been calculated, which is given in Table 11.2 and Table 11.3. The higher the correlation coefficient the better is the mechanism function [5].

To determine the kinetic model and the rate controlling steps in the reaction, the experimental data are analysed by using reduced time plots shown in Fig. 11.6 and Fig. 11.7 for C3 and C4 coke samples, respectively. From these figures and the calculated correlation coefficient given in Table 11.2 and Table 11.3, the models with the highest R squared values and those matching the experimental reduced time plots are selected to be the governing reaction mechanism for the individual coke samples [6]. It has been found that the experimental (α, θ) points coincide very well with the theoretical curve for CG3 and R2 for the standard C3 and C4 respectively, as shown in figures below. It can be seen that with the addition of alkali the experimental points coincide well with different theoretical curves for different coke samples as given below.

Sample	**C3**	**C4**
Standard	CG3	R2
Medium Sodium	R1	R3
High Sodium	R1	R1
Medium Potassium	R3	R2
High Potassium	R2	R2

Table 11.4: Reaction Mechanisms followed by different coke samples with different alkali loading

In case of standard Coke samples, the gasses react with the surface. The inside of the coke is connected with the surface through pores but the concentration of carbon dioxide inside the pores declines as the distance from the surface increases [7]. The surface reaction dominates and it follows CG3 mechanisms. As the reacted surface increases and the distance to be travelled by carbon dioxide for reaction inside the pores decreases. The diffusion of gases leads to reaction inside the pores but in case of no added catalyst the surface reaction predominates and CG3 mechanism is followed.

The medium sodium and high sodium added C3 samples follow R1 mechanism. The medium and high potassium coke samples (C3) follow R3 and R2 mechanism, respectively. The medium sodium added C4 samples follow R3 mechanism while high sodium added samples follow R1 mechanism. It is observed that in case of sodium added coke the reaction mechanism being followed is first order reaction (R1) in the case of medium as well as high sodium added samples in case of C3. It is observed that in case of sodium added coke the reaction mechanism being followed is second order reaction (R3) in case of medium sodium added samples where as in case of high sodium added samples the reaction mechanism being followed is first order reaction (R1) in case of C4. The medium and high potassium coke samples (C3) follow R3 and R2 mechanism. Both the C4 coke samples containing medium and high level potassium followed R2 mechanism.

In sodium or potassium added coke samples when the gas diffuses into the pores the catalysts activate the reaction inside the pores at a high rate which widens the pores leading to greater diffusion of gasses inside the pores [7]. After this a mixed mode of reaction takes place. Potassium has higher catalytic effect on carbon gasification compared to sodium [8]. So, after a certain time when diffused gases react inside the pores the rate of reaction and fractional weight loss increases.

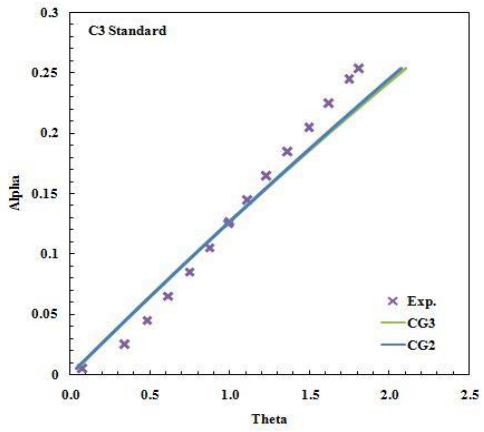
C3 Standard
Alpha
Theta
Exp.
CG3
CG2

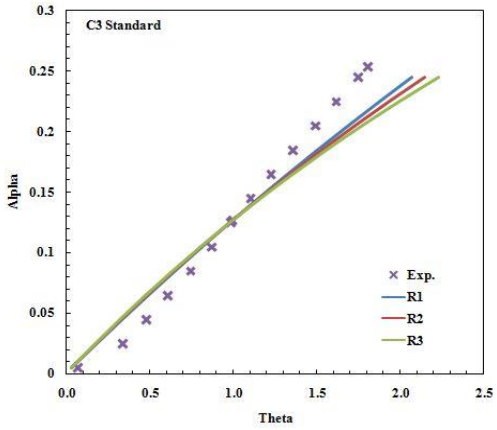
C3 Standard
Alpha
Theta
Exp.
R1
R2
R3

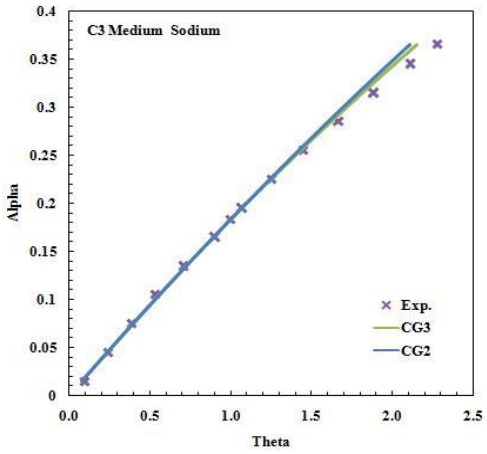
C3 Medium Sodium
Alpha
Theta
Exp.
CG3
CG2

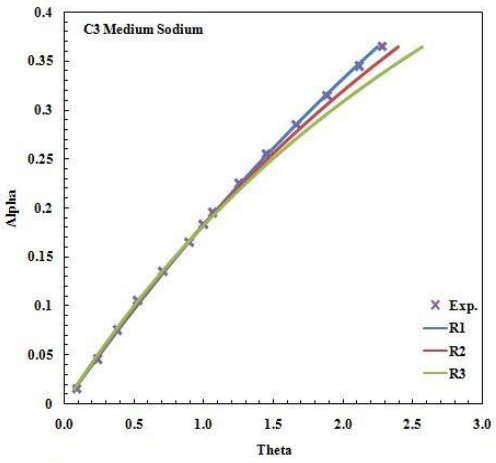
C3 Medium Sodium
Alpha
Theta
Exp.
R1
R2
R3

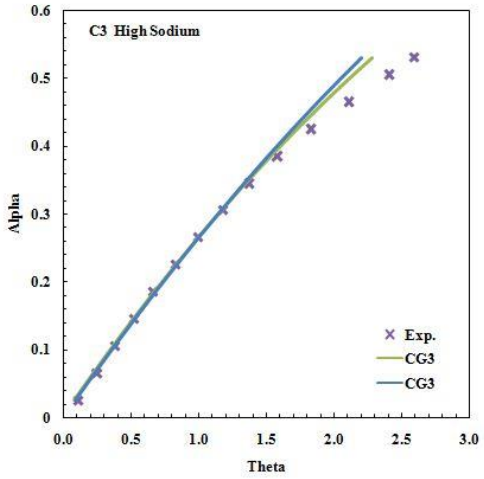
C3 High Sodium
Alpha
Theta
Exp.
CG3
CG3

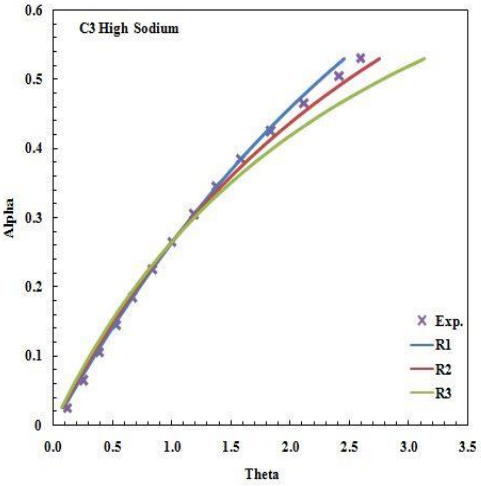
C3 High Sodium
Alpha
Theta
Exp.
R1
R2
R3

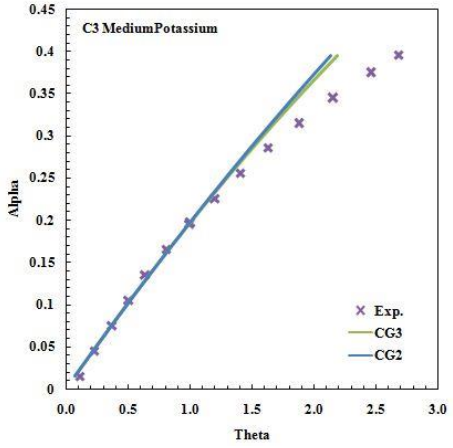
C3 MediumPotassium
Alpha
Theta
Exp.
CG3
CG2

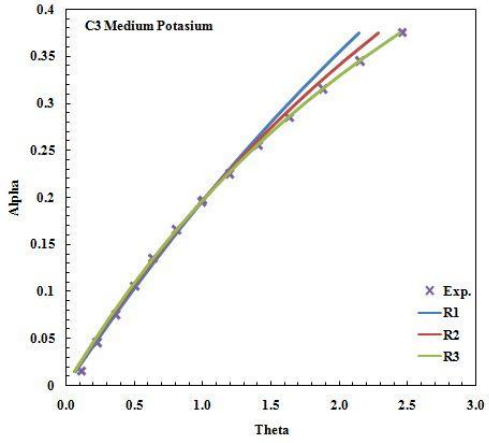
C3 Medium Potasium
Alpha
Theta
Exp.
R1
R2
R3

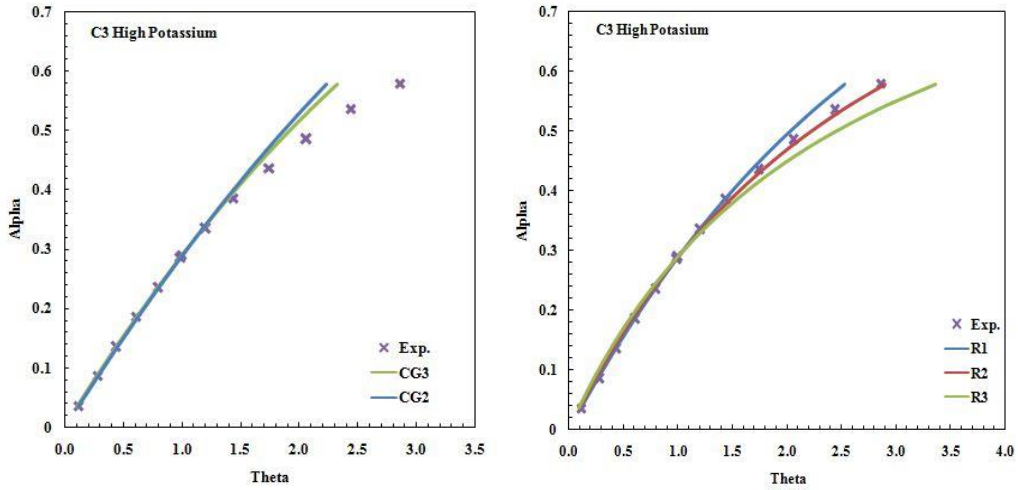

Fig. 11.6: Reduced time plot of fractional loss α along with the theoretical α vs. θ plot for different mechanism models of the C3

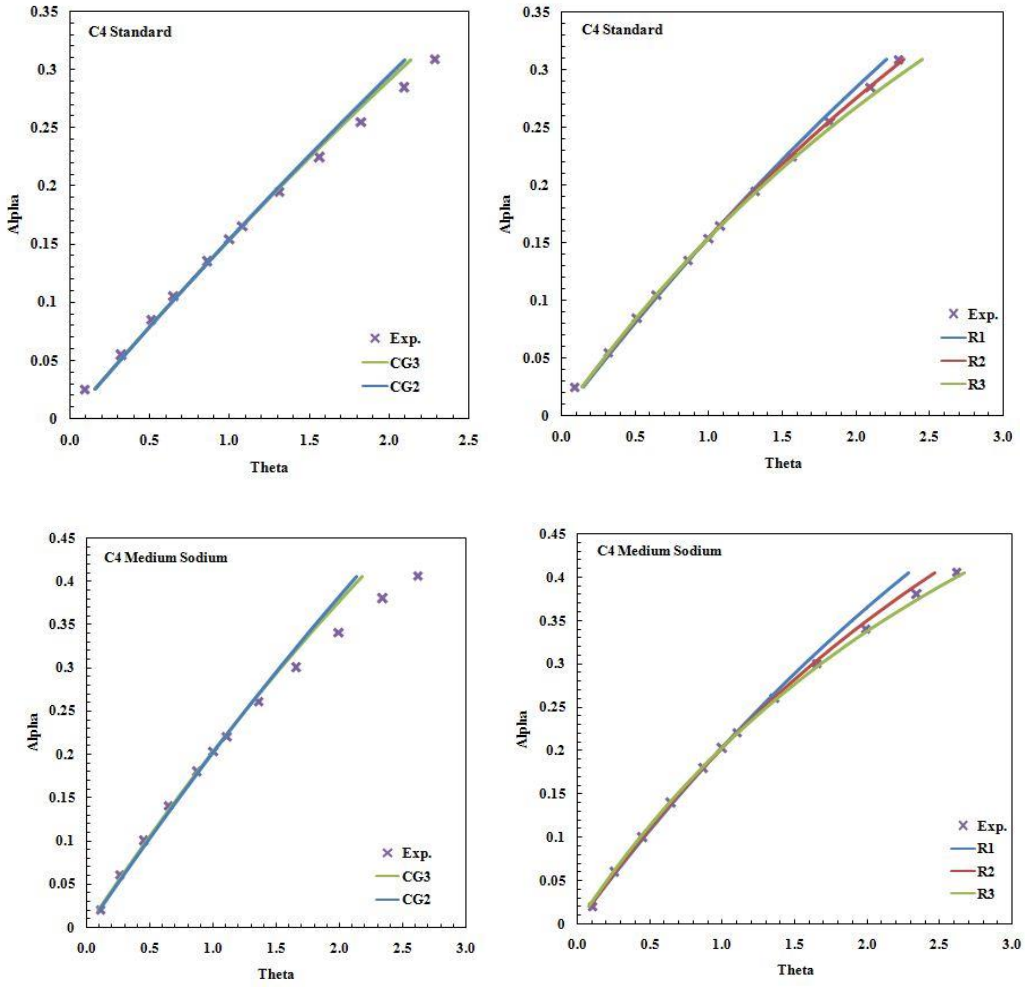

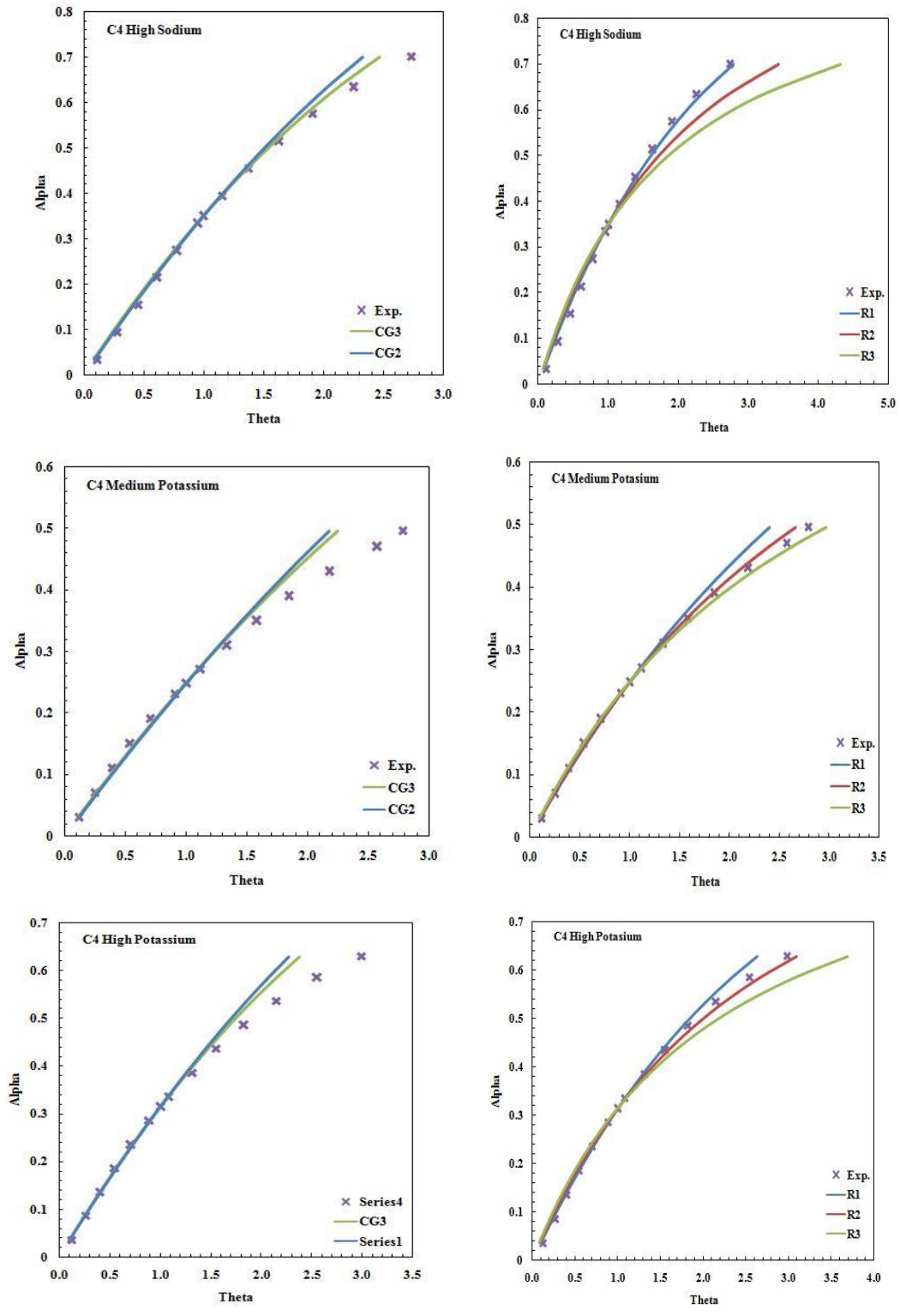

Fig. 11.7: Reduced time plot of fractional loss α along with the theoretical α vs. θ plot for different mechanism models of C4

11.4. Rate of Carbon Gasification

The rate of carbon gasification at 1100°C has been calculated using the following equation for the different set of samples to get a better understanding of the alkali effect on the reaction. The rate of gasification of carbon is calculated using the following formula:

$$-dN_C/dt = (M_c \text{ X } \alpha)/dt \quad (3)$$

Sample	Rate of reaction (mol/min)
C3 (Standard)	0.026070
C3 (medium Na)	0.037859
C3 (high Na)	0.054822
C3(medium K)	0.041220
C3(high K)	0.058883

Sample	Rate of reaction (mol/min)
C4 (Standard)	0.031693
C4 (medium Na)	0.042368
C4 (high Na)	0.073154
C4(medium K)	0.050866
C4(high K)	0.063776

Table 11.5: The rate of carbon gasification for different coke samples

M_c is the moles of carbon present in coke sample, α is the fractional weight loss and dt is the time from the start of weight loss till the end of test. The different rates have been listed in Table 11.5.

It can be seen from the data in Table 11.5 that the rate of carbon gasification increased gradually with the addition of alkali. The reaction rate for coke samples with added sodium is higher than that for the standard coke samples, whereas the coke samples with added potassium has higher reaction rate than the coke samples with added sodium for C3 samples. In case of C4 samples the rate of carbon gasification is the highest for high sodium samples. It has been reported previously that potassium has the highest catalytic effect on bouduard reaction compared to other alkali [8]. The data from the above table helps corroborate the results discussed in isothermal kinetics study part. Although, the highest rate of carbon

gasification is achieved by coke samples (C4) with high added sodium. The rate of carbon gasification is also higher in case of C4 samples compared to C3. The reaction mechanisms change depending upon the type of alkali as well as the type of coke as evident from this analytical study.

11.5 Comparison of Effect of Alkali (0.4-1.0%) on Different Coke Samples

The reaction mechanism followed during bouduard reaction and the rate of reaction of coke samples collected from India and Europe with the same level of sodium and potassium have been compared and the data has been given in Table 11.6 and Table 11.7, respectively.

Sample	C1	C2	C3	C4
Medium Sodium	R2	R2	R1	R3
Medium Potassium	R3	R3	R3	R2

Table 11.6: Reaction mechanisms followed by different coke samples for different alkali

Sample	C1	C2	C3	C4
Medium Sodium	0.0358	0.0379	0.03780	0.04236
Medium Potassium	0.0406	0.0436	0.04122	0.05086

Table 11.7: The rate of carbon gasification (mol/min) for different coke samples with medium alkali loading (0.4-1.0%)

All the coke samples with same level of alkali doping follow 1^{st}, one-half or 2^{nd} order chemical reaction mechanism. This mainly depends on the porosity and the available surface area of the different coke samples. It can be seen from Table 11.7; coke samples have higher rate of carbon gasification in case of potassium doped samples in comparison to samples with sodium. C3 and C4 have higher fixed carbon content compared to C1 and C2. The rate of carbon gasification is still greater in case of C2 compared to C3 for both sodium and potassium doped samples. The effect of alkali does not depend on the composition as much

as the porosity and specific surface area available for alkali penetration. Potassium has a much greater effect on carbon gasification compared to sodium on all the coke samples.

11.6. Conclusion

- Sodium and potassium addition to coke leads to an increased coke gasification.
- Sodium and potassium have different effects on the coke samples.
- Sodium and potassium added samples follow first order/ one half order or second order reaction mechanism depending on the coke samples.
- In case of C3 coke samples potassium has higher effect on the reaction rate than sodium.
- In case of C4 coke samples sodium (high) has higher effect on the reaction rate than potassium.
- Sodium and potassium both catalyse the bouduard reaction and lead to a higher coke gasification rate but the effect and its extent depends on the coke samples as evident from the results.

11.7 Reference

1. Bhattacharyya, A., Schenk, J., Rantitsch, G., Thaler, C., & Stocker, H. (2015). Effect of alkaline elements on the reactivity, strength and structural properties of blast furnace cokes. Metalurgija, 54(3), 503-506.
2. T. Lindstad, M. Syvertsen, R. J. Ishak, H. B. Arntzen, P. O. Grontvedt, Proceedings: INFACON X, Cape Town, 2004, 261-271.
3. J. Kaczorowski, T. Lindstad, M. Syvertsen, ISIJ International, 47 (2007) 11, 1599-1604.
4. Kaczorowski, T. Lindstad, Proceedings: INFACON XI, New Delhi, 2007, 584-593.
5. Wang H, Chu M, Guo B, Bao J, Zhao W, Liu Z, et al. Investigation on Gasification Reaction Behavior and Kinetic Analysis of Iron Coke Hot Briquette under Isothermal Conditions. Steel Res Int 2019; 90:1–10.
6. Sarkar BK, Kumar N, Dey R, Das GC. Optimization of Quenching Parameters for the Reduction of Titaniferous Magnetite Ore by Lean Grade Coal Using the Taguchi Method and Its Isothermal Kinetic Study. Metall Mater Trans B Process Metall Mater Process Sci 2018; 49:1822–33.
7. Nomura S, Naito M, Yamaguchi K. Post-reaction strength of catalyst-added highly reactive coke. ISIJ Int. 2007; 47:831–9. doi:10.2355/isijinternational.47.831.
8. Rao YK, Adjorlolo A, Haberman JH. On the mechanism of catalysis of the Boudouard reaction by alkali-metal compounds. Carbon N Y 1982; 20:207–212.

Chapter-12

Removal of Alkali from Iron via Smelting using Different Flux

12.1 Sample Selection

The iron ore sinters reduced under blast furnace conditions as shown in chapter 5B4 have been used for smelting purposes. The sinters with the highest alkali percentage have been used for this test. The sinters impregnated with 4M NaOH solution have been used, the amount of alkali present in the reduced sinter has been given below.

K = 0.477%

Na = 0.241%

Total Alkali % = 0.718%

The smelting has been carried out using two different combinations of fluxes.

12.2 Use of Dunite and Magnesium Hydroxide as Flux

The use of Dunite facilitates the alkali removal which leads to different problems like higher sulphur content in the hot metal [1, 2]. In this work we have used magnesium hydroxide alongside Dunite so as to provide the MgO required for removal of the sulphur from hot metal through slag. 50gms of reduced iron ore sinter samples have been taken it has been mixed with 2gms lime, 2gms Dunite and 1gm of magnesium hydroxide. The slag basicity is about 1.7. The mixture is taken in a graphite crucible. The raising hearth furnace is set to 1550^{o}C. The crucible containing the sinters and flux are put inside the furnace once the desired temperature is achieved. The smelting is carried on for about 30 minutes after which the crucible is taken out of the furnace and allowed to cool. The metal and slag are separately collected from the crucible and the metal is sent for ICP-OES analysis in Vizag Steel Plant (RINL). The ICP-OES result of the metal has been given in table 12.1.

Elements	%
Fe	91.05
Si	1.85
Mn	0.99
S	0.013
P	0.033
Ti	0.082
Zn	0.00176
Cr	0.00642
Alkali (Na+K %)	0.2832

Table 12.1: ICP-OES analysis of iron sinters smelted with dunite and magnesium hydroxide

12.3 Use of Magnesium Hydroxide and Magnesium Silicate

In this test magnesium silicate has been used as replacement for Dunite along with magnesium hydroxide which provides the MgO for sulphur removal. 50gms of reduced iron ore sinter samples have been taken it has been mixed with 2gms lime, 2gms magnesium silicate and 1gm of magnesium hydroxide. The slag basicity is about 1.6. The calculations have been shown in appendix. The mixture is taken in a graphite crucible. The raising hearth furnace is set to 1550^{o}C. The crucible containing the sinters and flux are put inside the furnace once the desired temperature is achieved. The smelting is carried on for about 30 minutes after which the crucible is taken out of the furnace and allowed to cool. The metal and slag are separately collected from the crucible and the metal is sent for ICP-OES analysis in Vizag Steel Plant (RINL). The ICP-OES result of the metal has been given in table 12.2.

Element	%
Fe	91.368
Si	1.98
Mn	1.4
S	0.008
P	0.036
Ti	0.102
Zn	0.0005
Cr	0.02376
Alkali (Na+K %)	**0.1614**

Table 12.2: ICP-OES analysis of iron sinters smelted with magnesium hydroxide and magnesium silicate

It can be seen from table 12.1 and 12.2 alkali has been removed from the hot metal during smelting with different fluxes. The alkali removal is more in case of lower basicity [3, 4]. The silicon pickup is more due to the higher percentage of silicates in slag [5]. The sulphur content of the metal is very low.

12.4 Conclusion

Alkali can be removed from hot metal with the help of silicates but it is important to keep in mind that the sulphur does not increase in turn [6]. The use of silicates makes silicon pickup in the hot metal inevitable. The use of magnesium hydroxide to supplement MgO in the slag and magnesium silicate in place of Dunite helped remove alkali and keep the sulphur content of hot metal in check.

12.5 Reference

1. A. Formoso, F.A. López, J.L.G. Fierro, M.T. Larrea and A. Cores: Ironmaking Steelmaking, 1997, vol. 24, pp. 288-92.
2. Lopez AF. Caloremetric and fourier transform infrared spectrophotometric studies of potassium elimination by dunite. Metallurgical and Materials Transactions B, 1995; 26(1): 51–58.
3. Polinov, A. & Pavlov, A. & Pishnograev, S. & Logachev, G. & Spirin, N. (2017). Effect of Slag Regime on Alkaline Compound Behavior in a Blast Furnace. Metallurgist. 61. 10.1007/s11015-017-0476-y.
4. Carlsson, J. (2018). Alkali Circulation in the Blast Furnace-Process Correlations and Counter Measures, Master's Thesis, Luleå University of Technology, Sweden.
5. Kundu, A.L. & Prasad, S.C. & Prakash, H.S. & Prasad, M., (2004). Strategies for the production of low silicon and low sulphur hot metal at Rourkela Steel Plant. Transactions- Indian Institute of Metals. 57. 109-121.
6. El-Geassy, A. A., Shehata, K. A., Nasr, M. I., & Fakhoury, S. S. (1986). Effect of alkalies on the performance of blast furnace. Transactions of the Iron and Steel Institute of Japan, 26(10), 865-874.

Chapter - 13

Interpretation and Future Scope of Work

13.1 Interpretation

- Alkali impregnated iron ore lumps and briquettes have been reduced and optimisation has been carried out in the frame work of BBD. The optimised conditions provided by BBD are close to experimental results.

- In iron ore lumps, sodium added samples showed increase in EOR with time and temperature even upto 0.35% Na. The potassium added samples showed an increase in EOR with time and temperature upto 0.15% K whereas when potassium increased to 0.4% the reducibility decreased at 1100^{o}C. Iron ore lumps reduction without and with added alkali follow chemical reaction mechanism at initial stages of reduction and diffusion mechanism at later stages of reduction.

- The EOR of alkali loaded briquettes increases with time and temperature. Potassium has higher effect than sodium. The EOR of briquettes increases with time even with alkali loading as high as 0.4% and 0.45% Na and K, respectively. Kinetics of briquette reduction is mixed mode type; initially it follows chemical reaction followed by diffusion in later stages of reduction.

- Alkali increases the degree of reduction and reducibility index of pellets. But alkali gives rise to swelling and sticking. Alkali as low as 0.15% (for both Na and K) also causes sticking and swelling. Kinetics followed by alkali loaded pellets is chemical reaction mechanism followed by diffusion in the later stages of reduction.

- Magnetite sinters from Donawitz, Austria with high alkali loading (0.4% K) have better LTD properties than hematite sinters from Tata Steel and Vizag Steel Plant, India with lower alkali loading of 0.15% and 0.2% K respectively. Alkali increases the degree of reduction and the reducibility index of magnetite sinters. The

degradation tendency and abrasion tendency improves with increase in alkali percentage. The LTD properties of the magnetite sinters improve initially upto 0.4%K and 0.15% Na but deteriorate as alkali increases to 0.4%K and 0.3%Na.

- Alkali increases the reactivity of coke but has negative effect on the strength (i.e. CSR and AV) of coke. The kinetics followed during Bouduard reaction is mixed mode type; initially contracting geometry (CG3) is followed after which one-half order or second order chemical reaction is followed. Effect of potassium is much more dominant. The activation energy is reduced due to the presence of alkali.

- Different alkali percentages impact the reaction mechanism followed during Bouduard reaction. The higher alkali percentage (1.0-2.0%) coke samples follow faster chemical reaction rates compared to the lower alkali (standard and 0.4-1.0%) percentage coke.

- The addition of different fluxes has helped remove alkali form iron during smelting. Best result has been achieved while smelting using lime, dunite, magnesium silicate and magnesium hydroxide. The silicon pickup is inevitable under conditions for alkali removal. In the other case the alkali removal is not efficient.

Modern iron and steel making has moved away from using only high grade iron ore lumps and coke. The utilisation of iron ore fines to improve sustainability and productivity of the iron making processes in form of sinters and pellets has been going on for a long time now. We are forced to use various other iron bearing resources i.e. non hematite ores, agglomerated iron ore fines (briquettes and nuggets) DRI using low grade iron ore with non-coking coal, etc. These practices pose a new challenge through incorporation of a significant alkali load in blast furnace operation. Some operational difficulties have been attributed to increased alkali load from time to time from various plants globally. Some temporal

rectification measures have also been reported and implemented with varying degree of success. But a comprehensive analytical study to understand the various qualitative effects advantageous or otherwise of the alkali load – Na, K or both, enumerate quantitatively the effects on various physico-chemical phenomenon, possibilities of removal of alkali load through modifying the flux composition and content has remained unattended. The present research is an attempt to fill in the gap. Interpretations of the experimental observation and analysis of the evolved data help to conclude:

- Box Behnken Design modelling can be used to find the optimum conditions using lower set of tests and provide results which resemble the experimental results very closely.
- Alkali (Na, K) improve the reducibility of iron ore lumps but after a certain level it has detrimental effect on the reducibility as well as strength of lumps.
- Alkali (Na, K) improve the reducibility of iron ore briquettes, the permissible amount of alkali load is higher and the effect on strength is lower compared to lumps.
- Alkali (Na, K) have the most damaging effect on pellets, even at low levels of alkali loading the strength of pellets deteriorate drastically by swelling and sticking.
- Alkali (Na, K) have lower effect on the strength of magnetite sinters as compared to hematite sinters. The permissible amount of alkali loading in case of magnetite sinters is higher compared to hematite sinters.
- Alkali can be removed from the furnace through slag during smelting with use of different combination of fluxes like Dunite, magnesium silicate and magnesium hydroxide along with lime.

6.2 Future Scope of Work

- The alkali effect on magnetite lumps, pellets and sinters can be studied on an industrial scale.
- The alkali effect on briquette reduction can be studied on an industrial scale.
- Alkali effect on some of the iron making processes like ITmK3, COREX, etc. which do not require air to be blown can be studied. In these cases, the problem of alkali recirculation can be avoided.

Chapter - 14

Appendix

Appendix-I

Hematite = 160gm

$Fe_2O_3 + 3C = 2Fe + 3CO$

For the removal of oxygen from hematite = 36gm carbon is required.

The ore in hand has 92% hematite.

92 gm hematite present in 100gm of iron ore.

To remove oxygen from 92 gm hematite: (36/160) 95.92 = 20.7gm carbon.

To remove oxygen from 100gm of given ore 20.7gm carbon is required.

For 10 gm ore 2.07gm carbon will be required.

Coal used has 28.08% carbon.

The amount of boiler grade coal for removal of oxygen from 10gm ore: 2.07/.2808 = 7.37gm

160 gm hematite – 48gm oxygen is removed.

92gm hematite – (48/160) * 95.92=27.6gm

From 100 gm of given ore 27.6gm oxygen removed.

EOR calculation for the 2M KOH lump sample reduced at 1100^{o}C for 60 minutes is shown below:

Sample Initial weight: 8.665gm; Amount of oxygen: 2.39gm

Final weight: 6.553

Loss in weight: 2.112gm Loss in weight (%): 24.37

Extent of reduction (%): (24.37/28.77)*100 = 88.33 or (2.112/2.39)*100=88.33

Various mechanism models fitting showing the lump reduction vs. time for different iron ore lump samples (Initial and final stages of reduction, respectively)

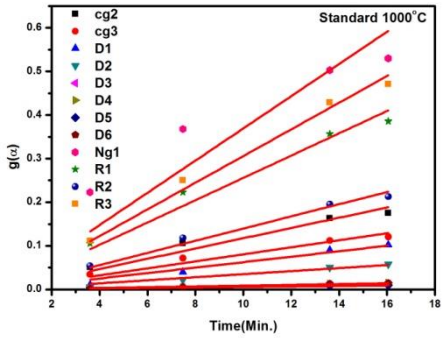

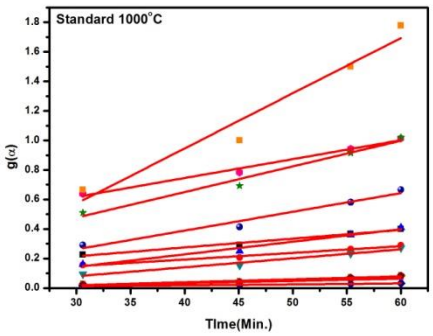

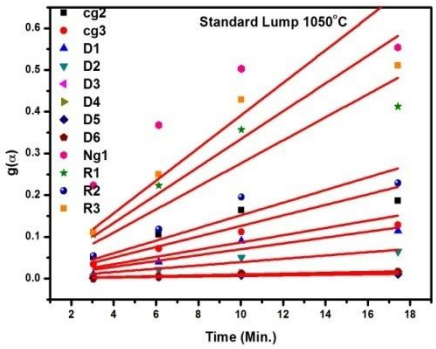

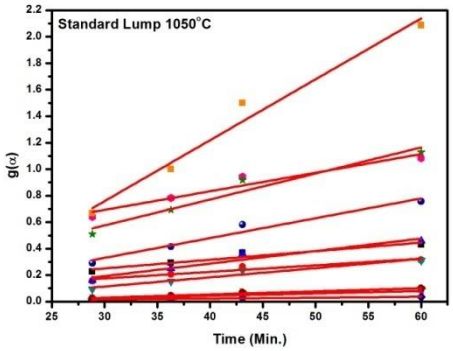

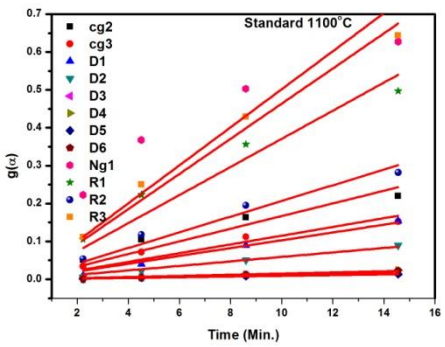

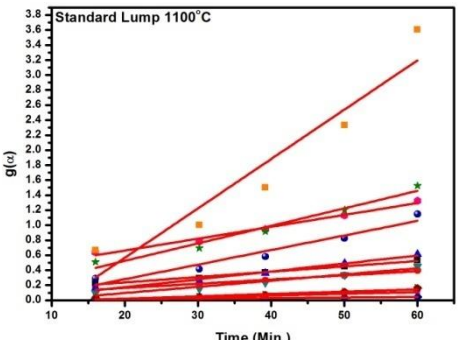

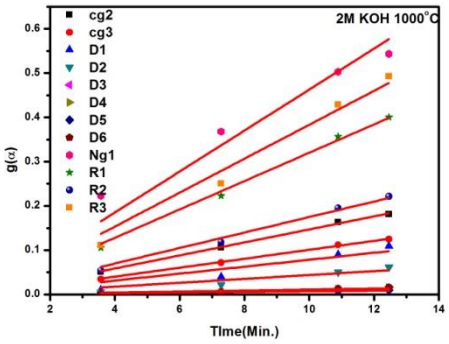

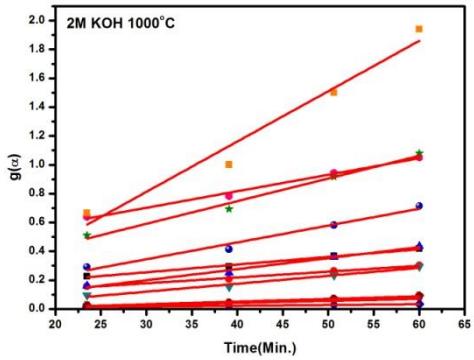

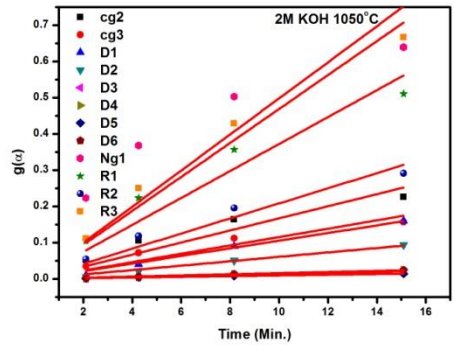
2M KOH 1050°C
cg2
cg3
D1
D2
D3
D4
D5
D6
Ng1
R1
R2
R3
g(α)
Time (Min.)

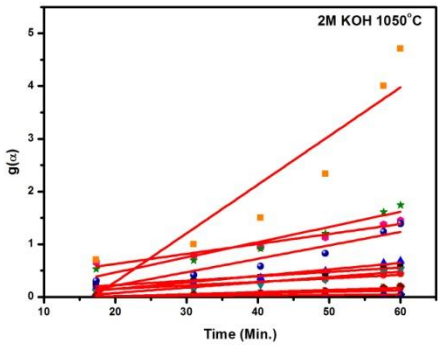
2M KOH 1050°C
g(α)
Time (Min.)

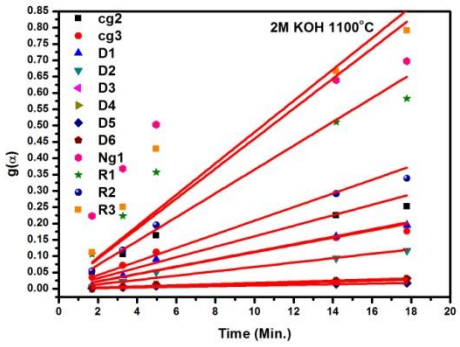
2M KOH 1100°C
cg2
cg3
D1
D2
D3
D4
D5
D6
Ng1
R1
R2
R3
g(α)
Time (Min.)

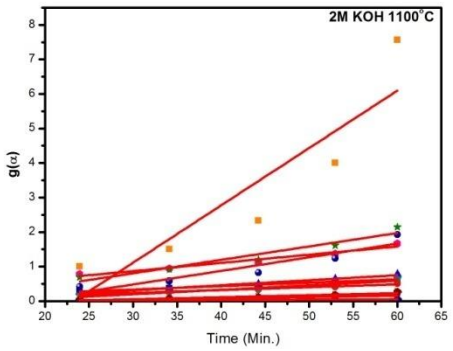
2M KOH 1100°C
g(α)
Time (Min.)

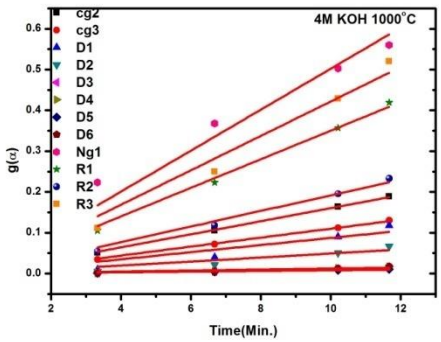
4M KOH 1000°C
cg2
cg3
D1
D2
D3
D4
D5
D6
Ng1
R1
R2
R3
g(α)
Time(Min.)

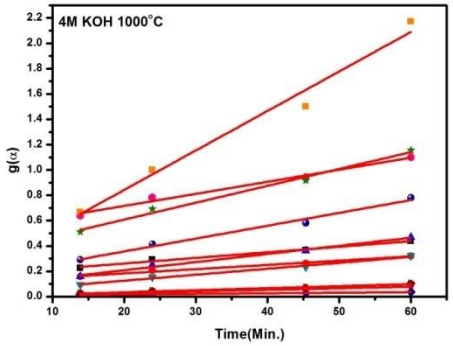
4M KOH 1000°C
g(α)
Time(Min.)

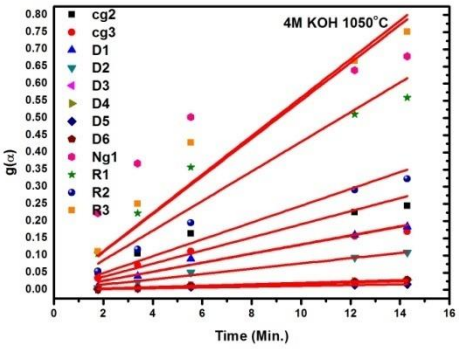
4M KOH 1050°C
cg2
cg3
D1
D2
D3
D4
D5
D6
Ng1
R1
R2
R3
g(α)
Time (Min.)

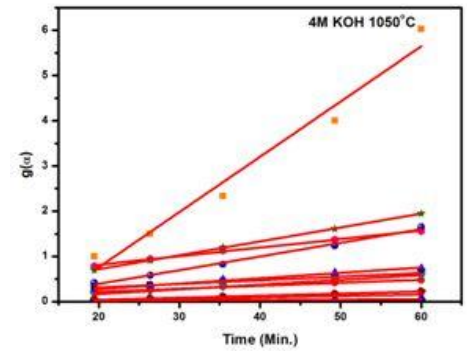
4M KOH 1050°C
g(α)
Time (Min.)

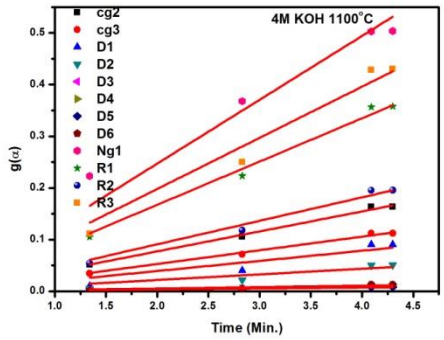
4M KOH 1100°C
cg2
cg3
D1
D2
D3
D4
D5
D6
Ng1
R1
R2
R3
g(α)
Time (Min.)

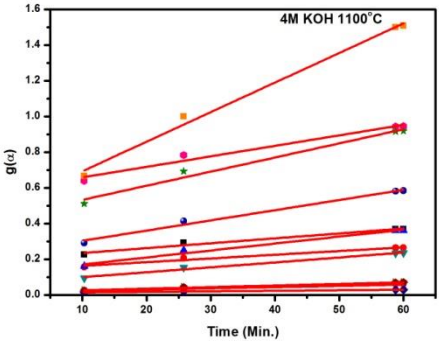
4M KOH 1100°C
g(α)
Time (Min.)

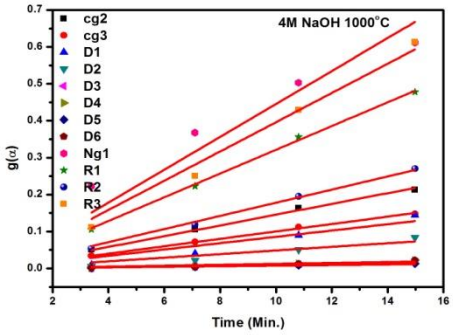
4M NaOH 1000°C
cg2
cg3
D1
D2
D3
D4
D5
D6
Ng1
R1
R2
R3
g(α)
Time (Min.)

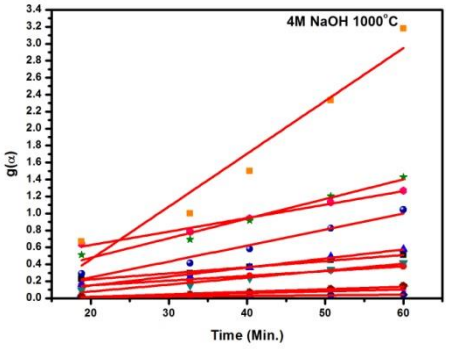
4M NaOH 1000°C
g(α)
Time (Min.)

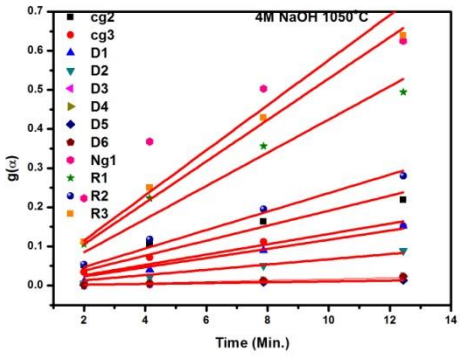
4M NaOH 1050°C
cg2
cg3
D1
D2
D3
D4
D5
D6
Ng1
R1
R2
R3
g(α)
Time (Min.)

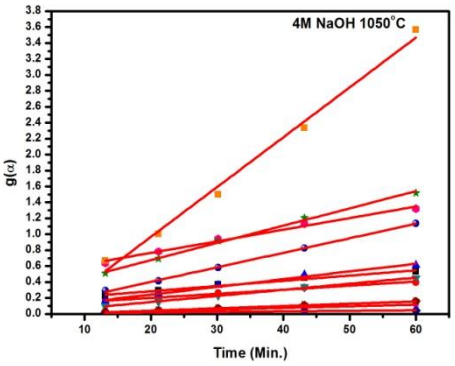
4M NaOH 1050°C
g(α)
Time (Min.)

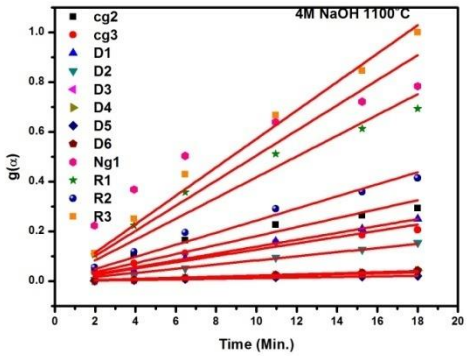
4M NaOH 1100°C
cg2
cg3
D1
D2
D3
D4
D5
D6
Ng1
R1
R2
R3
g(α)
Time (Min.)

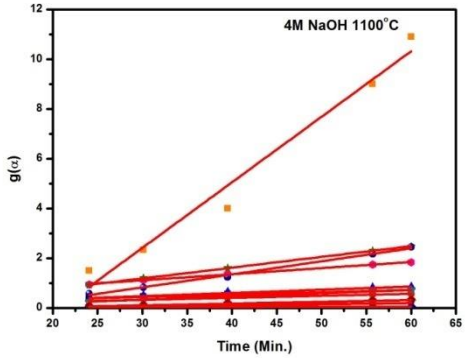
4M NaOH 1100°C
g(α)
Time (Min.)

Appendix-II

A briquette contains: 10gm iron ore + 2 % bentonite + 2 % moisture.

In case of alkali added briquettes the alkali is added using micropipettes.

4M NaOH in 500ml water contains 80gm NaOH.

Per ml of solution contains 0.16gm NaOH.

In 0.1ml solution - 0.016gm NaOH.

In 0.4ml solution 0.064gm NaOH.

0.064gm NaOH leads to addition of ~0.04gm Na.

For 4M solution of sodium we add 4 drops using a micropipette having a 0.1ml tip.

4M KOH in 500ml water contains 112gm KOH.

Per ml of solution contains 0.224gm KOH.

In 0.1ml solution - 0.0224gm NaOH.

In 0.3ml solution - 0.0672gm NaOH.

0.064gm NaOH leads to addition of ~0.045gm K.

For 4M solution of potassium we add 3 drops using a micropipette having a 0.1ml tip.

Similar calculation and technique has been used for the alkali addition to briquettes using 2M alkali solutions.

Extent of reduction (EOR) calculation for the 2M KOH briquette sample reduced at 1100^{o}C for 60 minutes is shown below:

Initial weight: 9.502gm; Iron ore: 9.502-0.2gm Bentonite-0.0336gm KOH=9.2684gm.

Oxygen: 2.558gm 18% bentonite is removed during reduction= 0.036gm

Total weight loss for 100% reduction: 2.594gm; Final weight: 7.069

Loss in weight: 2.433gm EOR (%): (2.433/2.594)*100=93.79%

Various mechanism models fitting showing the briquette reduction vs. time for different iron ore lump samples (Initial and final stages of reduction, respectively)

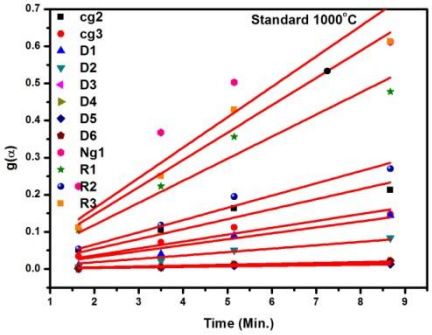

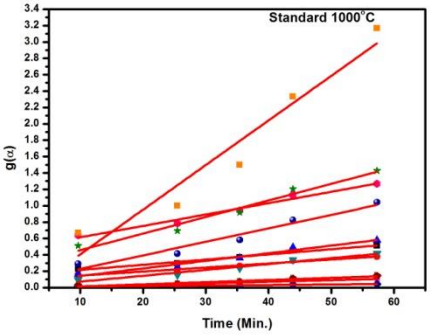

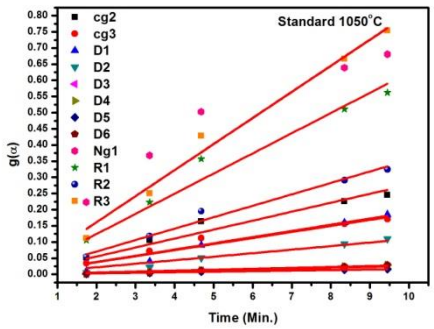

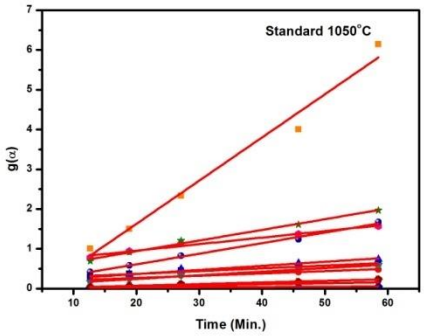

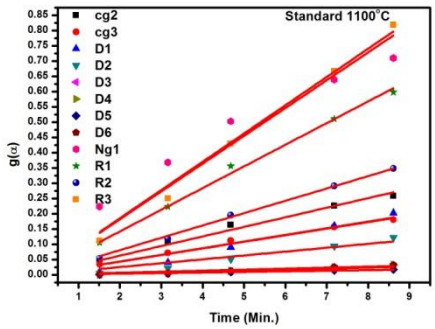

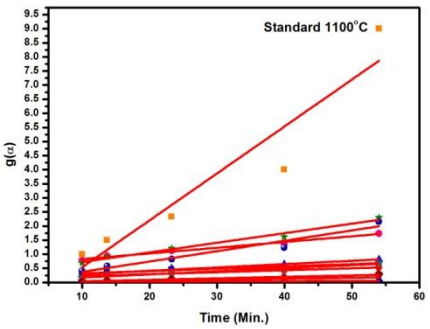

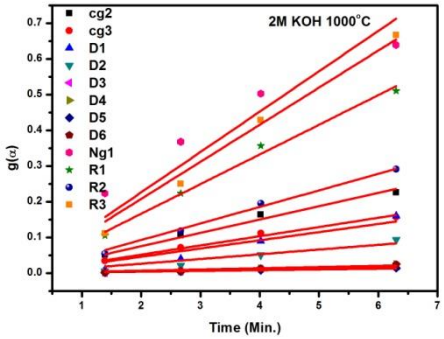

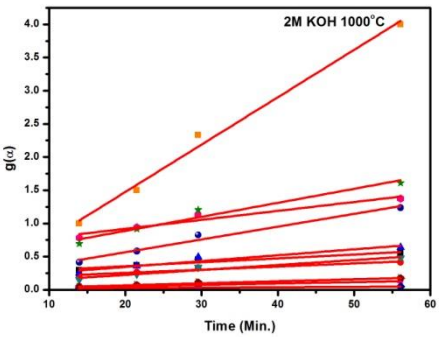

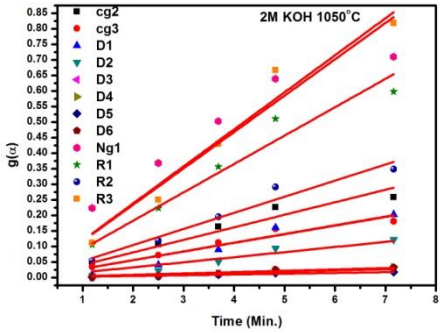
2M KOH 1050°C
cg2
cg3
D1
D2
D3
D4
D5
D6
Ng1
R1
R2
R3
g(α)
Time (Min.)

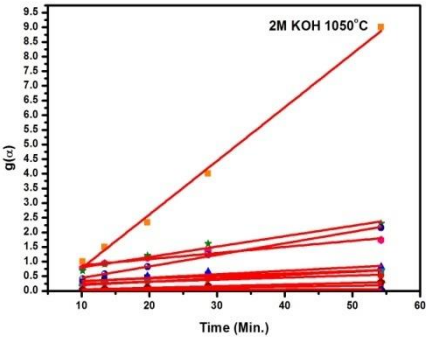
2M KOH 1050°C
g(α)
Time (Min.)

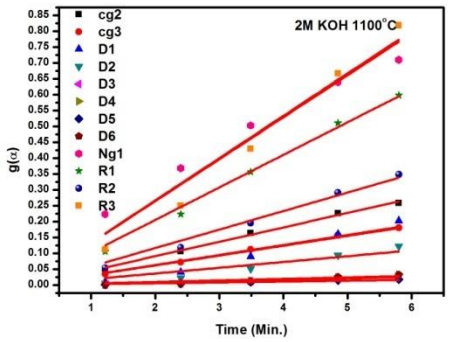
2M KOH 1100°C
cg2
cg3
D1
D2
D3
D4
D5
D6
Ng1
R1
R2
R3
g(α)
Time (Min.)

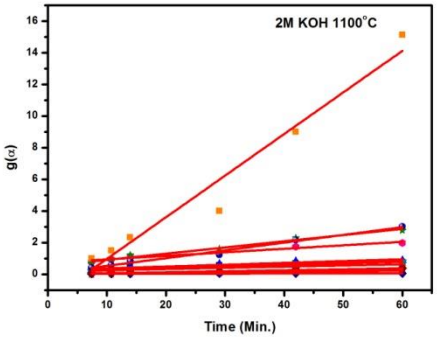
2M KOH 1100°C
g(α)
Time (Min.)

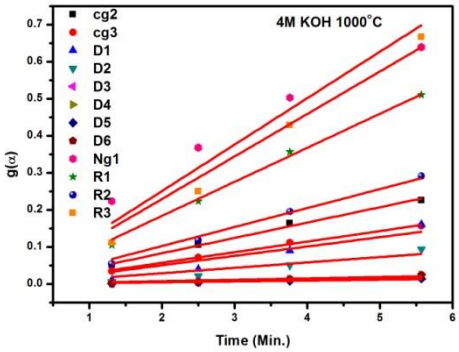
4M KOH 1000°C
cg2
cg3
D1
D2
D3
D4
D5
D6
Ng1
R1
R2
R3
g(α)
Time (Min.)

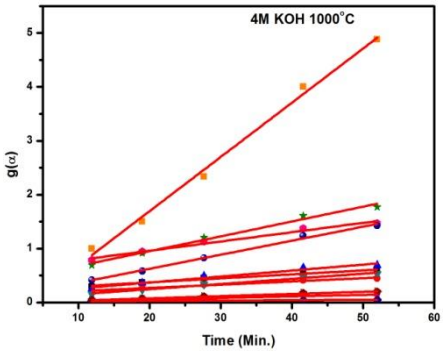
4M KOH 1000°C
g(α)
Time (Min.)

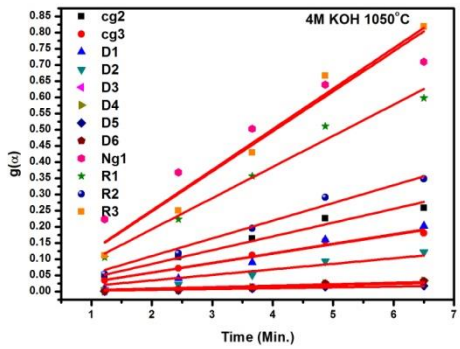
4M KOH 1050°C
cg2
cg3
D1
D2
D3
D4
D5
D6
Ng1
R1
R2
R3
g(α)
Time (Min.)

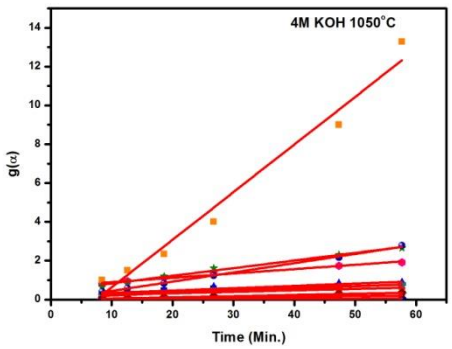
4M KOH 1050°C
g(α)
Time (Min.)

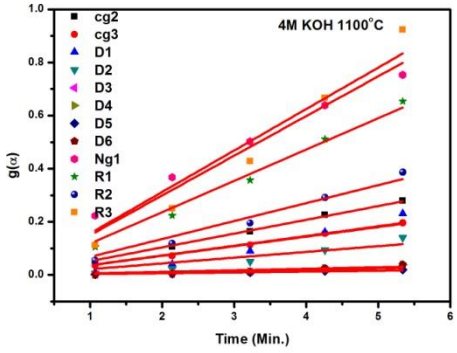
4M KOH 1100°C
cg2
cg3
D1
D2
D3
D4
D5
D6
Ng1
R1
R2
R3
g(α)
Time (Min.)

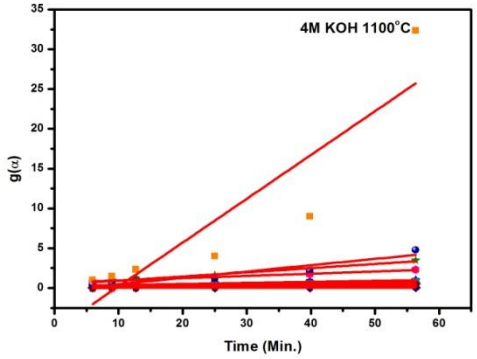
4M KOH 1100°C
g(α)
Time (Min.)

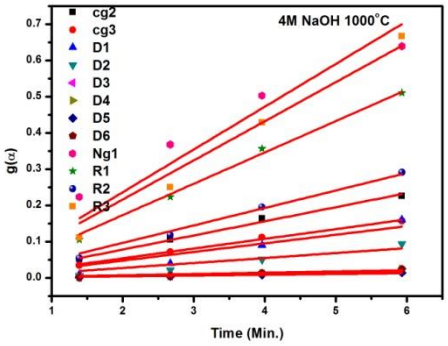
4M NaOH 1000°C
cg2
cg3
D1
D2
D3
D4
D5
D6
Ng1
R1
R2
R3
g(α)
Time (Min.)

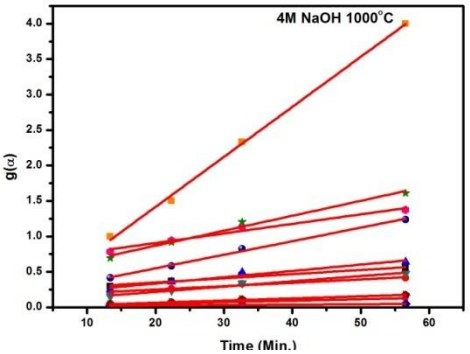
4M NaOH 1000°C
g(α)
Time (Min.)

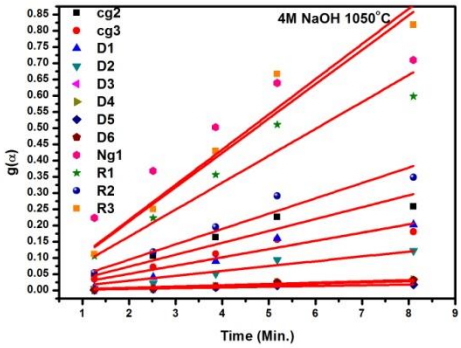
4M NaOH 1050°C
cg2
cg3
D1
D2
D3
D4
D5
D6
Ng1
R1
R2
R3
g(α)
Time (Min.)

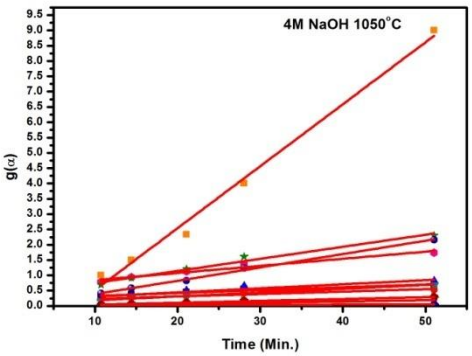
4M NaOH 1050°C
g(α)
Time (Min.)

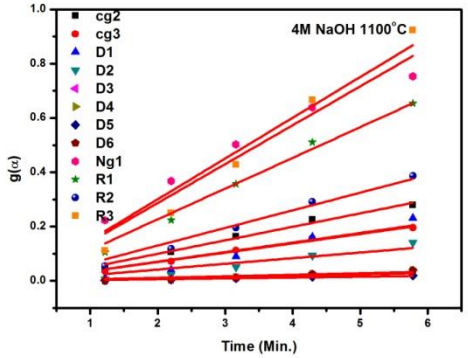
4M NaOH 1100°C
cg2
cg3
D1
D2
D3
D4
D5
D6
Ng1
R1
R2
R3
g(α)
Time (Min.)

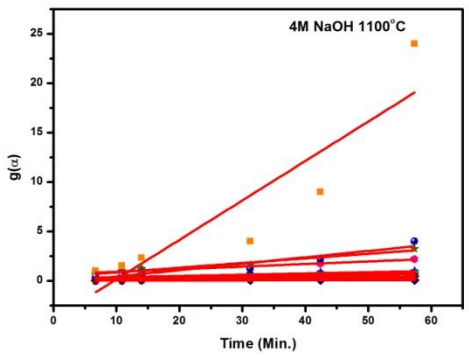
4M NaOH 1100°C
g(α)
Time (Min.)

Appendix-III

Tasmanian Pellet contains 92.74% Fe_2O_3 and 0.8% FeO.

Oxygen from Fe_2O_3=27.82gm

Oxygen from FeO=0.18gm

Total oxygen in 100gm Pellet: 28gm.

500gm Pellet contains: 140gm oxygen.

65% loss means 91gm. (for ISO-4695 test)

For standard Pellets:

Initial Weight (m_o): 499.9gm

$$R_t = \left(\frac{0.111\, w_1}{0.430\, w_2} + \frac{m_1 - m_t}{m_0 \times 0.430\, w_2} \times 100 \right) \times 100$$

w_1=0.8, w_2=92.74

After 60min reduction, m_t=417.9gm

$$R_t = 58.58\%$$

$$\frac{dR}{dt} = \frac{33.6}{t_{60} - t_{30}}$$

t_{60}=63min, t_{30}=20min

$$\frac{dR}{dt} = 0.78$$

(Calculation of degree of reduction and reducibility index for sinters has been done in a similar way)

Appendix-IV

Tata Steel coke (C1) added sodium

Amount of coke = 199.4 ≈153.2 g carbon ≈ 12.77 mol C

Master chemical equation: $CO_2 + C = 2CO$

Time span (straight line part of the kinetic curve) = 117.92 min

Mass loss = 33.09%

The gas flow control valves are calibrated at 298 K.

Calculation of molar flow rate of CO_2 –

Molar flow rate of CO_2 = 0.2 mol/min

The rate of gasification of carbon –

$-dN_C/dt = (12.77 * 0.33099)/117.92 = 0.035844$ mol/min